frontiers | Research Topics

Functional screening for cancer drug discovery: From experimental approaches to data integration

Edited by
Wenyu Wang, Jing Tang and Kecheng Zhou

Published in
Frontiers in Genetics

FRONTIERS EBOOK COPYRIGHT STATEMENT

The copyright in the text of individual articles in this ebook is the property of their respective authors or their respective institutions or funders. The copyright in graphics and images within each article may be subject to copyright of other parties. In both cases this is subject to a license granted to Frontiers.

The compilation of articles constituting this ebook is the property of Frontiers.

Each article within this ebook, and the ebook itself, are published under the most recent version of the Creative Commons CC-BY licence. The version current at the date of publication of this ebook is CC-BY 4.0. If the CC-BY licence is updated, the licence granted by Frontiers is automatically updated to the new version.

When exercising any right under the CC-BY licence, Frontiers must be attributed as the original publisher of the article or ebook, as applicable.

Authors have the responsibility of ensuring that any graphics or other materials which are the property of others may be included in the CC-BY licence, but this should be checked before relying on the CC-BY licence to reproduce those materials. Any copyright notices relating to those materials must be complied with.

Copyright and source acknowledgement notices may not be removed and must be displayed in any copy, derivative work or partial copy which includes the elements in question.

All copyright, and all rights therein, are protected by national and international copyright laws. The above represents a summary only. For further information please read Frontiers' Conditions for Website Use and Copyright Statement, and the applicable CC-BY licence.

ISSN 1664-8714
ISBN 978-2-8325-3444-1
DOI 10.3389/978-2-8325-3444-1

About Frontiers

Frontiers is more than just an open access publisher of scholarly articles: it is a pioneering approach to the world of academia, radically improving the way scholarly research is managed. The grand vision of Frontiers is a world where all people have an equal opportunity to seek, share and generate knowledge. Frontiers provides immediate and permanent online open access to all its publications, but this alone is not enough to realize our grand goals.

Frontiers journal series

The Frontiers journal series is a multi-tier and interdisciplinary set of open-access, online journals, promising a paradigm shift from the current review, selection and dissemination processes in academic publishing. All Frontiers journals are driven by researchers for researchers; therefore, they constitute a service to the scholarly community. At the same time, the *Frontiers journal series* operates on a revolutionary invention, the tiered publishing system, initially addressing specific communities of scholars, and gradually climbing up to broader public understanding, thus serving the interests of the lay society, too.

Dedication to quality

Each Frontiers article is a landmark of the highest quality, thanks to genuinely collaborative interactions between authors and review editors, who include some of the world's best academicians. Research must be certified by peers before entering a stream of knowledge that may eventually reach the public - and shape society; therefore, Frontiers only applies the most rigorous and unbiased reviews. Frontiers revolutionizes research publishing by freely delivering the most outstanding research, evaluated with no bias from both the academic and social point of view. By applying the most advanced information technologies, Frontiers is catapulting scholarly publishing into a new generation.

What are Frontiers Research Topics?

Frontiers Research Topics are very popular trademarks of the *Frontiers journals series*: they are collections of at least ten articles, all centered on a particular subject. With their unique mix of varied contributions from Original Research to Review Articles, Frontiers Research Topics unify the most influential researchers, the latest key findings and historical advances in a hot research area.

Find out more on how to host your own Frontiers Research Topic or contribute to one as an author by contacting the Frontiers editorial office: frontiersin.org/about/contact

Functional screening for cancer drug discovery: From experimental approaches to data integration

Topic editors

Wenyu Wang — University of Helsinki, Finland
Jing Tang — University of Helsinki, Finland
Kecheng Zhou — Anhui Medical University, China

Citation

Wang, W., Tang, J., Zhou, K., eds. (2023). *Functional screening for cancer drug discovery: From experimental approaches to data integration*. Lausanne: Frontiers Media SA. doi: 10.3389/978-2-8325-3444-1

Table of contents

frontiers | Frontiers in Genetics

TYPE Editorial
PUBLISHED 06 July 2023
DOI 10.3389/fgene.2023.1201454

Check for updates

OPEN ACCESS

EDITED BY
Dimple Chakravarty,
Icahn School of Medicine at Mount Sinai, United States

REVIEWED BY
Michael Lee,
University of Massachusetts Medical School, United States

*CORRESPONDENCE
Kecheng Zhou,
zhoukecheng@ahmu.edu.cn
Jing Tang,
jing.tang@helsinki.fi

RECEIVED 06 April 2023
ACCEPTED 30 June 2023
PUBLISHED 06 July 2023

CITATION
Zhou K, Wang W and Tang J (2023), Editorial: Functional screening for cancer drug discovery: from experimental approaches to data integration. *Front. Genet.* 14:1201454. doi: 10.3389/fgene.2023.1201454

COPYRIGHT
© 2023 Zhou, Wang and Tang. This is an open-access article distributed under the terms of the Creative Commons Attribution License (CC BY). The use, distribution or reproduction in other forums is permitted, provided the original author(s) and the copyright owner(s) are credited and that the original publication in this journal is cited, in accordance with accepted academic practice. No use, distribution or reproduction is permitted which does not comply with these terms.

Editorial: Functional screening for cancer drug discovery: from experimental approaches to data integration

Kecheng Zhou[1]*, Wenyu Wang[2] and Jing Tang[2]*

[1]School of Life Sciences, Anhui Medical University, Hefei, China, [2]Research Program in Systems Oncology, Faculty of Medicine, University of Helsinki, Helsinki, Finland

KEYWORDS

functional screening, cancer drug discovery, experimental approaches, data integration, editorial

Editorial on the Research Topic
Functional screening for cancer drug discovery: from experimental approaches to data integration

Cancer is still one of the leading causes of death worldwide, despite that tremendous resources are being invested in drug discovery (Siegel et al., 2022). Recent developments in uncovering the molecular biology of oncogenesis and tumor development (Zhou et al., 2018; Liu M. et al., 2022; Yan et al., 2023), and the studies on cancer polypharmacology (Pushpakom et al., 2019; Cohen et al., 2021) have challenged researchers to come up with new strategies for integrating ever-growing data at the molecular levels.

The majority of cancer medications consist of small molecule inhibitors. These inhibitors are engineered to enhance their efficacy by binding to specific cellular protein targets, which in turn initiate a series of downstream changes in cancer signaling and metabolic pathways (Yang et al., 2019; Goel et al., 2020). High-throughput phenotype-based drug screening has proven successful in identifying compounds that demonstrate promising cytotoxic effects (Letai et al., 2022). However, it is essential to further investigate the processes occurring between drug administration and the ultimate phenotypic response. Additionally, determining the genetic factors that influence variations in drug sensitivity or resistance is crucial for advancing cancer treatment strategies (Kuusanmäki et al., 2020).

Depending on the study's focus, high-throughput genetic perturbation experiments can yield results related to either 1) proliferation-associated phenotypes, or 2) intermediate phenotypes, such as transcriptomic alterations. Numerous well-established data portals, including The Cancer Genome Atlas (TCGA), DepMap Portal (Gonçalves et al., 2020), and The cBioPortal for Cancer Genomics (Cerami et al., 2012), have curated and standardized experimental data from tissues and cell lines, facilitating an easy access for subsequent systems medicine approaches (Wang et al., 2019). Moreover, cutting-edge studies are increasingly generating new data types, such as those derived from 3D organoids (Weeber et al., 2017; Hahn et al., 2021) and *in vivo* patient-derived xenograft (PDX) samples (Gao et al., 2015; Zanella et al., 2022). These innovative techniques hold the potential to bring researchers closer to a more biologically relevant foundation, moving beyond flat biological platforms. To fully utilize data from these advanced methodologies in identifying genetic signatures and molecular mechanisms for cancer drug discovery, versatile and robust

data integration and curation efforts are developped (Zheng et al., 2021; Tanoli et al., 2022). These tools are expected to pave the way for computational and artificial intelligence research, propelling the field towards clinical translation (Ma et al., 2021; Douglass et al., 2022). The selected acticles in this Research Topic will focus on both experimental approaches and data integration, aiming at facilitating the drug and target discovery in cancer.

The goal of the Research Topic "*Functional screening for cancer drug discovery: from experimental approaches to data integration*" is to highlight the recent advances in high-throughput functional genetic approaches, especially how results from such new technologies can be applied for future studies in cancer drug mechanisms of action. To achieve this goal, we carefully reviewed every submitted manuscript and screened for highly qualified reviewers. Eventually, we accepted and published nine articles including eight "Original Research" articles, and one systematical "Review" article on the mechanism and clinical trials of hepatocellular carcinoma immunotherapy (Huang et al., 2021).

The research articles presented in this Research Topic encompass efforts in cancer drug discovery from both experimental and computational perspectives. Jiang et al. identified the crucial role of RNA polymerase II subunit A (POLR2A) in the onset and progression of gastric cancer (GC). Ren et al. developed a necroptosis-related prognostic signature to reveal immune infiltration, which could predict drug sensitivity and inform personalized drug therapy for hepatocellular carcinoma (HCC) patients. Wang et al. reported a novel hub gene signature closely associated with ferroptosis, serving as a potentially effective biomarker for predicting the prognosis of HCC patients.

Liu et al. conducted a comprehensive analysis to elucidate the roles of cuproptosis-associated genes in tumor biology and cancer drug sensitivity across various cancers. Chen et al. discovered a novel diagnostic four-gene signature for hepatocellular carcinoma based on an artificial neural network, with applications in drug screening. Li et al. explored the functional effects of FDX1 in tumors, and further validated the inhibitory effect of FDX1 in copper-induced cell death, confirming FDX1's role as a cuproptosis biomarker. Ruan et al. leveraged pan-cancer analysis to identify DDX56 as a prognostic biomarker associated with immune infiltration and drug sensitivity. Zhang et al. uncovered an LncRNA signature related to cuproptosis, serving as a novel biomarker of prognosis in immunotherapy and drug screening for clear cell renal cell carcinoma.

We believe that the articles featured in this Research Topic can offer valuable insights into the application of functional screening methods for cancer drug discovery. The findings presented in these studies are anticipated to enhance our understanding of the molecular mechanisms governing cancer progression and, ultimately, we hope they will positively impact drug and target discovery in the near future.

Author contributions

KZ, WW and JT jointly wrote the manuscript. All authors contributed to the article and approved the submitted version.

Conflict of interest

The authors declare that the research was conducted in the absence of any commercial or financial relationships that could be construed as a potential conflict of interest.

Publisher's note

All claims expressed in this article are solely those of the authors and do not necessarily represent those of their affiliated organizations, or those of the publisher, the editors and the reviewers. Any product that may be evaluated in this article, or claim that may be made by its manufacturer, is not guaranteed or endorsed by the publisher.

References

Cerami, E., Gao, J., Dogrusoz, U., Gross, B. E., Sumer, S. O., Aksoy, B. A., et al. (2012). The cBio cancer genomics portal: An open platform for exploring multidimensional cancer genomics data. *Cancer Discov.* 2, 401–404. doi:10.1158/2159-8290.CD-12-0095

Cohen, P., Cross, D., and Jänne, P. A. (2021). Kinase drug discovery 20 years after imatinib: Progress and future directions. *Nat. Rev. Drug Discov.* 20, 551–569. doi:10.1038/S41573-021-00195-4

Douglass, E. F., Allaway, R. J., Szalai, B., Wang, W., Tian, T., Fernández-Torras, A., et al. (2022). A community challenge for a pancancer drug mechanism of action inference from perturbational profile data. *Cell Rep. Med.* 3, 100492. doi:10.1016/J.XCRM.2021.100492

Gao, H., Korn, J. M., Ferretti, S., Monahan, J. E., Wang, Y., Singh, M., et al. (2015). High-throughput screening using patient-derived tumor xenografts to predict clinical trial drug response. *Nat. Med.* 21, 1318–1325. doi:10.1038/NM.3954

Goel, B., Tripathi, N., Bhardwaj, N., and Jain, S. K. (2020). Small molecule CDK inhibitors for the therapeutic management of cancer. *Curr. Top. Med. Chem.* 20, 1535–1563. doi:10.2174/1568026620666200516152756

Gonçalves, E., Segura-Cabrera, A., Pacini, C., Picco, G., Behan, F. M., Jaaks, P., et al. (2020). Drug mechanism-of-action discovery through the integration of pharmacological and CRISPR screens. *Mol. Syst. Biol.* 16, e9405. doi:10.15252/MSB.20199405

Hahn, W. C., Bader, J. S., Braun, T. P., Califano, A., Clemons, P. A., Druker, B. J., et al. (2021). An expanded universe of cancer targets. *Cell* 184, 1142–1155. doi:10.1016/J.CELL.2021.02.020

Huang, S. L., Wang, Y. M., Wang, Q. Y., Feng, G. G., Wu, F. Q., Yang, L. M., et al. (2021). Mechanisms and clinical trials of hepatocellular carcinoma immunotherapy. *Front. Genet.* 12, 1159. doi:10.3389/fgene.2021.691391

Kuusanmäki, H., Kytölä, S., Vänttinen, I., Ruokoranta, T., Ranta, A., Huuhtanen, J., et al. (2020). *Ex vivo* venetoclax sensitivity testing predicts treatment response in acute myeloid leukemia. *Haematologica* 108, 1768–1781. doi:10.3324/HAEMATOL.2022.281692

Letai, A., Bhola, P., and Welm, A. L. (2022). Functional precision oncology: Testing tumors with drugs to identify vulnerabilities and novel combinations. *Cancer Cell* 40, 26–35. doi:10.1016/J.CCELL.2021.12.004

Liu, M., Yan, R., Wang, J., Yao, Z., Fan, X., and Zhou, K. (2022b). LAPTM4B-35 promotes cancer cell migration via stimulating integrin beta1 recycling and focal adhesion dynamics. *Cancer Sci.* 113, 2022–2033. doi:10.1111/CAS.15362

Ma, J., Fong, S. H., Luo, Y., Bakkenist, C. J., Shen, J. P., Mourragui, S., et al. (2021). Few-shot learning creates predictive models of drug response that translate from high-throughput screens to individual patients. *Nat. cancer* 2, 233–244. doi:10.1038/S43018-020-00169-2

Pushpakom, S., Iorio, F., Eyers, P. A., Escott, K. J., Hopper, S., Wells, A., et al. (2019). Drug repurposing: Progress, challenges and recommendations. *Nat. Rev. Drug Discov.* 18, 41–58. doi:10.1038/NRD.2018.168

Siegel, R. L., Miller, K. D., Fuchs, H. E., and Jemal, A. (2022). Cancer statistics, 2022. *Ca. Cancer J. Clin.* 72, 7–33. doi:10.3322/CAAC.21708

Tanoli, Z., Aldahdooh, J., Alam, F., Wang, Y., Seemab, U., Fratelli, M., et al. (2022). Minimal information for chemosensitivity assays (MICHA): A next-generation pipeline to enable the FAIRification of drug screening experiments. *Brief. Bioinform.* 23, 350. doi:10.1093/BIB/BBAB350

Wang, W., Malyutina, A., Pessia, A., Saarela, J., Heckman, C. A., and Tang, J. (2019). Combined gene essentiality scoring improves the prediction of cancer dependency maps. *EBioMedicine* 50, 67–80. doi:10.1016/J.EBIOM.2019.10.051

Weeber, F., Ooft, S. N., Dijkstra, K. K., and Voest, E. E. (2017). Tumor organoids as a pre-clinical cancer model for drug discovery. *Cell Chem. Biol.* 24, 1092–1100. doi:10.1016/J.CHEMBIOL.2017.06.012

Yan, R., Liu, D., Wang, J., Liu, M., Guo, H., Bai, J., et al. (2023). miR-137-LAPTM4B regulates cytoskeleton organization and cancer metastasis via the RhoA-LIMK-Cofilin pathway in osteosarcoma. *Oncogenesis* 12, 25. doi:10.1038/S41389-023-00471-5

Yang, L., Lin, S., Xu, L., Lin, J., Zhao, C., and Huang, X. (2019). Novel activators and small-molecule inhibitors of STAT3 in cancer. *Cytokine Growth Factor Rev.* 49, 10–22. doi:10.1016/J.CYTOGFR.2019.10.005

Zanella, E. R., Grassi, E., and Trusolino, L. (2022). Towards precision oncology with patient-derived xenografts. *Nat. Rev. Clin. Oncol.* 19, 719–732. doi:10.1038/S41571-022-00682-6

Zheng, S., Aldahdooh, J., Shadbahr, T., Wang, Y., Aldahdooh, D., Bao, J., et al. (2021). DrugComb update: A more comprehensive drug sensitivity data repository and analysis portal. *Nucleic Acids Res.* 49, W174–W184. doi:10.1093/NAR/GKAB438

Zhou, K., Dichlberger, A., Martinez-Seara, H., Nyholm, T. K. M., Li, S., Kim, Y. A., et al. (2018). A ceramide-regulated element in the late endosomal protein LAPTM4B controls amino acid transporter interaction. *ACS Cent. Sci.* 4, 548–558. doi:10.1021/acscentsci.7b00582

frontiers in Genetics

REVIEW
published: 08 July 2021
doi: 10.3389/fgene.2021.691391

Mechanisms and Clinical Trials of Hepatocellular Carcinoma Immunotherapy

Shao-Li Huang[1,2,3†], Yu-Ming Wang[4,5†], Quan-Yue Wang[6†], Guang-Gui Feng[1,3], Fu-Qing Wu[1,3], Liu-Ming Yang[2,3,7], Xi-He Zhang[2,3*] and Hong-Wu Xin[8,9*]*

[1] Department of Clinical Laboratory, Lianjiang People's Hospital, Zhanjiang, China, [2] Doctoral Scientific Research Center, Lianjiang People's Hospital, Zhanjiang, China, [3] Guangdong Medical University Affiliated Lianjiang People's Hospital, Zhanjiang, China, [4] Department of Spinal and Neural Functional Reconstruction, Beijing Bo'ai Hospital, China Rehabilitation Research Center, Beijing, China, [5] School of Rehabilitation Medicine, Capital Medical University, Beijing, China, [6] Qinghai Institute of Health Sciences, Xining, China, [7] Department of Gastroenterology and Hepatology, Lianjiang People's Hospital, Zhanjiang, China, [8] Laboratory of Oncology, Center for Molecular Medicine, School of Basic Medicine, Faculty of Medicine, Yangtze University, Jingzhou, China, [9] Department of Biochemistry and Molecular Biology, School of Basic Medicine, Faculty of Medicine, Yangtze University, Jingzhou, China

OPEN ACCESS

Edited by:
Kecheng Zhou,
Anhui Medical University, China

Reviewed by:
Martin Perez-Santos,
Benemérita Universidad Autónoma de Puebla, Mexico
Ankur Sharma,
Harry Perkins Institute of Medical Research, Australia

***Correspondence:**
Liu-Ming Yang
yw13813198@163.com
Xi-He Zhang
hljsnjx@163.com
Hong-Wu Xin
hongwu_xin@126.com

† These authors have contributed equally to this work

Specialty section:
This article was submitted to Cancer Genetics and Oncogenomics, a section of the journal Frontiers in Genetics

Received: *06 April 2021*
Accepted: *08 June 2021*
Published: *08 July 2021*

Citation:
Huang S-L, Wang Y-M, Wang Q-Y, Feng G-G, Wu F-Q, Yang L-M, Zhang X-H and Xin H-W (2021) Mechanisms and Clinical Trials of Hepatocellular Carcinoma Immunotherapy. Front. Genet. 12:691391. doi: 10.3389/fgene.2021.691391

Hepatocellular carcinoma (HCC), one of the most common and lethal tumors worldwide, is usually not diagnosed until the disease is advanced, which results in ineffective intervention and unfavorable prognosis. Small molecule targeted drugs of HCC, such as sorafenib, provided only about 2.8 months of survival benefit, partially due to cancer stem cell resistance. There is an urgent need for the development of new treatment strategies for HCC. Tumor immunotherapies, including immune check point inhibitors, chimeric antigen receptor T cells (CAR-T) and bispecific antibodies (BsAb), have shown significant potential. It is known that the expression level of glypican-3 (GPC3) was significantly increased in HCC compared with normal liver tissues. A bispecific antibody (GPC3-S-Fabs) was reported to recruit NK cells to target GPC3 positive cancer cells. Besides, bispecific T-cell Engagers (BiTE), including GPC3/CD3, an aptamer TLS11a/CD3 and EpCAM/CD3, were recently reported to efficiently eliminate HCC cells. It is known that immune checkpoint proteins programmed death-1 (PD-1) binding by programmed cell death-ligand 1 (PD-L1) activates immune checkpoints of T cells. Anti-PD-1 antibody was reported to suppress HCC progression. Furthermore, GPC3-based HCC immunotherapy has been shown to be a curative approach to prolong the survival time of patients with HCC in clinically trials. Besides, the vascular endothelial growth factor (VEGF) inhibitor may inhibit the migration, invasion and angiogenesis of HCC. Here we review the cutting-edge progresses on mechanisms and clinical trials of HCC immunotherapy, which may have significant implication in our understanding of HCC and its immunotherapy.

Keywords: hepatocellular carcinoma, immunotherapy, bispecific T-cell Engagers, bispecific antibody, aptamer, vascular endothelial growth factor (VEGF)

INTRODUCTION

Hepatocellular carcinoma (HCC) is caused by genetic and epigenetic changes of tissue stem cells and progressed through the interaction between cancer cells and tumor microenvironment (Hari et al., 2011; Xin et al., 2012, 2016; Xin et al., 2013; Xin H. W. et al., 2013; Ellison et al., 2017; Liu et al., 2017). Infection with hepatitis B virus and hepatitis C virus is the major cause of chronic hepatitis and HCC. Besides, aflatoxin, smoking, obesity, excessive alcoholic drink and hyperlipidemia also play significant roles in the process of HCC. Consequently, high incidence and mortality rate have made HCC to be one of the deadliest cancers and severe health issue (Guo et al., 2018; Hu et al., 2018; Jin et al., 2018).

Hepatocellular carcinoma progresses with no clinical symptoms in the early stage, whereas clinical symptoms become obvious in the advanced stage, leading to ineffective intervention and poor prognosis. Current prevailing medical treatments for HCC, including surgical ablation, chemotherapy (including chemoembolization), radiotherapy (including proton beam therapy), targeted therapy, and virotherapy, can generally achieve limited overall survival time (Xiang et al., 2015). The effective approach for the treatment of HCC is excision of cancerous tissue in early phases. The target selectivity of radiotherapy for HCC patients is not sensitive enough (Zhu et al., 1998). Sorafenib, an multi-kinase inhibitor, is one of the recommended medicine for patients with advanced HCC and has been shown to improve the overall survival, but with various side effects such as diarrhea, fatigue, and skin reaction of hand and foot. Furthermore, the drug resistance is the major issue for the treatment of HCC patients at advanced stages. Only 30% of HCC patients obtain survival benefits from sorafenib (Su et al., 2018). Other multikinase inhibitors such as lenvatinib and regorafenib have also been approved for the treatment of HCC patients. Lenvatinib is approved as the first-line therapy and regorafenib, which is an inhibitor closely associated with sorafenib, is approved as the second-line therapy. However, lenvatinib and regorafenib have limited survival benefit for the patients with HCC (Ruiz De Galarreta et al., 2019). In addition, cancer stem cells (CSCs) display cellular hierarchies with self-renewing tumor-initiating cells at the apex and are believed to cause drug resistance of tumors (Yamashita and Wang, 2013; De Angelis et al., 2019). Studies have demonstrated that ten of label-retaining cancer cells (LRCC) of human HCC are able to initiate tumors. Unfortunately, LRCC is relatively resistant to sorafenib and metformin (a reported potential drug against CSC) (Xin H. W. et al., 2013).

Therefore, there is an urgent need for effective therapeutic strategies for HCC. Recently, tumor immunotherapies, including immune check point inhibitors, chimeric antigen receptor T cells (CAR-Ts), and bispecific antibodies (BsAb), have shown great clinical benefit for HCC patients. BiTE, a form of BsAb that binds CD3 and tumor-associated antigens (TAA) (Frankel and Baeuerle, 2013; Sedykh et al., 2018), capable to recruit T cells to cancer cells for elimination (Oberst et al., 2014). The specific killing of the cancer cells by BiTE was mediated by concomitant cytokine release and HCC cell lysis (**Figure 1**). Here we review recent research progresses in the mechanisms and clinical trials of HCC immunotherapies against glypican-3 (GPC3), epithelial cell adhesion molecule (EpCAM) and TLS11a, and programmed death-1 (PD-1).

MECHANISMS OF HCC IMMUNOTHERAPY

GPC3-Based Immunotherapy: GPC3/NK BsAb, GPC3/BiTE, GPC3/CAR-Ts and GPC3 Peptide Vaccine

Glypican-3 belongs to heparin sulfate (HS) protein polysaccharide family and anchors to cell surface by glycosylphosphatidylinositol (GPI) (Filmus and Selleck, 2001; Sun et al., 2017). Glypicans interact with growth factors and play significant roles in cell proliferation, differentiation, and migration (Filmus and Selleck, 2001). The growth of HCC cells can be stimulated by GPC3 by the means of typical Wnt signaling pathway (**Figure 1**; Capurro et al., 2005; Chen et al., 2018). A frizzled-like cysteine-rich domain of GPC3 can regulate Wnt binding and mediate the growth of mouse HCC tumors (Li et al., 2019). Besides, GPC3 can negatively regulate bone morphogenesis protein 7 (BMP-7) to modulate cell proliferation (Midorikawa et al., 2003; Chen et al., 2018). Overexpression of GPC3 in the cell membrane can induce M2-polarized tumor-associated macrophages to enter human HCC tissues that may stimulate the progression and metastasis of HCC (Takai et al., 2009). GPC3 is absent in normal and benign tissues, whereas expresses in human embryo and many kinds of neoplastic cells such as HCC, melanoma, and squamous non-small cell lung cancer (Sun et al., 2017). GPC3 accounts for the initiation and progression of HCC (Llovet et al., 2006; Baumhoer et al., 2008). A meta-analysis found that GPC3 was highly expressed in high-grade and advanced stage HCC cells, and tumor vascular cells in HCC (Liu H. et al., 2018). The expression of GPC3 is relate with tumor size of HCC, which suggest that GPC3 may potentially become an early diagnosis biomarker of HCC. Research has suggested that the accuracy and sensitivity for early diagnosis of HCC by using combined serum GPC3 and alpha fetoprotein (AFP) were better than AFP alone. AFP is a glycoprotein, which is mainly synthesized by fetal liver cells and yolk sac. Elevated AFP in adulthood is considered as a pathological condition. AFP Levels are elevated in many diseases including HCC, stomach cancer, yolk sac tumors and so on. Besides, more than 70% liver cancer patients show positive AFP. Therefore, serum AFP is considered as the standard biomarker for clinical diagnosis of liver cancer. A study showed that AFP stimulated the progression of HCC by inhibiting human antigen R (HuR)-mediated Fas/FADD (Fas-associating protein with a novel death domain) apoptotic pathway (Chen et al., 2020). The diagnosis by AFP or GPC3 could be improved by combining GPC3 and AFP (El-Saadany et al., 2018). Another research showed that patients with high preoperative plasma level of GPC3 was more likely to undergo postoperative recurrence (Ofuji et al., 2017). Furthermore, it was shown that GPC3

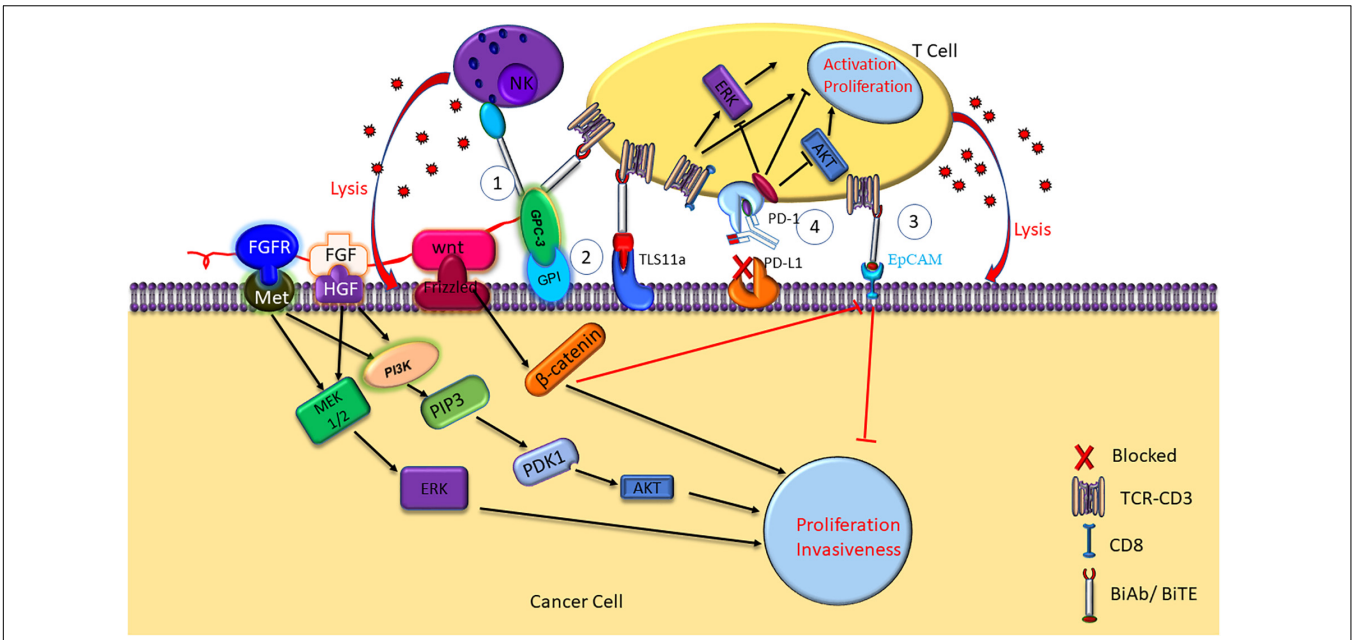

FIGURE 1 | Mechanisms of HCC immunotherapy targeting GPC3, TLS11a, EpCAM, and PD-1. NK BsAb and BiTE mediate T cell immunotherapy targeting GPC3 + HCC. GPC3 promotes HCC growth by upregulating the Wnt-β-catenin and FGF signaling. Aptamer bispecific antibody TLS11a/CD3 can mediate T cell immunotherapy by binding to both the HCC cancer cell and the T cell, inducing T cell cytotoxicity and proinflammatory cytokine release, such as IL-2, IL-6, IL-10, TNF-α, and IFN-γ. BiTE mediates T cell immunotherapy targeting EpCAM + HCC. Antibodies against PD-1 or PD-L1/2 on the cell surface inhibit the immune check point, and block the immune escape in HCC.

promotes HCC growth by upregulating the expression of Wnt as well as insulin-like growth factors (Cheng et al., 2008). GPC3 was found to be significantly related to HCC tumorigenesis through Wnt-5,6,7, Yap8, transforming growth factor-β29 (TGF-β29), and human growth factor 10 (HGF10) signaling (Ho and Kim, 2011). Most importantly, apoptosis was induced in HCC cell lines when GPC3 was silenced, which suggest that GPC3 play an important role in HCC carcinogenesis (Liu et al., 2012).

The high expression of GPC3 preferentially in HCC suggest that it can be used as a target for immunotherapy and the GPC3 expression on the surface of HCC cells makes it a good target for antibody therapy (Wang Y. et al., 2018). GPC3-binding antibodies have indeed been developed for immunotherapies of HCC, such as unmodified antibodies, immunotoxin bound antibodies, GPC3/NK BsAb, BiTE, and other BsAb (Lipovšek et al., 2018). GPC3-S-Fab, is an antibody Fab fragment based BiAb, and recruits NK cells to eliminate GPC3 positive cancer cells by linking the Fab of anti-GPC3 antibody to anti-CD16 single domain antibody (**Table 1** and **Figure 1**). In another BiAb, the GPC3/CD3 BiTE was also developed to recruit cytotoxic T lymphocyte (CTL) cells for clearance of $GPC3^{+}$ HCC cells (Lampen et al., 2018; **Table 1** and **Figure 1**). The therapeutic effect of BiTE depends on the concentration of GPC3/CD3 BiTE and the expression level of GPC3 on target cells. It has been demonstrated that the effect of BiTE is strongly GPC3-dependent *in vitro* and *in vivo* (Bi et al., 2017). In addition, GPC3-targeted CAR-T cells with CD28 co-stimulatory domain were also developed and showed anti-HCC effect in xenograft tumors (Guo et al., 2018). Furthermore, GPC3 peptide vaccine was also demonstrated to reduce recurrence rate of HCC patients (Sawada et al., 2016).

TLS11a Aptamer

Aptamers are ssDNA or ssRNA that are selected via library screening using SELEX (systematic evolution of ligands by exponential enrichment). They can combine with various targets such as small dyes, proteins, peptides, the whole cells, tissues and toxins, as it can fold into a variety of forms of three-dimensional (3D) structure (Kumar Kulabhusan et al., 2020). An aptamer bispecific antibody TLS11a/CD3 (Sulfo-SMCC, Thermo Scientific Co.) has been constructed by combining TLS11a-SH or S2.2-SH with the anti-CD3-NH2 at 4°C for 24 h, and the non-crosslinked aptamers of the reaction mixture was removed by centrifuging at 14000 rpm for 10 min. TLS11a/CD3 can bind to both HCC cells and T cells by aptamer TLS11a and anti-CD3 single chain variable region, respectively (**Figure 1**). TLS11a/CD3 was capable to guide T cells to target and kill HCC cells with high specificity and affinity and was shown to repress the proliferation of HCC H22 cells *in vitro* and prolong mouse survival time by inhibiting the progression of xenograft tumor *in vivo* (**Table 2**). T cell proliferation and the production of multiple cytokines, such as interleukin-2 (IL-2), IL-6, IL-10, tumor necrosis factor-alpha (TNF-α), and interferon-gamma (IFN-γ), were significantly higher in the T cells + H22 + TL11a/CD3 + group than in the control group, which also supported the anti-tumor effect of TL11a/CD3. Compared to other lower concentration groups, TLS11a/CD3 (20 μg) group had the best effect in tumor inhibition and prolonging survival on the hepatoma xenograft

model. The tumor inhibition efficacy of TLS11a/CD3 was found to be dose dependent (Hu Z. et al., 2018).

EpCAM-BiTE

Epithelial cell adhesion molecule is a transmembrane glycoprotein and its expression was increased in HCC tissues compared with adjacent normal liver tissues (Schmelzer et al., 2006). EpCAM expression in HCC was positively correlated with chemotherapy resistance and recurrence (Li Y. et al., 2016). Importantly, EpCAM-positive cells showed characteristics of CSC and $EpCAM^{+}AFP^{+}$ HCC was associated with poor prognosis. High tumorigenicity, high colony formation and low differentiation potency were found in EpCAM-positive HCC cell line PLC/PRF/5 and the proliferation and invasiveness of HCC cells were significantly reduced when EpCAM expression was downregulated (Kimura et al., 2014). EpCAM was found to be one of the Wnt-β-catenin signaling direct transcription target in normal human hepatocytes and hepatoma cells (Yamashita et al., 2007). CSC enrichment promotes the HCC tumorigenesis by Wnt-β-catenin signaling (Pandit et al., 2018). In response to Wnt-β-catenin signaling antagonists (natural compounds PKF118-310, PKF115-584, and CGP049090) (Lepourcelet et al., 2004), EpCAM expression was significantly decreased, suggesting Wnt-β-catenin signaling promoted EpCAM expression (Yamashita et al., 2007). A Study found that liver cancer CSCs with EpCAM-high upregulated the expression of carcinoembryonic antigen-related adhesion molecule 1 (CEACAM1) to resist the natural killer (NK) cell mediated cytotoxicity (Park et al., 2020). Moreover, EpCAM positive circulatory stem-like cells were associated with unfavorable prognosis of HCC patients who underwent radical resection. Therefore, EpCAM is considered as a CSC marker and a potential target for immunotherapy of HCC (Yamashita et al., 2007, 2009).

An anti-EpCAM BiTE, 1H8/CD3, has been constructed and was shown to inhibit the growth of xenograft tumors from HCC cell lines Hep3B and Huh-7 *in vivo* (**Figure 1**). Xenografts from the 1H8/CD3 treated mice showed decreased expression of majority CSC markers. However, the function of 1H8/CD3 was inhibited when galectin-1 (Gal-1) was overexpressed in HCC tumors (Zhang et al., 2014).

PD-1 Immune Check Point Inhibitor

Programmed death-1 is a transmembrane receptor that belongs to the immunoglobulin super family (IgSF) (Ohaegbulam et al., 2015) and is mainly expressed on the surface of $CD3^{+}$ T lymphocytes and NK cells, and functions as an inhibitory receptor (Gros et al., 2014). A study showed that both T-cell immunoglobulin domain and mucin domain containing molecule-3 (TIM-3) and PD-1 were highly expressed on the infiltrating lymphocytes of hepatitis B-related HCC tumors and adjacent tissues (Li Z. et al., 2016). PD-L1/2 on the surface of cancer cells inhibits activation and proliferation of T cell, resulting in cancer cell escape from the immune response (Zou et al., 2016). Besides, a study showed that MYC (one of the frequently altered ongenes in patients with HCC) in the tumor suppressor p53−/− HCC upregulated β-catenin signaling to promote immune escape. More importantly, the activation of β-catenin repressed the recruitment of DCs, accelerated

TABLE 1 | Features of the tumor associated antigens of HCC.

	GPC3	TLS11a target	EpCAM	PD-1
Expression in normal tissues	Low	None	Low	T cells
Expression in HCC tumors	High in about 70%	High	High	PD-L1/2 high
Function	Cancer cell proliferation, migration, metastasis	TLS11a-BiTE Inhibits HCC cells Hep3B and Huh-7	A CSC marker	Inhibiting T cells
McAb scFv or gRNA sequence	Not found	5-ACA GCATCC CCA TGT GAA CAATCGCATTGTGATTGTTA CGGTTTCCGCCTCATGGACG TGCTGTTTTTTTTTT-SH-3	Not found	PD-1-gRNA-1: GTCTGGGCGG TGCTACAACT; PD-1-RNA-2: GGCCAGGATG GTTCTTAGGT.
Ref	Wang Y. et al., 2018	Hu Z. et al., 2018	Zhang et al., 2014	Guo et al., 2018

TABLE 2 | BiAb-based immunotherapy against the tumor associated antigens of HCC.

Target	Drug	Methods	Effect	Adverse effect	Ref
GPC3 + HCC	GPC3/CD16 GPC3-S-Fab BiAb/BiTE	Cell culture, xenograft	Effective against tumors.	Not found	Wang Y. et al., 2018
H22 or BNL CL2 HCC	TLS11a aptamer/ CD3 BiTE	Mouse xenograft	Mediated effective tumor lysis.	Poor stability, immunogenicity and high cost production	Hu Z. et al., 2018
EpCAM + HCC	anti-EpCAM BiTE (1H8/CD3)	Hep3B, Huh-7, mouse xenograft	Significantly suppressed tumor growth and CSC marker expression.	Gal-1 may be conducive to resistance to 1H8/CD3-induced lysis.	Zhang et al., 2014

the immune escape and caused the resistance of the anti-PD-1 therapy (Ruiz De Galarreta et al., 2019). In addition, the up-regulation of Toll-like receptor 9 (TLR9) by PD-L1 induces immune escape in HCC (Zhou et al., 2020). Researchers demonstrated that blocking PD-1 or PD-L1 induce activation of T cells with increased IFN-γ release and T cell proliferation (**Figure 1**). PD-1 inhibits the consumption of oxygen, represses glutaminolysis and glycolysis of the activated T cells and reshapes their metabolism appropriately to change T cell differentiation. Besides, the PD-1 pathway induces PD-L1 by proinflammatory signal to inhibit the effector T cells and maintain self-tolerance. In addition, low levels of PD-1 expression are needed to suppress the expansion of T-cell as well as the IFN-γ, IL-2, and TNF-α production (Boussiotis, 2016). High PD-L1 expression in HCC tumors were an index of unfavorable prognosis for HCC patients who underwent surgical resection (Wang et al., 2017) and the level of serum PD-L1 is also positively correlated with HCC stages and mortality risk (Finkelmeier et al., 2016).

PD-1^{+} tumor infiltrating lymphocytes were an effective prognostic biomarker to predict the survival benefit for HCC patients who underwent the immunotherapy with cytokine induced killer (CIK) (Chang et al., 2018). PD-1 knockout was found to significantly enhance the anti-HCC efficacy of CIK cells. Study have shown that the combination of human telomerase reverse transcriptase (hTERT) transduction and PD-1 knockout of CIK cells improved the anti-HCC efficacy of CIK cells (Huang et al., 2018). In addition, PD-1 disruption was found to enhance the anti-HCC effect of GPC3 CAR-T cells in NOD-scid-IL-2Rγ/−/− (NSG) mice *in vivo* (Guo et al., 2018). Furthermore, Nivolumab, a complete human IgG4 monoclonal antibody against PD-1, has been approved by the United States Food and Drug Administration (FDA) for late stage melanoma and metastatic non-small cell lung cancer. Research have showed that Nivolumab also get an acceptable effectiveness in HCC patients and may become an alternative therapy for HCC patients who have failed routine treatments (Feng et al., 2017). Besides, pembrolizumab, another FDA approved anti-PD-1 antibody, also demonstrated that the anti-tumor activity and safety in previously treated patients with HCC in clinical trials (Finn et al., 2020a).

VEGF

The vascular endothelial growth factor (VEGF), a signaling ligand released by epithelial cells, is an important positive angiogenesis regulator (Yang et al., 2014; Zhang et al., 2020) and VEGF signaling plays a significant role in inhibiting the apoptosis and promoting proliferation in tumor cells (Liu et al., 2016). Highly vascularized tissue of adult liver is an important feature for its function, each liver cell is lined with sinusoidal endothelial cells (SEC) on both sides. It was reported that SEC fenestration was regulated by hepatocyte-mediated VEGF signaling during liver angiogenesis (Carpenter et al., 2005; Sharma et al., 2020). In addition, a study demonstrated that HCC shared the immune microenvironment and stromal microenvironment with fetal liver and suggested that VEGF and NOTCH signaling play important role in the maintenance of onco-fetal ecosystem. Importantly, it was shown that VEGF was also related with the metastasis and recurrence of HCC (Minata et al., 2013). Moreover, the down-regulation of exosmosis tumor C-Type Lectin Domain Family 3 Member B (CLEC3B) could accelerate the angiogenesis and metastasis of HCC by VEGF and AMP-activated protein kinase (AMPK) pathways (Dai et al., 2019). Research has indicated that tumor immune microenvironment and VEGF signaling pathway in HCC patients are synergistically activated, which suggests a prominent mechanism of combined therapy including immune checkpoint blockades (ICBs) and anti-VEGF drugs (Liu et al., 2020). Atezolizumab and bevacizumab are PD-L1 inhibitor and VEGF inhibitor, respectively, and a recent study of IMBrave150 trial indicated that comparing with sorafenib, atezolizumab in combination with bevacizumab improved overall response rate, overall survival and progression-free survival dramatically in patients with unresectable HCC (Finn et al., 2020b; Hack et al., 2020). Furthermore, FDA approved the combination of atezolizumab with bevacizumab as a new first-line treatment for advanced or unresectable HCC patients (Liu et al., 2020). The IMBrave150 trial also suggested that double blockade of PD-L1/VEGF can effectively reduce the recurrence of HCC by creating a more immunologically advantageous microenvironment (Hack et al., 2020). Apatinib is a specific inhibitor of VEGF-receptor 2 (VEGFR2) (Tian et al., 2011) and a recent study showed that apatinib blocked the VEGF and PI3K/AKT signaling pathways to inhibit the migration, invasion and angiogenesis of HCC cells (Song et al., 2021). Besides, lots of clinical trials involving as the VEGFR2 inhibitor apatinib in HCC are ongoing as showed in **Table 3**, most of which are exploring the combination of apatinib with other drugs or therapies to treat HCC to extend the survival time or to reduce the adverse side-effects. Furthermore, ramucirumab, another inhibitor of VEGF-receptor 2, was showed to have survival benefit in an age subgroup with safety tolerance, which supported its use in late stage HCC with elevated AFP, regardless of age (Kudo et al., 2020). Therefore, as a second line drug, ramucirumab was approved by FDA for the advanced HCC patients with AFP $\geq$ 400 ng/mL after sorafenib treatment (De Luca et al., 2020).

CLINICAL TRIALS OF HCC IMMUNOTHERAPY

A series of anti-GPC3 chimeric antigen receptor modified T cells (GPC3-CAR-T) had being tested in phase I/II trials (**Table 4**). In addition, a humanized anti-human GPC3 antibody, GC33, was tested in clinical trials to examine the pharmacokinetics, dosage and duration of treatment, safety and tolerability, and antitumor activity in GPC3 high expression hepatoma cells (**Tables 4**, **5**). The adverse reactions of GC33 were mainly fatigue (50%), constipation (35%), headache (35%), and hyponatremia (35%), most of which were grade 1 or 2. The number of peripheric NK cells was decreased after GC33 treatment, but no increased incidence of infection was observed. These research have showed that GC33 had potential antitumor activity in patients with high GPC3 expression HCC tumors and provided a preliminary

TABLE 3 | Ongoing clinical trials involving Apatinib (VEGFR2 inhibitor) in HCC.

Name	Trail ID	Phase	Study population	Intervention	Status
Apatinib	NCT03046979	II	Advanced HCC patients	Apatinib	Unknown
Apatinib and TACE	NCT03066557	Not Applicable	HCC patients	TACE and Apatinib	Unknown
Apatinib	NCT01192971	II	Advanced HCC patients	Apatinib	Completed
Apatinib	NCT02727309	I/II	Advanced HCC patients	Apatinib after TACE	Unknown
Apatinib and Camrelizumab	NCT04521153	Not Applicable	Resectable HCC patients	Camrelizumab and Apatinib Mesylate Procedure: TACE treatment and radical surgery	Recruiting
SHR-1210 and Apatinib	NCT04297202	II	HCC patients	Apatinib combined with SHR-1210 injection	Recruiting
Apatinib and Capecitabine	NCT03114085	II	Advanced HCC patients	Capecitabine and Apatinib compared with Apatinib	Unknown
Cryoablation, Camrelizumab and Apatinib	NCT04724226	II	Advanced HCC patients	Cryoablation, Camrelizumab, Apatinib	Not yet recruiting
SHR-1210 Plus Apatinib	NCT04014101	II	Advanced stage HCC	SHR-1210 and Apatinib	Recruiting
Apatinib	NCT02772029	I/II	Advanced HCC Patients After First-line Treatment Failure	Apatinib Mesylate Tablets	Unknown
SHR-1210 Plus Apatinib	NCT03722875	Not Applicable	BCLC B and C stage HCC after surgery	SHR-1210 and Apatinib	Unknown
Sintilimab, Apatinib and Capecitabine	NCT04411706	II	Advanced HCC patients	Sintilimab Combined With Apatinib and Capecitabine	Recruiting
Apatinib	NCT03511703	II	Advanced HCC	Postoperative adjuvant Apatinib vs. TACE, chemotherapy drugs + iodized	Unknown
Apatinib and Camrelizumab	NCT04191889	II	C-staged HCC patients	Hepatic Arterial Infusion with Apatinib and Camrelizumab	Recruiting
Apatinib plus radiotherapy	NCT03520257	II	HCC patients with BCLC-C stage I and II portal vein tumor thrombus	Apatinib plus radiotherapy vs. Apatinib	Unknown
Camrelizumab, Apatinib and Oxaliplatin	NCT04850040	II	Patients with potentially resectable HCC	Apatinib Mesylate, Camrelizumab and Oxaliplatin	Not yet recruiting
Camrelizumab and Apatinib	NCT04701060	II	Resectable primary HCC patients	Camrelizumab Combined With Apatinib	Recruiting
Camrelizumab, Apatinib and chemotherapy	NCT04479527	II	Advanced HCC patients	(cTACE or DEB-TACE + FOLFOX regimen HAIC) combined with Camrelizumab and Apatinib	Not yet recruiting
Apatinib and SHR-1210	NCT02942329	I/II	HCC or gastric cancer patients	Apatinib and SHR-1210	Unknown
Camrelizumab and Apatinib	NCT04826406	II	HCC patients previously treated with immune checkpoint inhibitors	Camrelizumab combined with Apatinib regimen	Recruiting
SHR-1210 and Apatinib	NCT03793725	II	Patients with unresectable HCC	SHR1210 combined with Apatinib	Unknown
Apatinib and SHR-1210	NCT03839550	II	HCC patients with high risk of recurrence after radical resection	Hepatic Arterial Infusion (HAI) of Apatinib Mesylate + PD-1 antibody SHR-1210.	Not yet recruiting
Camrelizumab Plus Apatinib	NCT04639180	III	Patients with HCC at high risk of recurrence after surgical	Camrelizumab plus Apatinib as adjuvant therapy in HCC	Not yet recruiting
M1-c6v1, SHR-1210 and Apatinib	NCT04665362	I	HCC patients	Recombinant oncolytic virus M1-c6v1, anti-PD-1 antibody SHR-1210, and Apatinib	Not yet recruiting
Camrelizumab plus Apatinib	NCT04035876	I/II	Downstaging/bridging of HCC patients before liver transplant	Camrelizumab (SHR-1210) and Apatinib combination	Recruiting
Radiotherapy, and Apatinib	NCT03732105	II	HCC patients received curative resection with microvascular invasion	Radiotherapy, Apatinib, or radiotherapy + Apatinib	Not yet recruiting
TACE, Camrelizumab and Apatinib	NCT04559607	Not Applicable	Intermediate and advanced HCC patients	TACE combined with Camrelizumab and Apatinib	Recruiting

(Continued)

TABLE 3 | Continued

Name	Trail ID	Phase	Study population	Intervention	Status
SHR-1210 and Apatinib	NCT03463876	II	Advanced HCC patients	SHR 1210 + Apatinib	Active, not recruiting
Camrelizumab and Apatinib	NCT04523662	II	Advanced liver cancer patients	Carrelizumab combined with Apatinib Mesylate and radiotherapy	Not yet recruiting
Apatinib	NCT02329860	III	HCC patients after systemic therapy	Apatinib or placebo	Completed
Apatinib and TACE	NCT02702323	II/III	Patients with pulmonary metastasis of liver cancer	Apatinib combined with TACE	Unknown
Thermal Ablation, Apatinib and Carilimub	NCT04204577	II	Advanced liver cancer patients	Thermal ablation combined with Apatinib and Carilimub	Recruiting
Apatinib	NCT03261791	II	HCC patients with PVTT who underwent radical resection	Adjuvant therapy with Apatinib	Unknown
SHR-1210 and Apatinib	NCT03764293	III	Advanced HCC patients	SHR-1210 in Combination With Apatinib as first-line therapy vs. Sorafenib	Recruiting

TABLE 4 | Ongoing clinical trials involving GPC3 in HCC.

Name	Trail ID	Phase	Study population	Intervention	Status
GC33	japicCTI 101255	I	HCC with no preferred treatment	GC33	Unknown
GPC3 CAR-T	NCT02395250	I	GPC3 + HCC patients	GPC3 CAR-T cells	Completed
GPC3 CAR-T	NCT02723942	I/II	GPC3 + HCC patients	GPC3 CAR-T cells	Completed
GPC3 CAR-T	NCT03084380	I/II	GPC3 + HCC patients	Anti-GPC3 CAR-T cells	Unknown
GLY CAR-T	NCT02905188	I	Unresectable, recurrent metastatic GPC3 + HCC patients	GLYCAR T cells; Fludarabine	Recruiting
GPC3 CAR-T	NCT03884751	I	Late stage HCC patients, unresectable	GPC3 CAR-T cells	Recruiting
GPC3-T2 CAR-T	NCT03198546	I	GPC3 + advanced HCC patients	GPC3 and/or TGFβ targeting CAR-T cells	Recruiting
GPC3 CAR-T	NCT04506983	I	GPC3 + HCC patients after failure or intolerance of first-line treatment	GPC3 CAR-T cells	Not yet recruiting
GPC3 CAR-T	NCT03146234	Not Applicable	GPC3 + relapsed or refractory HCC patients	GPC3 CAR-T cells	Completed
GPC3 CAR-T	NCT04121273	I	GPC3 + advanced HCC patients	GPC3 CAR-T cells	Recruiting
GPC3 CAR-T	NCT03980288	I	Refractory or intolerant to current standard systemic treatment, GPC3 + advanced HCC patients	GPC3 CAR-T cells	Recruiting
GPC3 CAR-T	NCT02715362	I/II	Unresectable, at least one prior standard of care chemotherapy, GPC3 + advanced HCC patients	TAI-GPC3 CART cells	Unknown
GPC3 CAR-T	NCT03130712	I/II	GPC3 + advanced HCC patients with one prior standard of chemotherapy or surgery	GPC3 CART cells	Unknown
CT0180 Cells	NCT04756648	I	GPC3 + advanced HCC patients	CT0180 humanized anti GPC3 autogenous T cell injection	Not yet recruiting
GPC3 CAR-T	NCT04121273	I	GPC3 + advanced HCC patients	CAR-T cell immunotherapy	Recruiting
ECT204 T-Cell therapy (ARYA3)	NCT04864054	I/II	GPC3 + adults advanced HCC patients with failure or intolerance of at least two different anti-HCC systemic agents	ECT204 T cells	Not yet recruiting
GC33 (RO5137382)	NCT01507168	II	Unresectable advanced or metastatic GPC3 + HCC patients	GC33	Completed
GPC3 CAR-T	NCT02959151	I/II	GPC3 + advanced liver malignancy	CAR-T cell	Unknown

clinical basis for further trials in advanced HCC (Zhu et al., 2013). However, grade 3 adverse events were shown as blood pressure increase, lymphocyte and platelet count decrease in two or more patients when the same agent was tested in Japan (Ikeda et al., 2014). Furthermore, a phase I clinical trial was performed on a GPC3 derived peptide vaccine (**Table 5**; Sawada et al., 2012). The peptide vaccine caused grade III hematologic adverse events (impaired liver function) in 4 out of 33 patients, although lymph node regression in 24/33 patients and liver tumor disappearance in 2/33 patients were observed (Sawada et al., 2012).

PF-03446962 is an activin receptor-like kinase-1 (ALK-1) monoclonal antibody. A phase I clinical trial had explored the safety, pharmacokinetics and antitumor activity of PF-03446962 in total of 24 HCC patients. The most common treatment-related adverse events were thrombocytopenia (33.3%), fatigue (29.2%), shivering (16.7%), fever epistaxis and anemia, and ENT-associated telangiectasia (2 patients). Based on the trial, the disease control rate was 29% (Simonelli et al., 2016) and a phase II trial was suggested to have a dose of 7 mg/kg of PF-03446962 for single drug treatment of HCC patients.

Antibodies against PD-1 and its ligand PD-L1 have shown anti-tumor effects in many cancers including liver cancer (Apolo et al., 2017). SHR-1210 is an anti-PD-1 antibody and phase Ia and Ib clinical trials that combined SHR-1210 with apatinib (VEGFR2 inhibitor) for the treatment of advanced HCC, stomach and esophageal cancers were performed. Phase Ia was designed to identify the maximum tolerated dose (MTD) and the recommended phase II dose (RP2D) of SHR-1210 when combined with apatinib. The combination of SHR-1210 and apatinib showed controllable toxicity in HCC and GC/EGJC patients with recommended single dose. The RP2D of SHR-1210 in the apatinib combined treatment was 250 mg, demonstrating encouraging clinical activity in patients with advanced liver cancer. SHR-1210 combined with apatinib showed the objective response rate of 30.8% (95% CI: 17.0–47.6%) as observed in 39 patients. Of the 16 evaluable HCC patients, 8 patients obtained partial responses (50.0%, 95% CI: 24.7–75.4%). The grade 3 adverse events observed are hypertension (15.2%) and elevated aspartate aminotransferase (AAT, 15.2%) (Xu et al., 2019). In brief, the combination of SHR-1210 and apatinib demonstrated encouraging results in patients with advanced liver cancer. Moreover, there are lots of ongoing clinical trials involving PD-1 treatment in HCC as shown in **Supplementary Table 1**, which mostly explore the efficacy and safety of new drugs and new therapies of existing drugs on HCC. However, most of these clinical trials are in phase I/II without published results.

SUMMARY AND FUTURE PERSPECTIVES

Hepatocellular carcinoma is one of the most common and lethal tumors worldwide. Small molecule targeted drugs, such as sorafenib, have only about 3 months survival benefit due to drug resistance to cancer stem cells (Xin H. W. et al., 2013). Therefore, further improvement of HCC therapy is urgent. Tumor immunotherapy has shown significant potential. GPC3 based HCC immunotherapies included GPC3/NK BsAb, GPC3/BiTE, GPC3/CAR-T, GPC3 mAb, and GPC3 peptide vaccine. These HCC immunotherapies have showed promising results in preclinical studies, ongoing phase I/II clinical trials and published phase I/II clinical trials. The published clinical trials demonstrated their preliminary safety and effectiveness, which warranted for their phase II trials in future. In addition, TLS11a aptamer-BiTE and EpCAM/BiTE showed their effectiveness in eliminating HCC tumors in mouse models. Anti-PD-1 antibody was also reported to suppress HCC progression in mouse xenograft and to be preliminarily safe and effective in clinical trials.

Nevertheless, most of the current specific antibodies applied in the HCC treatment are in preclinical experimental stage or early phase clinical trials. The antibodies that worked on animals may not work well on humans due to heterogeneity and complex immunogenicity, as different species have different immune rejection response and human body may produce rejection reaction to the animal source antibodies in different degree. Their effectiveness and safety need to be improved. The antibodies used in the immunotherapy had immunogenicity, poor stability,

TABLE 5 | Published clinical trials involving GPC3, ALK-1, and PD-1 in HCC immunotherapy.

Drug	Combination	Route, dose	Enrollment	Efficacy	Adverse effect	Phase	Ref
GPC3 derived peptide vaccine	None	Intracutaneously, on days 1, 15 and 29, at doses 0.3, 1.0, 3.0, 10, 30 mg/body surface area.	Non-randomized, open label	24/33 lymph node regression, 2 liver tumors disappeared.	Grade III hematologic adverse events (impaired liver function) in 4 patients	I	Sawada et al., 2012
GC33	75% patients received sorafenib	Dose escalation, 2.5–20 mg/kg, weekly i.v.	Multicenter, open label, single arm	AFP levels decreased or stabilized	Grade III, NK cell numbers in plasma decreased.	I	Zhu et al., 2013
Anti-ALK-1 McAb PF-03446962	Antiangiogenic or sorafenib therapy	1 h iv on days 1 and 29 and every 2 weeks thereafter, RP2D of 7 mg/kg.	Single-arm	Disease control rate at 12 weeks was 29%.	Grade III Thrombocytopenia in 33%, grade IV abdominal pain in 1 patient.	I	Simonelli et al., 2016
SHR-1210, an anti-PD-1 McAb	Apatinib, a VEGFR2 Inhibitor	Oral apatinib once-daily combined with SHR-1210 administered intravenously every 2 weeks.	Single center, open label.	Objective response rate is 30.8%, partial response is 50%.	Grade III Lipases rise (6.7%), preumonitis (20%) Hypertension (15.2%), increased AAT 15.2%.	Ia and Ib	Xu et al., 2019

and high cost, which may limit their clinical application. CAR-T modification, in combination with the disruption of inhibitory immune checkpoints, represents a promising method of tumor immunotherapy. Moreover, the HCC immunotherapy has not achieved significant results in clinical trials and further effective approaches are needed to explore for HCC immunotherapy. In future, we suggest that dendritic cell (DC) based tumor immunotherapy may be studied in HCC, as DC-derived exons was found to be involved in antigen presentation during anti-tumor immune response, besides, DC is the most important monitoring sentinel cell in tumor microenvironment (Wang et al., 2020). Oncolytic viruses may also be applied for HCC tumor immunotherapy. It is superior to conventional tumor treatments due to a relatively shorter period of treatment, reduction of toxicity, as well as the possibility of targeting micro-metastases (Wu et al., 2018; Cai et al., 2020; Wang et al., 2020). Engineered viral envelope glycoproteins can specifically target tumors (Liu X. Q. et al., 2018) and the technology of clustered regularly interspaced short palindromic repeats/CRISPR-associated protein 9 (CRISPR/Cas9) genomic editing has prominently promoted the study of oncolytic viruses (Wang D. et al., 2018).

AUTHOR CONTRIBUTIONS

S-LH, L-MY, and H-WX designed this research. S-LH contributed to literature search and drafted the manuscript. S-LH, Y-MW, Q-YW, G-GF, F-QW, L-MY, X-HZ, and H-WX revised and edited the manuscript. L-MY, X-HZ, and H-WX approved the final version of the manuscript. All authors contributed to the article and approved the submitted version.

FUNDING

This work was partly supported by the National Natural Science Foundation of China (81872412).

SUPPLEMENTARY MATERIAL

The Supplementary Material for this article can be found online at: https://www.frontiersin.org/articles/10.3389/fgene.2021.691391/full#supplementary-material

REFERENCES

Apolo, A. B., Infante, J. R., Balmanoukian, A., Patel, M. R., Wang, D., Kelly, K., et al. (2017). Avelumab, an anti-programmed death-ligand 1 antibody, in patients with refractory metastatic urothelial carcinoma: results from a multicenter, phase Ib study. *J. Clin. Oncol.* 35, 2117–2124. doi: 10.1200/jco.2016.71.6795

Baumhoer, D., Tornillo, L., Stadlmann, S., Roncalli, M., Diamantis, E. K., and Terracciano, L. M. (2008). Glypican 3 expression in human nonneoplastic, preneoplastic, and neoplastic tissues: a tissue microarray analysis of 4,387 tissue samples. *Am. J. Clin. Pathol.* 129, 899–906. doi: 10.1309/hcqwpwd50xhd2dw6

Bi, Y., Jiang, H., Wang, P., Song, B., Wang, H., Kong, X., et al. (2017). Treatment of hepatocellular carcinoma with a GPC3-targeted bispecific T cell engager. *Oncotarget* 8, 52866–52876. doi: 10.18632/oncotarget.17905

Boussiotis, V. A. (2016). Molecular and biochemical aspects of the PD-1 checkpoint pathway. *N. Engl. J. Med.* 375, 1767–1778. doi: 10.1056/nejmra1514296

Cai, W., Zeng, L., Wang, L., Wang, Y., Cheng, J., Zhang, Y., et al. (2020). The latest battles between EGFR monoclonal antibodies and resistant tumor cells. *Front. Oncol.* 10:1249. doi: 10.3389/fonc.2020.01249

Capurro, M. I., Xiang, Y. Y., Lobe, C., and Filmus, J. (2005). Glypican-3 promotes the growth of hepatocellular carcinoma by stimulating canonical Wnt signaling. *Cancer Res.* 65, 6245–6254. doi: 10.1158/0008-5472.can-04-4244

Carpenter, B., Lin, Y., Stoll, S., Raffai, R. L., McCuskey, R., and Wang, R. (2005). VEGF is crucial for the hepatic vascular development required for lipoprotein uptake. *Development* 132, 3293–3303. doi: 10.1242/dev.01902

Chang, B., Shen, L., Wang, K., Jin, J., Huang, T., Chen, Q., et al. (2018). High number of PD-1 positive intratumoural lymphocytes predicts survival benefit of cytokine-induced killer cells for hepatocellular carcinoma patients. *Liver Int.* 38, 1449–1458. doi: 10.1111/liv.13697

Chen, G., Chen, Y. C., Reis, B., Belousov, A., Jukofsky, L., Rossin, C., et al. (2018). Combining expression of GPC3 in tumors and CD16 on NK cells from peripheral blood to identify patients responding to codrituzumab. *Oncotarget* 9, 10436–10444. doi: 10.18632/oncotarget.23830

Chen, T., Dai, X., Dai, J., Ding, C., Zhang, Z., Lin, Z., et al. (2020). AFP promotes HCC progression by suppressing the HuR-mediated Fas/FADD apoptotic pathway. *Cell Death Dis.* 11:822.

Cheng, W., Tseng, C. J., Lin, T. T., Cheng, I., Pan, H. W., Hsu, H. C., et al. (2008). Glypican-3-mediated oncogenesis involves the Insulin-like growth factor-signaling pathway. *Carcinogenesis* 29, 1319–1326. doi: 10.1093/carcin/bgn091

Dai, W., Wang, Y., Yang, T., Wang, J., Wu, W., and Gu, J. (2019). Downregulation of exosomal CLEC3B in hepatocellular carcinoma promotes metastasis and angiogenesis via AMPK and VEGF signals. *Cell Commun. Signal.* 17:113.

De Angelis, M. L., Francescangeli, F., La Torre, F., and Zeuner, A. (2019). Stem cell plasticity and dormancy in the development of cancer therapy resistance. *Front. Oncol.* 9:626. doi: 10.3389/fonc.2019.00626

De Luca, E., Marino, D., and Di Maio, M. (2020). Ramucirumab, a second-line option for patients with hepatocellular carcinoma: a review of the evidence. *Cancer Manag. Res.* 12, 3721–3729. doi: 10.2147/cmar.s216220

Ellison, L. M., Man, Y., Stojadinovic, A., Xin, H., and Avital, I. (2017). Cytoreductive surgery and hyperthermic intraperitoneal chemotherapy in treatment of gastric cancer with peritoneal carcinomatosis. *Chin. J. Cancer Res.* 29, 86–92.

El-Saadany, S., El-Demerdash, T., Helmy, A., Mayah, W. W., El-Sayed, H. B., Hassanien, M., et al. (2018). Diagnostic value of Glypican-3 for hepatocellular carcinomas. *Asian Pac. J. Cancer Prev.* 19, 811–817.

Feng, D., Hui, X., Shi-Chun, L., Yan-Hua, B., Li, C., Xiao-Hui, L., et al. (2017). Initial experience of anti-PD1 therapy with nivolumab in advanced hepatocellular carcinoma. *Oncotarget* 8, 96649–96655. doi: 10.18632/oncotarget.20029

Filmus, J., and Selleck, S. B. (2001). Glypicans: proteoglycans with a surprise. *Clin. Invest.* 108, 497–501. doi: 10.1172/jci200113712

Finkelmeier, F., Canli, O., Tal, A., Pleli, T., Trojan, J., Schmidt, M., et al. (2016). High levels of the soluble programmed death-ligand (sPD-L1) identify hepatocellular carcinoma patients with a poor prognosis. *Eur. J. Cancer* 59, 152–159. doi: 10.1016/j.ejca.2016.03.002

Finn, R. S., Ryoo, B. Y., Merle, P., Kudo, M., Bouattour, M., Lim, H. Y., et al. (2020a). Pembrolizumab as second-line therapy in patients with advanced hepatocellular carcinoma in KEYNOTE-240: a randomized, double-blind, phase iii trial. *J. Clin. Oncol.* 38, 193–202. doi: 10.1200/jco.19.01307

Finn, R. S., Qin, S., Ikeda, M., Galle, P. R., Ducreux, M., Kim, T., et al. (2020b). Atezolizumab plus bevacizumab in unresectable hepatocellular carcinoma. *N. Engl. J. Med.* 382, 1894–1905.

Frankel, S. R., and Baeuerle, P. A. (2013). Targeting T cells to tumor cells using bispecific antibodies. *Curr. Opin. Chem. Biol.* 17, 385–392. doi: 10.1016/j.cbpa.2013.03.029

Gros, A., Robbins, P. F., Yao, X., Li, Y. F., Turcotte, S., Tran, E., et al. (2014). PD-1 identifies the patient-specific CD8(+) tumor-reactive repertoire infiltrating human tumors. *J. Clin. Invest.* 124, 2246–2259. doi: 10.1172/jci73639

Guo, X., Jiang, H., Shi, B., Zhou, M., Zhang, H., Shi, Z., et al. (2018). Disruption of PD-1 enhanced the anti-tumor activity of chimeric antigen receptor T cells against hepatocellular carcinoma. *Front. Pharmacol.* 9:1118. doi: 10.3389/fphar.2018.01118

Hack, S. P., Spahn, J., Chen, M., Cheng, A., Kaseb, A., Kudo, M., et al. (2020). IMbrave 050: a phase III trial of atezolizumab plus bevacizumab in high-risk hepatocellular carcinoma after curative resection or ablation. *Future Oncol.* 16, 975–989. doi: 10.2217/fon-2020-0162

Hari, D., Xin, H., Jaiswal, K., Wiegand, G., Kim, B., Ambe, C., et al. (2011). Isolation of live label-retaining cells and cells undergoing asymmetric cell division via nonrandom chromosomal cosegregation from human cancers. *Stem Cells Dev.* 20, 1649–1658. doi: 10.1089/scd.2010.0455

Ho, M., and Kim, H. (2011). Glypican-3: a new target for cancer immunotherapy. *Eur. J. Cancer* 47, 333–338. doi: 10.1016/j.ejca.2010.10.024

Hu, J., Li, P., Song, Y., Ge, Y. X., Meng, X. M., Huang, C., et al. (2018). Progress and prospects of circular RNAs in hepatocellular carcinoma: novel insights into their function. *J. Cell Physiol.* 233, 4408–4422. doi: 10.1002/jcp.26154

Hu, Z., He, J., Gong, W., Zhou, N., Zhou, S., Lai, Z., et al. (2018). TLS11a Aptamer/CD3 antibody anti-tumor system for liver cancer. *J. Biomed. Nanotechnol.* 14, 1645–1653. doi: 10.1166/jbn.2018.2619

Huang, K., Sun, B., Luo, N., Guo, H., Hu, J., and Peng, J. (2018). Programmed Death Receptor 1 (PD1) knockout and Human Telomerase Reverse Transcriptase (hTERT) transduction can enhance persistence and antitumor efficacy of cytokine-induced killer cells against hepatocellular carcinoma. *Med. Sci. Monit.* 24, 4573–4582. doi: 10.12659/msm.910903

Ikeda, M., Ohkawa, S., Okusaka, T., Mitsunaga, S., Kobayashi, S., Morizane, C., et al. (2014). Japanese phase I study of GC33, a humanized antibody against glypican-3 for advanced hepatocellular carcinoma. *Cancer Sci.* 105, 455–462. doi: 10.1111/cas.12368

Jin, L., He, Y., Tang, S., and Huang, S. (2018). LncRNA GHET1 predicts poor prognosis in hepatocellular carcinoma and promotes cell proliferation by silencing KLF2. *J. Cell Physiol.* 233, 4726–4734. doi: 10.1002/jcp.26257

Kimura, O., Kondo, Y., Kogure, T., Kakazu, E., Ninomiya, M., Iwata, T., et al. (2014). Expression of EpCAM increases in the hepatitis B related and the treatment-resistant hepatocellular carcinoma. *Biomed. Res. Int.* 2014:172913.

Kudo, M., Galle, P. R., Llovet, J. M., Finn, R. S., Vogel, A., Motomura, K., et al. (2020). Ramucirumab in elderly patients with hepatocellular carcinoma and elevated alpha-fetoprotein after sorafenib in REACH and REACH-2. *Liver Int.* 40, 2008–2020. doi: 10.1111/liv.14462

Kumar Kulabhusan, P., Hussain, B., and Yüce, M. (2020). Current perspectives on aptamers as diagnostic tools and therapeutic agents. *Pharmaceutics* 12:646. doi: 10.3390/pharmaceutics12070646

Lampen, M. H., Uchtenhagen, H., Blom, K., Varnaite, R., Pakalniene, J., Dailidyte, L., et al. (2018). Breadth and dynamics of HLA-A2- and HLA-B7-Restricted CD8(+) T cell responses against nonstructural viral proteins in acute human tick-borne encephalitis virus infection. *Immunohorizons* 2, 172–184. doi: 10.4049/immunohorizons.1800029

Lepourcelet, M., Chen, Y. N., France, D. S., Wang, H., Crews, P., Petersen, F., et al. (2004). Small-molecule antagonists of the oncogenic Tcf/beta-catenin protein complex. *Cancer Cell* 5, 91–102. doi: 10.1016/s1535-6108(03)00334-9

Li, N., Wei, L., Liu, X., Bai, H., Ye, Y., Li, D., et al. (2019). A frizzled-like cysteine-rich domain in glypican-3 mediates Wnt binding and regulates hepatocellular carcinoma tumor growth in mice. *Hepatology* 70, 1231–1245. doi: 10.1002/hep.30646

Li, Y., Farmer, R. W., Yang, Y., and Martin, R. C. G. (2016). Epithelial cell adhesion molecule in human hepatocellular carcinoma cell lines: a target of chemoresistence. *BMC Cancer* 16:228. doi: 10.1186/s12885-016-2252-y

Li, Z., Li, N., Li, F., Zhou, Z., Sang, J., Chen, Y., et al. (2016). Immune checkpoint proteins PD-1 and TIM-3 are both highly expressed in liver tissues and correlate with their gene polymorphisms in patients with HBV-related hepatocellular carcinoma. *Medicine* 95:e5749. doi: 10.1097/md.0000000000005749

Lipovšek, D., Carvajal, I., Allentoff, A. J., Barros, A., Brailsford, J., Cong, Q., et al. (2018). Adnectin–drug conjugates for Glypican-3-specific delivery of a cytotoxic payload to tumors. *Protein Eng. Des. Sel.* 31, 159–171. doi: 10.1093/protein/gzy013

Liu, H., Yang, C., Lu, W., and Zeng, Y. (2018). Prognostic significance of glypican-3 expression in hepatocellular carcinoma: a meta-analysis. *Medicine* 97:e9702. doi: 10.1097/md.0000000000009702

Liu, S., Li, Y., Chen, W., Zheng, P., Liu, T., He, W., et al. (2012). Silencing glypican-3 expression induces apoptosis in human hepatocellular carcinoma cells. *Biochem. Biophys. Res. Commun.* 419, 656–661. doi: 10.1016/j.bbrc.2012.02.069

Liu, X. Q., Xin, H. Y., Lyu, Y. N., Ma, Z. W., Peng, X. C., Xiang, Y., et al. (2018). Oncolytic herpes simplex virus tumor targeting and neutralization escape by engineering viral envelope glycoproteins. *Drug Deliv.* 25, 1950–1962. doi: 10.1080/10717544.2018.1534895

Liu, Y., Qiao, Y., Hu, C., Liu, L., Zhou, L., Liu, B., et al. (2016). VEGFR2 inhibition by RNA interference affects cell proliferation, migration, invasion, and response to radiation in Calu-1 cells. *Clin. Transl. Oncol.* 18, 212–219. doi: 10.1007/s12094-015-1358-z

Liu, Y., Yu, C., Wu, Y., Sun, X., Su, Q., You, C., et al. (2017). CD44(+) fibroblasts increases breast cancer cell survival and drug resistance via IGF2BP3-CD44-IGF2 signalling. *J. Cell Mol. Med.* 21, 1979–1988. doi: 10.1111/jcmm.13118

Liu, Z., Zhu, L., Liu, J., Pu, Z., Ruan, Z., and Chen, J. (2020). Vascular endothelial growth factor receptor-2 and its association with tumor immune regulatory gene expression in hepatocellular carcinoma. *Aging* 12, 25172–25188. doi: 10.18632/aging.104119

Llovet, J. M., Chen, Y., Wurmbach, E., Roayaie, S., Fiel, M. I., Schwartz, M., et al. (2006). A molecular signature to discriminate dysplastic nodules from early hepatocellular carcinoma in HCV cirrhosis. *Gastroenterology* 131, 1758–1767. doi: 10.1053/j.gastro.2006.09.014

Midorikawa, Y., Ishikawa, S., Iwanari, H., Imamura, T., Sakamoto, H., Miyazono, K., et al. (2003). Glypican-3, overexpressed in hepatocellular carcinoma, modulates FGF2 and BMP-7 signaling. *Int. J. Cancer* 103, 455–465. doi: 10.1002/ijc.10856

Minata, M., Harada, K. H., Kudo, M., Ikai, I., and Nishida, N. (2013). The prognostic value of vascular endothelial growth factor in hepatocellular carcinoma for predicting metastasis after curative resection. *Oncology* 84(Suppl. 1), 75–81. doi: 10.1159/000345894

Oberst, M. D., Fuhrmann, S., Mulgrew, K., Amann, M., Cheng, L., Lutterbuese, P., et al. (2014). CEA/CD3 bispecific antibody MEDI-565/AMG 211 activation of T cells and subsequent killing of human tumors is independent of mutations commonly found in colorectal adenocarcinomas. *Mabs* 6, 1571–1584. doi: 10.4161/19420862.2014.975660

Ofuji, K., Saito, K., Suzuki, S., Shimomura, M., Shirakawa, H., Nobuoka, D., et al. (2017). Perioperative plasma glypican-3 level may enable prediction of the risk of recurrence after surgery in patients with stage I hepatocellular carcinoma. *Oncotarget* 8, 37835–37844. doi: 10.18632/oncotarget.14271

Ohaegbulam, K. C., Assal, A., Lazar-Molnar, E., Yao, Y., and Zang, X. (2015). Human cancer immunotherapy with antibodies to the PD-1 and PD-L1 pathway. *Trends Mol. Med.* 21, 24–33.

Pandit, H., Li, Y., Li, X., Zhang, W., Li, S., and Martin, R. (2018). Enrichment of cancer stem cells via beta-catenin contributing to the tumorigenesis of hepatocellular carcinoma. *BMC Cancer* 18:783. doi: 10.1186/s12885-018-4683-0

Park, D. J., Sung, P. S., Kim, J. H., Lee, G. W., Jang, J. W., Jung, E. S., et al. (2020). EpCAM-high liver cancer stem cells resist natural killer cell-mediated cytotoxicity by upregulating CEACAM1. *J. Immunother. Cancer* 8:e000301. doi: 10.1136/jitc-2019-000301

Ruiz De Galarreta, M., Bresnahan, E., Molina-Sánchez, P., Lindblad, K. E., Maier, B., Sia, D., et al. (2019). β-Catenin activation promotes immune escape and resistance to Anti-PD-1 therapy in hepatocellular carcinoma. *Cancer Discov.* 9, 1124–1141. doi: 10.1158/2159-8290.cd-19-0074

Sawada, Y., Yoshikawa, T., Nobuoka, D., Shirakawa, H., Kuronuma, T., Motomura, Y., et al. (2012). Phase I trial of a glypican-3-derived peptide vaccine for advanced hepatocellular carcinoma: immunologic evidence and potential for improving overall survival. *Clin. Cancer Res.* 18, 3686–3696. doi: 10.1158/1078-0432.ccr-11-3044

Sawada, Y., Yoshikawa, T., Ofuji, K., Yoshimura, M., Tsuchiya, N., Takahashi, M., et al. (2016). Phase II study of the GPC3-derived peptide vaccine as an adjuvant therapy for hepatocellular carcinoma patients. *Oncoimmunology* 5:e1129483. doi: 10.1080/2162402x.2015.1129483

Schmelzer, E., Wauthier, E., and Reid, L. M. (2006). The phenotypes of pluripotent human hepatic progenitors. *Stem Cells* 24, 1852–1858. doi: 10.1634/stemcells.2006-0036

Sedykh, S. E., Prinz, V. V., Buneva, V. N., and Nevinsky, G. A. (2018). Bispecific antibodies: design, therapy, perspectives. *Drug Des. Dev. Ther.* 12, 195–208. doi: 10.2147/dddt.s151282

Sharma, A., Seow, J., Dutertre, C. A., Pai, R., Bleriot, C., Mishra, A., et al. (2020). Onco-fetal reprogramming of endothelial cells drives immunosuppressive macrophages in hepatocellular carcinoma. *Cell* 183, 377–394.e21.

Simonelli, M., Zucali, P., Santoro, A., Thomas, M. B., de Braud, F. G., Borghaei, H., et al. (2016). Phase I study of PF-03446962, a fully human monoclonal antibody against activin receptor-like kinase-1, in patients with hepatocellular carcinoma. *Ann. Oncol.* 27, 1782–1787. doi: 10.1093/annonc/mdw240

Song, J., Guan, Z., Song, C., Li, M., Gao, Z., and Zhao, Y. (2021). Apatinib suppresses the migration, invasion and angiogenesis of hepatocellular carcinoma cells by blocking VEGF and PI3K/AKT signaling pathways. *Mol. Med. Rep.* 23:429.

Su, M., Zhao, Y., and Liu, J. (2018). The role of definitive local treatment in metastatic hepatocellular carcinoma patients: a SEER-based study. *Medicine* 97:e0020. doi: 10.1097/md.0000000000010020

Sun, B., Huang, Z., Wang, B., Yu, Y., Lin, S., Luo, L., et al. (2017). Significance of Glypican-3 (GPC3) expression in hepatocellular cancer diagnosis. *Med. Sci. Monit.* 23, 850–855. doi: 10.12659/msm.899198

Takai, H., Ashihara, M., Ishiguro, T., Terashima, H., Watanabe, T., Kato, A., et al. (2009). Involvement of glypican-3 in the recruitment of M2-polarized tumor-associated macrophages in hepatocellular carcinoma. *Cancer. Ther.* 8, 2329–2338. doi: 10.4161/cbt.8.24.9985

Tian, S., Quan, H., Xie, C., Guo, H., Lu, F., Xu, Y., et al. (2011). YN968D1 is a novel and selective inhibitor of vascular endothelial growth factor receptor-2 tyrosine kinase with potent activity in vitro and in vivo. *Cancer Sci.* 102, 1374–1380. doi: 10.1111/j.1349-7006.2011.01939.x

Wang, D., Wang, X. W., Peng, X. C., Xiang, Y., Song, S. B., Wang, Y. Y., et al. (2018). CRISPR/Cas9 genome editing technology significantly accelerated herpes simplex virus research. *Cancer Gene Ther.* 25, 93–105. doi: 10.1038/s41417-018-0016-3

Wang, Q., Liu, F., and Liu, L. (2017). Prognostic significance of PD-L1 in solid tumor: an updated meta-analysis. *Medicine* 96:e6369. doi: 10.1097/md.0000000000006369

Wang, Y., Liu, J., Pan, H., Xing, J., Wu, X., Li, Q., et al. (2018). A GPC3-targeting bispecific antibody, GPC3-S-Fab, with potent cytotoxicity. *J. Vis. Exp.* 12:57588.

Wang, Y., Xiang, Y., Xin, V. W., Wang, X., Peng, X., Liu, X., et al. (2020). Dendritic cell biology and its role in tumor immunotherapy. *J. Hematol. Oncol.* 13:107.

Wu, Z. J., Tang, F. R., Ma, Z. W., Peng, X. C., Xiang, Y., Zhang, Y., et al. (2018). Oncolytic viruses for tumor precision imaging and radiotherapy. *Hum. Gene Ther.* 29, 204–222. doi: 10.1089/hum.2017.189

Xiang, Q. F., Zhang, D. M., Wang, J. N., Zhang, H. W., Zheng, Z. Y., Yu, D. C., et al. (2015). Cabozantinib reverses multidrug resistance of human hepatoma HepG2/adr cells by modulating the function of P-glycoprotein. *Liver Int.* 35, 1010–1023. doi: 10.1111/liv.12524

Xin, H., Ambe, C. M., Ray, S., Kim, B., Koizumi, T., Wiegand, G. W., et al. (2013). Wnt and the cancer niche: paracrine interactions with gastrointestinal cancer cells undergoing asymmetric cell division. *J. Cancer* 4, 447–457. doi: 10.7150/jca.6896

Xin, H. W., Ambe, C. M., Hari, D. M., Wiegand, G. W., Miller, T. C., Chen, J. Q., et al. (2013). Label-retaining liver cancer cells are relatively resistant to sorafenib. *Gut* 62, 1777–1786. doi: 10.1136/gutjnl-2012-303261

Xin, H. W., Ambe, C. M., Miller, T. C., Chen, J. Q., Wiegand, G. W., Anderson, A. J., et al. (2016). Liver label retaining cancer cells are relatively resistant to the reported anti-cancer stem cell drug metformin. *J. Cancer* 7, 1142–1151. doi: 10.7150/jca.10047

Xin, H., Hari, D. M., Mullinax, J. E., Ambe, C. M., Koizumi, T., Ray, S., et al. (2012). Tumor-initiating label-retaining cancer cells in human gastrointestinal cancers undergo asymmetric cell division. *Stem Cells* 30, 591–598. doi: 10.1002/stem.1061

Xu, J., Zhang, Y., Jia, R., Yue, C., Chang, L., Liu, R., et al. (2019). Anti-PD-1 antibody SHR-1210 combined with apatinib for advanced hepatocellular carcinoma, gastric, or esophagogastric junction cancer: an open-label, dose escalation and expansion study. *Clin. Cancer Res.* 25, 515–523. doi: 10.1158/1078-0432.ccr-18-2484

Yamashita, T., and Wang, X. W. (2013). Cancer stem cells in the development of liver cancer. *J. Clin. Invest.* 123, 1911–1918.

Yamashita, T., Budhu, A., Forgues, M., and Wang, X. W. (2007). Activation of hepatic stem cell marker EpCAM by Wnt-beta-catenin signaling in hepatocellular carcinoma. *Cancer Res.* 67, 10831–10839. doi: 10.1158/0008-5472.can-07-0908

Yamashita, T., Ji, J., Budhu, A., Forgues, M., Yang, W., Wang, H. Y., et al. (2009). EpCAM-positive hepatocellular carcinoma cells are tumor-initiating cells with stem/progenitor cell features. *Gastroenterology* 136, 1012–1024. doi: 10.1053/j.gastro.2008.12.004

Yang, X., Zhang, X. F., Lu, X., Jia, H. L., Liang, L., Dong, Q. Z., et al. (2014). MicroRNA-26a suppresses angiogenesis in human hepatocellular carcinoma by targeting hepatocyte growth factor-cMet pathway. *Hepatology* 59, 1874–1885. doi: 10.1002/hep.26941

Zhang, P., Shi, B., Gao, H., Jiang, H., Kong, J., Yan, J., et al. (2014). An EpCAM/CD3 bispecific antibody efficiently eliminates hepatocellular carcinoma cells with limited galectin-1 expression. *Cancer Immunol. Immunother.* 63, 121–132. doi: 10.1007/s00262-013-1497-4

Zhang, Z. B., Shi, Z., Yang, L. F., and Gao, H. B. (2020). Caveolin-1 knockdown decreases SMMC7721 human hepatocellular carcinoma cell invasiveness by inhibiting vascular endothelial growth factor-induced angiogenesis. *Can. J. Gastroenterol. Hepatol.* 2020:8880888.

Zhou, B., Yan, J., Guo, L., Zhang, B., Liu, S., Yu, M., et al. (2020). Hepatoma cell-intrinsic TLR9 activation induces immune escape through PD-L1 upregulation in hepatocellular carcinoma. *Theranostics* 10, 6530–6543. doi: 10.7150/thno.44417

Zhu, A. X., Gold, P. J., El-Khoueiry, A. B., Abrams, T. A., Morikawa, H., Ohishi, N., et al. (2013). First-in-man phase i study of GC33, a novel recombinant humanized antibody against Glypican-3, in patients with advanced hepatocellular carcinoma. *Clin. Cancer Res.* 19, 920–928. doi: 10.1158/1078-0432.ccr-12-2616

Zhu, H., Jain, R. K., and Baxter, L. T. (1998). Tumor pretargeting for radioimmunodetection and radioimmunotherapy. *J. Nucl. Med.* 39, 65–76.

Zou, W., Wolchok, J. D., and Chen, L. (2016). PD-L1 (B7-H1) and PD-1 pathway blockade for cancer therapy: mechanisms, response biomarkers, and combinations. *Sci. Transl. Med.* 8:328rv4. doi: 10.1126/scitranslmed.aad7118

Conflict of Interest: The authors declare that the research was conducted in the absence of any commercial or financial relationships that could be construed as a potential conflict of interest.

Copyright © 2021 Huang, Wang, Wang, Feng, Wu, Yang, Zhang and Xin. This is an open-access article distributed under the terms of the Creative Commons Attribution License (CC BY). The use, distribution or reproduction in other forums is permitted, provided the original author(s) and the copyright owner(s) are credited and that the original publication in this journal is cited, in accordance with accepted academic practice. No use, distribution or reproduction is permitted which does not comply with these terms.

frontiers in Genetics

ORIGINAL RESEARCH
published: 25 November 2021
doi: 10.3389/fgene.2021.688575

POLR2A Promotes the Proliferation of Gastric Cancer Cells by Advancing the Overall Cell Cycle Progression

Qiuyu Jiang[1], Jinyuan Zhang[1], Fang Li[1], Xiaoping Ma[1], Fei Wu[2], Jiyu Miao[3], Qian Li[4], Xiaofei Wang[5], Ruifang Sun[1], Yang Yang[6], Lingyu Zhao[1] and Chen Huang[1]**

[1]Institute of Genetics and Development Biology, Translational Medcine Institute, Xi'an Jiaotong University, Xi'an, China, [2]Department of Oncology, The Second Affiliated Hospital, Xi'an Jiaotong University, Xi'an, China, [3]Department of Hematology, The Second Affiliated Hospital, Xi'an Jiaotong University, Xi'an, China, [4]Department of Gastroenterology, The First Affiliated Hospital of Xi'an Medical University, Xi'an, China, [5]Biomedical Experiment Center, Xian Jiaotong University, Xi'an, China, [6]Department of Toxicology and Sanitary Analysis, School of Public Health, Xi'an Jiaotong University, Xi'an, China

RNA polymerase II subunit A (POLR2A) is the largest subunit encoding RNA polymerase II and closely related to cancer progression. However, the biological role and underlying molecular mechanism of POLR2A in gastric cancer (GC) are still unclear. Our study demonstrated that POLR2A was highly expressed in GC tissue and promoted the proliferation of GC *in vitro* and *in vivo*. We also found that POLR2A participated in the transcriptional regulation of cyclins and cyclin-dependent kinases (CDKs) at each stage and promoted their expression, indicated POLR2A's overall promotion of cell cycle progression. Moreover, POLR2A inhibited GC cell apoptosis and promoted GC cell migration. Our results indicate that POLR2A play an oncogene role in GC, which may be an important factor involved in the occurrence and development of GC.

Keywords: PolR2a, gastric cancer, transcriptional regulation, cell cycle, oncogene

OPEN ACCESS

Edited by:
Kecheng Zhou,
Anhui Medical University, China

Reviewed by:
Jozsef Dudas,
Innsbruck Medical University, Austria
Niraj Lodhi,
Mirna Analytics, United States

****Correspondence:***
Lingyu Zhao
zhaolingyu@xjtu.edu.cn
Chen Huang
hchen@xjtu.edu.cn

Specialty section:
This article was submitted to Cancer Genetics and Oncogenomics, a section of the journal Frontiers in Genetics

Received: *31 March 2021*
Accepted: *01 November 2021*
Published: *25 November 2021*

Citation:
Jiang Q, Zhang J, Li F, Ma X, Wu F, Miao J, Li Q, Wang X, Sun R, Yang Y, Zhao L and Huang C (2021) POLR2A Promotes the Proliferation of Gastric Cancer Cells by Advancing the Overall Cell Cycle Progression. Front. Genet. 12:688575. doi: 10.3389/fgene.2021.688575

INTRODUCTION

Gastric cancer (GC) is one of the most common malignant tumors in the digestive system. In accordance with global cancer statistics in 2018, the incidence of GC ranked fifth, and the mortality rate ranked third in malignant tumors worldwide, while its incidence in East Asia ranked first in the world (Bernecky et al., 2016). In recent years, the incidence of GC has increased year by year, and the burden of social and health expenditure has also increased. Surgery combined with radiotherapy and chemotherapy is currently the main method for the treatment of GC. However, because the early symptoms of GC are hidden and most of them are in the middle and late stages of diagnosis, the 5-years survival rate is still less than 20% (Bertoli et al., 2013; Bray et al., 2018). General resistance to chemotherapy drugs is also one of the main reasons for poor efficacy. GC is a heterogeneous disease, the differences of epidemiological and histopathological between countries are the main cause of cancer-related deaths (Chapman et al., 2008). The occurrence and development of GC is a multi-step process involving many genetic and environmental factors. According to histopathological classification, it can be divided into adenocarcinoma, squamous cell carcinoma, and adenosquamous carcinoma. The currently widely used histopathological classification has gradually become difficult to adapt to the needs of clinical individualized diagnosis and treatment. With the development of gene chip and next-generation sequencing technology, the study on GC has entered the molecular level (Coffman, 2004; Chia and Tan, 2016; Clark et al., 2016). Therefore, understanding the molecular mechanism of the occurrence and development of GC is extremely crucial for its diagnosis and treatment.

RNA polymerase (RNAP) is the most critical enzyme in the transcription process, and it plays an extremely significant role in gene expression. Unlike prokaryotic cells where there is only one RNAP responsible for all mRNA, rRNA, and tRNA synthesis, eukaryotes have three different RNAPs, which specifically transcribe different genes to produce different products. Among them, RNAP Ⅱ is involved in the transcription of all protein-coding genes, snoRNA and some snRNA, and it is located in the nucleoplasm of cells (Das et al., 2004). RNAP Ⅱ requires the participation of a variety of transcription factors when initiating transcription, in order to form an active transcription initiation complex that binds to the promoter, so there are more studies on it (Errico, 2015). RNAP Ⅱ consists of 12 subunits, of which the largest subunit is encoded by the POLR2A gene (Gao and Liu, 2019). The human POLR2A gene is located on chromosome 17p13.1. The carboxyl end of its product has a 7-amino acid common repeat sequence of Tyr-Ser-Pro-Thr-Ser-Pro-Ser, called the carboxy-terminal domain (CTD), which is essential for polymerase activity and also necessary for maintaining cell activity. The CTD structure is unique to RNAP Ⅱ, not in RNAPⅠ and RNAP Ⅲ (Griesenbeck et al., 2017; Harlen and Churchman, 2017; Hou et al., 2019). In addition, this subunit combines with several other polymerase subunits to form the DNA binding domain of the polymerase, which is the groove where the DNA template is transcribed into RNA (Hsin and Manley, 2012).

Studies have shown that, the expression of POLR2A was significantly lower expressed in normal elderly and Werner syndrome patients compared with young donor cells, suggesting that POLR2A may be involved in regulating cell senescence (Jeronimo et al., 2013). Moreover, Hou et al. proved that POLR2A is the main target gene down-regulated after Xeroderma pigmentosum group A (XPA)-binding protein 2 (XAB2) is depleted (Hou et al., 2019). XAB2 depletion leads to massive loss of POLR2A and triggers a cascade of global transcription and cellular senescence (Jeronimo et al., 2016). Repeated mutations of POLR2A were found in samples lacking known meningioma driver genes, suggesting that POLR2A may play a role in tumorigenesis (Koumenis and Giaccia, 1997). Furthermore, in triple negative breast cancer (TNBC) and colorectal cancer (CRC), inhibition of POLR2A has a selective inhibitory effect on the growth of tumors with loss of POLR2A hemizygotes. Homozygous deletion of POLR2A is lethal in human cells, shows that POLR2A is essential for cell survival (Kurokawa et al., 2017; Gao and Liu, 2019). However, the biological effects and molecular mechanisms of POLR2A in GC cells are rarely studied.

In the present study, we investigated the role and the molecular mechanism of POLR2A in regulating GC cell proliferation and migration. Our study showed that POLR2A was highly expressed in GC tissues, and promoted the proliferation of GC *in vivo* and *in vitro*. Futhermore, POLR2A significantly promoted the overall cell cycle progression in GC by facilitating cyclins and CDKs transcription. POLR2A also inhibited GC cell apoptosis and accelerated GC cell migration. These results indicate that POLR2A plays the role of oncogene in GC and is expected to become a potential therapeutic target for GC.

MATERIALS AND METHODS

Collection of Human GC Tissue Samples

GC tumor and adjacent normal tissue samples from 39 patients were randomly collected from the First Affiliated Hospital of Xi'an Jiaotong University, PR China. The tissues were divided into two parts, one part was fixed in 4% paraformaldehyde for paraffin embedding, and the other part was stored at −80°C for further analysis. The clinicopathological characteristics of the patients are summarized in **Supplementary Table S1**. The consent of each patient was obtained before the samples were collected. The study was approved by the Biomedical Ethics Committee of the Medical Department of Xi'an Jiaotong University.

Cell Culture

Human GC cell lines MKN-28, MKN-45, AGS, SGC-7901, BGC-823 and normal gastric mucosal epithelial cell line GES-1 were obtained from Cell Bank (Genechem, Shanghai, China). All the cell lines had been authenticated by the Cell Bank. The cells had been tested for mycoplasma before all experiments began. All cell lines were cultured in RPMI-1640 or DMEM (Basalmedia, Shanghai, China) medium containing 10% fetal bovine serum (FBS, Biological Industries, Israel) and 1% penicillin-streptomycin solution (solarbio, Beijing, China), and incubated in a humidified incubator at 37°C with 5% CO_2.

Immunohistochemistry

GC tissues were fixed in 4% paraformaldehyde, then embedded in paraffin. The tissues were cut to a thickness of 5 microns with a microtome. The sections were treated with xylene to deparaffinize, and graded alcohol treated for hydration, and then antigen retrieval was applied. The rabbit SP kit (rabbit streptavidin-biotin detection system, OriGene, United States) was performed to break the endogenous peroxidase and block according to the manufacturer's instructions. The slides were incubated with the POLR2A specific primary antibody overnight at 4°C, and then the secondary antibody was incubated at room temperature, and the horseradish enzyme-labeled streptavidin working solution was processed. DAB staining kit (OriGene, United States) and hematoxylin were used for staining. The slides were dehydrated and sealed prior to microscopic analysis (Media Cybernetics, United States). The primary antibody for IHC are listed in **Supplementary Table S2**.

RNA Extraction and Quantitative Real-Time Polymerase Chain Reaction

Total RNA was extracted from cell lines or frozen tissue using TRIzol reagent (Genestar, Shanghai, China) according to the manufacturer's instructions. RNA sample concentrations were measured using Spectrophotometer (DeNovix, United States) spectrophotometrically. Complementary DNA (cDNA) was synthesized by cDNA Synthesis Kit (Yeasen, Shanghai, China) according to the manufacturer's instructions. qRT-PCR was performed using the SYBR Green PCR kit (Yeasen, Shanghai, China). The three-step method was applied as the amplification

procedure. First, pre-denatured at 95°C for 5 min. Then denatured at 95°C for 10 s, annealed at 55–60°C for 20 s, and extended at 72°C for 20 s, this step requires 40 cycles. The default setting of the instrument was adopted for the melting curve stage. The primers are listed in Table S3. All qRT-PCR reactions for each sample were performed in triplicate, using the IQ5 multicolor qRT-PCR detection system (Bio-Rad, United States). GAPDH were used as control for messenger RNA (mRNA). The $2^{-\Delta\Delta Ct}$ method was utilized for the qRT-PCR analysis.

Protein Extraction and Western Blotting

Human GC cells were lysed with precooled RIPA buffer (Pioneer, Xi'an, China) with protease inhibitor (Pioneer, Xi'an, China) for 30 min on ice. The samples were then centrifuged (14,000 rpm for 20 min at 4°C), supernatants were collected. The protein concentrations were determined by the BCA quantification kit (Fdbio, Hangzhou, China). Protein samples (20 μg) were separated by sodium dodecyl sulfate-polyacrylamide gel electrophoresis and transferred to polyvinylidene difluoride membranes (Merck Millipore, Germany). The membranes were blocked with 5% skim milk for 1 h at room temperature and incubated with specific primary antibodies at 4°C overnight. Before and after incubation with the secondary antibody for 1 h at room temperature, the membranes were thoroughly washed with TBST buffer containing Tween-20 (Fdbio, Hangzhou, China) for 10 min, a total of three times. Finally, the membranes were exposured with an enhanced chemiluminescence detection kit (Fdbio, Hangzhou, China) to show protein bands. GAPDH was performed as an internal control. Imaging signals were acquired and analyzed by ChemiDoc™ Touch (Bio-Rad, United States). The primary and secondary antibodies used are listed in **Supplementary Table S2**.

siRNA Synthesis, Plasmid Construction and Transfection

Small interfering RNAs (siRNAs) targeting human POLR2A were designed and generated by GenePharma (Shanghai, China). A sequence with no homology to mammalian genes was used as a negative control (NC, GenePharma). The sequences are listed in **Supplementary Table S4**. The full-length human POLR2A cDNA was cloned into the pCMV2-GV219 vector (Genechem, Shanghai, China) to construct its overexpression plasmid. After culturing MKN-45 and SGC-7901 cells in the plate for 24 h, siRNA or plasmids were transfected into the cells using jetPRIME® *in vitro* DNA and siRNA transfection reagent (PolyPlus, France) according to the manufacturer's protocol and the usage of transfection reagent is listed in **Supplementary Table S4**.

MTT Assay

MKN-45, SGC-7901 cells were seeded in a 96-well plate at a density of 3,000 cells/well. Five repeats were set. 24, 48, and 72 h after transfection, 10 μLMTT (sigma, United States) was added to each well and then incubated at 37°C for 4 h. Discarded the supernatant and added dimethyl sulfoxide (DMSO, 150 μL per well) to dissolve the purple crystals. Then, the absorbance of each well was measured with a microplate reader (FLUOstar Omega, BMG, Germany) at 492 nm and the cell proliferation curves were plotted.

Colony Formation Assay

24 h after transfection, MKN-45 and SGC-7901 cells were seeded in a 12-well plate at a density of 2000 cells/well and cultured for 7–10 days. Cell colonies were fixed with 4% paraformaldehyde for 15 min and stained with 0.1% crystal violet for 30 min. After washing out the excess dye twice with phosphate-buffered saline (PBS), photographed the stained cell clones and recorded the number of colonies (>10 cells) to analyze the cell cloning efficiency with Quantity One® software (Bio-Rad, United States).

Cell Cycle Analysis

24 h after transfection, MKN-45 and SGC-7901 cells were harvested by trypsinization, the cells were washed twice with PBS, and fixed with 70% ice-cold ethanol at 4°C overnight. After two more washes, the cells were incubated with 0.1 mg/ml RNase A and 0.05 mg/ml propidium iodide (Sigma, United States) for 15 min at room temperature. The distribution of the cell cycle stages was examined by flow cytometer (BD, United States).

Cell Apoptosis Analysis

48 h after transfection, MKN-45 and SGC-7901 cells were harvested by trypsinization, the cells were washed twice with PBS and treated with Annexin V-FITC/PI Apoptosis Detection Kit (7 sea, Shanghai, China) according to the manufacturer's instructions. Flow cytometry was used to detect stained cells and analyze the level of apoptosis.

Tumorigenesis Experiment in Nude Mice

MKN-45 cells were infected with a lentiviral vector with luciferase, and also infected with lentiviral vector that knocks down POLR2A (Lv-shPOLR2A, GenePharma, Shanghai, China) and its control (Lv-Control, GenePharma, Shanghai, China) according to the manufacturer's instructions, then a stable cell line knocked down POLR2A and its control were constructed. Four-week-old male nude mice were purchased from the Experimental Animal Center of Xi'an Jiaotong University and were injected subcutaneously at 1×10^7 cells/mouse. In order to eliminate individual differences, we injected cells of Lv-Control and Lv-shPOLR2A subcutaneously on both sides of the mice's groin. Tumor growth was observed every 5 days. Four weeks after the injection, the mice were intraperitoneally injected with D-luciferin potassium to stimulate the expression of luciferase (MedChemExpress, United States), anesthetized with isoflurane, and photographed by bioluminescence imaging system (Xenogen, United States) to observe the growth of tumors in living mice by observing the expression of luciferase. The mice were euthanized by cervical dislocation method, the tumors were taken out to measure the volume and weight, and then divided into two parts for RNA and protein extraction. This study was approved by the Biomedical Ethics Committee of the Medical Department of Xi'an Jiaotong University.

Transwell Migration Assay

Migration assays were performed using transwell chambers with a porous polycarbonate filter (8.0 mm; Merck Millipore,

Germany) and inserted into a 24-well plate. Cells in 200 μl of serum-free medium (3×10^4 cells) were added to the upper chamber, and 600 μl of 10% FBS medium was added to the lower chamber. The 24-well plate was incubated in a 5% CO2 cell incubator at 37°C for 24 h. At room temperature, the chambers were fixed with 4% paraformaldehyde for 15 min, and 0.1% crystal violet stained for 30 min. Cells which did not migrate through the wells were wiped by a cotton swab. A microscope imaging system (Nikon, Japan) was used to take pictures to determine the migrating cells.

Chromatin Immunoprecipitation and ChIP-qRT-PCR

ChIP was conducted as described (Kyng et al., 2003). In brief, MKN-45 and SGC-7901 cells were cross-linked with 1% formaldehyde for 15 min at room temperature and quenched with glycine (125 mmol/L). The nuclear lysate were sonicate by a cell lyser so that the chromatin was sonicated into a fragment of approximately 200 bp. The lysate was divided into two parts and incubated with 5 μg of anti-POLR2A or IgG antibody (Abcam, United Kingdom) at 4°C overnight. DNA-protein complexes were captured by Dynabeads Protein G (Invitrogen, United States) and eluted in TE buffer at 65°C. Decrosslinking was performed at 65°C for 8 h. DNA was extracted using the QIA Rapid PCR Purification Kit (Qiagen, Germany) according to the manufacturer's instructions, and the DNA was analyzed by qRT-PCR with gene-specific primers. The primer sequences used for ChIP-qRT-PCR are listed in **Supplementary Table S6**.

Statistical Analysis

Unless otherwise stated, all experiments were performed at least in triplicate. All statistical analyses were performed using SPSS Statistics 18.0 (Chicago, IL, United States). Datas were expressed as the mean ±SEM of at least three independent experiments, and Student t test was used to calculate the statistical significance of the differences between the groups. All tests were double-sided, and $p < 0.05$ was considered statistically significant.

RESULTS

POLR2A Was Highly Expressed in GC Tissues and Showed Differential Expression in GC Cell Lines

The Cancer Genome Atlas (TCGA) data showed that the expression of POLR2A in GC samples was significantly higher than that of normal samples (**Figure 1A**). Its expression was significantly related to the size or depth of invasion of the primary GC (T stage, **Figure 1B**). Patients with high expression of POLR2A had a lower survival rate (**Figure 1C**). We examined the expression of POLR2A at mRNA and protein levels in 39 GC patients' GC tissue samples and adjacent normal (non-tumor) tissue samples by qRT-PCR and IHC staining. The results showed that the expression of POLR2A in GC tissues was significantly higher than that in adjacent normal tissues (**Figures 1D,E**). The mRNA and protein levels of POLR2A in established GC cell lines were detected by qRT-PCR and Western Blotting. However, compared to normal gastric epithelial cells GES-1, POLR2A was highly expressed in MKN-28 and MKN-45 cells, not significantly altered in AGS cells, and significantly low expressed in BGC-823 and SGC-7901 cells (**Figures 1F,G**).

POLR2A Promoted the Proliferation of GC Cells *In Vitro*

In order to examine the role of POLR2A in the progression of GC cells, siRNAs targeting POLR2A and its negative control were transfected into MKN-45 cells, and the POLR2A overexpression plasmid and its control empty vector were transfected into SGC-7901 cells. qRT-PCR and Western Blotting were performed to detect the expression of POLR2A at the mRNA and protein levels. Our data showed that, in MKN-45 cells transfected with POLR2A siRNAs, the mRNA and protein levels of POLR2A were significantly down-regulated, while SGC-7901 cells transfected with the POLR2A overexpression plasmid, the mRNA and protein levels of POLR2A were significantly up-regulated, which suggested that siRNAs and overexpression plasmids were successfully constructed (**Figures 2A,B**). In order to analyze the function of POLR2A in GC cell proliferation, MTT and colony formation assays were performed. MTT analysis showed that knockdown of POLR2A in MKN-45 cells significantly inhibited cell viability at 72 h, while overexpression of POLR2A in SGC-7901 cells significantly improved cell viability at 72 h (**Figures 2C,D**). Consistent results were also observed in the colony formation assay. As shown in **Figures 2E,F**, knockdown of POLR2A significantly reduced MKN-45 cell colony formation, and overexpressing POLR2A markedly increased colony formation in SGC-7901 cells. These data indicated that POLR2A promoted the vitality and colony forming ability of GC cells, that is, POLR2A promoted the proliferation of GC cells *in vitro*.

POLR2A Promoted the Overall Progression of GC Cell Cycle

Since cell proliferation was regulated by the cell cycle, we wondered whether POLR2A affects GC cell proliferation by affecting the cycle checkpoint. Flow cytometry was employed to detect the distribution of each phase of the GC cell cycle. Our data showed that knockdown of POLR2A significantly increased the distribution of G1 and S phases in MKN-45 cells, while M phase decreased. Moreover, overexpressing POLR2A decreased the percentage of G1 phase in SGC-7901 cells, and M phase increased (**Figures 3A,B**). We found that the influence of POLR2A on the GC cell cycle was not reflected in a certain phase, since POLR2A was involved in transcription, we guessed whether POLR2A played a transcriptional regulatory role on all cyclins and cyclin-dependent kinases (CDKs), thereby promoted the overall progression of cell cycle. In order to verify our conjecture, first, the GEPIA database was used to predict the correlation between POLR2A and all cyclins/CDKs at the mRNA expression level. The results showed a significant positive

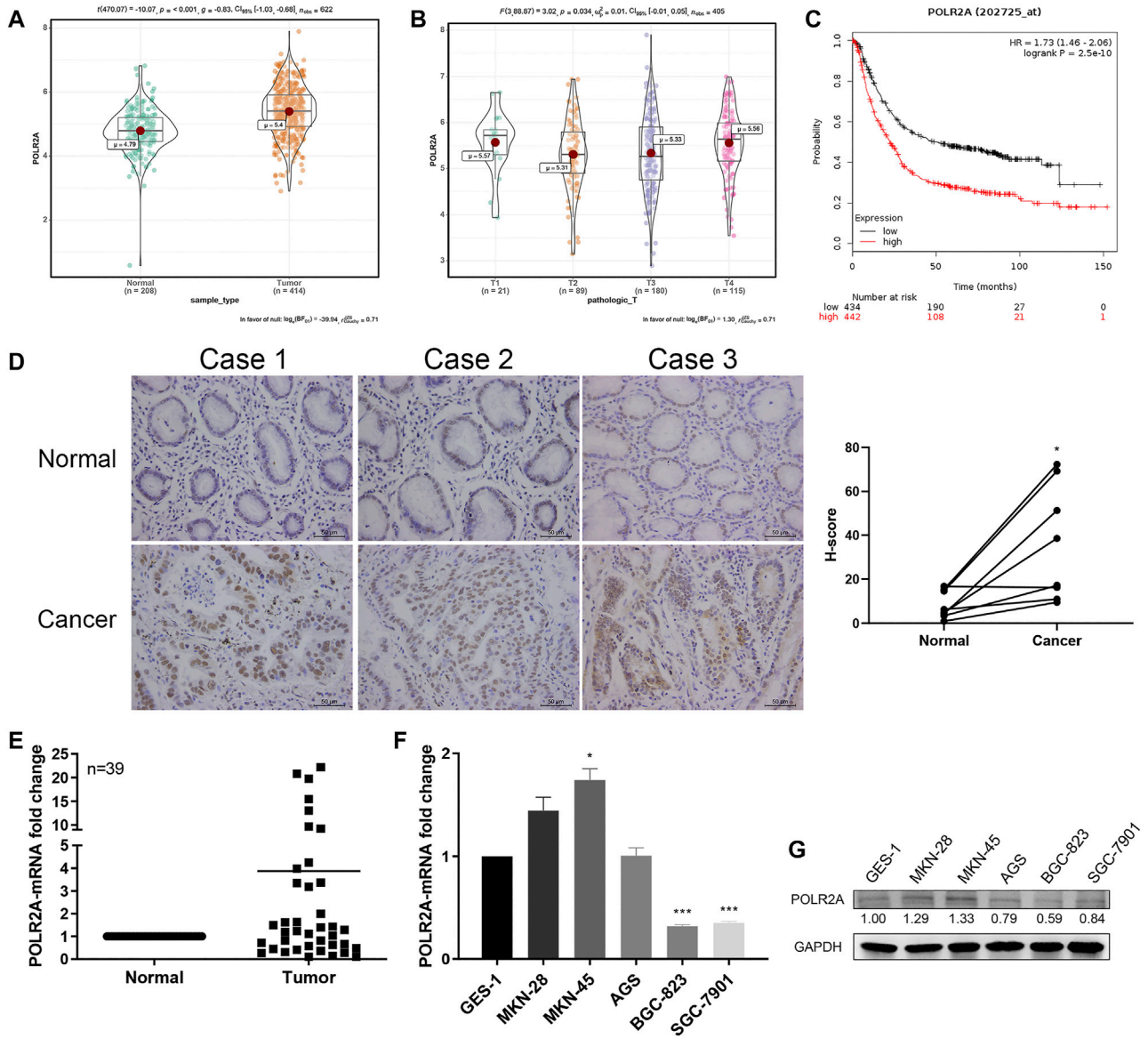

FIGURE 1 | POLR2A was highly expressed in GC tissues and showed differential expression in GC cell lines. **(A)** Bioinformatics analysis of POLR2A expression in GC (n = 414) and normal tissues (n = 208) based on TCGA data. **(B)** The expression of POLR2A analyzed by TCGA data in T-stage GC tissue samples. **(C)** Kaplan-Meier Plotter based on the expression of POLR2A in GC tissue from the TCGA database. **(D)** Representative images of IHC of POLR2A in paired GC and adjacent normal tissue samples. **(E)** POLR2A mRNA expression in 39 pairs of GC and adjacent normal tissues. **(F,G)** mRNA and protein expression of POLR2A in GC cell lines (MKN-28, MKN-45, AGS, BGC-823 and SGC-7901) and gastric mucosal epithelial cells (GES-1). *p < 0.05; **p < 0.01; ***p < 0.001.

correlation between them (**Figure 3C**). Then, we searched molecules in the promoter region of cyclins (CCNA2/CCNB1/CCND1/CCNE2) and CDKs (CDK1/CDK2/CDK4) by the UCSC database, and found that POLR2A existed in all (**Supplementary Figure S1**). Next, primers were designed based on the binding sites of POLR2A and their promoter regions, and ChIP experiments was performed to capture the DNA fragments that bind to the POLR2A antibody and verified by qRT-PCR. Experiment results showed that POLR2A could capture at least one DNA fragment at the binding site of each molecule (**Figures 3D,E**).

The binding effect of POLR2A with the promoter region of cyclins/CDKs was clarified, so did POLR2A affect their expression? qRT-PCR and Western Blotting were applied to detect the changes of cyclins and CDKs. The results showed that the mRNA and protein expression levels of cyclins and CDKs were down-regulated in MKN-45 cells after knockdown of POLR2A, and up-regulated in SGC-7901 cells after overexpressing POLR2A (**Figures 3F–H**). Our data demonstrated that POLR2A bound to the promoter regions of cyclins and CDKs to promote their transcription, thereby causing the overall progression of

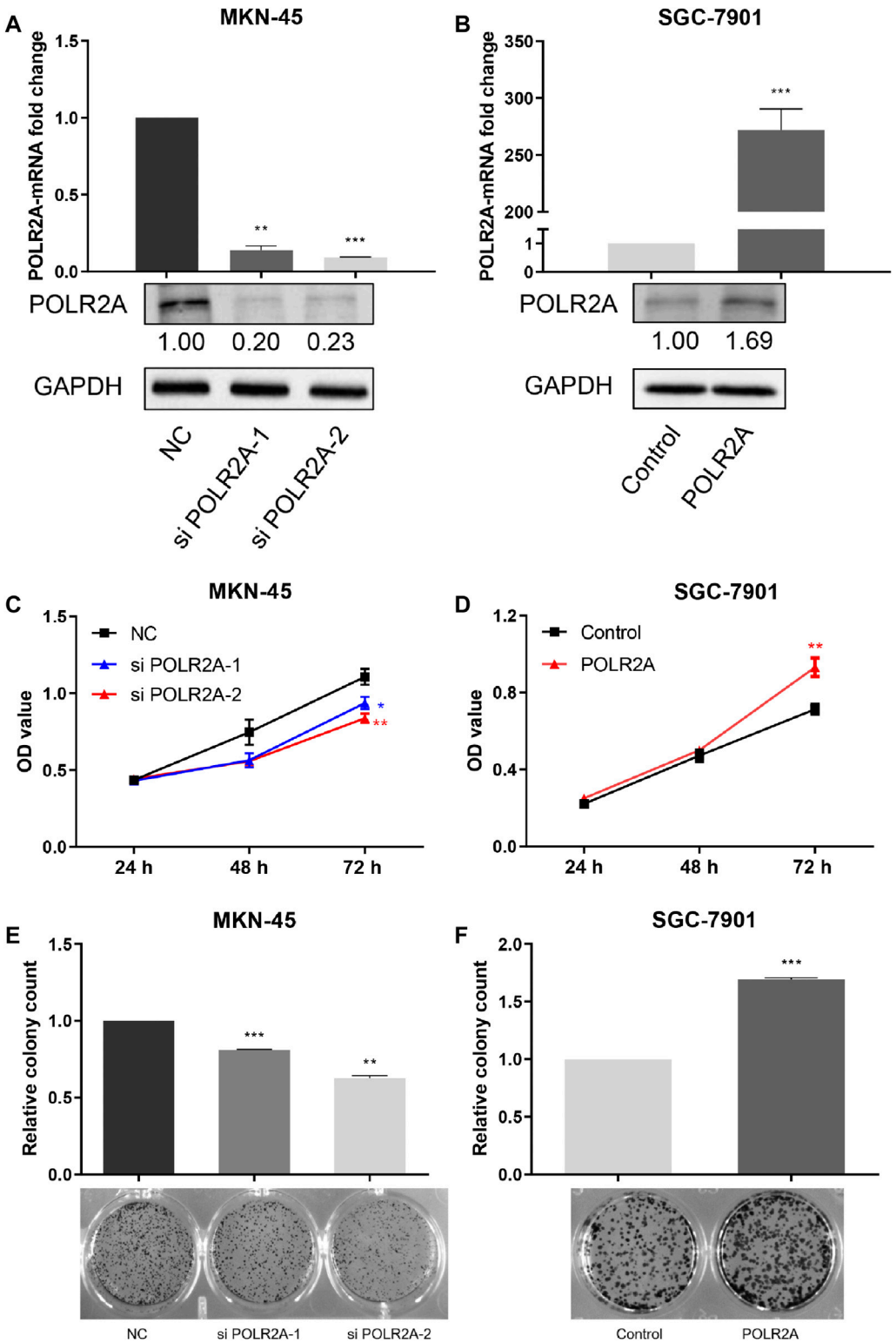

FIGURE 2 | POLR2A promoted the proliferation of GC cells *in vitro*. **(A,B)** POLR2A mRNA and protein expression in MKN-45 cells transfected with POLR2A siRNAs and SGC-7901 cells transfected with POLR2A overexpression plasmid. The mRNA and protein expression of POLR2A in the two cells was detected by qRT-PCR and Western Blotting. **(C,D)** The effect of knockdown/overexpression of POLR2A on the viability of MKN-45/SGC-7901 cells measured by MTT assay. **(E,F)** Colony formation assay 7–10 days after knockdown/overexpression of POLR2A in MKN-45/SGC-7901 cells. $^{*}p < 0.05$; $^{**}p < 0.01$; $^{***}p < 0.001$.

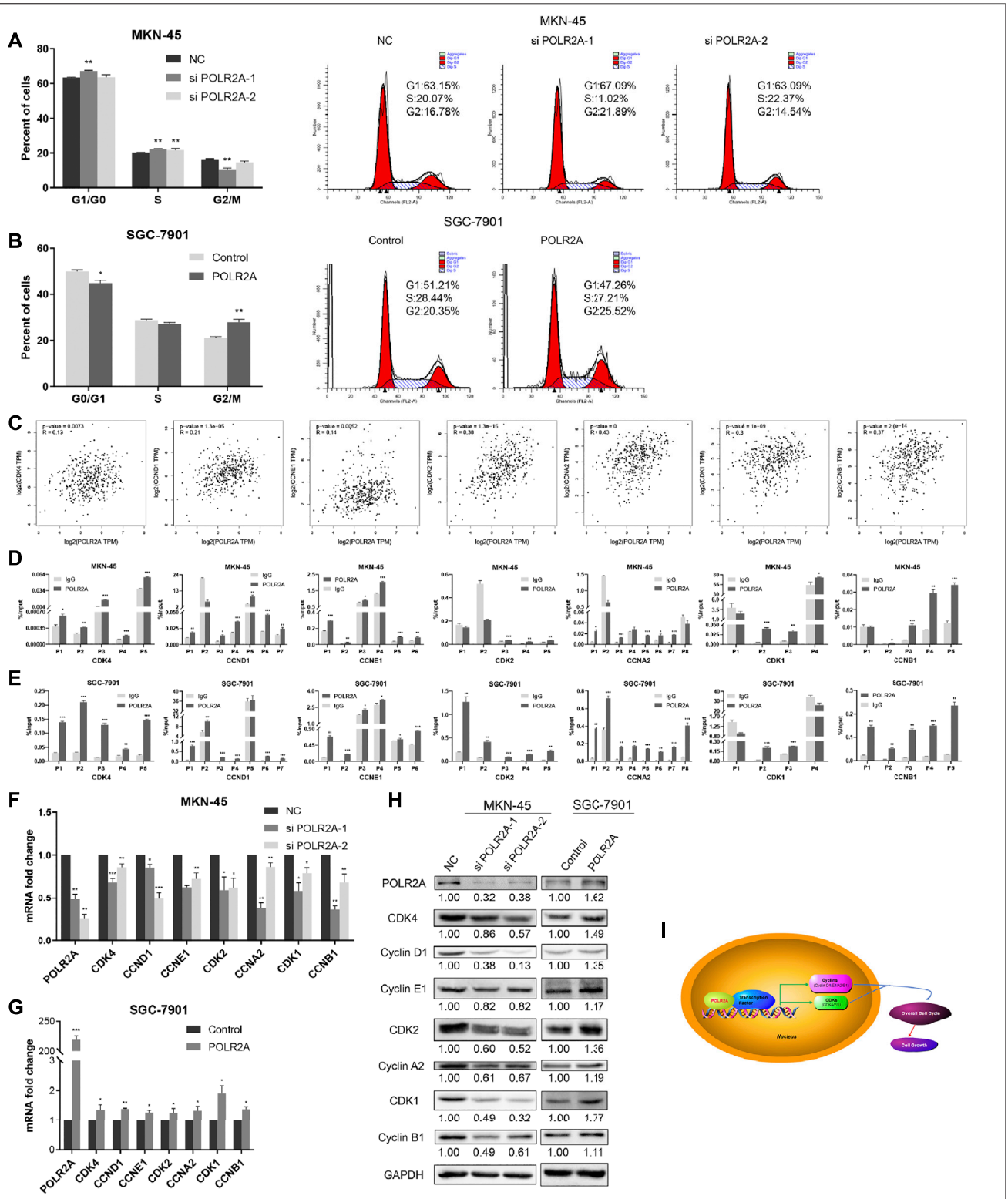

FIGURE 3 | POLR2A promoted the overall progression of GC cell cycle. **(A,B)** Cell cycle changes of MKN-45/SGC-7901 cells that knock down/overexpress POLR2A was measured by flow cytometry. **(C)** The correlation between POLR2A and cyclins/CDKs mRNA expression predicted by the GEPIA database. **(D,E)** Whether the POLR2A antibody captures the target DNA fragment was detected by ChIP-qRT-PCR. **(F,G)** The mRNA level changes of all cyclins and CDKs after knockdown/overexpression of POLR2A in MKN-45/SGC-7901 cells. **(H)** The protein level changes of all cyclins and CDKs after knockdown/overexpression of POLR2A in MKN-45/SGC-7901 cells. **(I)** Schematic diagram of ChIP-qRT-PCR primer design. $^{*}p < 0.05$; $^{**}p < 0.01$; $^{***}p < 0.001$.

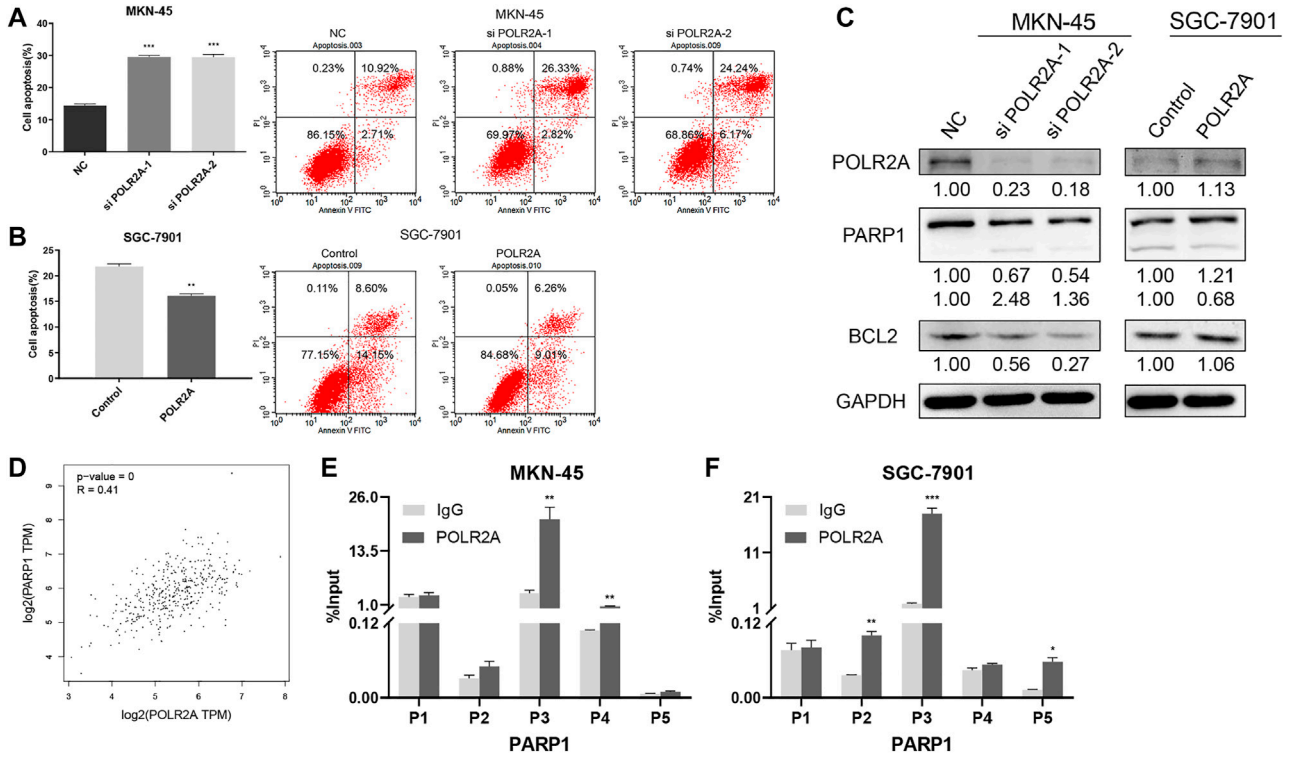

FIGURE 4 | POLR2A inhibited the apoptosis of GC cells. **(A,B)** Cell apoptosis of MKN-45/SGC-7901 cells that knock down/overexpress POLR2A was measured by flow cytometry. **(C)** The protein level changes of apoptosis-related molecules after knockdown/overexpression of POLR2A in MKN-45/SGC-7901 cells. **(D)** The correlation between POLR2A and PARP1 mRNA expression predicted by the GEPIA database. **(E,F)** Whether the POLR2A antibody captures the target DNA fragment was detected by ChIP-qRT-PCR. $^{*}p < 0.05$; $^{**}p < 0.01$; $^{***}p < 0.001$.

all stages of the cell cycle and promoting cell proliferation (**Figure 3I**).

POLR2A Inhibited the Apoptosis of GC Cells

Apoptosis plays a considerable role in the development of cancer. To investigate whether POLR2A affected apoptosis of GC cells, flow cytometry was performed, and Western Blotting was applied to detect changes in apoptosis-related proteins. The results showed that apoptosis was increased in MKN-45 cells after knockdown of POLR2A. In addition, knockdown of POLR2A in MKN-45 cells inhibited the protein expression of anti-apoptotic molecules poly ADP-ribose polymerase 1 (PARP1) and B-cell lymphoma 2 (BCL2). At the same time, apoptosis was reduced in SGC-7901 cells after overexpressing POLR2A, and PARP and BCL2 expression were significantly up-regulated (**Figures 4A–C**). These results suggested that POLR2A inhibited the apoptosis in GC cells.

PARP1 was an anti-apoptotic molecule, was POLR2A involved in PARP transcriptional regulation? In order to verify this conjecture, the GEPIA database was applied to analyze the correlation between POLR2A and PARP1 mRNA expression, as shown in **Figure 4D**, there was a significant positive correlation between them. Then we searched PARP promoter region molecules through the UCSC database, and found that POLR2A existed (**Supplementary Figure S2**). The experimental results of ChIP-qRT-PCR in MKN-45 and SGC-7901 cells also showed that POLR2A captured DNA fragments at the binding site of PARP1 (**Figures 4E,F**). The above results suggested that POLR2A may inhibit apoptosis through transcriptional regulation of PARP1.

POLR2A Promoted the Proliferation of GC Cells *In Vivo*

In order to explore the role of POLR2A in the progression of GC *in vivo*, we successfully constructed a stable MKN-45 cell line that knocked down POLR2A and its control (**Figure 5A**), and then performed tumorigenesis experiment in nude mice. The two groups of cells were injected subcutaneously into the groin on both sides of nude mice to observe tumor growth. Four weeks after the injection, the bioluminescence imaging system showed that the tumor volume of Lv-shPOLR2A was significantly smaller than that of Lv-Control (**Figure 5B**). The volume and weight of the removed solid tumor were measured, and the results showed that the tumor volume and weight of Lv-shPOLR2A were significantly smaller than that of Lv-Control (**Figures 5C–E**). The qRT-PCR and Western Blotting results of solid tumors showed that compared with Lv-Control, the expression of POLR2A of Lv-shPOLR2A was significantly down-regulated at the RNA and protein levels (**Figures 5F,G**). We also tested the expression of the cycle and apoptosis-related

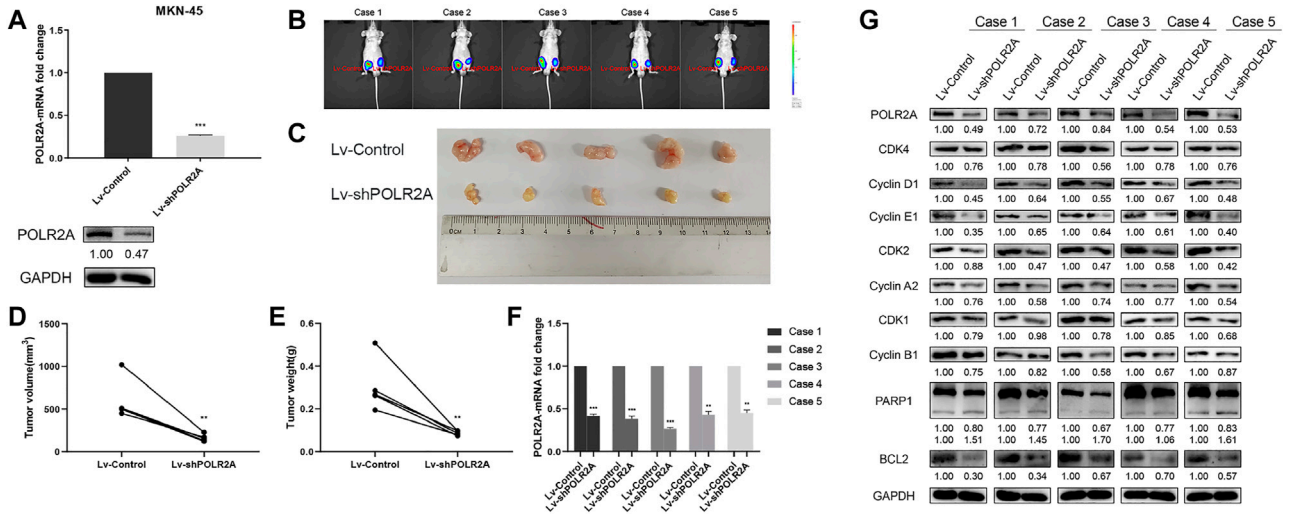

FIGURE 5 | POLR2A promoted the proliferation of GC cells *in vivo*. **(A)** The mRNA and protein expression of POLR2A in MKN-45 cells infected with Lv-shPOLR2A. **(B)** Tumor growth presented by bioluminescence imaging system. The right side of the mice groin was the Lv-Control group, and the left side was the Lv-POLR2A group. **(C)** The tumors were removed to observe its size. **(D,E)** The volume and weight of tumors. **(F)** The mRNA expression of POLR2A in tumors. **(G)** The protein expression of POLR2A and cycle and apoptosis-related molecules in tumors. $^{*}p < 0.05$; $^{**}p < 0.01$; $^{***}p < 0.001$.

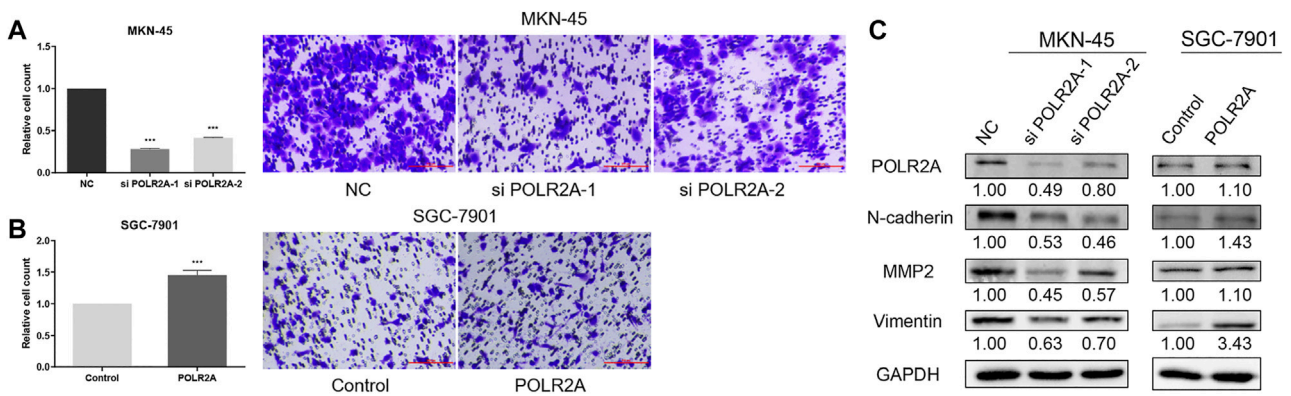

FIGURE 6 | POLR2A promoted the migration of GC cells. **(A,B)** Cell migration of MKN-45/SGC-7901 cells that knock down/overexpress POLR2A was measured by transwell migration assay. **(C)** The protein level changes of migration-related molecules after knockdown/overexpression of POLR2A in MKN-45/SGC-7901 cells. $^{*}p < 0.05$; $^{**}p < 0.01$; $^{***}p < 0.001$.

molecules involved in the aforementioned *in vitro* experiments at the protein level, and the results were consistent with the previous *in vitro* experiments. As shown in **Figure 5G**, compared to Lv-Control, the protein expression levels of cyclins and CDKs of Lv-shPOLR2A were down-regulated, and the protein expression levels of PARP and BCL2 were also down-regulated. These findings were consistent with the *in vitro* results, indicated that POLR2A also had the effect of promoting GC proliferation *in vivo*.

POLR2A Promoted the Migration of GC Cells

To investigate the effect of POLR2A on the migration of GC cells, we employed the transwell migration assay. The migration of MKN-45 cells was inhibited after knockdown of POLR2A, while the migration was promoted after POLR2A overexpressed in SGC-7901 cells (**Figures 6A,B**). The levels of Matrix Metallopeptidase 2 (MMP2), Vimentin, and N-cadherin were decreased in POLR2A-knockdown MKN-45 cells, while their expression levels were up-regulated in SGC-7901 cells after overexpressing POLR2A (**Figure 6C**). The above results indicated that POLR2A had enhancement in the migration of GC cells.

DISCUSSION

More and more evidences show that POLR2A plays an oncogene in tumors. Highly expressed POLR2A was

associated with the poor prognosis of TNBC patients, inhibition of POLR2A would reduce tumor growth (Kurokawa et al., 2017). In CRC, silencing POLR2A led to inhibition of cell proliferation, cycle arrest and increased apoptosis (Liu et al., 2015; Gao and Liu, 2019). Similarly, POLR2A was highly expressed in acute myeloid leukemia (AML) cells and tissue samples, and positively correlated with the malignant proliferation of leukemia cells. AML patients with high POLR2A expression also had a poor prognosis (Radhakrishnan and Gartel, 2006). Besides, studies had reported that POLR2A gene polymorphism was associated with lower survival outcomes in patients with non-small cell lung cancer (Sainsbury et al., 2015). In addition, Zhang et al. discovered the key potential transcription axis of CTCF/POLR2A—SYNJ2/INPP5B in metabolic programs based on the ChIP-seq data set, speculated that CTCF/POLR2A could directly dysregulate SYNJ2 levels and that increased SYNJ2 would affect HCC development via metabolic perturbation pathways (Zhang et al., 2021). The above studies consistently show that POLR2A promotes tumor growth and is related to poor prognosis. However, as far as we know, the expression and role of POLR2A in GC have not been reported. We used bioinformatics to predict the survival rate of POLR2A in GC and found that patients with high POLR2A expression have a lower survival rate. We also proved that POLR2A was highly expressed in GC tissues through bioinformatics and experiments, which is consistent with the results of studies in other tumors.

The basic biological processes of cells, such as survival, growth and differentiation, are inseparable from transcription (Saldi et al., 2016). Tumor cells require higher levels of transcription to meet their rapid proliferation characteristics (Radhakrishnan and Gartel, 2006). POLR2A, as the core of the transcription mechanism, is considered to be an essential transcriptional oncogene and anti-apoptotic factor, which could maintain the rapid growth and apoptosis resistance of tumor cells (Schafer, 1998; Serra et al., 2019). Therefore, POLR2A is highly expressed in tumor tissues compared with normal tissues. Our results also confirmed this. Furthermore, the biological function experiments of GC cells *in vitro* showed that the proliferation of MKN-45 cells was inhibited after knockdown POLR2A, the overall cell cycle was suppressed, the expression of cyclins and CDKs was down-regulated, apoptosis increased, and the expression of anti-apoptotic proteins PARP and BCL2 is down-regulated, and the overexpression of POLR2A in SGC-7901 cells has the opposite effect of knockdown POLR2A in MKN-45 cells, these results indicated that POLR2A promoted the proliferation of GC by advancing the cell cycle and inhibiting apoptosis. *In vivo* experiments in mice further confirmed the promoting effect of POLR2A on GC. Apart from this, we also found that POLR2A promoted the migration of GC cells, and up-regulated the expression of N-cadherin, MMP2 and Vimentin, which were involved in epithelial-mesenchymal transition (EMT) (Nfonsam et al., 2019; Xu et al., 2021). However, the specific molecular mechanism needs to be further studied.

The cell cycle of eukaryotic cells is a relatively complex process. The changes in the biochemical and morphological structure of the cell, as well as the transition between adjacent phases, are carried out in an orderly manner under the strict control of the cell itself and environmental factors (Villicana et al., 2014; Song et al., 2017). The cell cycle process is driven by an evolutionary conserved central mechanism. Cyclins and CDKs(Cyclin-CDK) form the core of the cell cycle control system (Wenzel and Singh, 2018; Xu et al., 2019). The periodic formation and degradation of Cyclin-CDK complex triggers the emergence of specific events in the cell cycle process, and promotes the irreversible transformation of key processes from G1 phase to S phase, G2 phase to M phase, and mid to late phases. Therefore, the correct cooperation between them is essential to ensure the orderly progression of the complete cell cycle. Additionally, the detection point monitors important events and malfunctions that occur in the cell cycle (Yoo et al., 2017) Our study demonstrates that POLR2A has an overall effect on the cell cycle. The cell cycle that knockdown POLR2A shows an overall blockage phenomenon, while an overall advancement of POLR2A overexpression, indicating that POLR2A does not only act on a certain checkpoint of the cell cycle, but also promotes each phase of the cell cycle. Furthermore, our chromatin immunoprecipitation experiments confirmed that POLR2A could capture DNA fragments of cyclins (CCNA2/CCNB1/CCND1/CCNE1) and CDKs (CDK1/CDK2/CDK4) genes in each phase. As we all know, transcription is not an independent process. When RNAP II initiates transcription, it needs the participation of universal transcription factors to form an active transcription complex (Zhao et al., 2017; Yu et al., 2019). POLR2A is the largest subunit of RNAP II, its role in transcription regulation is by recruiting transcription factors to the promoter region of target genes to promote the transcription of target genes, instead of directly playing the role of the transcription factor (Zhou et al., 2016).

In summary, we report here the high expression of POLR2A in GC and its promotion to GC *in vitro* and *in vivo*. POLR2A promoted the overall process of the GC cell cycle by regulating the transcription of cyclins and CDKs. In addition, POLR2A inhibited GC cell apoptosis and promoted GC cell migration. Our data suggest that POLR2A plays an oncogene role in the progression of GC and is expected to become a potential therapeutic target for GC. This study explains the role of POLR2A in the progession of GC, and its specific molecular mechanism and targeted drugs in GC need to be further studied.

DATA AVAILABILITY STATEMENT

The original contributions presented in the study are included in the article/**Supplementary Material**, further inquiries can be directed to the corresponding authors.

ETHICS STATEMENT

The studies involving human participants were reviewed and approved by the Biomedical Ethics Committee of the Medical

Department of Xi'an Jiaotong University. The patients/participants provided their written informed consent to participate in this study. The animal study was reviewed and approved by the Biomedical Ethics Committee of the Medical Department of Xi'an Jiaotong University. Written informed consent was obtainedfrom the individual(s) for the publication of any potentially identifiable images or data included in this article. At the same time, we have also made changes to the ethics statement mentioned in the material method.

AUTHOR CONTRIBUTIONS

QYJ, LYZ and CH design the study. QYJ, RFS and YY collected clinical data and sample. QYJ, JYZ, FL, FW, JYM and QL carry out the experiment. XPM and XFW performed the bioinformatic analysis. QYJ and LYZ wrote and edited the manuscript. CH supervised the work.

FUNDING

This work was supported by the National Natural Science Foundation of China (Nos 81972603, 81874192, 81772985), the Natural Science Foundation of Shaanxi Province (No. 2020JM-074), and Shaanxi Province Key Science and Technology Innovation Team (No. 2020TD-039).

SUPPLEMENTARY MATERIAL

The Supplementary Material for this article can be found online at: https://www.frontiersin.org/articles/10.3389/fgene.2021.688575/full#supplementary-material

Supplementary Figure S1 | Transcriptional regulatory molecules in the promoter region of cyclins and CDKs searched by the UCSC database.

Supplementary Figure S2 | Transcriptional regulatory molecules in the promoter region of PARP1 searched by the UCSC database.

REFERENCES

Bernecky, C., Herzog, F., Baumeister, W., Plitzko, J. M., and Cramer, P. (2016). Structure of Transcribing Mammalian RNA Polymerase II. *Nature* 529 (7587), 551–554. doi:10.1038/nature16482

Bertoli, C., Skotheim, J. M., and de Bruin, R. A. M. (2013). Control of Cell Cycle Transcription during G1 and S Phases. *Nat. Rev. Mol. Cel Biol* 14 (8), 518–528. doi:10.1038/nrm3629

Bray, F., Ferlay, J., Soerjomataram, I., Siegel, R. L., Torre, L. A., and Jemal, A. (2018). Global Cancer Statistics 2018: GLOBOCAN Estimates of Incidence and Mortality Worldwide for 36 Cancers in 185 Countries. *CA: A Cancer J. Clinicians* 68 (6), 394–424. doi:10.3322/caac.21492

Chapman, R. D., Heidemann, M., Hintermair, C., and Eick, D. (2008). Molecular Evolution of the RNA Polymerase II CTD. *Trends Genet.* 24 (6), 289–296. doi:10.1016/j.tig.2008.03.010

Chia, N.-Y., and Tan, P. (2016). Molecular Classification of Gastric Cancer. *Ann. Oncol.* 27 (5), 763–769. doi:10.1093/annonc/mdw040

Clark, V. E., Harmancı, A. S., Bai, H., Youngblood, M. W., Lee, T. I., Baranoski, J. F., et al. (2016). Recurrent Somatic Mutations in POLR2A Define a Distinct Subset of Meningiomas. *Nat. Genet.* 48 (10), 1253–1259. doi:10.1038/ng.3651

Coffman, J. A. (2004). Cell Cycle Development. *Develop. Cel* 6 (3), 321–327. doi:10.1016/S1534-5807(04)00067-X

Das, P. M., Ramachandran, K., vanWert, J., and Singal, R. (2004). Chromatin Immunoprecipitation Assay. *Biotechniques* 37 (6), 961–969. doi:10.2144/04376RV01

Errico, A. (2015). POLR2A Deletion with TP53 Opens a Window of Opportunity for Therapy. *Nat. Rev. Clin. Oncol.* 12 (7), 374. doi:10.1038/nrclinonc.2015.94

Gao, S.-w., and Liu, F. (2019). Novel Insights into Cell Cycle Regulation of Cell Fate Determination. *J. Zhejiang Univ. Sci. B* 20 (6), 467–475. doi:10.1631/jzus.B1900197

Griesenbeck, J., Tschochner, H., and Grohmann, D. (2017). Structure and Function of RNA Polymerases and the Transcription Machineries. *Subcell Biochem.* 83, 225–270. doi:10.1007/978-3-319-46503-6_9

Harlen, K. M., and Churchman, L. S. (2017). The Code and beyond: Transcription Regulation by the RNA Polymerase II Carboxy-Terminal Domain. *Nat. Rev. Mol. Cel Biol* 18 (4), 263–273. doi:10.1038/nrm.2017.10

Hou, S., Qu, D., Li, Y., Zhu, B., Liang, D., Wei, X., et al. (2019). XAB2 Depletion Induces Intron Retention in POLR2A to Impair Global Transcription and Promote Cellular Senescence. *Nucleic Acids Res.* 47 (15), 8239–8254. doi:10.1093/nar/gkz532

Hsin, J.-P., and Manley, J. L. (2012). The RNA Polymerase II CTD Coordinates Transcription and RNA Processing. *Genes Develop.* 26 (19), 2119–2137. doi:10.1101/gad.200303.112

Jeronimo, C., Bataille, A. R., and Robert, F. (2013). The Writers, Readers, and Functions of the RNA Polymerase II C-Terminal Domain Code. *Chem. Rev.* 113 (11), 8491–8522. doi:10.1021/cr4001397

Jeronimo, C., Collin, P., and Robert, F. (2016). The RNA Polymerase II CTD: The Increasing Complexity of a Low-Complexity Protein Domain. *J. Mol. Biol.* 428 (12), 2607–2622. doi:10.1016/j.jmb.2016.02.006

Koumenis, C., and Giaccia, A. (1997). Transformed Cells Require Continuous Activity of RNA Polymerase II to Resist Oncogene-Induced Apoptosis. *Mol. Cel Biol* 17 (12), 7306–7316. doi:10.1128/mcb.17.12.7306

Kurokawa, Y., Yang, H.-K., Cho, H., Ryu, M.-H., Masuzawa, T., Park, S. R., et al. (2017). Phase II Study of Neoadjuvant Imatinib in Large Gastrointestinal Stromal Tumours of the Stomach. *Br. J. Cancer* 117 (1), 25–32. doi:10.1038/bjc.2017.144

Kyng, K. J., May, A., Kolvraa, S., and Bohr, V. A. (2003). Gene Expression Profiling in Werner Syndrome Closely Resembles that of normal Aging. *Proc. Natl. Acad. Sci.* 100 (21), 12259–12264. doi:10.1073/pnas.2130723100

Liu, Y., Zhang, X., Han, C., Wan, G., Huang, X., Ivan, C., et al. (2015). TP53 Loss Creates Therapeutic Vulnerability in Colorectal Cancer. *Nature* 520 (7549), 697–701. doi:10.1038/nature14418

Nfonsam, L. E., Jandova, J., Jecius, H. C., Omesiete, P. N., and Nfonsam, V. N. (2019). SFRP4 Expression Correlates with Epithelial Mesenchymal Transition-Linked Genes and Poor Overall Survival in colon Cancer Patients. *Wjgo* 11 (8), 589–598. doi:10.4251/wjgo.v11.i8.589

Radhakrishnan, S. K., and Gartel, A. L. (2006). A Novel Transcriptional Inhibitor Induces Apoptosis in Tumor Cells and Exhibits Antiangiogenic Activity. *Cancer Res.* 66 (6), 3264–3270. doi:10.1158/0008-5472.CAN-05-3940

Sainsbury, S., Bernecky, C., and Cramer, P. (2015). Structural Basis of Transcription Initiation by RNA Polymerase II. *Nat. Rev. Mol. Cel Biol* 16 (3), 129–143. doi:10.1038/nrm3952

Saldi, T., Cortazar, M. A., Sheridan, R. M., and Bentley, D. L. (2016). Coupling of RNA Polymerase II Transcription Elongation with Pre-mRNA Splicing. *J. Mol. Biol.* 428 (12), 2623–2635. doi:10.1016/j.jmb.2016.04.017

Schafer, K. A. (1998). The Cell Cycle: A Review. *Vet. Pathol.* 35 (6), 461–478. doi:10.1177/030098589803500601

Serra, O., Galán, M., Ginesta, M. M., Calvo, M., Sala, N., and Salazar, R. (2019). Comparison and Applicability of Molecular Classifications for Gastric Cancer. *Cancer Treat. Rev.* 77, 29–34. doi:10.1016/j.ctrv.2019.05.005

Song, Z., Wu, Y., Yang, J., Yang, D., and Fang, X. (2017). Progress in the Treatment of Advanced Gastric Cancer. *Tumour Biol.* 39 (7), 101042831771462. doi:10.1177/1010428317714626

Villicaña, C., Cruz, G., and Zurita, M. (2014). The Basal Transcription Machinery as a Target for Cancer Therapy. *Cancer Cel Int* 14, 18. doi:10.1186/1475-2867-14-18

Wenzel, E. S., and Singh, A. T. K. (2018). Cell-cycle Checkpoints and Aneuploidy on the Path to Cancer. *Iv* 32 (1), 1–5. doi:10.21873/invivo.11197

Xu, J., Liu, Y., Li, Y., Wang, H., Stewart, S., Van der Jeught, K., et al. (2019). Precise Targeting of POLR2A as a Therapeutic Strategy for Human Triple Negative Breast Cancer. *Nat. Nanotechnol.* 14 (4), 388–397. doi:10.1038/s41565-019-0381-6

Xu, Y. J., Hu, Y. M., Qin, C., Wang, F., Cao, W., Yu, Y. W., et al. (2021). CacyBP Promotes the Proliferation and Invasion of Non-small Cell Lung Cancer. *Zhonghua Zhong Liu Za Zhi* 43 (9), 924–931. doi:10.3760/cma.j.cn112152-20210421-00329

Yoo, S. S., Hong, M. J., Lee, J. H., Choi, J. E., Lee, S. Y., Lee, J., et al. (2017). Association between Polymorphisms in microRNA Target Sites and Survival in Early-Stage Non-small Cell Lung Cancer. *Thorac. Cancer* 8 (6), 682–686. doi:10.1111/1759-7714.12478

Yu, Q., Xu, Y., Zhuang, H., Wu, Z., Zhang, L., Li, J., et al. (2019). Aberrant Activation of RPB1 Is Critical for Cell Overgrowth in Acute Myeloid Leukemia. *Exp. Cel Res.* 384 (2), 111653. doi:10.1016/j.yexcr.2019.111653

Zhang, R., Mo, W.-J., Huang, L.-S., Chen, J.-T., Wu, W.-Z., He, W.-Y., et al. (2021). Identifying the Prognostic Risk Factors of Synaptojanin 2 and its Underlying Perturbations Pathways in Hepatocellular Carcinoma. *Bioengineered* 12 (1), 855–874. doi:10.1080/21655979.2021.1890399

Zhao, L. Y., Tong, D. D., Xue, M., Ma, H. L., Liu, S. Y., Yang, J., et al. (2017). MeCP2, a Target of miR-638, Facilitates Gastric Cancer Cell Proliferation through Activation of the MEK1/2-Erk1/2 Signaling Pathway by Upregulating GIT1. *Oncogenesis* 6 (7), e368. doi:10.1038/oncsis.2017.60

Zhou, M., Li, G., and Zhang, Z. (2016). Research Progress in Molecular Classification of Gastric Cancer. *Zhonghua Wei Chang Wai Ke Za Zhi* 19 (9), 1072–1076. doi:10.3760/cma.j.issn.1671-0274

Conflict of Interest: The authors declare that the research was conducted in the absence of any commercial or financial relationships that could be construed as a potential conflict of interest.

Publisher's Note: All claims expressed in this article are solely those of the authors and do not necessarily represent those of their affiliated organizations, or those of the publisher, the editors and the reviewers. Any product that may be evaluated in this article, or claim that may be made by its manufacturer, is not guaranteed or endorsed by the publisher.

Copyright © 2021 Jiang, Zhang, Li, Ma, Wu, Miao, Li, Wang, Sun, Yang, Zhao and Huang. This is an open-access article distributed under the terms of the Creative Commons Attribution License (CC BY). The use, distribution or reproduction in other forums is permitted, provided the original author(s) and the copyright owner(s) are credited and that the original publication in this journal is cited, in accordance with accepted academic practice. No use, distribution or reproduction is permitted which does not comply with these terms.

frontiers | Frontiers in Genetics

ORIGINAL RESEARCH
published: 22 July 2022
doi: 10.3389/fgene.2022.907331

Ferroptosis-Related Hub Genes in Hepatocellular Carcinoma: Prognostic Signature, Immune-Related, and Drug Resistance Analysis

Wei Wang[1], *Fan Pan*[2], *Xinrong Lin*[2], *Jiakai Yuan*[2], *Chunyu Tao*[2] *and Rui Wang*[1,2]*

[1]*Department of Medical Oncology, Jinling Hospital, Nanjing Medical University, Nanjing, China,* [2]*Department of Medical Oncology, School of Medicine, Jinling Hospital, Nanjing University, Nanjing, China*

Background: Hepatocellular carcinoma (HCC) is the most prevalent type of primary liver cancer with a high fatality rate and dismal prognosis because of frequent recurrence and lack of efficient therapies. Ferroptosis is a recently recognized iron-dependent cell death distinct from necroptosis and apoptosis. The relationship between ferroptosis-related hub gene expression and prognosis in HCC remains to be further elucidated.

Methods: Ferroptosis-related genes from the FerrDb database and the mRNA sequencing data and clinical information of HCC patients were obtained from The Cancer Genome Atlas (TCGA) database. The least absolute shrinkage and selection operator (LASSO) Cox regression was applied to identify a prognostic signature consisting of five ferroptosis-related hub genes in the TCGA cohort. The International Cancer Genome Consortium (ICGC) database was utilized to validate the reliability of the signature. Functional enrichment and immune-related analysis, including single-sample gene set enrichment analysis (ssGSEA), immune checkpoints, TIP-related genes, tumor stemness, and m6A-related genes, were performed to analyze the underlying mechanism. Additionally, the correlations between ferroptosis and drug resistance were evaluated using the NCI-60 database.

Results: A 5–hub-gene signature associated with ferroptosis was constructed by multivariate Cox regression analysis to stratify patients into two risk groups. Patients with high risk had worse prognosis than those with low risk. Multivariate Cox regression analysis uncovered that the risk score was an independent prognostic indicator. We also proved the signature's predictive capacity using the Kaplan–Meier method and receiver operating characteristic (ROC) curve analysis. Functional analysis showed that nuclear division and the cell cycle were enriched. Immune-related analysis revealed that the signature was enriched in immune-related pathways. Moreover, the risk signature was significantly associated with immune cell infiltration, immune checkpoints, TIP-related genes, tumor stem cells, as well as m6A-related genes. Furthermore, these genes were crucial regulators of drug resistance.

Conclusion: We identified and validated a novel hub gene signature that is closely associated with ferroptosis as a new and efficient biomarker with favorable potential for predicting the prognosis of HCC patients. In addition, it also offers new insights into the

OPEN ACCESS

Edited by:
Xiao Zhu,
Guangdong Medical University, China

Reviewed by:
Anjali Lathwal,
Indraprastha Institute of Information Technology Delhi, India
Ming Sun,
Nanjing Medical University, China
Yunfei Wang,
Moffitt Cancer Center, United States

***Correspondence:**
Rui Wang
wangrui218@163.com

Specialty section:
This article was submitted to Cancer Genetics and Oncogenomics, a section of the journal Frontiers in Genetics

Received: *29 March 2022*
Accepted: *20 June 2022*
Published: *22 July 2022*

Citation:
Wang W, Pan F, Lin X, Yuan J, Tao C and Wang R (2022) Ferroptosis-Related Hub Genes in Hepatocellular Carcinoma: Prognostic Signature, Immune-Related, and Drug Resistance Analysis. Front. Genet. 13:907331. doi: 10.3389/fgene.2022.907331

molecular mechanisms of HCC and provides an effective approach for the treatment of HCC. Further studies are necessary to validate the results of our study.

Keywords: ferroptosis, hepatocellular carcinoma, prognostic model, immune, drug resistance, bioinformatics analysis

INTRODUCTION

Hepatocellular carcinoma (HCC) is a major type of adult liver malignancy. The latest global cancer statistics suggest that primary liver cancer is the sixth most commonly diagnosed cancer and the third leading cause of cancer death, with about 906,000 new cases and 830,000 deaths (8.3%) in 2020 (Sung et al., 2021). The major risk factors include hepatitis virus (hepatitis B virus, HBV, or hepatitis C virus, HCV) infection, heavy alcohol intake, nonalcoholic fatty liver disease, type 2 diabetes, and dietary toxins (aflatoxins and aristolochic acid) (Yang et al., 2019). Moreover, HCC shows high heterogeneity. As a result, many molecular targeted anticancer therapies are ineffective or even face resistance from some patients (Cancer Genome Atlas Research Network, 2017). The prognosis of HCC is very poor, with a 5-year survival rate of 14.1% (Allemani et al., 2018). At present, the diagnosis and treatment of HCC are not satisfactory.

In general, 80% of advanced HCC patients miss opportunities for surgery and ablation, but palliative treatments for HCC exhibit limited efficacy (Liu and Qin, 2019). In recent years, increasing attention has been paid to immunotherapy, and animal experiments and clinical trials have confirmed that immunotherapy plays an imperative role in the treatment of HCC patients (Zongyi and Xiaowu, 2020). Immunotherapy has been proven to be safe and effective for HCC treatment, which includes vaccines, immune checkpoint blockade, and adoptive cell transfer (ACT) (Li et al., 2015). The advent of immunotherapy has shed new light on the therapeutic strategies of HCC. Currently, immune checkpoint inhibitor (ICI) monotherapy using drugs such as nivolumab, pembrolizumab, and camrelizumab are primarily used for the second-line treatment of HCC patients at an advanced stage, and a series of relevant clinical trials are being conducted (El-Khoueiry et al., 2017; Llovet et al., 2018; Qin et al., 2020). Therefore, there is an urgent need to explore immunity-related analysis which can lay the foundation stone for immunotherapy treatment of HCC.

Ferroptosis is a newly discovered type of programmed cell death modality which is iron-dependent and mediated by lipid peroxidation. Typical morphological features include membrane rupture and blebbing, normal-sized nuclei without chromatin condensation, and mitochondrial changes, such as size reduction, increased membrane density, decreased or disappearance of mitochondrial cristae, and disruption of the mitochondrial outer membranes (Dixon et al., 2012). Extensive evidence has demonstrated that ferroptosis is closely associated with many diseases, such as cancer (Liang et al., 2019; Perez et al., 2020). It also plays a very critical role in gastric cancer, colorectal cancer, pancreatic cancer, and especially HCC (Nie et al., 2018). It has been reported that ferroptosis has become a promising treatment option for cancer cell death, especially for HCC resistant to traditional treatment (Tang et al., 2020; Yu and Wang, 2021). For instance, sorafenib could hinder cystine–glutamate antiporter and result in glutathione depletion, which induces ferroptosis in HCC cells (Hassannia et al., 2019; Liang et al., 2019). Emerging evidence suggests that ferroptosis can improve the immunotherapy response and inhibit tumor progression. Wang and coauthors have found that immunotherapy-activated $CD8^+$ T cells could enhance ferroptosis by downregulating the expression of SLC7A11 and SLC3A2. The activation of ferroptosis further contributes to the anti-tumor effect of immunotherapy (Wang et al., 2019). However, a comprehensive analysis of the relationship between ferroptosis and immunotherapy response in HCC is not well characterized.

In this study, we obtained RNA expression data and clinical information from the TCGA and ICGC databases and analyzed them using bioinformatics tools. Thereafter, we constructed a protein–protein interaction (PPI) network to screen for hub genes. Next, we constructed a ferroptosis-related hub gene signature in the TCGA cohort, and the ICGC cohort was used to verify the reliability of the prognostic signature. In addition, functional enrichment analysis was conducted based on differentially expressed ferroptosis–related genes (FRGs) between the high-risk and low-risk groups. Finally, we further performed immune, tumor stemness, N6-methyladenosine (m6A) mRNA status, drug sensitivity, and immunohistochemical analysis. All of these might not only offer insight into the molecular mechanisms that participate in the tumorigenesis and progression of HCC but also provide an efficient method to predict the outcomes in HCC patients as well as contribute to selecting effective immunotherapy for HCC patients based on biomarkers.

MATERIALS AND METHODS

Data Collection

The mRNA expression data [level 3; fragment per kilobase million (FPKM) normalized] from 374 tumor samples and 50 adjacent normal samples with corresponding clinicopathological information was downloaded from The Cancer Genome Atlas (TCGA) database (https://portal.gdc.cancer.gov/). RNA-seq data and clinical information of another cohort with 260 patients were obtained from the International Cancer Genome Consortium (ICGC) database (https://dcc.icgc.org/). After removing patients without significant clinical information, a total of 371 HCC patients in the TCGA database were included in the training cohort, and 260 patients in the ICGC database were included in the validation cohort. At the same time, the 382 ferroptosis-related genes were

downloaded from the FerrDb database (http://www.zhounan.org/ferrdb/). All data analyzed in this study were publicly accessible. Ethics committee approval was not required.

Model Establishment and Validation of Prognostic Ferroptosis-Related Hub Gene Signatures

The differentially expressed genes (DEGs) related to ferroptosis between tumor tissues and adjacent normal tissues were screened out by the "limma" package (Ritchie et al., 2015) using the Wilcoxon test in the TCGA cohort. The cutoff values were determined according to the parameters, $p < 0.05$ and false discovery rate (FDR) < 0.05. A univariate Cox analysis of overall survival (OS) was conducted to determine prognostic FRGs. The intersection of ferroptosis-related DEGs and prognostic genes was demonstrated using the "venn" R package.

An interaction network for the prognostic ferroptosis-related DEGs was plotted by the STRING (Search Tool for the Retrieval of Interacting Genes) database (version 11.0) (Szklarczyk et al., 2019). Then, we applied Cytoscape MCODE (Molecular Complex Detection) for screening hub genes (Jin et al., 2015). In addition, the MCODE app in Cytoscape software (version 3.9.1) was applied to check modules of the PPI network (degree cutoff = 2, max. depth = 100, k-core = 2, and node score cutoff = 0.2). The top ranked 10 genes in all modules were considered to be the hub genes. The expressions of these genes in tumor and normal samples were visualized using the "pheatmap" package in R.

The R packages "glmnet" and "survival" were utilized to further develop a prognostic risk signature with the least absolute shrinkage and selection operator (LASSO) method (Tibshirani, 1997; Simon et al., 2011).

The risk score was calculated based on the normalized expression level of each gene and its corresponding regression coefficients. The formula was as follows: risk score = $\sum_{n=1}^{j}(Coef\,j*Xj)$, with *Coefj* representing the coefficient and *Xj* representing the expression level of each selected gene. We stratified patients into low- and high-risk subgroups according to the risk score. To detect internal correlation in these two groups, principal component analysis (PCA) and t-distributed stochastic neighbor embedding (t-SNE) were carried out using R packages "stats" and "Rtsne." Survival analysis between the two subgroups was conducted through R package "surviminer" using the Kaplan–Meier curve and log-rank test. The predictive power of the gene signature was verified by the receiver operator characteristics (ROC) curve using the R package "timeROC."

Nomogram Construction and Assessment

Based on the variables identified with the univariate and multivariate Cox regression analyses, we also constructed the nomogram based on our prognostic gene signature using the R package "rms." The calibration curve was plotted to assess the fitting and predictive ability of our prognostic model.

Functional Enrichment Analysis

The DEGs between the low- and high-risk groups were screened out using the criteria: $|\log2FC| \geq 1$ and FDR <0.05. Based on these DEGs, we then applied the "clusterProfiler" R package to perform the functional enrichment analysis of Gene Ontology (GO), which consists of biological processes, cellular component, and molecular functions. The Kyoto Encyclopedia of Genes and Genomes (KEGG) analysis was also conducted using the same method.

Immune, Stem Cell-Like Features and M6A Correlation Analysis

We used the single-sample gene set enrichment analysis (ssGSEA) to further assess the infiltration scores of 16 immune cells and the activity of 13 immune-related functions using the "gsva" R package (Rooney et al., 2015).

Potential immune checkpoints retrieved from previous published literatures (Tang et al., 2021) were applied to investigate the correlation between immune checkpoint–related genes and risk signatures using Wilson's test. Tumor immunological phenotype (TIP) is an emerging concept to assess the immunological heterogeneity according to the relative infiltration of immune cells, and tumors are generally categorized into two TIPs: "hot" (inflamed) and "cold" (non-inflamed) (Nagarsheth et al., 2017). A total of 12 hot tumor–related genes and three cold tumor–related genes (Wang et al., 2021) were extracted, and correlations between the risk signature and TIP-related genes were evaluated using Wilson's test. Spearman correlation analysis was carried out to examine the relationship between the risk score and tumor stemness.

Several studies in recent years have confirmed that 13 m6A regulator genes could influence tumor development, which comprise the "writers" (KIAA1429, METTL3, METTL14, RBM15, WTAP, and ZC3H13), the "erasers" (ALKBH5 and FTO), and the "readers" (HNRNPC, YTHDC1, YTHDC2, YTHDF1, and YTHDF2) (Wang et al., 2020a; Zhao et al., 2021). The relationship between m6A-related genes and risk signatures was evaluated using Wilson's test.

Drug Sensitivity Analysis

The NCI-60 database and information on 218 Food and Drug Administration–approved drugs were obtained from the Cell Miner interface (https://discover.nci.nih.gov/cellminer). NCI-60 is a free online database of nine cancer types and 60 cancer cell lines, which contains mRNA expression levels and corresponding z scores of cell sensitivity data (GI50) after drug treatment. A Pearson correlation analysis was then conducted to investigate the association between drug sensitivity and the prognostic ferroptosis-related hub genes.

Analysis of the Protein Expression of Prognostic Ferroptosis-Related Hub Genes Between Normal Liver Tissue and Hepatocellular Carcinoma Tissue Using Immunohistochemistry

The Human Protein Atlas (HPA, version: 21.0) (Uhlén et al., 2015; Uhlen et al., 2017) is an open online database which

TABLE 1 | Clinical characteristics of patients in the TCGA and ICGC cohorts.

Characteristic	TCGA cohort	ICGC cohort
n	377	260
Age (median, range)	61 (16–90)	69 (31–89)
Gender (%)		
Female	122 (32.4%)	68 (26.2%)
Male	255 (67.6%)	192 (73.8%)
TNM stage		
I	175 (46.4%)	40 (15.4%)
II	87 (23.1%)	117 (45.0%)
III	86 (22.8%)	80 (30.8%)
IV	5 (1.3%)	23 (8.8%)
Unknown	24 (6.4%)	0 (0.0%)
Grade		
Grade 1	55 (14.6%)	NA
Grade 2	180 (47.7%)	NA
Grade 3	124 (32.9%)	NA
Grade 4	13 (3.4%)	NA
Unknown	5 (1.3%)	NA
Status		
Alive	245 (65.0%)	214 (82.3%)
Dead	132 (35.0%)	46 (17.7%)

comprises various protein expression images in normal and tumor tissues. The immunohistochemistry images of the corresponding genes in the prognosis model were obtained from the HPA database to verify the bioinformatics analysis results in our study.

Statistical Analysis

The Student's t test was used to identify gene expression differences between tumor and normal tissues, while the chi-square test was employed to compare differences in proportions. The OS between subgroups was compared using Kaplan–Meier analysis with the log-rank test. Univariate and multivariate Cox regression analyses were conducted to determine the independent predictors of OS. Comparisons of the ssGSEA scores of immune cells or pathways, immune checkpoints, TIP-related genes, and m6A-related genes between the high- and low-risk groups were drawn using the Wilcoxon test. Spearman correlation analysis was used to measure the relationship between the risk score and tumor stemness. Pearson correlation analysis was conducted to explore the correlation between drug sensitivity and the signature. All statistical analyses were executed using R software (Version 4.1.0). p value <0.05 was set as statistically significant.

RESULTS

In total, 377 HCC samples in the TCGA cohort and 260 HCC samples in the ICGC cohort were incorporated into the study. The detailed clinicopathological characteristics of these patients are listed in **Table 1**.

Candidate Prognostic Ferroptosis-Related Hub Gene Screening in the Cancer Genome Atlas Cohort

A total of 84 ferroptosis-related DEGs were identified in HCC, and 41 of them were associated with OS (**Figure 1A**). Among the 41 prognostic FRDEGs, all of them were upregulated in tumor tissue except ALB, which was visualized using a heatmap (**Figure 1B**). We used STRING and Cytoscape to find the intrinsic connections between these 41 genes. The interaction network and correlation among these genes are shown in **Figures 1C,D**. The hub genes including SRC, ALB, HRAS, SLC2A1, NRAS, CDKN2A, MAPK3, FANCD2, HELLS, and RRM2 were identified using Cytoscape, implying that these genes were key components of this biological network. The detailed flow diagram of this study is shown in **Figure 2**.

Development of the Prognostic Model in The Cancer Genome Atlas Cohort

To evaluate the prognostic value of the 10 aforementioned hub genes, we further used LASSO Cox regression analysis to set up a prognostic model. Finally, five genes, namely, HRAS, SLC2A1, NRAS, MAPK3, and RRM2, were identified based on the penalty parameter (λ) determined by the minimum criteria. The risk score was calculated using the formula: risk score = (0.151 × Exp HRAS) + (0.273 × Exp SLC2A1) + (0.276 × Exp NRAS) + (0.003 × Exp MAPK3) + (0.053 × Exp RRM2). According to the median risk score, the patients in the TCGA cohort were stratified into either high- or low-risk groups (**Figure 3C**). The results of the PCA and t-SNE analysis implied that the patients in the different risk groups were well distributed between two trends (**Figures 3D,F**). As shown in **Figure 3E**, patients with high risk had a higher rate of earlier death and poorer survival time than those with low risk. The survival analysis between the two groups is displayed in **Figure 3G**. Notably, the OS in the high-risk group was lower ($p < 0.001$). The time-dependent receiver operating characteristic (ROC) curve was used to evaluate the predictive ability of the model, and the area under the curve (AUC) reached 0.758 at 1 year, 0.698 at 2 years, and 0.658 at 3 years (**Figure 3H**).

External Validation of the Risk Signature in the International Cancer Genome Consortium Cohort

To test the reliability of the model established using the TCGA cohort, the patients from the ICGC cohort were also categorized into low- or high-risk groups by the median risk score calculated with the same formula used for the TCGA cohort. Similarly, PCA and t-SNE analysis also showed excellent separations between the two groups (**Figures 4B,D**). We also found that patients in the high-risk group had a higher possibility of encountering earlier death (**Figure 4C**) and had a significantly lower survival possibility than those in the low-risk group (**Figure 4E**). Meanwhile, the time–ROC curve also showed great predictive ability of our model in the ICGC cohort, and the AUC predictive value of the 5-gene signature for 1-, 2-, and 3-year survival rates was 0.749, 0.708, and 0.722, respectively (**Figure 4F**).

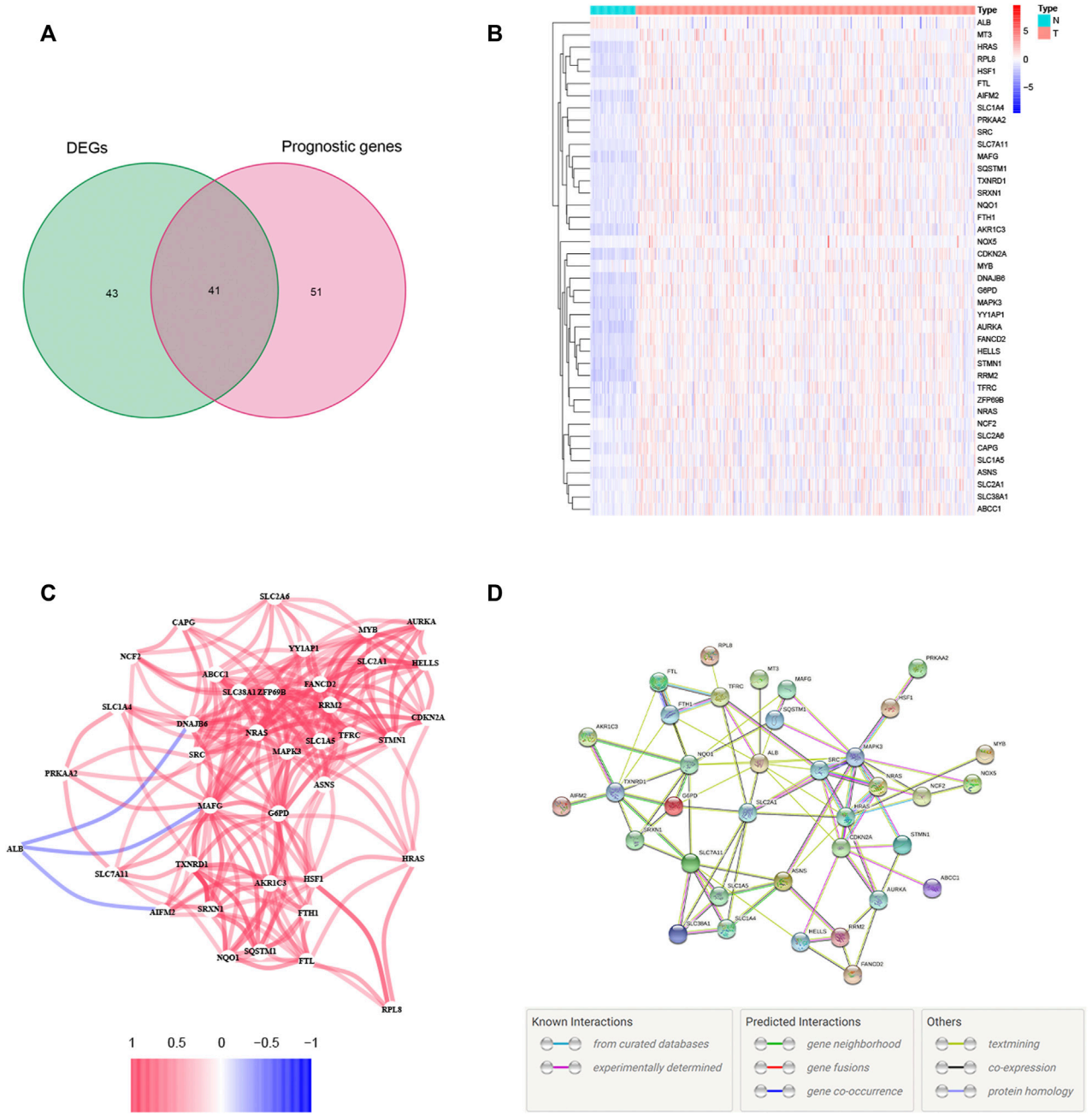

FIGURE 1 | Identification of the candidate ferroptosis-related genes (FRGs) with differential expression and prognostic value in the TCGA cohort. **(A)** Venn diagram showing identified ferroptosis-related DEGs with prognostic value. **(B)** Heatmap showing the expression of the 41 overlapping genes between tumor and adjacent tissues. **(C)** The correlation network of candidate genes. The red line represents the positive correlation, while the blue line represents the negative correlation. **(D)** The PPI network indicated the interactions among the candidate genes.

Independent Prognostic Value of the Risk Model

A heatmap of clinical characteristics and risk subgroups in the TCGA cohort is shown in **Figure 5**. All five genes (HRAS, SLC2A1, NRAS, MAPK3, and RRM2) were upregulated in the low-risk subgroup. Univariate and multivariable Cox regression analyses were generated to determine whether a signature-based risk score could be an independent prognostic indicator. The risk score was significantly associated with OS in the TCGA (HR = 3.242, 95% CI: 2.217–4.741, **Figure 6A**) and ICGC cohort (HR: 2.901, 95% CI: 1.859–4.526, **Figure 6C**) according to univariate regression analysis results. Subsequently, multivariate Cox

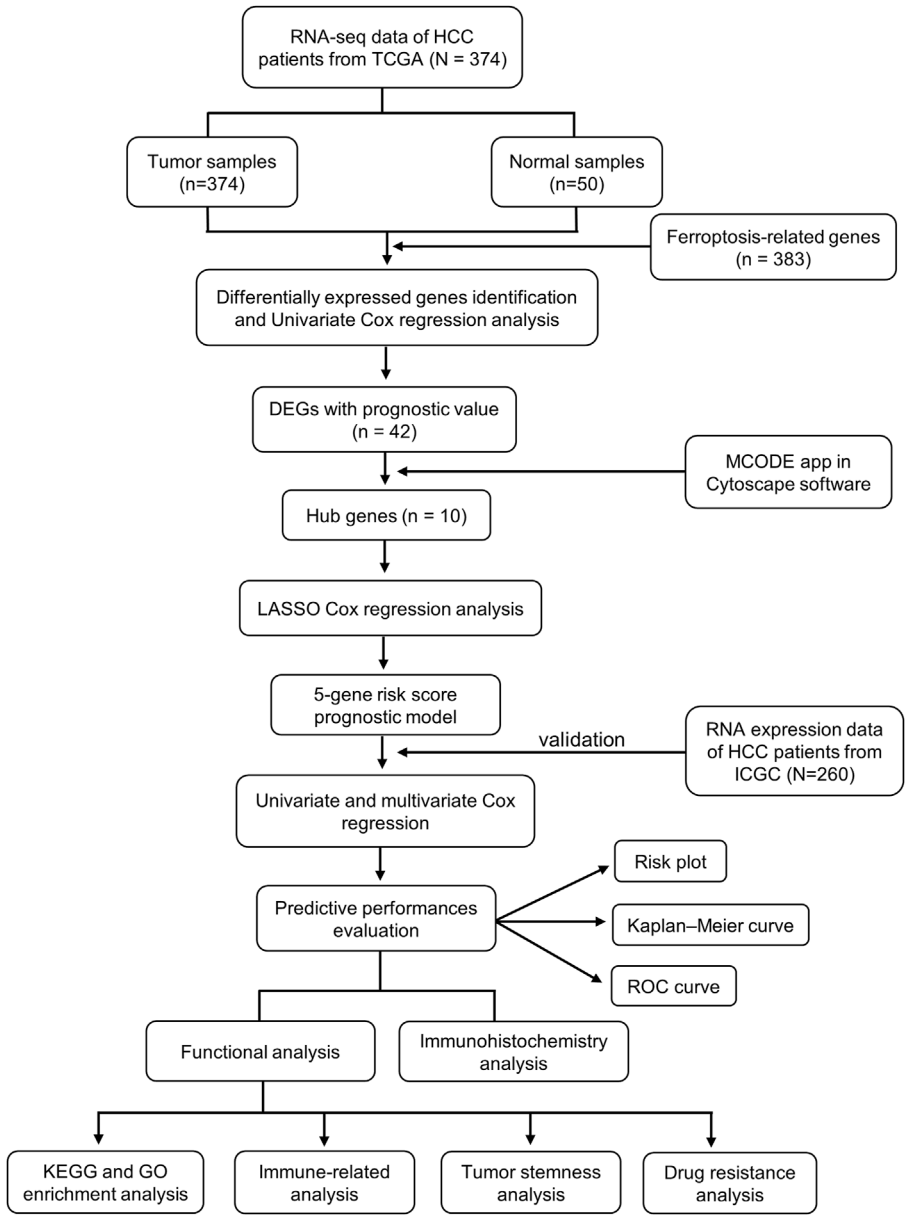

FIGURE 2 | The flow diagram of data collection and analysis in the present study.

regression analysis demonstrated that the risk scores were independent predictors connected with OS (TCGA cohort: HR = 2.756, 95% CI = 1.867–4.068, $p < 0.001$; ICGC cohort: HR = 2.361, 95% CI = 1.490–3.740, $p < 0.001$; **Figures 6B,D**).

Establishment of the Nomogram

To better apply the signature to clinical practice, we developed a nomogram based on risk score and other independent prognostic factors (TNM stage) in the TCGA cohort (**Figure 6E**). Moreover, calibration plots of 1-, 2- and 3-year survival probabilities also showed excellent consistency between nomogram predictions and actual observations (**Figure 6F**).

Functional Analyses

In order to figure out the biological functions and pathways related to the risk score, we quantified the enrichment analysis of GO and KEGG pathways in high-risk and low-risk patients in the TCGA and ICGC cohorts.

As shown in **Figures 7C,D**, GO enrichment analysis between the two cohorts was significantly enriched in nuclear division and mitotic nuclear division. KEGG pathway analysis (**Figures 7A,B**) revealed that these DEGs were closely associated with the cell cycle, human T-cell leukemia virus infection, the metabolism of xenobiotics by cytochrome P450, extracellular matrix (ECM)–receptor interactions, and so on. Thus, these results indicate the

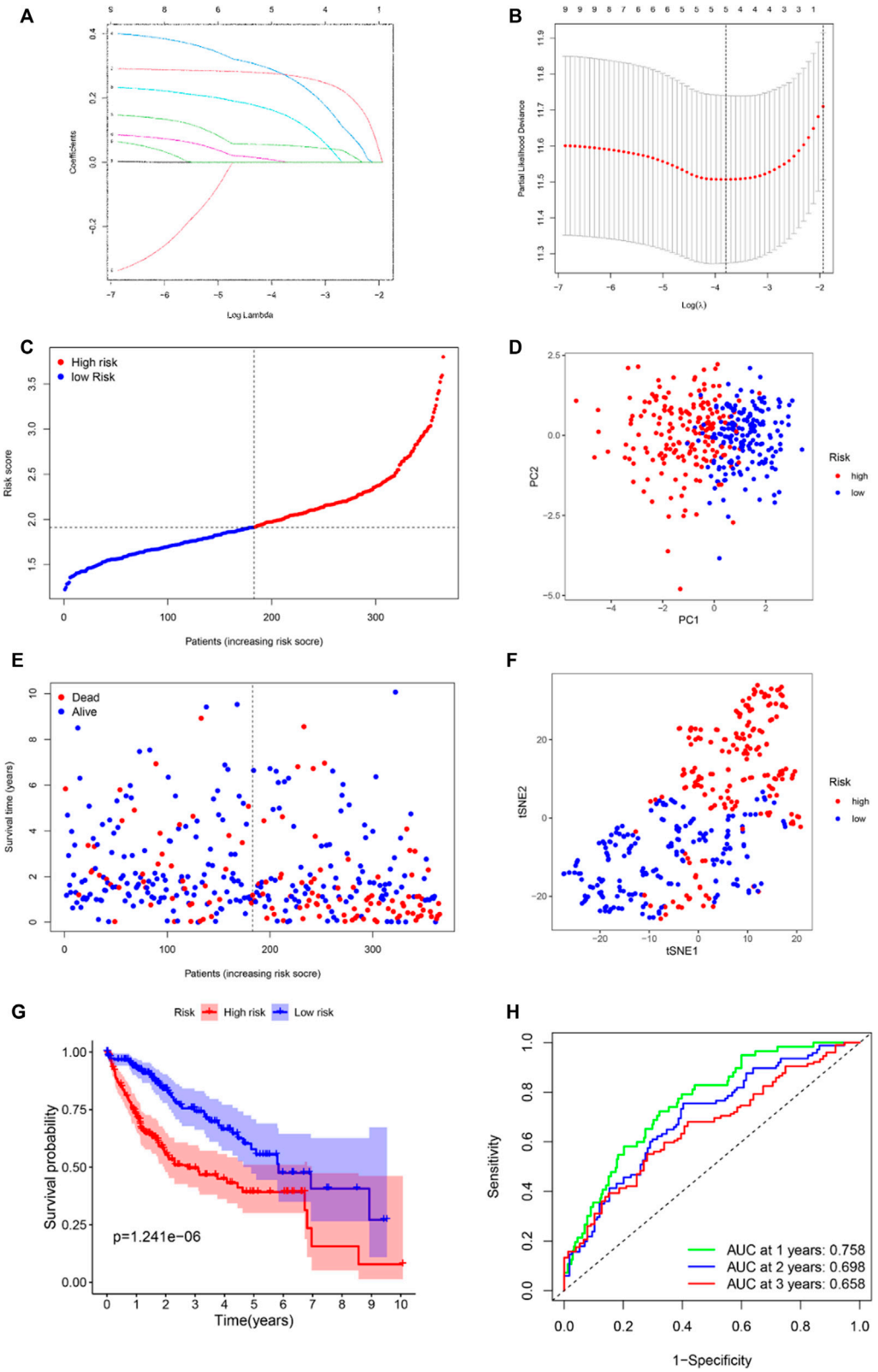

FIGURE 3 | Establishment of ferroptosis-related hub gene signature in the TCGA set. **(A)** LASSO coefficient profiles of the expression of 41 candidate genes. **(B)** Selection of the penalty parameter (λ) in the LASSO model *via* 10-fold cross-validation. An optimal log λ value is indicated by the vertical black line in the plot. Risk score distribution **(C)**, PCA plot **(D)**, overall survival (OS) status **(E)**, and t-SNE **(F)** analysis of TCGA cohort. **(G)** Kaplan–Meier curves for comparison of the OS between low- and high-risk groups. **(H)** Receiver operating characteristic (ROC) curves verified the prognostic performance of the risk score.

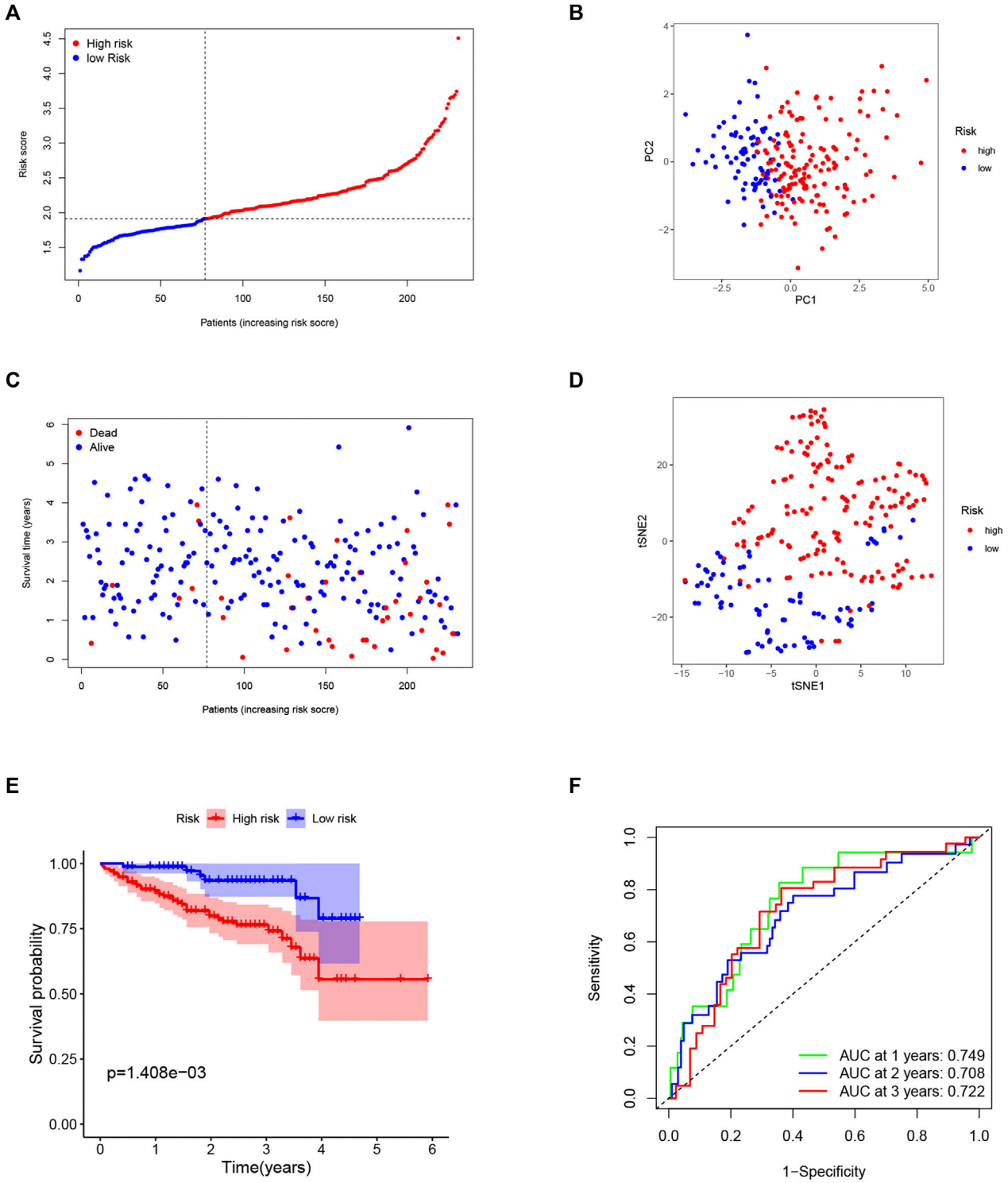

FIGURE 4 | Validation of the 5-gene signature in the ICGC cohort. **(A)** The distribution and median value of the risk scores in the ICGC cohort. **(B)** The distributions of overall survival (OS) status. **(C)** PCA plot of the ICGC cohort. **(D)** t-SNE analysis of the ICGC cohort. **(E)** Kaplan–Meier curves for the OS of patients in the high- and low-risk groups. **(F)**. ROC curves in the ICGC cohort.

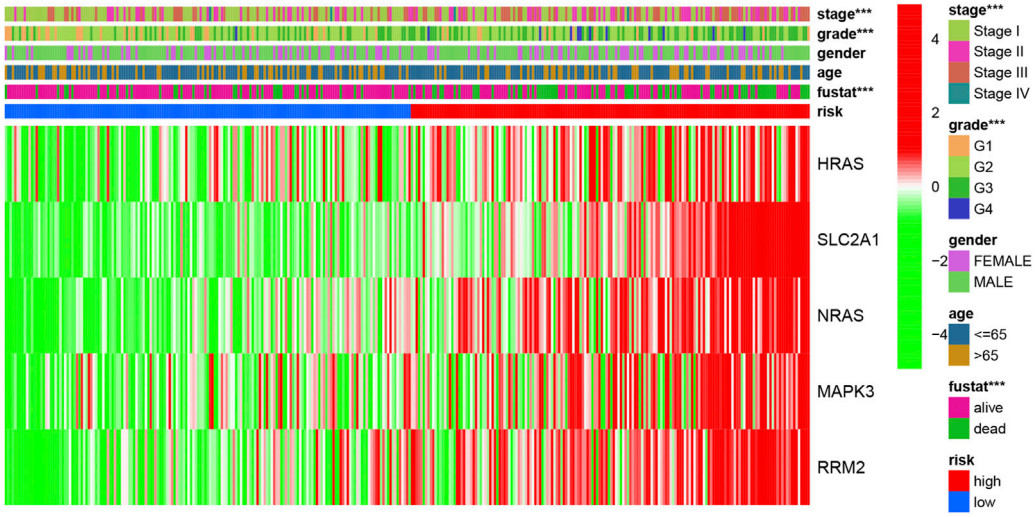

FIGURE 5 | The heatmap of clinicopathological features and ferroptosis-related hub gene expression in two risk subgroups.

correlation between ferroptosis and these essential biological processes.

Associations With Immunity, Tumor Stemness, and M6A-Related Genes

Since ferroptosis is linked with tumor immunity and can affect the outcomes of tumor immunotherapy, it is worth calculating the enrichment scores of diverse immune cells, related functions, or pathways using ssGSEA in both the TCGA and ICGC cohorts. As shown in **Figures 8A,C**, aDCs, macrophages, T helper cells, Th2 cells, and Treg cells showed high infiltration in the high-risk group in both TCGA and ICGC cohorts (all $p < 0.05$). With respect to the immune-related pathways, checkpoint and MHC class I were significantly upregulated in the high-risk group, while type I IFN response and type II IFN response were opposite in the TCGA cohorts (all adjusted $p < 0.05$, **Figure 8B**). In the ICGC cohorts, checkpoint, HLA, and MHC class I were significantly upregulated in the high-risk group, while type II IFN responses were converse (all adjusted $p < 0.05$, **Figure 8D**). These enriched immune-related pathways implied that the ferroptosis participates in the development of tumor immune evasion.

To the best of our knowledge, tumor cells can escape from immune surveillance and promote tumor growth and progression through the activation of distinct immune checkpoint pathways. Considering the important role of immune checkpoints in immunotherapy, we further explored the difference in immune checkpoint expression between the two groups. The expression levels of all identified immune-related genes were higher in the high-risk subgroup, except for ADORA2A in the TCGA cohort and TNFSF14 in the ICGC cohort. We also found an obvious difference in the expression of PDCD1 (PD-1), CTLA-4, and HHLA2 between the two groups of patients (**Figures 9A,C**), indicating a potential role of the risk model in predicting immune responses to immunotherapy in HCC patients.

Tumor immunological phenotype has been reported to be significantly associated with prognosis and therapeutic responses in various cancers by accumulating evidence (Fu et al., 2018; Zhou et al., 2019a; Wang et al., 2020b; Sui et al., 2020; Wang et al., 2021). Wang and coauthors recently reported 12 hot tumor-related genes (CXCR3, CXCR4, CXCL9, CXCL10, CXCL11, CCL5, CD3, CD4, CD8a, CD8b, CD274, and PDCD1) and three cold tumor-related genes (CXCL1, CXCL2, and CCL20) constitute the TIP gene signature using a text-mining approach (Wang et al., 2021), which is significantly associated with the survival outcomes of cancer patients and presents better predictive ability in immunotherapeutic responses than widely used immune signatures such as tumor mutation burden (TMB) and tumor immune dysfunction and exclusion (TIDE). Hence, we analyzed the relationships between the signature and TIP-related genes, and the results showed that cold tumor genes such as CXCL2 and CCL20 and hot tumor genes such as CXCR3, CXCL11, and PDCD1 were upregulated in the high-risk group in both cohorts (**Figures 9B,D**).

Tumor stemness (including the RNA stemness score and DNA methylation pattern) and m6A-related genes are critical regulators of tumor progression. The established risk signature was significantly positively correlated with RNA methylation patterns (RNAss; **Figures 10A,C**). In addition, the expression levels of m6A-related genes FTO, HNRNPC, METTL3, RBM15, WTAP, YTHDC1, YTHDF1, and YTHDF2 were significantly higher in the high-risk subgroup than in the low-risk subgroup in both TCGA and ICGC cohorts (**Figures 10B,D**). These findings imply that these ferroptosis-related hub genes may be closely associated with the immune state of HCC.

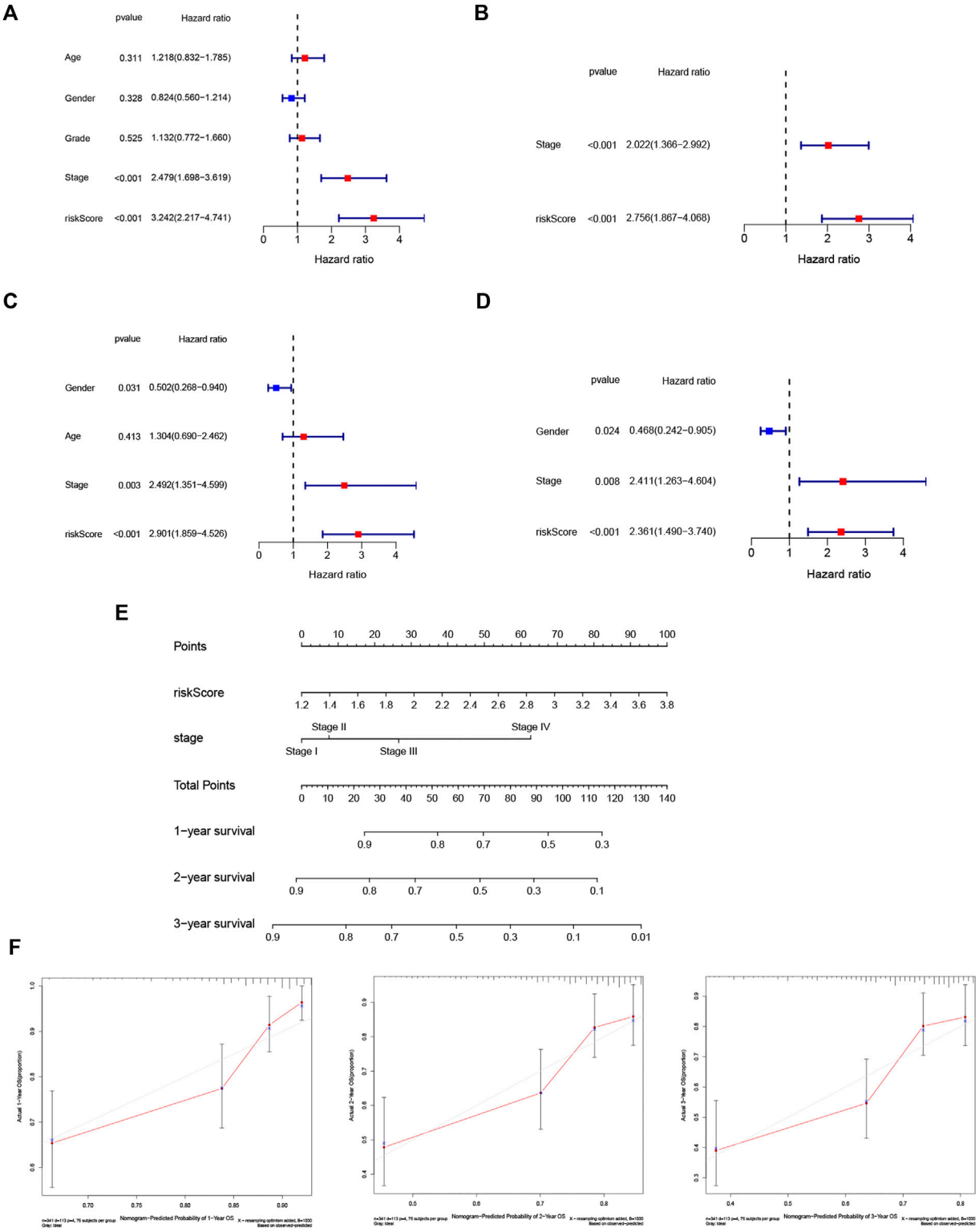

FIGURE 6 | Risk score is an independent prognostic signature for HCC and nomogram with calibration curves of the prognostic factor screened by multivariate Cox regression. Results of the univariate **(A)** and multivariate **(B)** Cox regression analyses of OS in the TCGA cohort. Univariate **(C)** and multivariate **(D)** Cox regression analyses of OS in the ICGC cohort. **(E)** Nomogram of the TCGA cohort. **(F)** Calibration curve of the TCGA cohort.

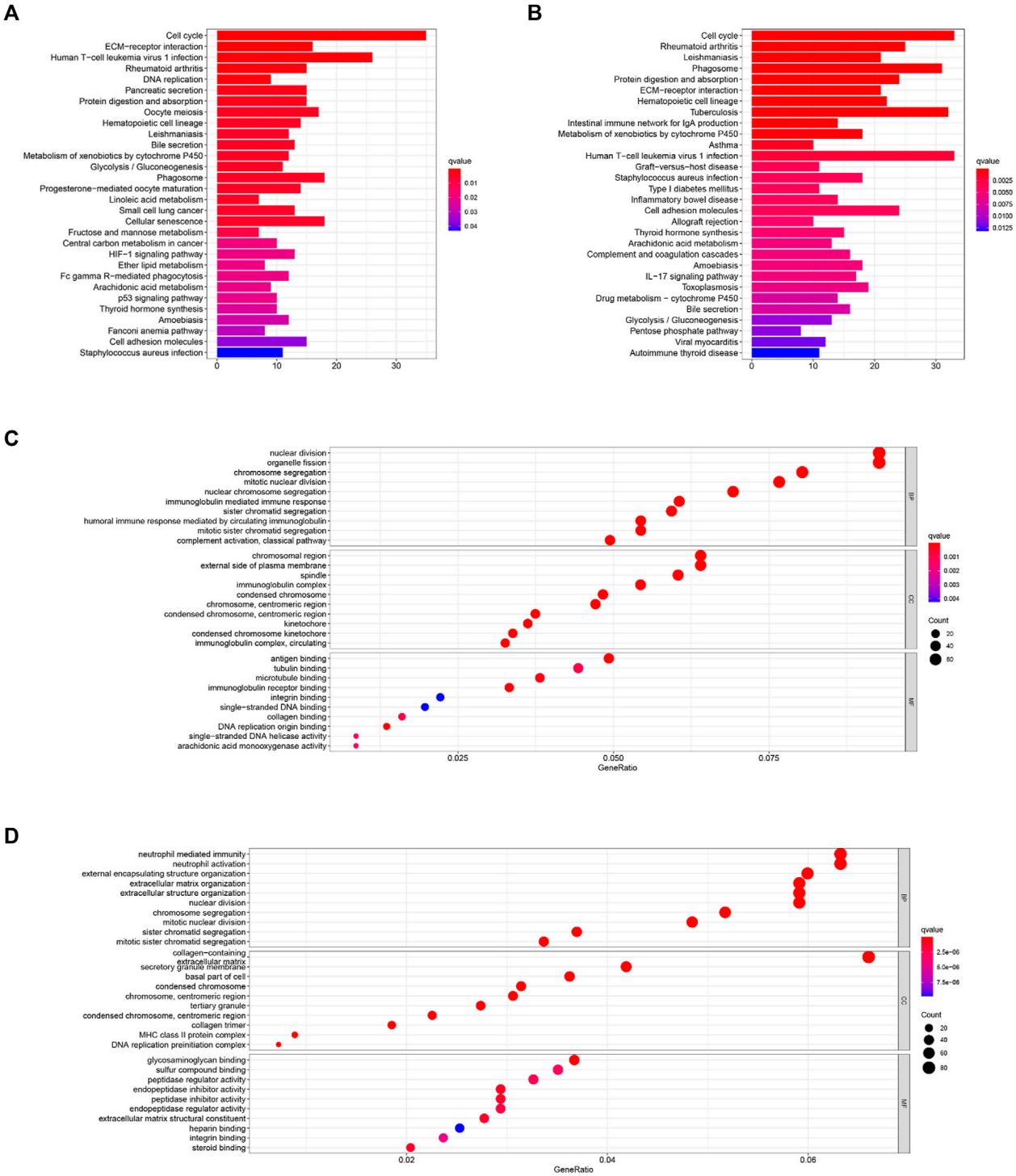

FIGURE 7 | KEGG **(A,B)** and GO **(C,D)** enrichment analyses were conducted between the high- and low-risk groups in the TCGA **(A,C)** and ICGC **(B,D)** cohorts.

Relationship Between Prognostic Ferroptosis-Related Hub Genes and Drug Sensitivity

Ferroptosis has been reported to play a crucial role in modulating drug resistance. Herein, we used the NCI-60 database to explore the connection between prognostic ferroptosis-related hub genes and drug sensitivity using Pearson correlation. The top 16 gene–drug pairs ranked by Pearson correlation coefficient are displayed in **Figure 11**. We found that RRM2 was positively associated with chemotherapy sensitivity, while SLC2A1 was negatively associated with

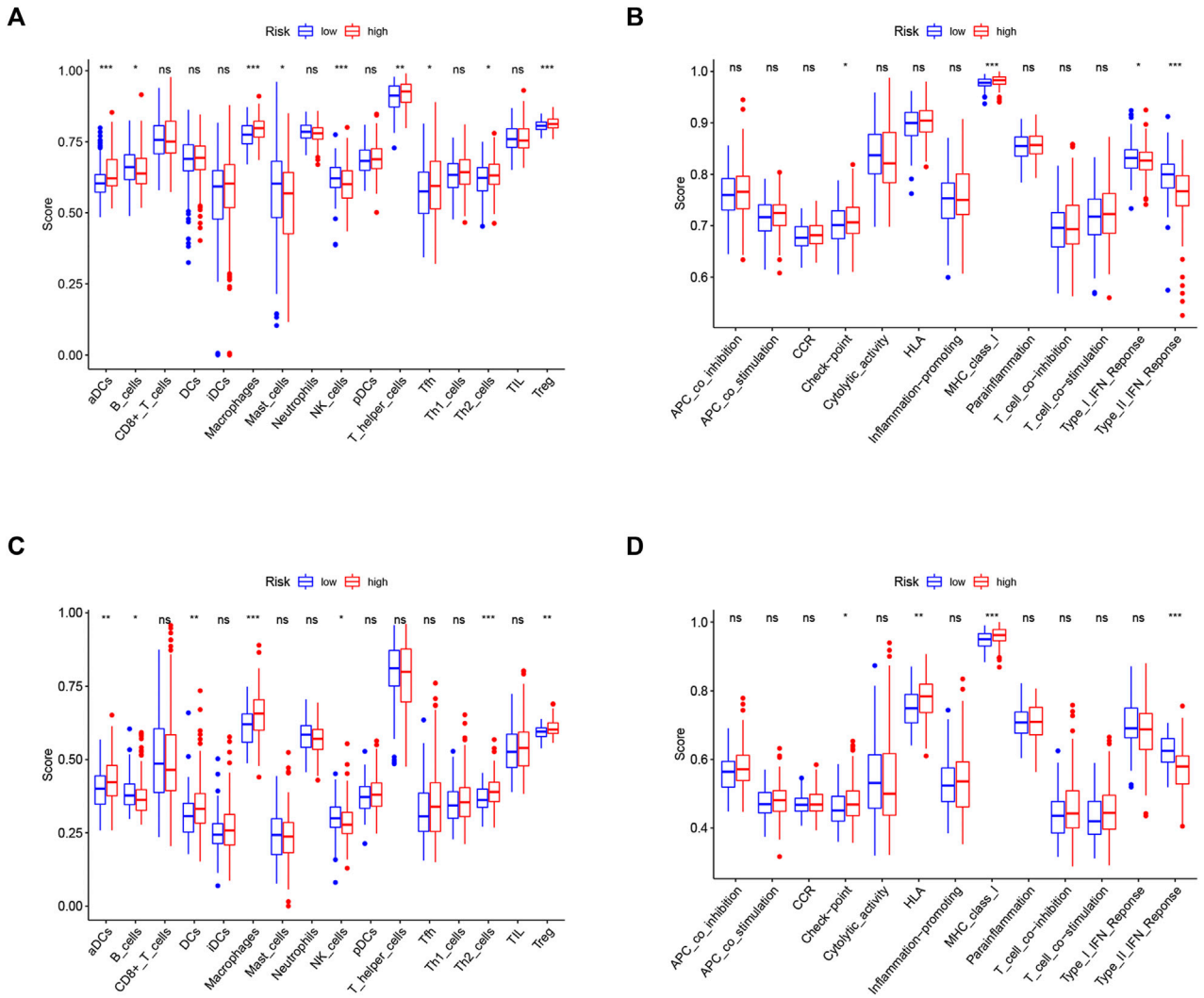

FIGURE 8 | Comparison of the ssGSEA scores between different risk groups in the TCGA cohort **(A,B)** and ICGC cohort **(C,D)**. The scores of 16 immune cells **(A,C)** and 13 immune-related functions **(B,D)** are displayed in boxplots. CCR, cytokine–cytokine receptor. Adjusted *p* values were shown as ns, not significant; *, $p < 0.05$; **, $p < 0.01$; and ***, $p < 0.001$.

targeted drug sensitivity. Intriguingly, MAPK3 was positively related to eight drug sensitivity tests, including chemotherapy and targeted drugs. These results proved that ferroptosis was involved in targeted therapies in HCC.

Differences in the Protein Expression of Five Prognostic Ferroptosis-Related Hub Genes Between Normal Liver Tissue and Hepatocellular Carcinoma Tissue

As shown in **Figure 12**, we found that the expression of MAPK3 in liver cancer tissue is higher than that in normal tissue by immunohistochemical staining in the HPA database. In contrast, the protein expression of HRAS, SLC2A1, NRAS, and RRM2 showed no significant difference between normal liver tissues and HCC tissues.

DISCUSSION

Despite tremendous and rapid progress in the present diagnosis and treatment of HCC, patients with HCC still have low OS rate and poor prognosis (Anwanwan et al., 2020). Hence, it is necessary to identify new biomarkers and targets that affect the prognosis of HCC, so as to optimize the early diagnosis of HCC and improve treatment to enhance the clinical efficacy against HCC. Distinct from apoptosis, autophagy and necrosis, ferroptosis is a novel form of programmed cell death characterized by unique morphology, gene expression, and molecular pathways (Tang et al., 2019). Though the underlying mechanisms of tumor susceptibility to ferroptosis have been a research hotspot over the past few years, the potential regulatory roles between ferroptosis and tumor immunity have not been systemically studied.

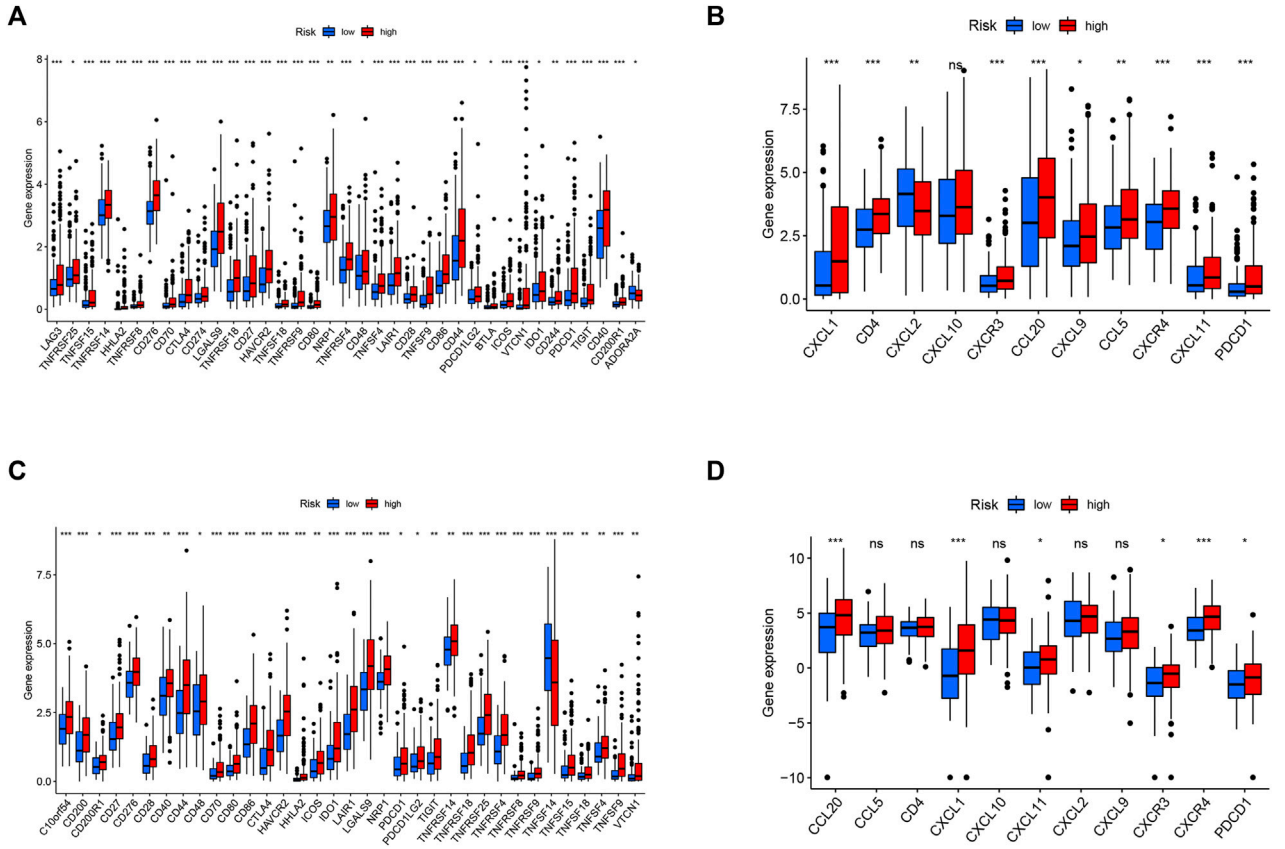

FIGURE 9 | Correlation between the risk score, immune checkpoints, and TIP-related genes. Expression of immune checkpoints between two risk subgroups in the TCGA cohort **(A)** and ICGC cohort **(C)**. The expression of TIP-related genes between high- and low-risk groups in the TCGA cohort **(B)** and ICGC cohort **(D)**. Adjusted *p* values were shown as *, $p < 0.05$; **, $p < 0.01$; and ***, $p < 0.001$.

Previously, FRG signatures have been established and applied to HCC in recent research (Liang et al., 2020; Wan et al., 2022). In contrast to previous studies, we screened out the ferroptosis-related hub genes and made the model we built more targeted. Moreover, we performed a comprehensive analysis of the relationship between ferroptosis-related hub genes and liver cancer. We not only constructed the prognostic model, but also emphasized the analysis between ferroptosis and immunotherapy in HCC.

In the present study, we constructed a ferroptosis-related model consisting of five Hub genes (HRAS, SLC2A1, NRAS, MAPK3, and RRM2) for predicting the prognosis of HCC according to the data from TCGA and verified its predictive ability in the ICGC cohort. Among the five genes in the risk signature, HRAS is a small G protein in the RAS subfamily of the RAS superfamily of small GTPases. The expression level of HRAS was higher in HCC cell lines and HCC tissues, suggesting a transcriptional activation mechanism of HRAS in HCC rather than oncogenic mutations (Dietrich et al., 2017). Moreover, activated HRAS mutations were detected in nonalcoholic fatty liver disease (NAFLD)–associated HCC in mice (Shen et al., 2016), which is increasingly regarded as a promotor of hepatocarcinogenesis.

Solute carrier family 2 member 1 (SLC2A1), also known as glucose transporter 1 (GLUT1), is an energy source for cell growth that lends favor to cancer development and progression (Min et al., 2021). In addition, SLC2A1-mediated glucose transport facilitates glycolysis, accelerates fatty acid synthesis, and eventually induces lipid peroxidation–dependent ferroptosis (Song et al., 2021). High expression of SLC2A1 has been found to be connected with inferior outcomes in various adult malignancies, including liver cancer (Chen et al., 2018), lung cancer (Zhang et al., 2019), breast cancer (Deng et al., 2018), colorectal cancer (Yang et al., 2017), and so on. Furthermore, it has been revealed that all-trans-retinoic acid (ATRA) could be a candidate drug for the treatment of gastric cancer patients with high SLC2A1 expression and resistance to conventional chemotherapy (Min et al., 2021).

A previous transcriptome profiling study demonstrated that neuroblastoma RAS viral oncogene homolog (NRAS) was dysregulated in fibrolamellar HCC, although the functions and clinical implications of NRAS were unknown (Sorenson et al., 2017). Another recent study found that NRAS and c-MYC are simultaneously upregulated by insulin-like growth factor II in HCC, but the specific function of NRAS was not investigated (Ji et al., 2017). Additionally, NRAS overexpression was related to

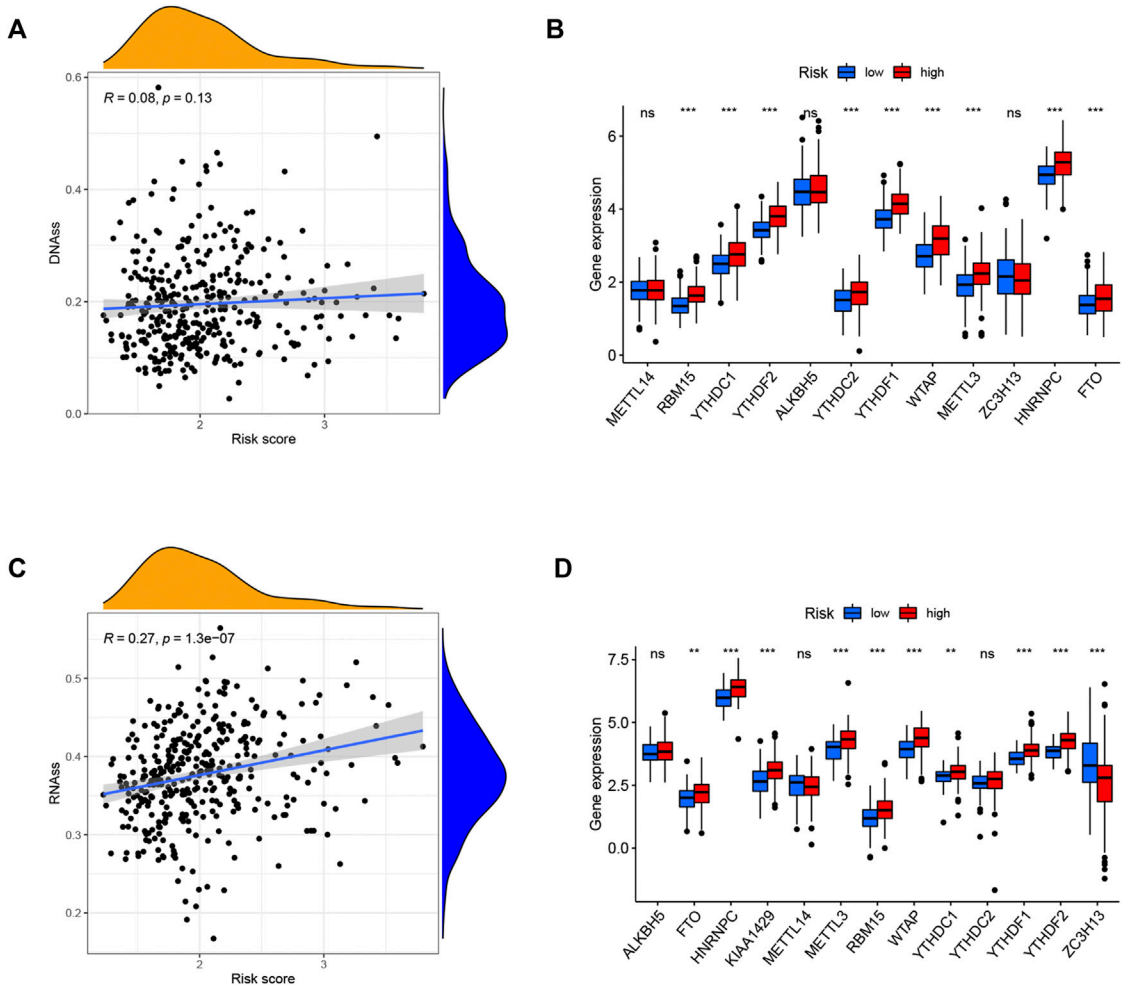

FIGURE 10 | Potential role of risk signature in HCC tumor stemness and m6A-related genes. Associations between risk signature and DNAss **(A)**, RNAss **(C)**. Comparison of the m6A-related genes between different risk groups in the TCGA cohort **(B)** and ICGC cohort **(D)**.

poor survival and proliferation *in vivo*. NRAS knockdown increased the efficacy of sorafenib in resistant cells and may be a promising prognostic predictor in HCC (Dietrich et al., 2019).

MAPK3, also called extracellular signal-regulated kinase-1 (ERK-1), is a protein that plays a critical part in the ERK signaling pathway. Specifically, it regulates cell proliferation, cycle, and apoptosis (McCubrey et al., 2007). Previous studies revealed that MAPK3 expression was upregulated in human HCC cells (Schmidt et al., 1997) and was related to drug resistance (Yan et al., 2009; Zhang et al., 2009). Similarly, Bendix and coauthors found that MAPK3 enabled the regulation of the activation of natural T cells by dendritic cells (DC) (Bendix et al., 2010).

Ribonucleotide reductase M2 subunit (RRM2) is a rate-limiting enzyme related to DNA synthesis and damage repair, which plays a momentous role in many crucial cellular processes including cell proliferation, invasiveness, migration, and angiogenesis (Nordlund and Reichard, 2006). It has been observed that the expression of RRM2 in HCC tissues was higher than that in normal tissues, and an anti-RRM2 siRNA duplex could inhibit proliferative activity in HCC (Gao et al., 2013). Moreover, Zhou and coauthors revealed that RRM2 overexpression was closely related to poor prognosis of HCC patients, and RRM2 was enriched in the p53 signaling pathway (Zhou et al., 2019b). RRM2 has been reported to be an independent predictor of early recurrence of HCC, indicating that RRM2 may facilitate tumor cells metastasis (Lee et al., 2014). According to recent reports, RRM2 could antagonize ferroptosis in liver cancer cells by sustaining glutathione (GSH) synthesis, which is a promising biomarker for the diagnosis of liver cancer (Yang et al., 2020a). Sorafenib is the first FDA-approved systemic molecular targeted therapy drug for advanced HCC, which can induce ferroptosis of cancer cells in HCC (Louandre et al., 2013). Interestingly, Yang and coworkers demonstrated that RRM2 overexpression partially rescues HCC cells from the cytotoxicity of sorafenib, and RRM2 is a novel target of sorafenib in HCC (Yang et al., 2020b).

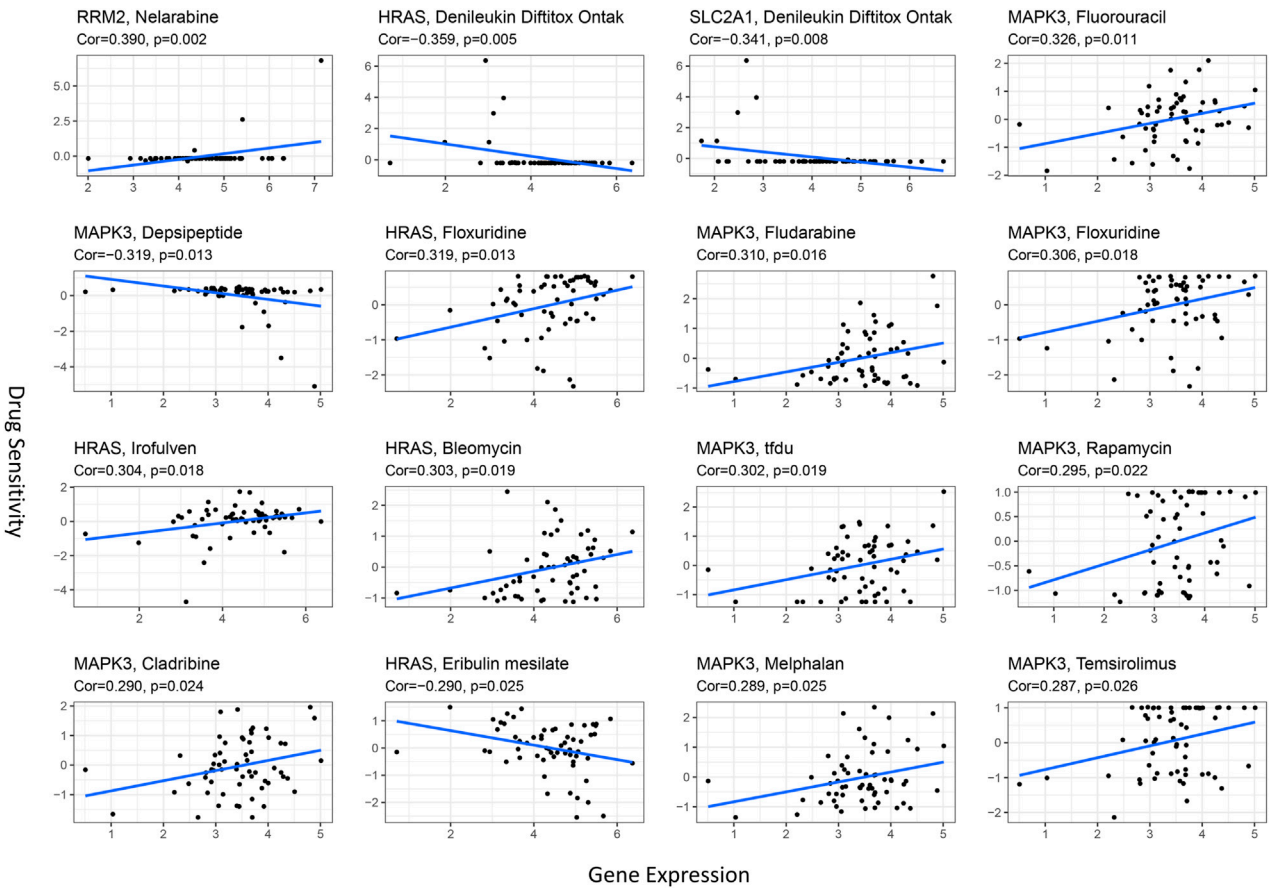

FIGURE 11 | Scatter plots for the association between prognostic hub gene expression in the model and drug sensitivity (top 16 ranked by *p*-value).

We further employed functional analysis and found that HCC-related biological processes such as nuclear division and the cell cycle were enriched. In addition, we found that the signature was significantly associated with immune cell infiltration and enriched in immunity-related pathways in HCC patients. In addition, we also found a substantial difference in TIP-related genes between high-risk and low-risk groups. Currently, cancer therapy has entered the era of immunity and iron (Tarangelo and Dixon, 2016; Jiang et al., 2019). Nanoparticles regulate iron and reactive oxygen species (ROS) levels to induce ferroptosis, providing a promising therapeutic strategy for cancer therapy (Xu et al., 2019). Immunotherapy has become a new criterion for treatment for advanced HCC worldwide (Wang and Wang, 2019). However, only a small proportion of HCC patients can respond to immunotherapies (Ramos-Casals et al., 2020), and the selection of available and suitable targets for individualized therapy remains a difficult problem for HCC patients. In our study, we also evaluated the correlation of the signature with response to immunotherapy. We discovered that PD-1 and CTLA-4 were dramatically upregulated in the high-risk group, indicating that immune checkpoint inhibitors could be more effective in HCC patients with the high-risk signature score. Although there are no available drugs or clinical trials targeting the identified hub genes at present, our findings suggest that ferroptosis may open a new chapter in the immunotherapy of tumors.

Cancer stem cell–like cells (CSCs) promote tumor growth due to their self-renewal and invasive abilities. In the current study, the risk signature was positively correlated with the stem cell score, confirming that our newly identified gene signature was a risk factor for HCC. M6A-related genes have also been an active area of recent tumor research (Liao et al., 2021). Our signature could accurately predict the expression levels of the m6A-related genes FTO, HNRNPC, METTL3, RBM15, WTAP, YTHDC1, YTHDF1, and YTHDF2 in HCC. However, the potential mechanisms of these relationships require further investigation.

Resistance of cancer cells to chemotherapy is a paramount challenge in cancer treatment. Ferroptosis inducers may provide new avenues to the problem of tumor drug resistance as they could overcome the disadvantages of traditional chemotherapeutic agents (Shen et al., 2018). Hence, we conducted drug sensitivity analysis and demonstrated that ferroptosis had a close correlation with chemotherapy resistance. Intriguingly, the results also provided a novel perspective that ferroptosis may be involved in some tumor-targeted therapy resistance.

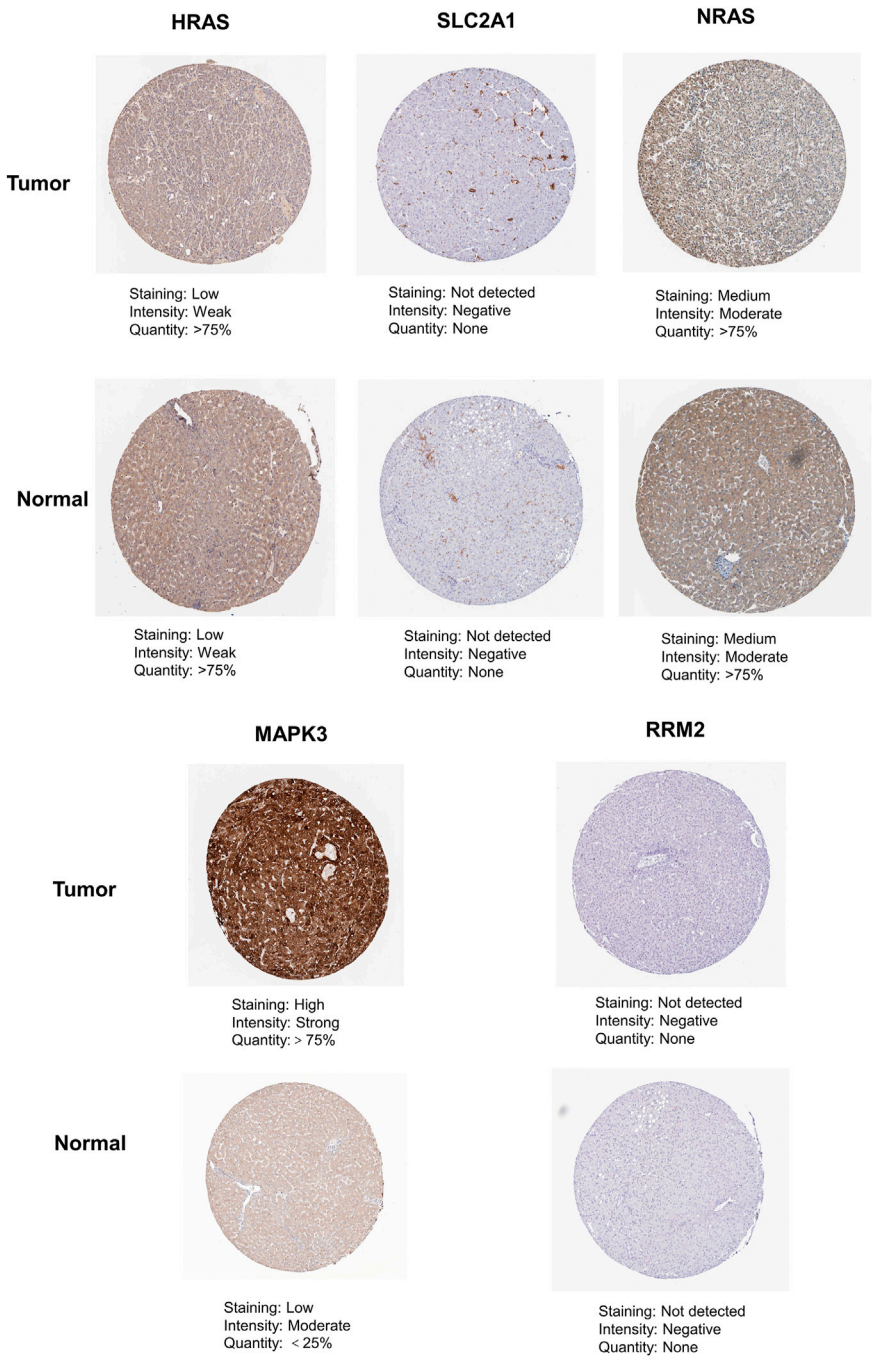

FIGURE 12 | The immunohistochemistry images of related hub genes from the HPA database in liver cancer tumor tissue and normal tissues.

However, many key issues such as the interrelation between ferroptosis and other cell deaths and host immunogenicity remain poorly understood. Therefore, our analysis offered new insights into the creation of effective clinical diagnostic and therapeutic strategies in HCC as well as a theoretical basis for future research. It is much less clear about the potential mechanisms between ferroptosis-related hub genes and tumor immunity in HCC and warrants further exploration.

Nevertheless, a few limitations of this study should be taken into consideration. First, we utilized retrospective data from public databases to construct and validate our prognostic model. Thus, some bias is unavoidable, and different cohorts are needed to validate its clinical utility henceforth. Second, the current study only included simple database analysis without any validation through experimental research to prove our conclusions. Therefore, the reliability of our results cannot be fully guaranteed.

CONCLUSION

In summary, our study established and verified a hub gene signature associated with ferroptosis that can precisely predict the prognosis of HCC patients. In addition, our proposed signature was closely associated with tumor immunity and drug resistance. Our study can not only provide innovative biomarkers for accessing HCC prognosis and uncover important evidence for future research on the mechanisms between ferroptosis-related hub genes and the immunity of liver cancer, but also offer new insights into drug resistance in liver cancer and can significantly guide improvements in the treatment of liver cancer.

DATA AVAILABILITY STATEMENT

The original contributions presented in the study are included in the article/Supplementary Material; further inquiries can be directed to the corresponding author.

AUTHOR CONTRIBUTIONS

WW contributed to conception, design, and data analysis of the study and wrote the manuscript. FP, XL, JY, and CT revised the manuscript and tables. RW reviewed and approved the final version of the manuscript. All the authors read and approved the final manuscript.

REFERENCES

Allemani, C., Matsuda, T., Di Carlo, V., Harewood, R., Matz, M., Nikšić, M., et al. (2018). Global Surveillance of Trends in Cancer Survival 2000-14 (CONCORD-3): Analysis of Individual Records for 37 513 025 Patients Diagnosed with One of 18 Cancers from 322 Population-Based Registries in 71 Countries. *Lancet* 391 (10125), 1023–1075. doi:10.1016/S0140-6736(17)33326-3

Anwanwan, D., Singh, S. K., Singh, S., Saikam, V., and Singh, R. (2020). Challenges in Liver Cancer and Possible Treatment Approaches. *Biochimica Biophysica Acta (BBA) - Rev. Cancer* 1873 (1), 188314. doi:10.1016/j.bbcan.2019.188314

Bendix, I., Pfueller, C. F., Leuenberger, T., Glezeva, N., Siffrin, V., Müller, Y., et al. (2010). MAPK3 Deficiency Drives Autoimmunity via DC Arming. *Eur. J. Immunol.* 40 (5), 1486–1495. doi:10.1002/eji.200939930

Cancer Genome Atlas Research Network (2017). Comprehensive and Integrative Genomic Characterization of Hepatocellular Carcinoma. *Cell.* 169 (7), 1327–e23. doi:10.1016/j.cell.2017.05.046

Chen, H.-L., OuYang, H.-Y., Le, Y., Jiang, P., Tang, H., Yu, Z.-S., et al. (2018). Aberrant MCT4 and GLUT1 Expression Is Correlated with Early Recurrence and Poor Prognosis of Hepatocellular Carcinoma after Hepatectomy. *Cancer Med.* 7 (11), 5339–5350. doi:10.1002/cam4.1521

Deng, Y., Zou, J., Deng, T., and Liu, J. (2018). Clinicopathological and Prognostic Significance of GLUT1 in Breast Cancer. *Med. Baltim.* 97 (48), e12961. doi:10.1097/MD.0000000000012961

Dietrich, P., Freese, K., Mahli, A., Thasler, W. E., Hellerbrand, C., and Bosserhoff, A. K. (2017). Combined Effects of PLK1 and RAS in Hepatocellular Carcinoma Reveal Rigosertib as Promising Novel Therapeutic "Dual-Hit" Option. *Oncotarget* 9 (3), 3605–3618. doi:10.18632/oncotarget.23188

Dietrich, P., Gaza, A., Wormser, L., Fritz, V., Hellerbrand, C., and Bosserhoff, A. K. (2019). Neuroblastoma RAS Viral Oncogene Homolog (NRAS) Is a Novel Prognostic Marker and Contributes to Sorafenib Resistance in Hepatocellular Carcinoma. *Neoplasia* 21 (3), 257–268. doi:10.1016/j.neo.2018.11.011

Dixon, S. J., Lemberg, K. M., Lamprecht, M. R., Skouta, R., Zaitsev, E. M., Gleason, C. E., et al. (2012). Ferroptosis: an Iron-dependent Form of Nonapoptotic Cell Death. *Cell.* 149 (5), 1060–1072. doi:10.1016/j.cell.2012.03.042

El-Khoueiry, A. B., Sangro, B., Yau, T., Crocenzi, T. S., Kudo, M., Hsu, C., et al. (2017). Nivolumab in Patients with Advanced Hepatocellular Carcinoma (CheckMate 040): an Open-Label, Non-comparative, Phase 1/2 Dose Escalation and Expansion Trial. *Lancet* 389 (10088), 2492–2502. doi:10.1016/S0140-6736(17)31046-2

Fu, H., Zhu, Y., Wang, Y., Liu, Z., Zhang, J., Xie, H., et al. (2018). Identification and Validation of Stromal Immunotype Predict Survival and Benefit from Adjuvant Chemotherapy in Patients with Muscle-Invasive Bladder Cancer. *Clin. Cancer Res.* 24 (13), 3069–3078. doi:10.1158/1078-0432.CCR-17-2687

Gao, J., Chen, H., Yu, Y., Song, J., Song, H., Su, X., et al. (2013). Inhibition of Hepatocellular Carcinoma Growth Using Immunoliposomes for Co-delivery of Adriamycin and Ribonucleotide Reductase M2 siRNA. *Biomaterials* 34 (38), 10084–10098. doi:10.1016/j.biomaterials.2013.08.088

Hassannia, B., Vandenabeele, P., and Vanden Berghe, T. (2019). Targeting Ferroptosis to Iron Out Cancer. *Cancer Cell.* 35 (6), 830–849. doi:10.1016/j.ccell.2019.04.002

Ji, Y., Wang, Z., Li, Z., Huang, N., Chen, H., Li, B., et al. (2017). Silencing IGF-II Impairs C-Myc and N-Ras Expressions of SMMC-7721 Cells via Suppressing FAK/PI3K/Akt Signaling Pathway. *Cytokine* 90, 44–53. doi:10.1016/j.cyto.2016.10.008

Jiang, Y., Han, Q.-J., and Zhang, J. (2019). Hepatocellular Carcinoma: Mechanisms of Progression and Immunotherapy. *Wjg* 25 (25), 3151–3167. doi:10.3748/wjg.v25.i25.3151

Jin, B., Wang, W., Du, G., Huang, G. Z., Han, L. T., Tang, Z. Y., et al. (2015). Identifying Hub Genes and Dysregulated Pathways in Hepatocellular Carcinoma. *Eur. Rev. Med. Pharmacol. Sci.* 19 (4), 592

Lee, B., Ha, S. Y., Song, D. H., Lee, H. W., Cho, S. Y., and Park, C.-K. (2014). High Expression of Ribonucleotide Reductase Subunit M2 Correlates with Poor Prognosis of Hepatocellular Carcinoma. *Gut Liver* 8 (6), 662–668. doi:10.5009/gnl13392

Li, S., Yang, F., and Ren, X. (2015). Immunotherapy for Hepatocellular Carcinoma. *DD&T* 9 (5), 363–371. doi:10.5582/ddt.2015.01054

Liang, C., Zhang, X., Yang, M., and Dong, X. (2019). Recent Progress in Ferroptosis Inducers for Cancer Therapy. *Adv. Mat.* 31 (51), 1904197. doi:10.1002/adma.201904197

Liang, J.-y., Wang, D.-s., Lin, H.-c., Chen, X.-x., Yang, H., Zheng, Y., et al. (2020). A Novel Ferroptosis-Related Gene Signature for Overall Survival Prediction in Patients with Hepatocellular Carcinoma. *Int. J. Biol. Sci.* 16 (13), 2430–2441. doi:10.7150/ijbs.45050

Liao, Y., Han, P., Zhang, Y., and Ni, B. (2021). Physio-pathological Effects of m6A Modification and its Potential Contribution to Melanoma. *Clin. Transl. Oncol.* 23 (11), 2269–2279. doi:10.1007/s12094-021-02644-3

Liu, X., and Qin, S. (2019). Immune Checkpoint Inhibitors in Hepatocellular Carcinoma: Opportunities and Challenges. *Oncologist* 24 (Suppl. 1), S3–S10. doi:10.1634/theoncologist.2019-IO-S1-s01

Llovet, J. M., Montal, R., Sia, D., and Finn, R. S. (2018). Molecular Therapies and Precision Medicine for Hepatocellular Carcinoma. *Nat. Rev. Clin. Oncol.* 15 (10), 599–616. doi:10.1038/s41571-018-0073-4

Louandre, C., Ezzoukhry, Z., Godin, C., Barbare, J.-C., Mazière, J.-C., Chauffert, B., et al. (2013). Iron-dependent Cell Death of Hepatocellular Carcinoma Cells Exposed to Sorafenib. *Int. J. Cancer* 133 (7), 1732–1742. doi:10.1002/ijc.28159

McCubrey, J. A., Steelman, L. S., Chappell, W. H., Abrams, S. L., Wong, E. W. T., Chang, F., et al. (2007). Roles of the Raf/MEK/ERK Pathway in Cell Growth, Malignant Transformation and Drug Resistance. *Biochimica Biophysica Acta (BBA) - Mol. Cell. Res.* 1773 (8), 1263–1284. doi:10.1016/j.bbamcr.2006.10.001

Min, K.-W., Kim, D.-H., Son, B. K., Moon, K. M., Kim, S. M., Intazur Rahaman, M., et al. (2021). High SLC2A1 Expression Associated with Suppressing CD8 T Cells and B Cells Promoted Cancer Survival in Gastric Cancer. *PLoS One* 16 (3), e0245075. doi:10.1371/journal.pone.0245075

Nagarsheth, N., Wicha, M. S., and Zou, W. (2017). Chemokines in the Cancer Microenvironment and Their Relevance in Cancer Immunotherapy. *Nat. Rev. Immunol.* 17 (9), 559–572. doi:10.1038/nri.2017.49

Nie, J., Lin, B., Zhou, M., Wu, L., and Zheng, T. (2018). Role of Ferroptosis in Hepatocellular Carcinoma. *J. Cancer Res. Clin. Oncol.* 144 (12), 2329–2337. doi:10.1007/s00432-018-2740-3

Nordlund, P., and Reichard, P. (2006). Ribonucleotide Reductases. *Annu. Rev. Biochem.* 75, 681–706. doi:10.1146/annurev.biochem.75.103004.142443

Perez, M. A., Magtanong, L., Dixon, S. J., and Watts, J. L. (2020). Dietary Lipids Induce Ferroptosis in Caenorhabditiselegans and Human Cancer Cells. *Dev. Cell.* 54 (4), 447–454. doi:10.1016/j.devcel.2020.06.019

Qin, S., Ren, Z., Meng, Z., Chen, Z., Chai, X., Xiong, J., et al. (2020). Camrelizumab in Patients with Previously Treated Advanced Hepatocellular Carcinoma: a Multicentre, Open-Label, Parallel-Group, Randomised, Phase 2 Trial. *Lancet Oncol.* 21 (4), 571–580. doi:10.1016/S1470-2045(20)30011-5

Ramos-Casals, M., Brahmer, J. R., Callahan, M. K., Flores-Chávez, A., Keegan, N., Khamashta, M. A., et al. (2020). Immune-Related Adverse Events of Checkpoint Inhibitors. *Nat. Rev. Dis. Prim.* 6 (1), 38. doi:10.1038/s41572-020-0160-6

Ritchie, M. E., Phipson, B., Wu, D., Hu, Y., Law, C. W., Shi, W., et al. (2015). Limma Powers Differential Expression Analyses for RNA-Sequencing and Microarray Studies. *Nucleic Acids Res.* 43 (7), e47. doi:10.1093/nar/gkv007

Rooney, M. S., Shukla, S. A., Wu, C. J., Getz, G., and Hacohen, N. (2015). Molecular and Genetic Properties of Tumors Associated with Local Immune Cytolytic Activity. *Cell.* 160 (1-2), 48–61. doi:10.1016/j.cell.2014.12.033

Schmidt, C. M., McKillop, I. H., Cahill, P. A., and Sitzmann, J. V. (1997). Increased MAPK Expression and Activity in Primary Human Hepatocellular Carcinoma. *Biochem. Biophysical Res. Commun.* 236 (1), 54–58. doi:10.1006/bbrc.1997.6840

Shen, J., Tsoi, H., Liang, Q., Chu, E. S. H., Liu, D., Yu, A. C.-S., et al. (2016). Oncogenic Mutations and Dysregulated Pathways in Obesity-Associated Hepatocellular Carcinoma. *Oncogene* 35 (49), 6271–6280. doi:10.1038/onc.2016.162

Shen, Z., Song, J., Yung, B. C., Zhou, Z., Wu, A., and Chen, X. (2018). Emerging Strategies of Cancer Therapy Based on Ferroptosis. *Adv. Mat.* 30, 1704007. doi:10.1002/adma.201704007

Simon, N., Friedman, J., Hastie, T., and Tibshirani, R. (2011). Regularization Paths for Cox's Proportional Hazards Model via Coordinate Descent. *J. Stat. Soft.* 39, 1–13. doi:10.18637/jss.v039.i05

Song, X., Liu, J., Kuang, F., Chen, X., Zeh, H. J., 3rd, Kang, R., et al. (2021). PDK4 Dictates Metabolic Resistance to Ferroptosis by Suppressing Pyruvate Oxidation and Fatty Acid Synthesis. *Cell. Rep.* 34 (8), 108767. doi:10.1016/j.celrep.2021.108767

Sorenson, E. C., Khanin, R., Bamboat, Z. M., Cavnar, M. J., Kim, T. S., Sadot, E., et al. (2017). Genome and Transcriptome Profiling of Fibrolamellar Hepatocellular Carcinoma Demonstrates P53 and IGF2BP1 Dysregulation. *PLoS One* 12 (5), e0176562. doi:10.1371/journal.pone.0176562

Sui, S., An, X., Xu, C., Li, Z., Hua, Y., Huang, G., et al. (2020). An Immune Cell Infiltration-Based Immune Score Model Predicts Prognosis and Chemotherapy Effects in Breast Cancer. *Theranostics* 10 (26), 11938–11949. doi:10.7150/thno.49451

Sung, H., Ferlay, J., Siegel, R. L., Laversanne, M., Soerjomataram, I., Jemal, A., et al. (2021). Global Cancer Statistics 2020: GLOBOCAN Estimates of Incidence and Mortality Worldwide for 36 Cancers in 185 Countries. *CA A Cancer J. Clin.* 71 (3), 209–249. doi:10.3322/caac.21660

Szklarczyk, D., Gable, A. L., Lyon, D., Junge, A., Wyder, S., Huerta-Cepas, J., et al. (2019). STRING V11: Protein-Protein Association Networks with Increased Coverage, Supporting Functional Discovery in Genome-wide Experimental Datasets. *Nucleic Acids Res.* 47 (D1), D607–D613. doi:10.1093/nar/gky1131

Tang, B., Zhu, J., Li, J., Fan, K., Gao, Y., Cheng, S., et al. (2020). The Ferroptosis and Iron-Metabolism Signature Robustly Predicts Clinical Diagnosis, Prognosis and Immune Microenvironment for Hepatocellular Carcinoma. *Cell. Commun. Signal* 18 (1), 174. doi:10.1186/s12964-020-00663-1

Tang, D., Kang, R., Berghe, T. V., Vandenabeele, P., and Kroemer, G. (2019). The Molecular Machinery of Regulated Cell Death. *Cell. Res.* 29, 347–364. doi:10.1038/s41422-019-0164-5

Tang, Y., Li, C., Zhang, Y.-J., and Wu, Z.-H. (2021). Ferroptosis-Related Long Non-coding RNA Signature Predicts the Prognosis of Head and Neck Squamous Cell Carcinoma. *Int. J. Biol. Sci.* 17 (3), 702–711. doi:10.7150/ijbs.55552

Tarangelo, A., and Dixon, S. J. (2016). An Iron Age for Cancer Therapy. *Nat. Nanotech* 11 (11), 921–922. doi:10.1038/nnano.2016.199

Tibshirani, R. (1997). The Lasso Method for Variable Selection in the Cox Model. *Stat. Med.* 16 (4), 385–395. doi:10.1002/(sici)1097-0258(19970228)16:4<385:aid-sim380>3.0.co

Uhlén, M., Fagerberg, L., Hallström, B. M., Lindskog, C., Oksvold, P., Mardinoglu, A., et al. (2015). Tissue-based Map of the Human Proteome. *Science* 347 (6220), 1260419. doi:10.1126/science.1260419

Uhlen, M., Zhang, C., Lee, S., Sjöstedt, E., Fagerberg, L., Bidkhori, G., et al. (2017). A Pathology Atlas of the Human Cancer Transcriptome. *Science* 357 (6352), eaan2507. doi:10.1126/science.aan2507

Wan, S., Lei, Y., Li, M., and Wu, B. (2022). A Prognostic Model for Hepatocellular Carcinoma Patients Based on Signature Ferroptosis-Related Genes. *Hepatol. Int.* 16 (1), 112–124. doi:10.1007/s12072-021-10248-w

Wang, H., Li, S., Wang, Q., Jin, Z., Shao, W., Gao, Y., et al. (2021). Tumor Immunological Phenotype Signature-Based High-Throughput Screening for the Discovery of Combination Immunotherapy Compounds. *Sci. Adv.* 7 (4), eabd7851. doi:10.1126/sciadv.abd7851

Wang, L., and Wang, F.-S. (2019). Clinical Immunology and Immunotherapy for Hepatocellular Carcinoma: Current Progress and Challenges. *Hepatol. Int.* 13 (5), 521–533. doi:10.1007/s12072-019-09967-y

Wang, S., Zhang, Q., Yu, C., Cao, Y., Zuo, Y., and Yang, L. (2020). Immune Cell Infiltration-Based Signature for Prognosis and Immunogenomic Analysis in Breast Cancer. *Brief. Bioinform* 22 (2), 2020–2031. doi:10.1093/bib/bbaa026

Wang, T., Kong, S., Tao, M., and Ju, S. (2020). The Potential Role of RNA N6-Methyladenosine in Cancer Progression. *Mol. Cancer* 19 (1), 88. doi:10.1186/s12943-020-01204-7

Wang, W., Green, M., Choi, J. E., Gijón, M., Kennedy, P. D., Johnson, J. K., et al. (2019). CD8+ T Cells Regulate Tumour Ferroptosis during Cancer Immunotherapy. *Nature* 569, 270–274. doi:10.1038/s41586-019-1170-y

Xu, T., Ding, W., Ji, X., Ao, X., Liu, Y., Yu, W., et al. (2019). Molecular Mechanisms of Ferroptosis and its Role in Cancer Therapy. *J. Cell. Mol. Med.* 23 (8), 4900–4912. doi:10.1111/jcmm.14511

Yan, F., Wang, X.-M., Pan, C., and Ma, Q.-M. (2009). Down-regulation of Extracellular Signal-Regulated Kinase 1/2 Activity in P-Glycoprotein-Mediated Multidrug Resistant Hepatocellular Carcinoma Cells. *Wjg* 15 (12), 1443–1451. doi:10.3748/wjg.15.1443

Yang, J. D., Hainaut, P., Gores, G. J., Amadou, A., Plymoth, A., and Roberts, L. R. (2019). A Global View of Hepatocellular Carcinoma: Trends, Risk, Prevention and Management. *Nat. Rev. Gastroenterol. Hepatol.* 16 (10), 589–604. doi:10.1038/s41575-019-0186-y

Yang, J., Wen, J., Tian, T., Lu, Z., Wang, Y., Wang, Z., et al. (2017). GLUT-1 Overexpression as an Unfavorable Prognostic Biomarker in Patients with Colorectal Cancer. *Oncotarget* 8 (7), 11788–11796. doi:10.18632/oncotarget.14352

Yang, P.-M., Lin, L.-S., and Liu, T.-P. (2020). Sorafenib Inhibits Ribonucleotide Reductase Regulatory Subunit M2 (RRM2) in Hepatocellular Carcinoma Cells. *Biomolecules* 10 (1), 117. doi:10.3390/biom10010117

Yang, Y., Lin, J., Guo, S., Xue, X., Wang, Y., Qiu, S., et al. (2020). RRM2 Protects against Ferroptosis and Is a Tumor Biomarker for Liver Cancer. *Cancer Cell. Int.* 20 (1), 587. doi:10.1186/s12935-020-01689-8

Yu, J., and Wang, J.-q. (2021). Research Mechanisms of and Pharmaceutical Treatments for Ferroptosis in Liver Diseases. *Biochimie* 180, 149–157. doi:10.1016/j.biochi.2020.11.002

Zhang, B., Xie, Z., and Li, B. (2019). The Clinicopathologic Impacts and Prognostic Significance of GLUT1 Expression in Patients with Lung Cancer: A Meta-Analysis. *Gene* 689, 76–83. doi:10.1016/j.gene.2018.12.006

Zhang, Z., Zhou, X., Shen, H., Wang, D., and Wang, Y. (2009). Phosphorylated ERK Is a Potential Predictor of Sensitivity to Sorafenib when Treating Hepatocellular Carcinoma: Evidence from an in Vitrostudy. *BMC Med.* 7, 41. doi:10.1186/1741-7015-7-41

Zhao, Z., Cai, Q., Zhang, P., He, B., Peng, X., Tu, G., et al. (2021). N6-Methyladenosine RNA Methylation Regulator-Related Alternative Splicing (AS) Gene Signature Predicts Non-small Cell Lung Cancer Prognosis. *Front. Mol. Biosci.* 8, 657087. doi:10.3389/fmolb.2021.657087

Zhou, R., Zhang, J., Zeng, D., Sun, H., Rong, X., Shi, M., et al. (2019). Immune Cell Infiltration as a Biomarker for the Diagnosis and Prognosis of Stage I-Iii Colon Cancer. *Cancer Immunol. Immunother.* 68 (3), 433–442. doi:10.1007/s00262-018-2289-7

Zhou, Z., Li, Y., Hao, H., Wang, Y., Zhou, Z., Wang, Z., et al. (2019). Screening Hub Genes as Prognostic Biomarkers of Hepatocellular Carcinoma by Bioinformatics Analysis. *Cell. Transpl.* 28 (1_Suppl. l), 76S–86S. doi:10.1177/0963689719893950

Zongyi, Y., and Xiaowu, L. (2020). Immunotherapy for Hepatocellular Carcinoma. *Cancer Lett.* 470, 8–17. doi:10.1016/j.canlet.2019.12.002

Conflict of Interest: The authors declare that the research was conducted in the absence of any commercial or financial relationships that could be construed as a potential conflict of interest.

Publisher's Note: All claims expressed in this article are solely those of the authors and do not necessarily represent those of their affiliated organizations, or those of the publisher, the editors, and the reviewers. Any product that may be evaluated in this article, or claim that may be made by its manufacturer, is not guaranteed or endorsed by the publisher.

Copyright © 2022 Wang, Pan, Lin, Yuan, Tao and Wang. This is an open-access article distributed under the terms of the Creative Commons Attribution License (CC BY). The use, distribution or reproduction in other forums is permitted, provided the original author(s) and the copyright owner(s) are credited and that the original publication in this journal is cited, in accordance with accepted academic practice. No use, distribution or reproduction is permitted which does not comply with these terms.

frontiers | Frontiers in Genetics

ORIGINAL RESEARCH
published: 25 July 2022
doi: 10.3389/fgene.2022.900713

Establishment of a Necroptosis-Related Prognostic Signature to Reveal Immune Infiltration and Predict Drug Sensitivity in Hepatocellular Carcinoma

Huili Ren[1], *Jianglin Zheng*[2], *Qi Cheng*[3], *Xiaoyan Yang*[1,4] *and Qin Fu*[1,4]*

[1]Department of Pharmacology, School of Basic Medicine, Tongji Medical College, Huazhong University of Science and Technology, Wuhan, China, [2]Department of Neurosurgery, Union Hospital, Tongji Medical College, Huazhong University of Science and Technology, Wuhan, China, [3]Hepatic Surgery Center, Tongji Hospital, Tongji Medical College, Huazhong University of Science and Technology, Wuhan, China, [4]Key Laboratory for Drug Target Research and Pharmacodynamic Evaluation of Hubei Province, Wuhan, China

Background: Hepatocellular carcinoma (HCC) is a common type of primary liver cancer and has a poor prognosis. In recent times, necroptosis has been reported to be involved in the progression of multiple cancers. However, the role of necroptosis in HCC prognosis remains elusive.

Methods: The RNA-seq data and clinical information of HCC patients were downloaded from The Cancer Genome Atlas (TCGA) and International Cancer Genome Consortium (ICGC) databases. Differentially expressed genes (DEGs) and prognosis-related genes were explored, and the nonnegative matrix factorization (NMF) clustering algorithm was applied to divide HCC patients into different subtypes. Based on the prognosis-related DEGs, univariate Cox and LASSO Cox regression analyses were used to construct a necroptosis-related prognostic model. The relationship between the prognostic model and immune cell infiltration, tumor mutational burden (TMB), and drug response were explored.

Results: In this study, 13 prognosis-related DEGs were confirmed from 18 DEGs and 24 prognostic-related genes. Based on the prognosis-related DEGs, patients in the TCGA cohort were clustered into three subtypes by the NMF algorithm, and patients in C3 had better survival. A necroptosis-related prognostic model was established according to LASSO analysis, and HCC patients in TCGA and ICGC were divided into high- and low-risk groups. Kaplan–Meier (K–M) survival analysis revealed that patients in the high-risk group had a shorter survival time compared to those in the low-risk group. Using univariate and multivariate Cox analyses, the prognostic model was identified as an independent prognostic factor and had better survival predictive ability in HCC patients compared with other clinical biomarkers. Furthermore, the results revealed that the high-risk patients had higher stromal, immune, and ESTIMATE scores; higher TP53 mutation rate; higher TMB; and lower tumor purities compared to those in the low-risk group. In addition, there were significant differences in predicting the drug response between the high- and low-risk

OPEN ACCESS

Edited by:
Le-Le Zhang,
Chengdu University, China

Reviewed by:
Xiaoming Jiang,
Zhejiang University, China
Jie Yu,
Wuhan Polytechnic University, China

***Correspondence:**
Qin Fu
fuqin@mails.tjmu.edu.cn

Specialty section:
This article was submitted to Cancer Genetics and Oncogenomics, a section of the journal Frontiers in Genetics

Received: *21 March 2022*
Accepted: *17 June 2022*
Published: *25 July 2022*

Citation:
Ren H, Zheng J, Cheng Q, Yang X and Fu Q (2022) Establishment of a Necroptosis-Related Prognostic Signature to Reveal Immune Infiltration and Predict Drug Sensitivity in Hepatocellular Carcinoma. Front. Genet. 13:900713. doi: 10.3389/fgene.2022.900713

groups. The protein and mRNA levels of these prognostic genes were upregulated in HCC tissues compared to normal liver tissues.

Conclusion: We established a necroptosis-related prognostic signature that may provide guidance for individualized drug therapy in HCC patients; however, further experimentation is needed to validate our results.

Keywords: hepatocellular carcinoma, necroptosis, prognostic, immune microenvironment, chemosensitivity

INTRODUCTION

Hepatocellular carcinoma (HCC) is the second mortality malignancy globally (Sung et al., 2021). Chemotherapy and molecular targeted therapies are the treatment modalities for patients with advanced HCC (Daher et al., 2018; Medavaram and Zhang, 2018), but the 5-year survival rate of patients is still low. The poor prognosis of HCC is mainly related to tumor heterogeneity, metastasis, recurrence, drug resistance, and the lack of predictive biomarkers in response to the treatment (Llovet et al., 2012; Llovet et al., 2015; Faivre et al., 2020). Thus, it is necessary to exploit novel therapeutic targets and reliable prognostic models for medical decision making.

Necroptosis, a form of programmed inflammatory cell death, was originally discovered as a form of cell death independent of caspase (Degterev et al., 2005). The canonical necroptotic pathway was triggered by tumor necrosis factor receptor (TNFR) family proteins, toll-like receptor 3 (TLR3)/TLR4, and lipopolysaccharide (LPS) (Yan et al., 2022). Thereafter, receptor-interacting serine/threonine-protein kinase 3 (RIPK3) is recruited and phosphorylated by RIPK1 in the absence of caspase-8, which is then phosphorylated by MLKL. Phosphorylation of MLKL leads to its oligomerization, and then translocate to cell membrane and form large pores that lead to necroptotic cell death by allowing ion influx, membrane lysis, followed by the uncontrollable release of intracellular material (Sun et al., 2012; Zhao et al., 2012). In recent times, necroptosis has been found to be involved in tumorigenesis, tumor progression, metastasis, and tumoral immune response (Hitomi et al., 2008; Yatim et al., 2015; Jiao et al., 2018). However, the exact function of necroptosis in tumor remains debatable. Findings imply that the exact role of necroptosis is dependent on the type of cancer and the different stages of disease development. The key molecular RIPK3 of necroptosis is required for tumorigenesis, such as in breast tumors (Lin et al., 2020). Inhibition the signal pathway by silence RIPK3 or suppresses the activity of RIPK3 may abolish inflammatory responses which is critical in modulating tumor initiation and progression (Seifert et al., 2016; Jayakumar and Bothwell, 2019). While necroptosis may also have tumor-suppressive properties. For acute myeloid leukemia, downregulation of RIPK3 is associated with poor survival (Najafov et al., 2017). For HCC, necroptosis inhibition may enhance the accumulation polarization of M2 TAMs, contributing to tumorigenesis (Wu et al., 2020) and sorafenib resistance (Liao et al., 2021). The mRNA level of RIPK3 might be a biomarker in tumor progression (Han et al., 2020).

However, the role of necroptosis in HCC prognosis is still unclear. In this study, we focused on the genes related to necroptosis regulation and constructed a prognostic model based on necroptosis-related genes (NRGs). Furthermore, we explored the relationship between prognosis and immune profiles, tumor mutational burden (TMB), and applications in predicting drug sensitivity. Our findings provide some new ideas for the diagnosis and treatment of HCC.

MATERIALS AND METHODS

Data Collection and Preprocessing

The mRNA sequencing (FPKM) data and corresponding clinical information of HCC patients were downloaded from The Cancer Genome Atlas (TCGA; /https://portal.gdc.cancer.gov/repository; including 370 HCC tissue samples and 50 adjacent normal tissue samples) and International Cancer Genome Consortium (ICGC; https://dcc.icgc.org/projects/LIRI-JP; including 231 HCC samples). The gene expression profiles were normalized using the Perl language (http://www.perl.org/). The clinicopathological characteristics of HCC patients in TCGA and ICGC cohorts were summarized in **Table 1**. A total of 69 NRGs were collected from prior studies (**Supplementary Table S1**).

Identification of Differentially Expressed and Prognosis-Related Necroptosis Genes

DEGs in tumor tissues and normal tissues were analyzed using the "limma" package in Bioconductor in the R software (version 4.1.0). DEGs were identified based on the following criteria: false discovery rate (FDR) < 0.05 and a log2 fold change >1. Univariate

TABLE 1 | Characteristics of hepatocellular carcinoma (HCC) patients in the training and validation cohorts.

Characteristics		Training cohort TCGA (*n* = 370)	Validation cohort ICGC (*n* = 231)
Age	≤65	232	90
	>65	138	141
Gender	Female	121	61
	Male	249	170
WHO grade	G1–2	232	—
	G3–4	133	—
	Unknown	5	—
TNM stage	I–II	256	141
	III–IV	90	90
	Unknown	34	—

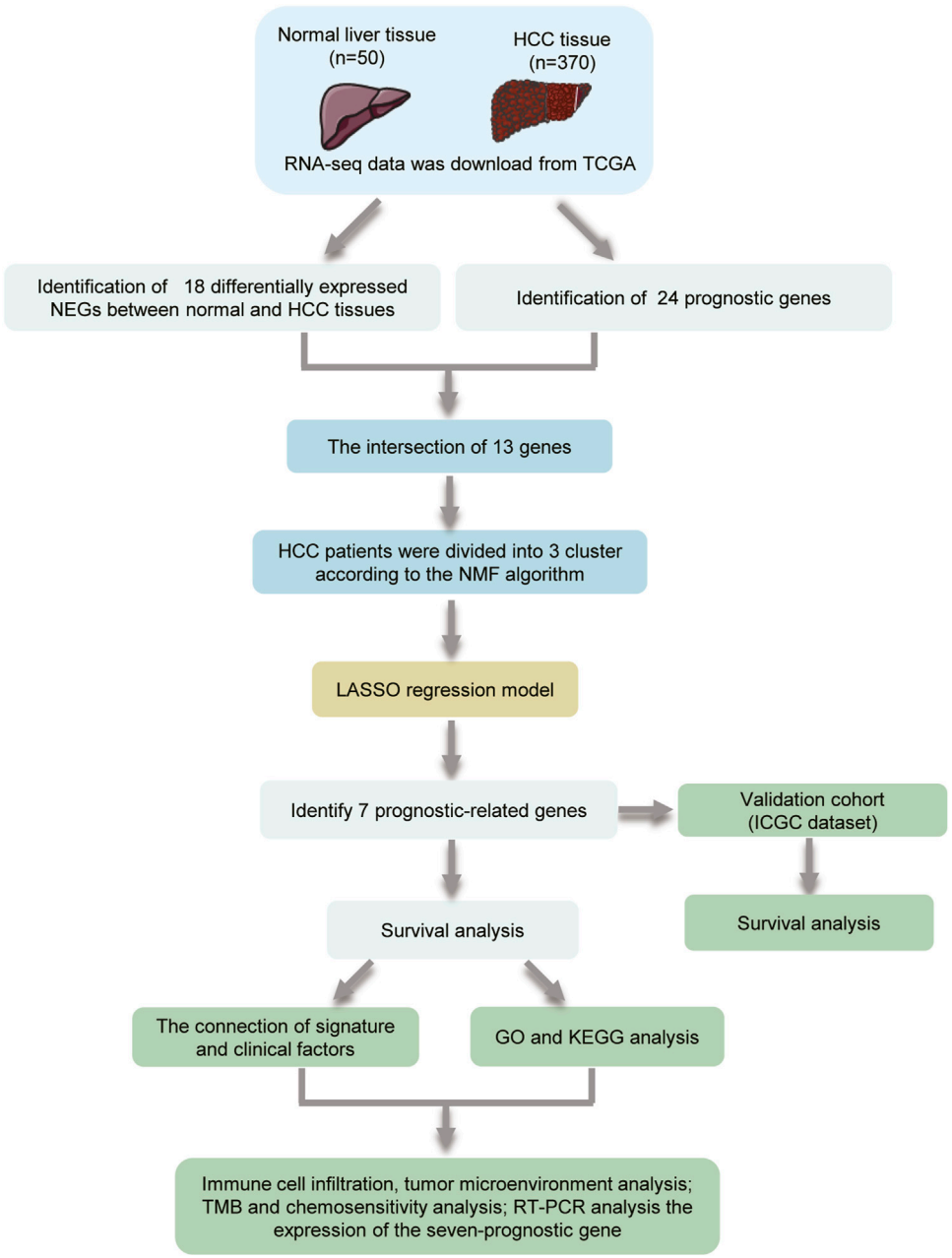

FIGURE 1 | Flowchart showing the scheme of the study.

analysis was applied in estimating the prognosis-related genes from the 69 NRGs. To analyze the correlation among the DEGs, a protein–protein interaction (PPI) network was built using the STRING (http://string-db.org/cgi/) online tool and the interaction score >0.2 was chosen as the cutoff criterion.

Molecular Subtype Identification

We extracted the expression profiles of prognostic DEGs from the TCGA and ICGC databases. Thereafter, the nonnegative matrix factorization (NMF) clustering algorithm was used to cluster the HCC samples, the standard "brunet" option was selected, and 50 iterations were carried out. The number of clusters k was set to 2–10. According to indexes, including cophenetic, dispersion, and silhouette, the optimal number of clusters was finally determined. Kaplan–Meier (KM) survival curves were analyzed to compare the difference in survival rates among different groups.

Construction of the Necroptosis-Related Gene Prognostic Model

The TCGA cohort was selected as the training cohort to construct the prognostic model. Univariate Cox analysis was applied to

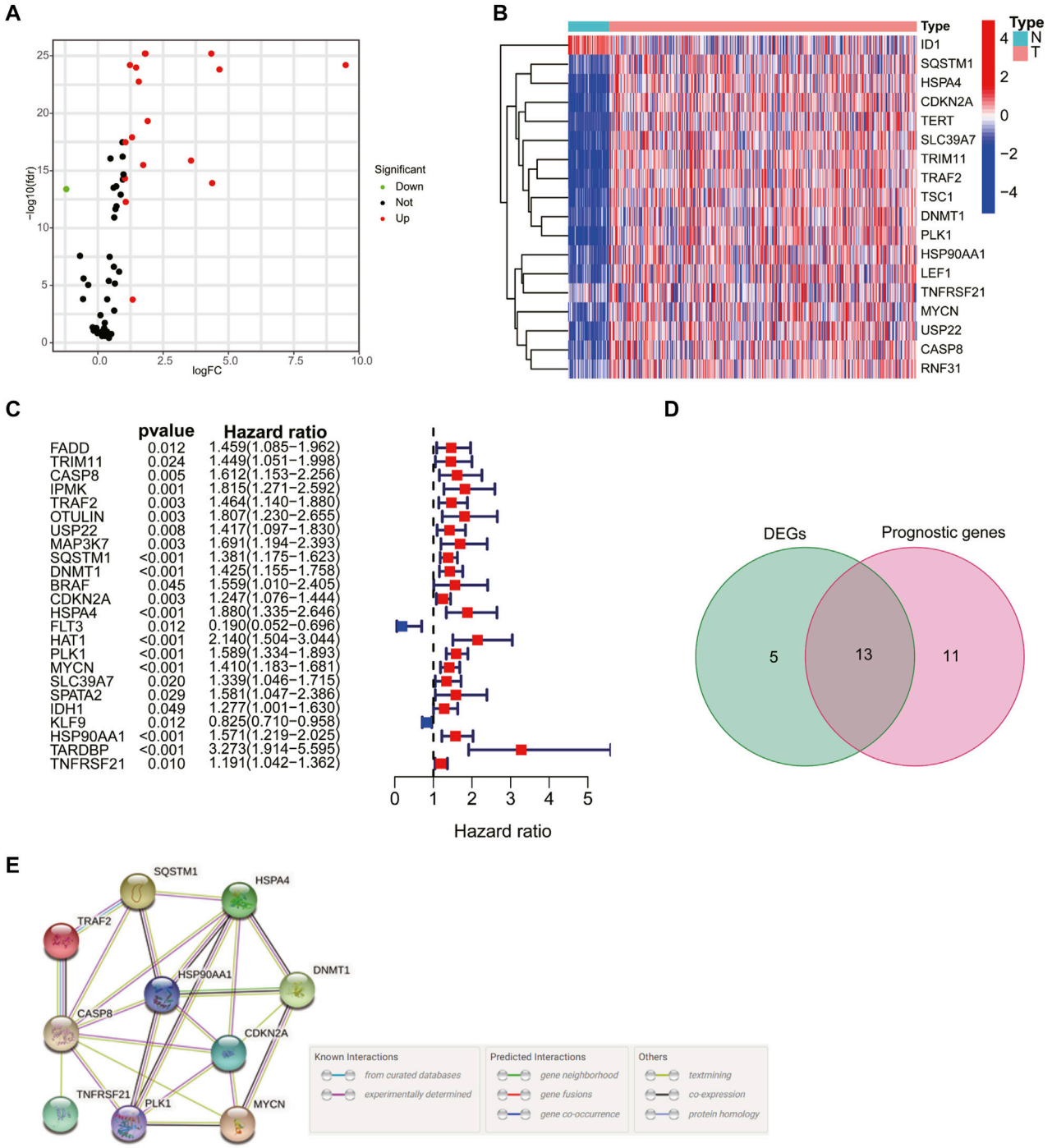

FIGURE 2 | Identification of prognosis-related genes in hepatocellular carcinoma (HCC) patients. Volcano plot **(A)** and heatmap **(B)** of 18 differentially expressed necroptosis-related genes (NRGs). **(C)** Univariate Cox regression analysis of prognosis-related genes. **(D)** Venn plot showing the 13 intersection genes. **(E)** Protein–protein interaction network of the interactions among intersection genes.

identify the NRGs that were significantly associated with HCC prognosis. Then, LASSO Cox regression analysis based on the "glmnet" R package was used to construct the prognostic signature. In time, the seven genes and their coefficients were retained, and the minimum criteria determined the penalty parameter (λ). The risk score of individual patients was also counted. Based on the median risk score value, the HCC patients in the TCGA and ICGC cohorts were divided into high- and low-risk groups, and ROC curves were utilized to predict the accuracy of prognostic signatures. Moreover, principal component analysis (PCA) and

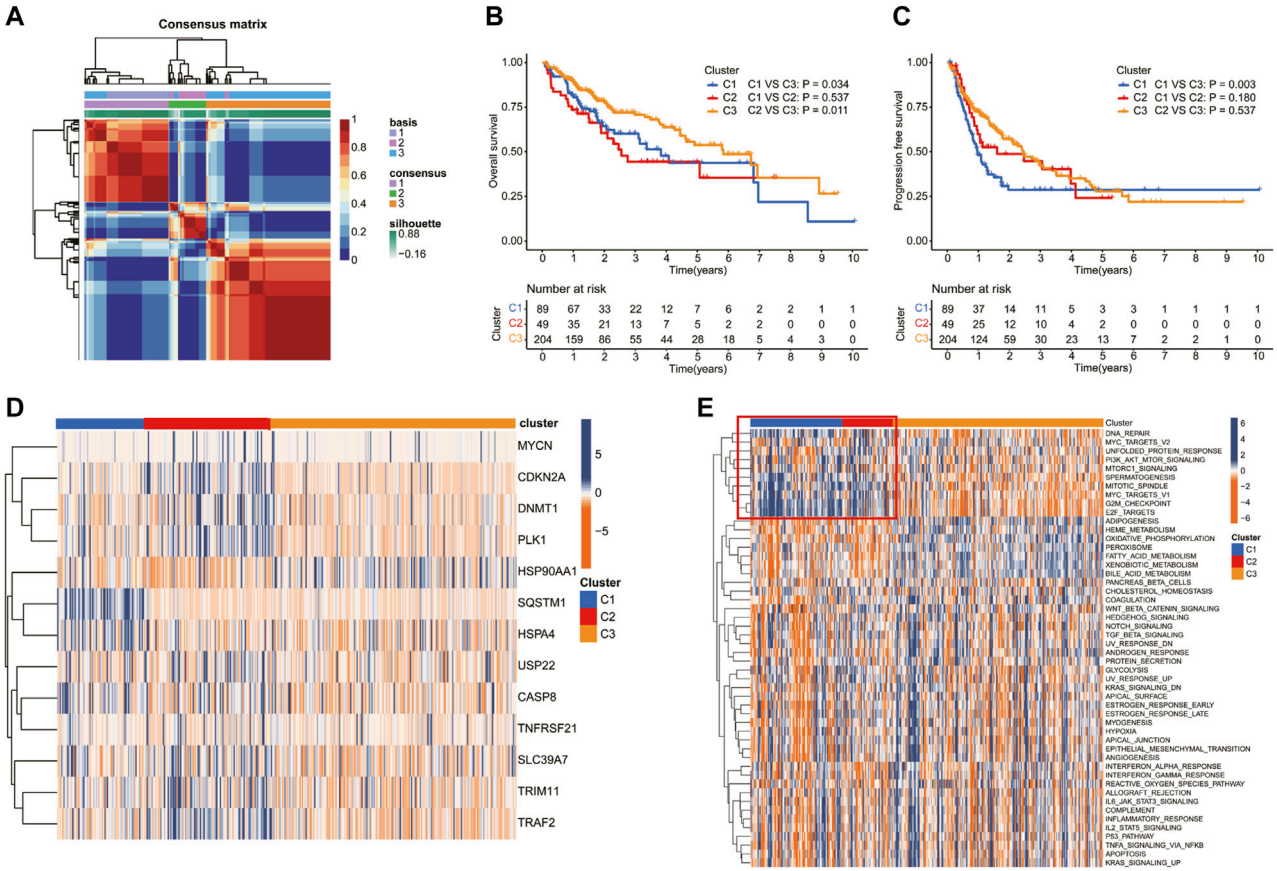

FIGURE 3 | Screening of molecular subgroups through the nonnegative matrix factorization (NMF) cluster. **(A)** Consensus map of NMF clustering. The Kaplan–Meier (K–M) analysis of **(B)** overall survival and **(C)** progression-free survival for patients in different clusters. **(D)** Heatmap of the NRG expression of the molecular subtypes. **(E)** Heatmap showed the ssGSEA Z-scores of 50 hallmarks among the three clusters.

the T-distributed stochastic neighbor embedding (t-SNE)-based approach were adopted to validate the subtype assignments.

Univariate and Multivariate Cox Regression Analysis

Univariate analysis was applied for estimating the associations between prognosis and age, gender, grade, stage, and risk score. Thereafter, multivariate analysis was presented for observing whether these factors were independently predictive of the prognosis of hepatocellular carcinoma. Hazard ratio (HR), 95% confidence interval (CI), and *p*-values were separately determined.

Gene Ontology and the Kyoto Encyclopedia of Genes and Genomes Analyses

Gene Ontology (GO) and Kyoto Encyclopedia of Genes and Genomes (KEGG) pathway functional enrichment analyses were conducted using cluster Profiler R package (version 3.14.3) to assign various biological processes (BPs), molecular functions (MFs), cellular components (CCs), and pathways of identified marker genes in the interested cluster, and $p < 0.05$ was regarded as statistically enriched.

Immune Cell Infiltration and Tumor Mutation Burden Analysis

The lollipop of immune responses is based on XCELL, TIMER, QUANTISEQ, MCPCOUNTER, EPIC, CIBERSORT-ABS, and CIBERSORT algorithms to analyze the Spearman correlation between risk score values and tumor-infiltrating immune cells. The tumor mutational data were downloaded from TCGA, and the "maftools" package was used to analyze the mutational data in both the high- and low-risk groups. The correlation between TMB and risk score was analyzed using the Pearson correlation test.

Drug Response Prediction

The responses to regorafenib, cisplatin, tipifarnib, atezolizumab, gefitinib, sorafenib, erlotinib, axitinib, and bevacizumab were predicted by the Genomics of Drug Sensitivity in Cancer (https://www.cancerrxgene.org/) to analyze the relationship between the signature and drug response. We used pRRophetic R package (version 0.5) to compare the half-maximal inhibitory concentration (IC_{50}) values between different risk groups by building a ridge regression model with 10-fold cross-validation.

Human Hepatocellular Carcinoma Samples

Ten HCC tissue specimens and adjacent nontumorous tissues were obtained by surgery at Tongji Hospital of Tongji Medical College, and informed consent was obtained from the patients. All study methodologies were strictly in accordance with the Helsinki declaration for the use of human subjects and were approved by the Ethics Committee of Tongji Medical College, Huazhong University of Science and Technology.

Realtime Quantitative PCR

Total RNA was extracted from HCC tissue using TRIzol Reagent (Life Technologies), and cDNA was generated using a PrimeScript RT reagent kit (TaKara, Japan). The RT-PCR reactions were followed according the instructions of SYBR® Green Realtime PCR Master Mix (TaKara, Japan). The relative mRNA levels of target genes and housekeeping genes were calculated using the $2^{-\Delta\Delta Ct}$ method. All primers used in this study are listed in **Supplementary Table S2**.

Statistical Analysis

Statistical analysis was conducted using R (version 4.1.0). Differential gene expression between two groups was identified using Wilcoxon rank sum test, with p value calculated for each gene. Pearson correlation analyses were performed to establish correlation coefficients. K–M survival analysis with log-rank test was used to assess survival differences between different groups. Data were depicted using the "ggplot2" package. The cutoff between high risk and low risk was determined using the "surv cutpoint" function in the "survminer" package, and all survival curves were visualized using the "survminer" package. $p < 0.05$ was considered statistically significant ($^{*}p < 0.05$, $^{**}p < 0.01$, $^{***}p < 0.001$).

RESULTS

Identification of Prognosis-Related Necroptosis Genes in Hepatocellular Carcinoma

The flowchart of the study is shown in **Figure 1**. A total of 69 NRG expression levels were evaluated in the TCGA cohort. Among the 69 NRGs, 18 DEGs were identified between normal and HCC samples as shown in the volcano plots and heatmap (**Figures 2A, B**; **Supplementary Table S3**), including 17 upregulated genes (*TSC1*, *TRIM11*, *CASP8*, *TRAF2*, *USP22*, *SQSTM1*, *DNMT1*, *CDKN2A*, *HSPA4*, *PLK1*, *MYCN*, *TERT*, *SLC39A7*, *RNF31*, *HSP90AA1*, *LEF1*, and *TNFRSF21*) and 1 downregulated gene (*ID1*). In addition, we determined 24 prognostic-related genes (PRGs) from the 69 NRGs by univariate Cox regression analyses (**Figure 2C**). Then, 13 prognostic DEGs were identified from the 18 DEGs and 24 PRGs (**Figure 2D**), and the PPI network provided interactive information among these 13 genes (**Figure 2E**).

Molecular Typing Based on Differentially Expressed Genes

Patients in the TCGA cohort were divided into three clusters (C1, C2, and C3) according to the NMF algorithm (**Figure 3A**, **Supplementary Figure S1**). We compared the overall survival (OS) and progression-free survival (PFS) of the three clusters and found that C3 had better OS and PFS (**Figures 3B, C**). In addition, the expression of 13 prognostic DEGs among the three clusters was observed in the heatmap (**Figure 3D**). To explore the underlying molecular mechanism related to the three subtypes of HCC, we performed ssGSEA based on the transcriptome data of 50 gene sets retrieved from MSigDB. As shown in the **Figure 3E**, compared with C3, C1, and C2 were more correlated with the hallmark related to DNA repair, which may suggest an active proliferation of cancer cells.

Establishment and Validation of an Necroptosis-Related Prognostic Model

To construct a necroptosis-related prognostic signature, we performed LASSO regression analysis based on the prognostic significance of 13 DEGs in the TCGA cohort. According to the minimum criteria, a risk model consisting of *TRAF2*, *SQSTM1*, *CDKN2A*, *PLK1*, *MYCN, HSP90AA1*, and *TNFRSF21* was built (**Figures 4A–C**). The risk score was calculated using the following: risk score = (*TRAF2* × 0.0344 + *SQSTM1* × 0.2163 + *CDKN2A* × 0.0309 + *PLK1* × 0.3262 + *MYCN* × 0.2680 + *HSP90AA1* × 0.0917 + *TNFRSF21* × 0.0352). According to the median risk score, patients in the TCGA cohort were separated into high-risk ($n = 170$) and low-risk groups ($n = 170$). Moreover, patients in the high-risk group had a higher probability of death, increased expression level of the seven risk genes (**Figure 4D**), and a shorter OS (**Figure 4E**) compared to those in the low-risk group. In addition, the time-dependent ROC curve analysis demonstrated that this seven-gene prognostic model could predict the survival of the HCC patients (1-year AUC = 0.804, cutoff value: 2.560; 2-year AUC = 0.706, cutoff value: 2.959; and 3-year AUC = 0.694, cutoff value: 2.590) (**Figure 4F**). The PCA and t-SNE plot confirmed that the necroptosis-related prognostic model could separate high-risk patients from low-risk patients in the TCGA cohort (**Figures 4G, H**).

The efficiency of the risk model was validated in the ICGC cohort. Patients in the ICGC validation cohort were split into the high- and low-risk groups according to the median risk score (**Supplementary Figure S2A**). Similar to the TCGA cohort, patients in the high-risk group had higher death and expression of risk genes in the ICGC cohort (**Supplementary Figure S2A**). Moreover, the K–M curve showed that the low-risk group had a higher OS (**Supplementary Figure S2B**), and the ROC curve analysis confirmed the potent capability of the risk model to predict the survival of the patients in the ICGC cohort (1-year AUC = 0.684, cutoff value: 3.449; 2-year AUC = 0.718, cutoff value: 3.477; and 3-year AUC = 0.671, cutoff value: 3.718) (**Supplementary Figure S2C**). At last, the PCA and t-SNE plot indicated that the prognostic model could also separate the two risk groups in the ICGC cohort (**Supplementary Figures S2D–E**).

Risk Score Is an Independent Prognostic Factor for Hepatocellular Carcinoma

Univariate and multivariate Cox analyses were used to check whether the risk score could serve as an independent and robust

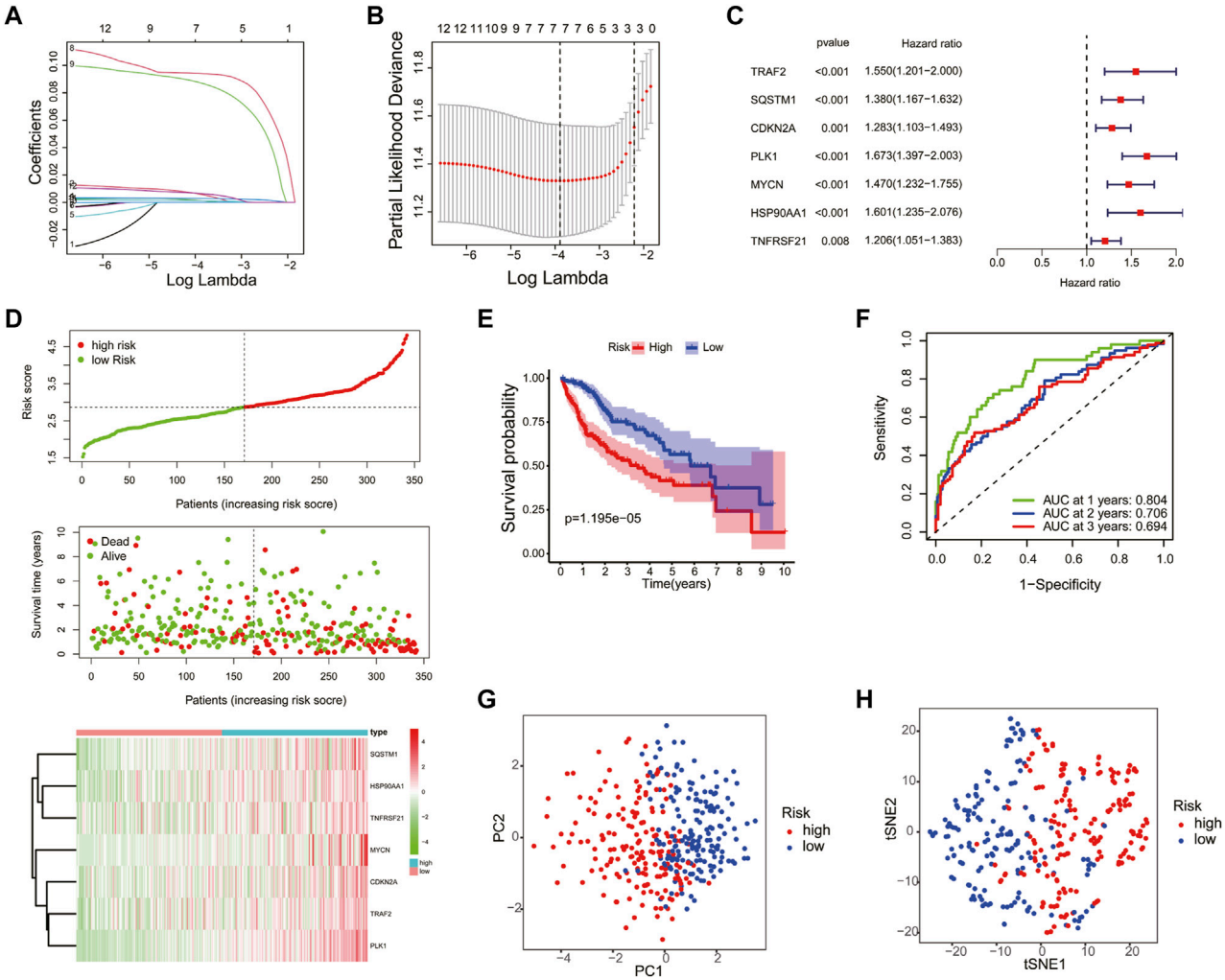

FIGURE 4 | Construction of the necroptosis gene-based prognostic model in the Cancer Genome Atlas (TCGA) training cohort. The association between log(lamba) and coefficients of genes **(A)** and deviance **(B)**. **(C)** Univariate Cox regression analysis was used to construct a prognostic model. **(D)** Distribution of the risk scores, survival status, and expression of the four necroptosis-related risk genes in the training cohort. **(E)** The K–M curve of the low- and high-risk groups based on the seven-necroptosis-related gene profile. **(F)** Time-dependent ROC analysis for the 1-, 2-, and 3-year OS of the prognosis. PCA **(G)** and t-SNE **(H)** analysis of the TCGA cohort based on the risk score.

biomarker to predict OS in HCC patients. As shown in **Figure 5A**, univariate Cox regression analysis showed that the risk score and stage were significantly correlated with the OS of HCC patients in the TCGA cohort. Thereafter, the risk score and stage were further identified as independent prognostic factors of OS by multivariate analysis (**Figure 5B**) (stage, HR = 2.345, 95% CI = 1.591–3.457, $p < 0.001$; risk score, HR = 3.190, 95% CI = 2.270–4.484, $p < 0.001$). In the ICGC cohort, the risk score was also confirmed as an independent prognostic factor (risk score, HR = 2.361, 95% CI = 1.380–4.042, $p = 0.002$) (**Figures 5C, D**). Furthermore, the accuracy of the risk score was highest in predicting 1-year, 3-year, and 5-year survival rates compared with other clinicopathological characteristics (**Figure 5E**). These results indicated that the risk score could be used as an independent prognostic factor to predict patient survival.

Relationship Between the Risk Score and Clinical Factors

To explore the connection between the necroptosis-related prognostic model and clinical factors, we separated the patients in the TCGA dataset into several subgroups according to the different clinical parameters. The K–M curve showed that the high-risk patients had a poorer survival probability compared to the low-risk patients under the conditions of age > 65, age ≤ 65, G1–G2, G3–G4, stages I–II, III–IV, T1–T2, and T3–T4 (**Supplementary Figures S3A–H**).

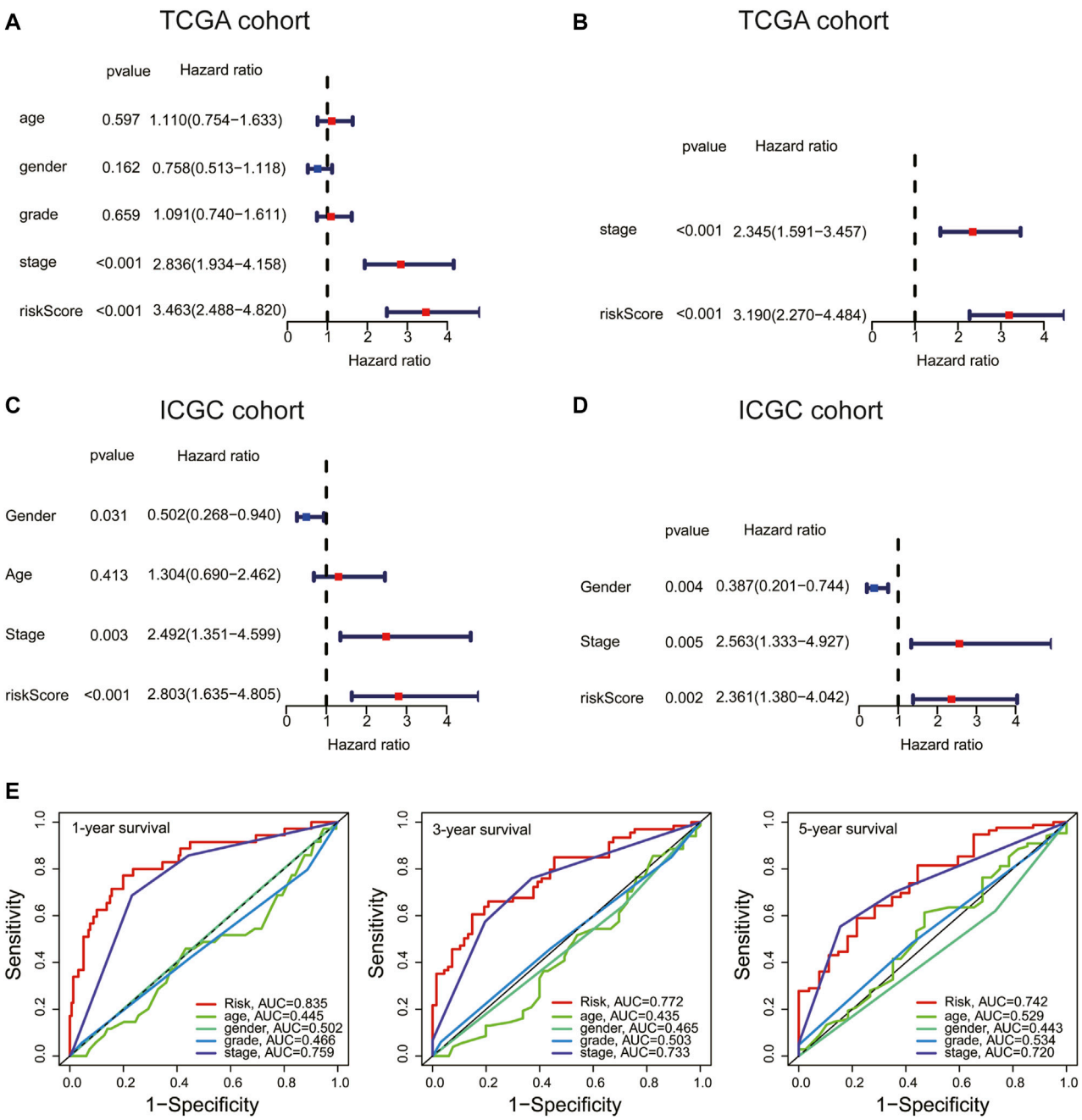

FIGURE 5 | Risk score is an independent prognostic factor for HCC. **(A,C)** Univariate and **(B,D)** multivariate Cox analyses of the risk score and clinical variables in the TCGA and International Cancer Genome Consortium (ICGC) cohort. **(E)** ROC curve analysis of the risk score and clinicopathological characteristics in predicting 1-, 3-, and 5-year survival rates.

Furthermore, the heatmap exhibited the relationship between the high- and low-risk groups and the clinical factors, including age, gender, grade, and T stage (**Figure 6A**). Our further analysis found that in the high-risk group, a higher proportion of patients died and there was a higher proportion of late-stage patients (**Figures 6B–D**). While, the high-risk group had a lower proportion of male than the low-risk group (**Figure 6E**).

Gene Ontology Enrichment and Kyoto Encyclopedia of Genes and Genomes Pathway Analyses

The biological functions and pathways related to the necroptosis-related prognostic model were measured by GO and KEGG analyses based on the DEGs between the high- and low-risk groups. GO analysis suggested that DEGs were mainly involved in

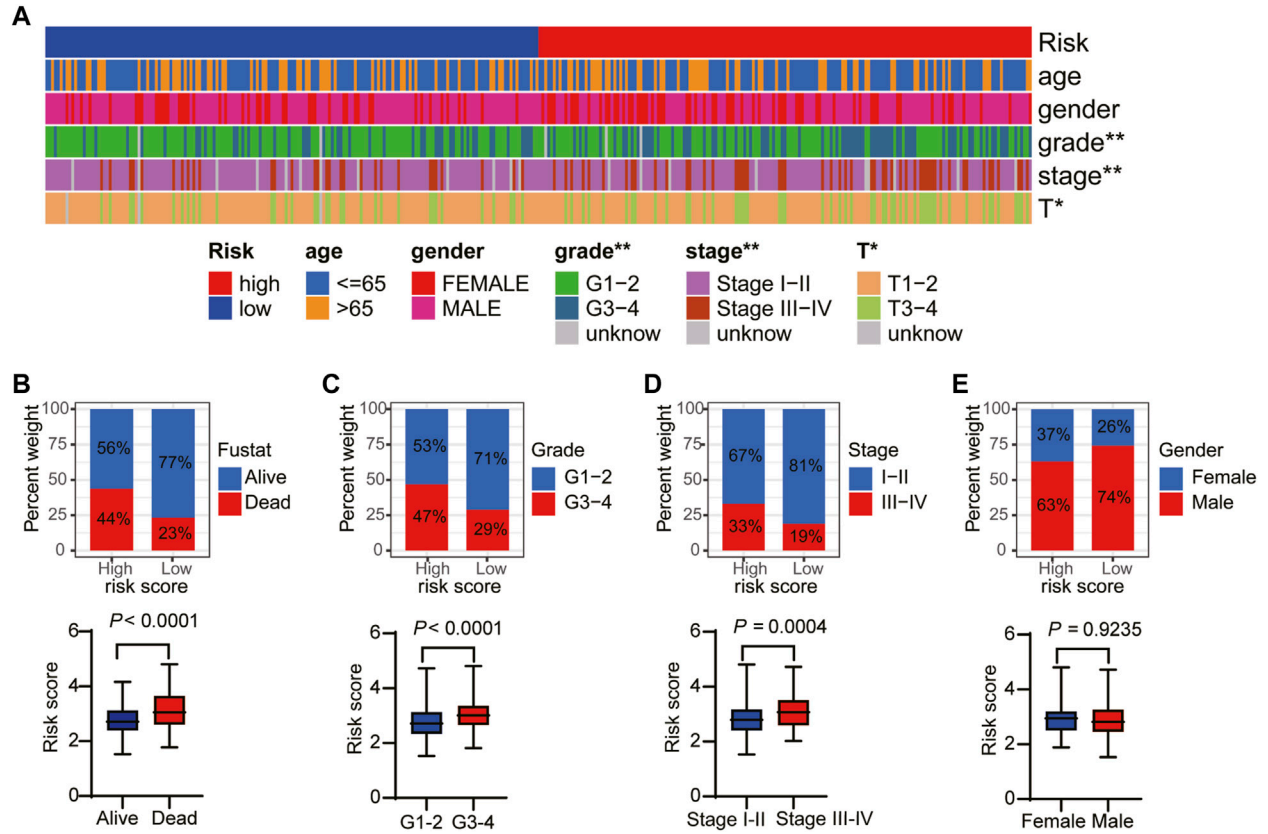

FIGURE 6 | The relationship between the risk score and clinical factors. **(A)** The overview of the correspondence between necroptosis-related prognostic and other features of HCC patients. The proportion of patients with alive and death **(B)**, G1–G2 and G3–G4 **(C)**, stage I–II and III–IV **(D)**, and female and male **(E)**.

chromosome segregation, mitotic nuclear division, humoral immune response, and B cell activation (**Figures 7A, B**). The KEGG results indicated that a number of DEGs were involved in the cell cycle, DNA replication, drug metabolism, and p53 signaling pathway (**Figures 7C, D**). These results demonstrated that the necroptosis-related prognostic signature may have a closed connection with the immune cell infiltration, tumor cell mutation, and metabolism of chemotherapeutic drugs.

Correlation of Immune Cell Infiltration and Tumor Mutational Burden With Prognostic Signature

Given the results of the GO and KEGG analyses, the XCELL, TIMER, QUANTISEQ, MCPCOUNTER, EPIC, CIBERSORT-ABS, and CIBERSORT algorithms were applied to explore the correlation between the prognostic model and immune cells. As shown in **Figure 8A**, the risk score was positively correlated to B cell and T-cell $CD4^+$ memory and negatively correlated to the infiltration macrophage and T-cell regulatory (Tregs). Next, the immune-related genes that were significantly different in the high- and low-risk groups were exhibited in the heatmap (**Figure 8B**). Thereafter, ssGSEA analysis showed that antigen-presenting cell costimulation, CCR, MHC class I, and parainflammation were more highly activated in HCC patients with high-risk scores and cytolytic activity and type II IFN response were more active in the low-risk group (**Figures 8C, D**). At last, we analyzed the prognostic model on the HCC tumor immune microenvironment. Patients in the high-risk group had a higher immune score, stromal score, and ESTIMATE score, and lower tumor purity (**Figures 8E–H**). These findings revealed that the high-risk group might have more immune cells. Considering the crucial role of immune checkpoints in immunotherapies, the expression of immune checkpoints was analyzed between the high- and low-risk groups. As shown in **Supplementary Figure S4**, the expressions of *CD40*, *CD44*, *CD80*, *CD86*, *CD200*, *CD200R1*, *PD-L1*, *LAG3*, *HAVCR2*, *LAIR1*, *LGALS9*, *TNFSF18*, *TNFSF4*, *VTCN1*, *CTLA4*, and *NRP1* were remarkably higher in the high-risk group, suggesting that the high-risk patients might have a better response to immunotherapy.

TMB is a biomarker that indicates a response to immunotherapy. In this study, the relation between the risk score and TMB was investigated. As shown in **Supplementary Figures S5A–B**, the top 20 driver genes with the highest alteration of TP53 were significantly different between the high- and low-risk groups. Meanwhile, the K–M survival

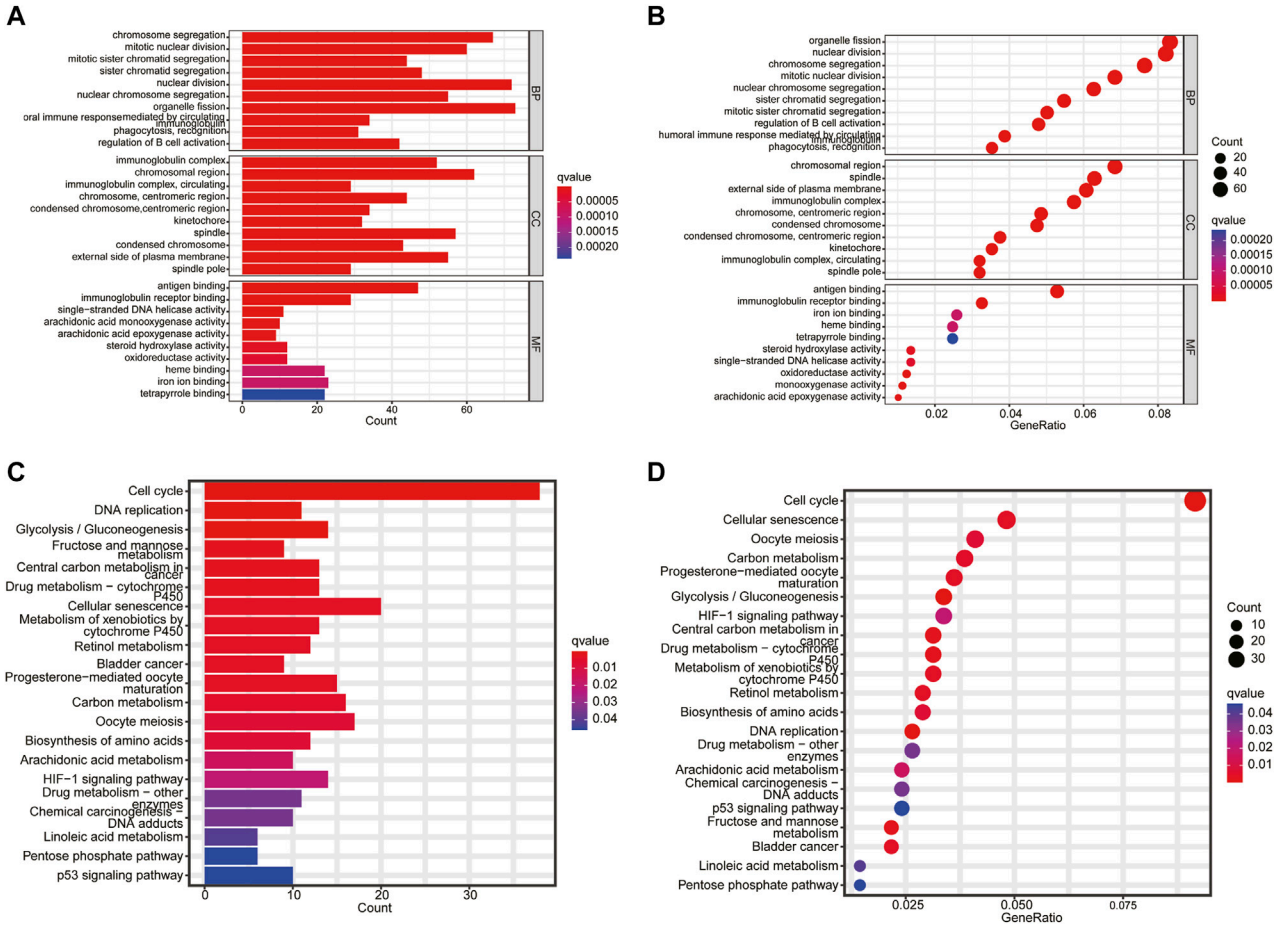

FIGURE 7 | Functional enrichment analysis. **(A,B)** The top 10 biological process (BP) terms, CC terms, and MF terms of gene ontology analysis. **(C,D)** Kyoto Encyclopedia of Genes and Genomes enrichment analysis indicating related genes and pathways.

curves revealed that the high-TMB group demonstrated a poor prognosis (**Supplementary Figure S5C**). Moreover, we found that patients with high TMB and a high-risk score had a poorer prognosis (**Supplementary Figure S5D**). These results indicate that the prognostic model based on the seven NRGs could reflect the genomic stability of patients with HCC.

Application of the Prognostic Model in Drug Sensitivity

Next, we explored the association between risk score and the efficacy of common chemotherapy drugs for HCC using IC_{50}. The results revealed that several drugs in high-risk patients had lower IC_{50} values, including regorafenib, cisplatin, tipifarnib, and atezolizumab (**Figures 9A–D**, $p < 0.05$). However, gefitinib, sorafenib, erlotinib, axitinib, and bevacizumab were more sensitive to the patients in the low-risk group (**Figures 9E–I**, $p < 0.05$). Altogether, this result suggested the possibility of the prognostic model as a predictor of drug sensitivity.

Expression of Prognostic Differentially Expressed Genes

We examined the protein levels of these seven genes in risk models using the Human Protein Atlas (HPA) database. The results showed that the HCC tissues had higher protein levels of *TRAF2*, *SQSTM1*, *CDKN2A*, *PLK1*, and *HSP90AA1* (**Figure 10A**). While, *MYCN* and *TNFRSF21* were not found in HPA database. At last, to better validate the results of the bioinformatic analysis, the mRNA levels of *TRAF2*, *SQSTM1*, *CDKN2A*, *PLK1*, *MYCN*, *HSP90AA1*, and *TNFRSF21* obtained from the HCC patients were measured by RT-PCR. As expected, these seven genes were upregulated in the tumor tissues compared to the tumor-adjacent tissue (**Figure 10B**).

DISCUSSION

It has reported that necroptosis was associated with aggressive tumorigenesis and was thought to be an indication of poor prognosis (Richards et al., 2011; Caruso et al., 2012). However,

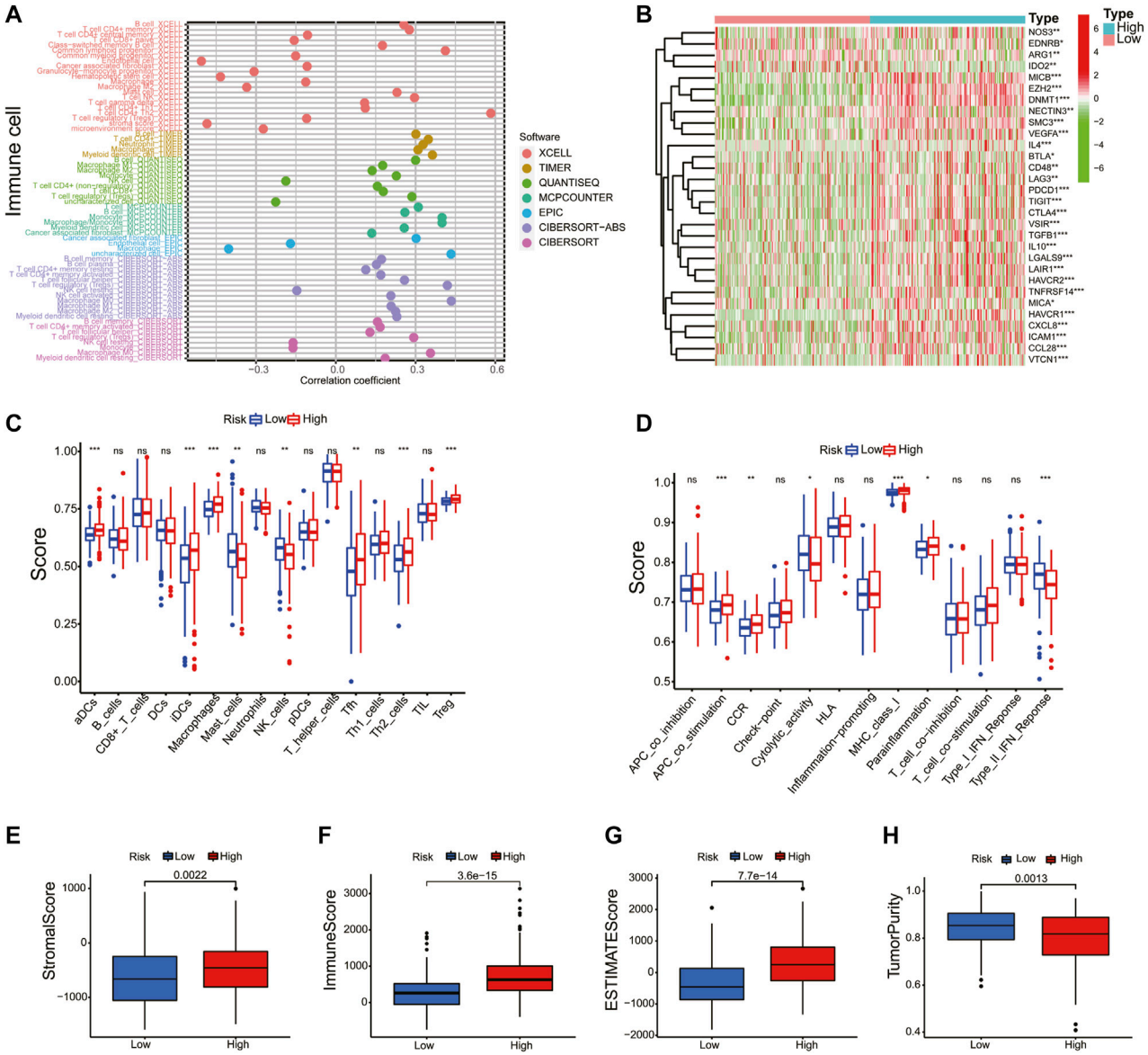

FIGURE 8 | Correlation of immune cell infiltration and tumor mutational burden with prognostic signature. **(A)** A detailed Spearman correlation analysis was also performed using different algorithms. **(B)** The heatmap revealed the immune-related genes between the high- and low-risk groups. The activity differences of immune cells **(C)** and immune function **(D)** between the high- and low-risk groups. The immune score **(E)**, stromal score **(F)**, ESTIMATE score **(G)**, and tumor purity **(H)** were compared in the high- and low-risk groups.

owing to the lack of knowledge about the molecular mechanism of necroptosis in different types of cancer, the exact function of necroptosis in tumor development remains elusive (Yan et al., 2022). In the present study, we identified 13 prognosis-related NRGs in HCC. According to the NMF clustering, patients with HCC were divided into three clusters. C3 had better survival based on OS and PFS analyses compared with C1 and C2. To further evaluate the prognostic value of the DEGs, we constructed a necroptosis-related prognostic model using univariate Cox analysis and LASSO Cox regression analysis, and patients in the TCGA and ICGC cohorts were divided into high- and low-risk groups. We found that patients in the high-risk group had a worse prognosis compared to patients in the low-risk group in both the TCGA and ICGC cohorts. Moreover, the prognosis signature was proven to be an independent prognostic factor to predict the OS by univariate and multivariate Cox regression analyses. These results confirmed that our risk score may be stable as a predictor of HCC patient survival.

The necroptosis-related prognostic signature was composed of seven genes (*TRAF2*, *SQSTM1*, *CDKN2A*, *PLK1*, *MYCN*, *HSP90AA1*, and *TNFRSF21*), which had been confirmed to be closely related to tumorigenesis and necroptosis. *TRAF2*, as an adaptor molecule, was related with multiple receptor-specific functions in tumorigenesis and progression (Borghi et al., 2016).

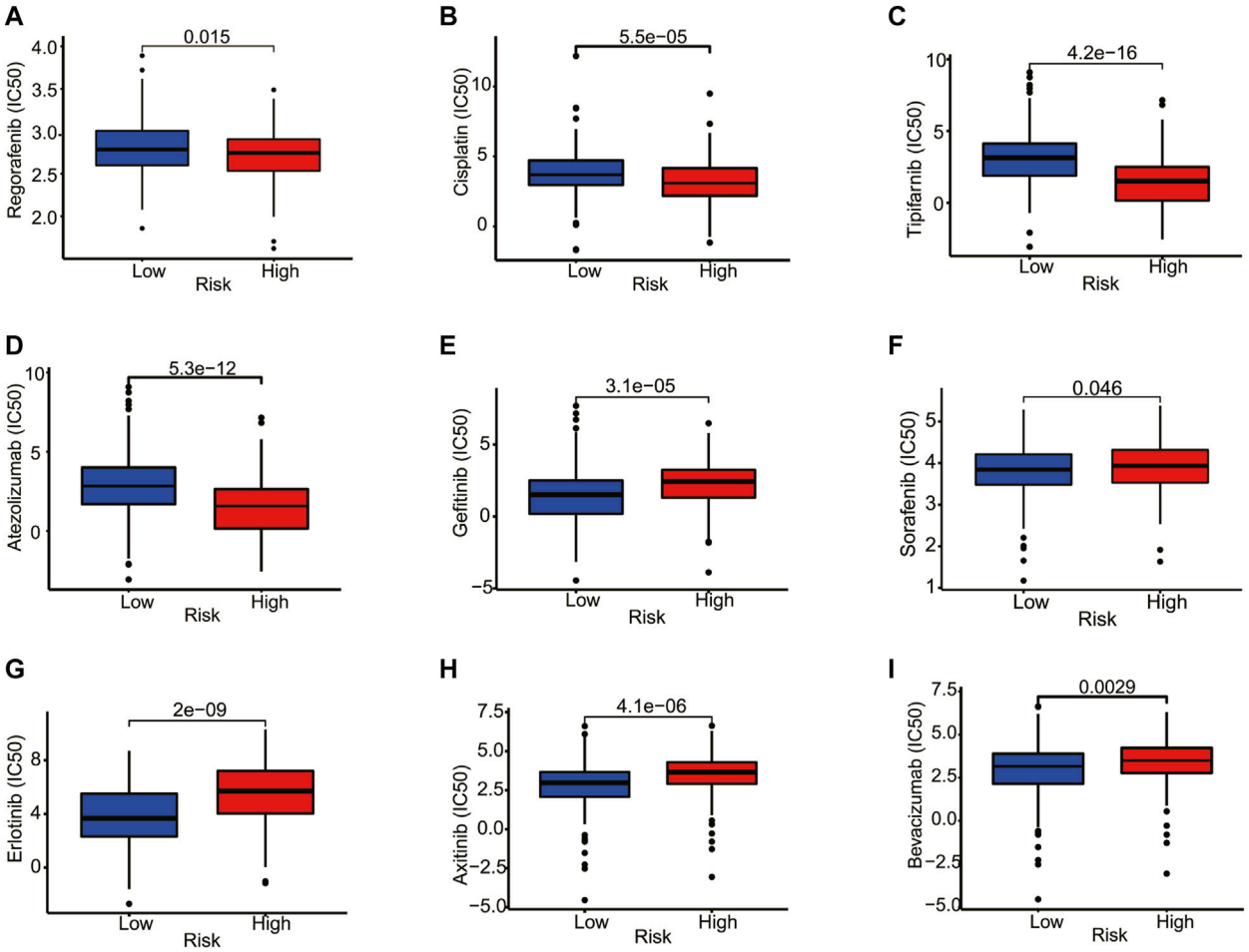

FIGURE 9 | Correlation analysis between the estimated IC_{50} values of chemotherapy drugs and the risk score in HCC patients from the TCGA database. **(A)** Regorafenib, **(B)** Cisplatin, **(C)** Tipifarnib, **(D)** Atezolizumab, **(E)** Gefitinib, **(F)** Sorafenib, **(G)** Erlotinib, **(H)** Axitinib, **(I)** Bevacizumab.

Moreover, *TRAF2* was identified as an important suppressor of necroptosis by directly binding to *MLKL* and recruiting cIAP1/2 (Karl et al., 2014; Petersen et al., 2015; Li et al., 2019). *SQSTM1*, also known as P62, is a multidomain scaffold protein with well-established roles in autophagy and tumor necrosis factor alpha (TNFα)- and NF-κB-related signaling pathways (Kirkin et al., 2009; Cha-Molstad et al., 2017; Cha-Molstad et al., 2018). However, researchers are increasingly finding that *SQSTM1* has an essential and complex role in tumor progression (Cuyler et al., 2022). Elevated *SQSTM1* expression had been reported to support tumorigenesis (Guo et al., 2011). Using 40 cases of tumor tissue chip, elevated *SQSTM1* expression was mainly observed in the cytoplasm of pancreatic carcinoma cells and differently expressed among the T stages (Mohamed et al., 2015; Zhang et al., 2020). MLKL deficiency prevents the accumulation of *SQSTM1* in the liver (Wu and Nagy, 2020). For age-related ischemia/reperfusion, *SQSTM1* forms a complex with RIP1–RIP3, which contributes to myocardial necroptosis (Li et al., 2020). *CDKN2A*, also known as the *P16* gene, had a crucial role in the regulation of the cell cycle (Luo et al., 2021). Although various studies have classified *CDKN2A* as a tumor suppressor, some studies have identified its complex role in tumors (Rangel et al., 2022). It was reported that the expression of the *CDKN2A* gene was significantly higher in 15 tumors, and the *CDKN2A* expression level was significantly correlated with the TMB, microsatellite instability, and infiltrating lymphocyte (Chen et al., 2021). In addition, high *CDKN2A* expression and low FGFR3 expression were statistically significantly associated with worse PFS (Breyer et al., 2018) and were associated with a higher grade (Quentin et al., 2004; Ploussard et al., 2011; Abat et al., 2014). Given the multiple roles of *CDKN2A*, further studies need to be done to validate the effects of *CDKN2* in tumor progression. *PLK1* is a serine/threonine-protein kinase involved in cell cycle regulation and mitotic progression (Xie et al., 2005). Overexpression of *PLK1* was observed in prostate cancer (Weichert et al., 2004), colorectal cancer (Takahashi et al., 2003), neuroblastomas (Ramani et al., 2015), and rectal cancer (Tut et al., 2015) and was associated with poor prognosis. *PLK1* knockout suppressed cancer cell survival, induced apoptosis, and increased the sensitivity to chemotherapy drugs (Reagan-Shaw and Ahmad, 2005; Weiss and Efferth, 2012). Moreover, *PLK* was identified as one of the necroptosis-related

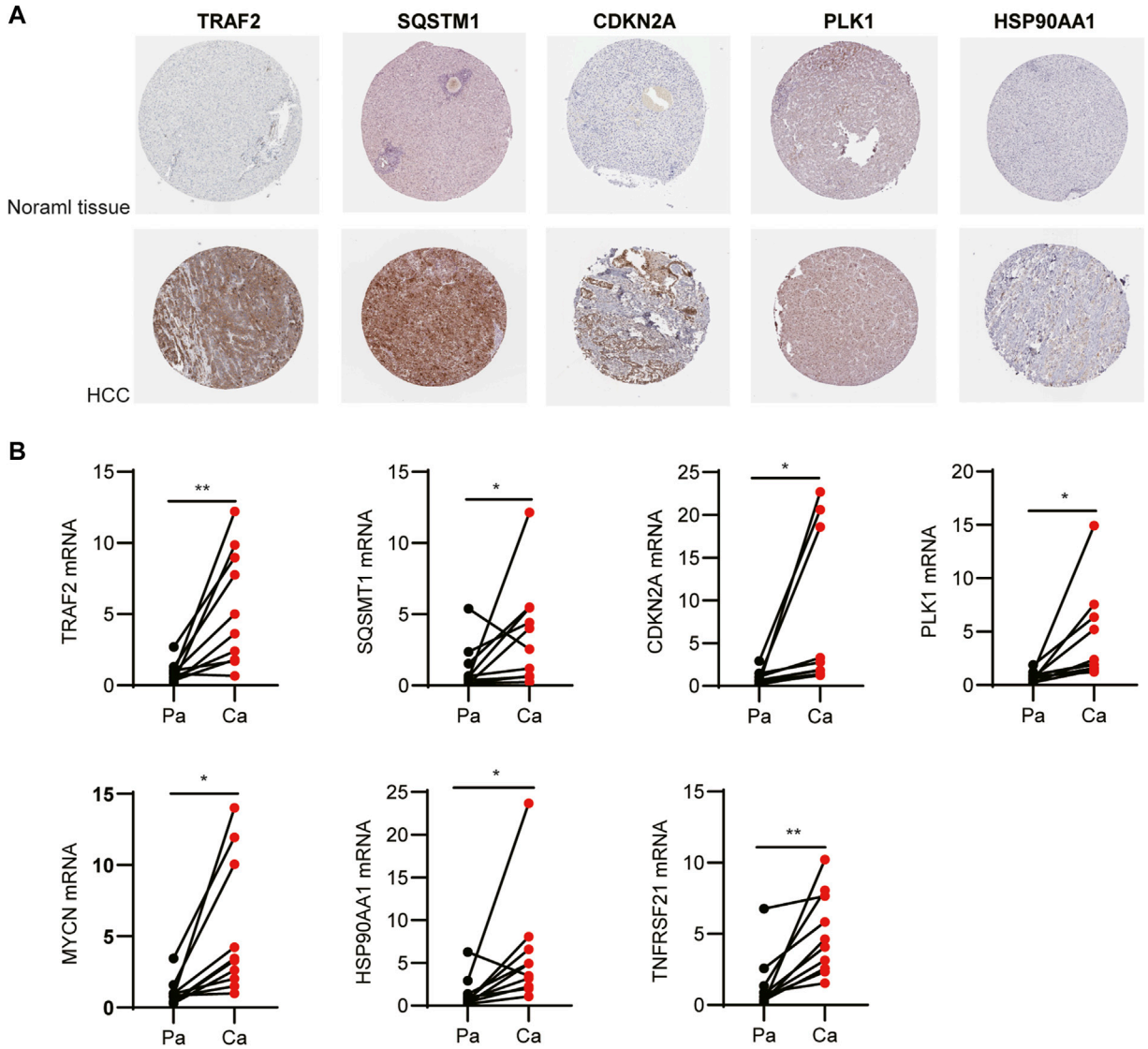

FIGURE 10 | Expression of the independent prognostic genes. **(A)** Immunohistochemistry of *TRAF2*, *SQSTM1*, *CDKN2A*, *PLK1*, and *HSP90AA1* in the normal and tumor groups from the Human Protein Atlas database. **(B)** The mRNA levels of *TRAF2*, *SQSTM1*, *CDKN2A*, *PLK1*, *MYCN*, *HSP90AA1*, and *TNFRSF21* were measured by RT-PCR.

prognosis genes of invasive breast carcinoma (Hu et al., 2022) and clear cell renal cell carcinoma (Xin et al., 2022). In addition, *PLK1* mediated the phosphorylation of RIPK3 by directly associated with RIPK3 as cell enter mitosis (Gupta and Liu, 2021). *MYCN*, one of the MYC families of oncogenes, was related to cell proliferation, cell adhesion, DNA repair, and metabolism (Arvanitis and Felsher, 2006; Chen et al., 2018). Studies found that 25% of patients with neuroblastoma showed an *MYCN* amplification and predicted poor prognosis independently of other factors (Brodeur et al., 1984; Seeger et al., 1985). *HSP90AA1*, one of the HSP90 isoforms, showed a significant correlation with survival time in lung cancer patients by inhibiting the AKT1 and ERK pathways (Niu et al., 2021) and was upregulated in colorectal cancer (Szczuka et al., 2021). *HSP90* regulates the stability of MLKL and RIP3 and is required for TNF-stimulated necrosome assembly (Zhao et al., 2016). *TNFRSF21* is the member of the TNF receptor superfamily. Studies suggested that *TNFRSF21* might serve as a prognostic marker for esophageal squamous cell carcinoma (Qiu et al., 2021) and esophagus adenocarcinoma (Zhang et al., 2021). Furthermore, it should be mentioned that the impact and mechanism of these seven NRGs in HCC have not been reported yet, and future experiments are needed to provide more evidence.

GO and KEGG analyses revealed that the gene sets of the high-risk patients were enriched in humoral immune response, DNA replication, and drug metabolism, which indicated that the necroptosis-related prognosis may be associated with the tumor immune environment and the sensitivity to chemotherapy drugs. In addition, necroptosis exhibited an important role in the

regulation of the immune response. In melanoma, a high level of potassium was released from the necrotic tumor cell, which inhibits $CD4^+$ and $CD8^+$ T-cell activities, resulting in the blockade of antitumor immunity (Vodnala et al., 2019). Moreover, upregulation of RIPK1 in tumor-associated macrophages (TAMs) contributes to immune tolerance and immunotherapeutic resistance in pancreatic ductal adenocarcinoma (Wang et al., 2020). Further analyses indicated that the composition of immune cells was different between high- and low-risk groups. Our results confirmed that higher immune, stromal, and ESTIMATE scores, and lower tumor purity were observed in patients with a high-risk score, which provided further evidence revealing the connection between the tumor microenvironment and necroptosis. In addition, our study confirmed that the expression of multiple immune checkpoints showed considerable difference between the high- and low-risk groups, which may offer underlying therapeutic targets for HCC.

Another biomarker that has recently garnered significant attention is TMB, which demonstrated reasonable prediction of immunotherapy responses (Lauss et al., 2017). In the present study, we found that the high-TMB group demonstrated a poorer prognosis in HCC patients. More importantly, HCC patients with high TMB combined with a high-risk score had a poorer prognosis. The *TP53* gene encodes the tumor protein p53, which is a tumor suppressor that prevents cell division and proliferation. We found that TP53 mutation is related to a poor prognosis of HCC, and it has a high mutation rate in the high-risk group. Drug sensitivity prediction revealed that regorafenib, cisplatin, tipifarnib, and atezolizumab showed lower IC_{50} values in patients with high-risk scores. The results confirmed that prognosis can be used to predict drug sensitivity.

Some limitations must be addressed in our research. First, owing to the heterogeneity of the HCC tissue, more samples should be included in the future to ensure the stability and accuracy of signature prediction. Second, molecular mechanism was not characterized. Further experiments are needed to explore the interaction between HCC and NRGs. Third, the data in our research were obtained from public databases and lacked more basic experimental verification. At last, the complex interaction between HCC and immune cells in necroptosis remains to be further explored.

In conclusion, our study provided a new marker for predicting the prognosis of patients with HCC and provided an important basis for the further study of the relationship among NRGs, the immune microenvironment, and chemotherapy treatment in HCC.

DATA AVAILABILITY STATEMENT

The original contributions presented in the study are included in the article/**Supplementary Material**. Further inquiries can be directed to the corresponding author.

ETHICS STATEMENT

The studies involving human participants were reviewed and approved by the Ethics Committee of Tongji Medical College, Huazhong University of Science and Technology. The patients/participants provided their written informed consent to participate in this study.

AUTHOR CONTRIBUTIONS

HR and QF conceived and designed the study. HR and JZ conducted the experiments. QC was responsible for the collection of the clinical samples. HR analyzed the data. HR and QF wrote and edited the manuscript. XY edited the manuscript and provided critical insights. All authors have approved the manuscript.

FUNDING

This study was supported by the National Natural Science Foundation of China (Nos. 81773730 and 81729004) to QF.

ACKNOWLEDGMENTS

The authors sincerely acknowledge the patients who provided research samples, their families, and the public databases: TCGA and ICGC.

SUPPLEMENTARY MATERIAL

The Supplementary Material for this article can be found online at: https://www.frontiersin.org/articles/10.3389/fgene.2022.900713/full#supplementary-material

REFERENCES

Abat, D., Demirhan, O., Inandiklioglu, N., Tunc, E., Erdogan, S., Tastemir, D., et al. (2014). Genetic Alterations of Chromosomes, P53 and P16 Genes in Low- and High-Grade Bladder Cancer. *Oncol. Lett.* 8 (1), 25–32. doi:10.3892/ol.2014.2108

Arvanitis, C., and Felsher, D. W. (2006). Conditional Transgenic Models Define How MYC Initiates and Maintains Tumorigenesis. *Seminars Cancer Biol.* 16 (4), 313–317. doi:10.1016/j.semcancer.2006.07.012

Borghi, A., Verstrepen, L., and Beyaert, R. (2016). TRAF2 Multitasking in TNF Receptor-Induced Signaling to NF-κB, MAP Kinases and Cell Death. *Biochem. Pharmacol.* 116, 1–10. doi:10.1016/j.bcp.2016.03.009

Breyer, J., Wirtz, R. M., Erben, P., Worst, T. S., Stoehr, R., Eckstein, M., et al. (2018). High CDKN2A/p16 and Low FGFR3 Expression Predict Progressive Potential of Stage pT1 Urothelial Bladder Carcinoma. *Clin. Genitourin. Cancer* 16 (4), 248–256. doi:10.1016/j.clgc.2018.01.009

Brodeur, G. M., Seeger, R. C., Schwab, M., Varmus, H. E., and Bishop, J. M. (1984). Amplification of N- Myc in Untreated Human Neuroblastomas Correlates with Advanced Disease Stage. *Science* 224 (4653), 1121–1124. doi:10.1126/science.6719137

Caruso, R., Parisi, A., Bonanno, A., Paparo, D., Quattrocchi, E., Branca, G., et al. (2012). Histologic Coagulative Tumour Necrosis as a Prognostic Indicator of Aggressiveness in Renal, Lung, Thyroid and Colorectal Carcinomas: A Brief Review. *Oncol. Lett.* 3 (1), 16–18. doi:10.3892/ol.2011.420

Cha-Molstad, H., Yu, J. E., Feng, Z., Lee, S. H., Kim, J. G., Yang, P., et al. (2017). p62/SQSTM1/Sequestosome-1 Is an N-Recognin of the N-End Rule Pathway Which Modulates Autophagosome Biogenesis. *Nat. Commun.* 8 (1), 102. doi:10.1038/s41467-017-00085-7

Cha-Molstad, H., Lee, S. H., Kim, J. G., Sung, K. W., Hwang, J., Shim, S. M., et al. (2018). Regulation of Autophagic Proteolysis by the N-Recognin SQSTM1/p62 of the N-End Rule Pathway. *Autophagy* 14 (2), 359–361. doi:10.1080/15548627.2017.1415190

Chen, H., Liu, H., and Qing, G. (2018). Targeting Oncogenic Myc as a Strategy for Cancer Treatment. *Sig. Transduct. Target Ther.* 3, 5. doi:10.1038/s41392-018-0008-7

Chen, Z., Guo, Y., Zhao, D., Zou, Q., Yu, F., Zhang, L., et al. (2021). Comprehensive Analysis Revealed that CDKN2A Is a Biomarker for Immune Infiltrates in Multiple Cancers. *Front. Cell Dev. Biol.* 9, 808208. doi:10.3389/fcell.2021.808208

Cuyler, J., Murthy, P., Spada, N. G., McGuire, T. F., Lotze, M. T., and Xie, X.-Q. (2022). Sequestsome-1/p62-targeted Small Molecules for Pancreatic Cancer Therapy. *Drug Discov. Today* 27 (1), 362–370. doi:10.1016/j.drudis.2021.09.011

Daher, S., Massarwa, M., Benson, A. A., and Khoury, T. (2018). Current and Future Treatment of Hepatocellular Carcinoma: An Updated Comprehensive Review. *J. Clin. Transl. Hepatol.* 6 (1), 1–10. doi:10.14218/JCTH.2017.00031

Degterev, A., Huang, Z., Boyce, M., Li, Y., Jagtap, P., Mizushima, N., et al. (2005). Chemical Inhibitor of Nonapoptotic Cell Death with Therapeutic Potential for Ischemic Brain Injury. *Nat. Chem. Biol.* 1 (2), 112–119. doi:10.1038/nchembio711

Faivre, S., Rimassa, L., and Finn, R. S. (2020). Molecular Therapies for HCC: Looking outside the Box. *J. Hepatol.* 72 (2), 342–352. doi:10.1016/j.jhep.2019.09.010

Guo, J. Y., Chen, H.-Y., Mathew, R., Fan, J., Strohecker, A. M., Karsli-Uzunbas, G., et al. (2011). Activated Ras Requires Autophagy to Maintain Oxidative Metabolism and Tumorigenesis. *Genes Dev.* 25 (5), 460–470. doi:10.1101/gad.2016311

Gupta, K., and Liu, B. (2021). PLK1-mediated S369 Phosphorylation of RIPK3 during G2 and M Phases Enables its Ripoptosome Incorporation and Activity. *iScience* 24 (4), 102320. doi:10.1016/j.isci.2021.102320

Han, L.-Y., Yang, J.-R., Zhao, Z.-H., Gao, S., Fan, Y.-C., and Wang, K. (2020). RIPK3 mRNA Level Acts as a Diagnostic Biomarker in Hepatitis B Virus-Associated Hepatocellular Carcinoma. *Pathol. Res. Pract.* 216 (10), 153147. doi:10.1016/j.prp.2020.153147

Hitomi, J., Christofferson, D. E., Ng, A., Yao, J., Degterev, A., Xavier, R. J., et al. (2008). Identification of a Molecular Signaling Network that Regulates a Cellular Necrotic Cell Death Pathway. *Cell* 135 (7), 1311–1323. doi:10.1016/j.cell.2008.10.044

Hu, T., Zhao, X., Zhao, Y., Cheng, J., Xiong, J., and Lu, C. (2022). Identification and Verification of Necroptosis-Related Gene Signature and Associated Regulatory Axis in Breast Cancer. *Front. Genet.* 13, 842218. doi:10.3389/fgene.2022.842218

Jayakumar, A., and Bothwell, A. L. M. (2019). RIPK3-Induced Inflammation by I-MDSCs Promotes Intestinal Tumors. *Cancer Res.* 79 (7), 1587–1599. doi:10.1158/0008-5472.CAN-18-2153

Jiao, D., Cai, Z., Choksi, S., Ma, D., Choe, M., Kwon, H.-J., et al. (2018). Necroptosis of Tumor Cells Leads to Tumor Necrosis and Promotes Tumor Metastasis. *Cell Res.* 28 (8), 868–870. doi:10.1038/s41422-018-0058-y

Karl, I., Jossberger-Werner, M., Schmidt, N., Horn, S., Goebeler, M., Leverkus, M., et al. (2014). TRAF2 Inhibits TRAIL- and CD95L-Induced Apoptosis and Necroptosis. *Cell Death Dis.* 5 (10), e1444. doi:10.1038/cddis.2014.404

Kirkin, V., McEwan, D. G., Novak, I., and Dikic, I. (2009). A Role for Ubiquitin in Selective Autophagy. *Mol. Cell* 34 (3), 259–269. doi:10.1016/j.molcel.2009.04.026

Lauss, M., Donia, M., Harbst, K., Andersen, R., Mitra, S., Rosengren, F., et al. (2017). Mutational and Putative Neoantigen Load Predict Clinical Benefit of Adoptive T Cell Therapy in Melanoma. *Nat. Commun.* 8 (1), 1738. doi:10.1038/s41467-017-01460-0

Li, J., Zhang, J., Zhang, Y., Wang, Z., Song, Y., Wei, S., et al. (2019). TRAF2 Protects against Cerebral Ischemia-Induced Brain Injury by Suppressing Necroptosis. *Cell Death Dis.* 10 (5), 328. doi:10.1038/s41419-019-1558-5

Li, C., Mu, N., Gu, C., Liu, M., Yang, Z., Yin, Y., et al. (2020). Metformin Mediates Cardioprotection against Aging-induced Ischemic Necroptosis. *Aging Cell* 19 (2), e13096. doi:10.1111/acel.13096

Liao, Y., Yang, Y., Pan, D., Ding, Y., Zhang, H., Ye, Y., et al. (2021). HSP90α Mediates Sorafenib Resistance in Human Hepatocellular Carcinoma by Necroptosis Inhibition under Hypoxia. *Cancers* 13 (2), 243. doi:10.3390/cancers13020243

Lin, C.-C., Mabe, N. W., Lin, Y.-T., Yang, W.-H., Tang, X., Hong, L., et al. (2020). RIPK3 Upregulation Confers Robust Proliferation and Collateral Cystine-Dependence on Breast Cancer Recurrence. *Cell Death Differ.* 27 (7), 2234–2247. doi:10.1038/s41418-020-0499-y

Llovet, J. M., Peña, C. E. A., Lathia, C. D., Shan, M., Meinhardt, G., Bruix, J., et al. (2012). Plasma Biomarkers as Predictors of Outcome in Patients with Advanced Hepatocellular Carcinoma. *Clin. Cancer Res.* 18 (8), 2290–2300. doi:10.1158/1078-0432.CCR-11-2175

Llovet, J. M., Villanueva, A., Lachenmayer, A., and Finn, R. S. (2015). Advances in Targeted Therapies for Hepatocellular Carcinoma in the Genomic Era. *Nat. Rev. Clin. Oncol.* 12 (7), 408–424. doi:10.1038/nrclinonc.2015.103

Luo, J.-p., Wang, J., and Huang, J.-h. (2021). CDKN2A Is a Prognostic Biomarker and Correlated with Immune Infiltrates in Hepatocellular Carcinoma. *Biosci. Rep.* 41 (10), BSR20211103. doi:10.1042/BSR20211103

Medavaram, S., and Zhang, Y. (2018). Emerging Therapies in Advanced Hepatocellular Carcinoma. *Exp. Hematol. Oncol.* 7, 17. doi:10.1186/s40164-018-0109-6

Mohamed, A., Ayman, A., Deniece, J., Wang, T., Kovach, C., Siddiqui, M. T., et al. (2015). P62/Ubiquitin IHC Expression Correlated with Clinicopathologic Parameters and Outcome in Gastrointestinal Carcinomas. *Front. Oncol.* 5, 70. doi:10.3389/fonc.2015.00070

Najafov, A., Chen, H., and Yuan, J. (2017). Necroptosis and Cancer. *Trends Cancer* 3 (4), 294–301. doi:10.1016/j.trecan.2017.03.002

Niu, M., Zhang, B., Li, L., Su, Z., Pu, W., Zhao, C., et al. (2021). Targeting HSP90 Inhibits Proliferation and Induces Apoptosis Through AKT1/ERK Pathway in Lung Cancer. *Front. Pharmacol.* 12, 724192. doi:10.3389/fphar.2021.724192

Petersen, S. L., Chen, T. T., Lawrence, D. A., Marsters, S. A., Gonzalvez, F., and Ashkenazi, A. (2015). TRAF2 Is a Biologically Important Necroptosis Suppressor. *Cell Death Differ.* 22 (11), 1846–1857. doi:10.1038/cdd.2015.35

Ploussard, G., Soliman, H., Dubosq, F., Méria, P., Vérine, J., Desgrand-Champs, F., et al. (2011). The Prognostic Value of FGFR3 Mutational Status for Disease Recurrence and Progression Depends on Allelic Losses at 9p22. *Am. J. Cancer Res.* 1 (4), 498–507.

Qiu, H., Song, H., Luo, M., Ke, S., Shi, W., Chen, J., et al. (2021). Dysfunction of Apoptosis and Autophagy Correlates with Local Recurrence in Esophageal Squamous Cell Carcinoma after Definitive Chemoradiation. *Cancer Cell Int.* 21 (1), 466. doi:10.1186/s12935-021-02171-9

Quentin, T., Henke, C., Korabiowska, M., Schlott, T., Zimmerman, B., and Kunze, E. (2004). Altered mRNA Expression of the Rb and P16 Tumor Suppressor Genes and of CDK4 in Transitional Cell Carcinomas of the Urinary Bladder Associated with Tumor Progression. *Anticancer Res.* 24 (2B), 1011–1023.

Ramani, P., Nash, R., Sowa-Avugrah, E., and Rogers, C. (2015). High Levels of Polo-like Kinase 1 and Phosphorylated Translationally Controlled Tumor Protein Indicate Poor Prognosis in Neuroblastomas. *J. Neurooncol.* 125 (1), 103–111. doi:10.1007/s11060-015-1900-4

Rangel, R., Pickering, C. R., Sikora, A. G., and Spiotto, M. T. (2022). Genetic Changes Driving Immunosuppressive Microenvironments in Oral Premalignancy. *Front. Immunol.* 13, 840923. doi:10.3389/fimmu.2022.840923

Reagan-Shaw, S., and Ahmad, N. (2005). Silencing of Polo-like Kinase (Plk) 1 via siRNA Causes Induction of Apoptosis and Impairment of Mitosis Machinery in Human Prostate Cancer Cells: Implications for the Treatment of Prostate Cancer. *FASEB J.* 19 (6), 1–14. doi:10.1096/fj.04-2910fje

Richards, C. H., Mohammed, Z., Qayyum, T., Horgan, P. G., and McMillan, D. C. (2011). The Prognostic Value of Histological Tumor Necrosis in Solid Organ Malignant Disease: A Systematic Review. *Future Oncol.* 7 (10), 1223–1235. doi:10.2217/fon.11.99

Seeger, R. C., Brodeur, G. M., Sather, H., Dalton, A., Siegel, S. E., Wong, K. Y., et al. (1985). Association of Multiple Copies of the N-mycOncogene with Rapid Progression of Neuroblastomas. *N. Engl. J. Med.* 313 (18), 1111–1116. doi:10.1056/NEJM198510313131802

Seifert, L., Werba, G., Tiwari, S., Giao Ly, N. N., Alothman, S., Alqunaibit, D., et al. (2016). The Necrosome Promotes Pancreatic Oncogenesis via CXCL1 and

Mincle-Induced Immune Suppression. *Nature* 532 (7598), 245–249. doi:10.1038/nature17403

Sun, L., Wang, H., Wang, Z., He, S., Chen, S., Liao, D., et al. (2012). Mixed Lineage Kinase Domain-like Protein Mediates Necrosis Signaling Downstream of RIP3 Kinase. *Cell* 148 (1-2), 213–227. doi:10.1016/j.cell.2011.11.031

Sung, H., Ferlay, J., Siegel, R. L., Laversanne, M., Soerjomataram, I., Jemal, A., et al. (2021). Global Cancer Statistics 2020: GLOBOCAN Estimates of Incidence and Mortality Worldwide for 36 Cancers in 185 Countries. *CA A Cancer J. Clin.* 71 (3), 209–249. doi:10.3322/caac.21660

Szczuka, I., Wierzbicki, J., Serek, P., Szczęśniak-Sięga, B. M., and Krzystek-Korpacka, M. (2021). Heat Shock Proteins HSPA1 and HSP90AA1 Are Upregulated in Colorectal Polyps and Can Be Targeted in Cancer Cells by Anti-inflammatory Oxicams with Arylpiperazine Pharmacophore and Benzoyl Moiety Substitutions at Thiazine Ring. *Biomolecules* 11 (11), 1588. doi:10.3390/biom11111588

Takahashi, T., Sano, B., Nagata, T., Kato, H., Sugiyama, Y., Kunieda, K., et al. (2003). Polo-Like Kinase 1 (PLK1) Is Overexpressed in Primary Colorectal Cancers. *Cancer Sci.* 94 (2), 148–152. doi:10.1111/j.1349-7006.2003.tb01411.x

Tut, T. G., Lim, S. H. S., Dissanayake, I. U., Descallar, J., Chua, W., Ng, W., et al. (2015). Upregulated Polo-Like Kinase 1 Expression Correlates with Inferior Survival Outcomes in Rectal Cancer. *PLoS One* 10 (6), e0129313. doi:10.1371/journal.pone.0129313

Vodnala, S. K., Eil, R., Kishton, R. J., Sukumar, M., Yamamoto, T. N., Ha, N.-H., et al. (2019). T Cell Stemness and Dysfunction in Tumors Are Triggered by a Common Mechanism. *Science* 363 (6434), eaau0135. doi:10.1126/science.aau0135

Wang, W., Marinis, J. M., Beal, A. M., Savadkar, S., Wu, Y., Khan, M., et al. (2020). RIP1 Kinase Drives Macrophage-Mediated Adaptive Immune Tolerance in Pancreatic Cancer. *Cancer Cell* 38 (4), 585–590. doi:10.1016/j.ccell.2020.09.020

Weichert, W., Schmidt, M., Gekeler, V., Denkert, C., Stephan, C., Jung, K., et al. (2004). Polo-Like Kinase 1 Is Overexpressed in Prostate Cancer and Linked to Higher Tumor Grades. *Prostate* 60 (3), 240–245. doi:10.1002/pros.20050

Weiss, L., and Efferth, T. (2012). Polo-Like Kinase 1 as Target for Cancer Therapy. *Exp. Hematol. Oncol.* 1 (1), 38. doi:10.1186/2162-3619-1-38

Wu, X., and Nagy, L. E. (2020). MLKL Contributes to Western Diet-Induced Liver Injury through Inhibiting Autophagy. *Autophagy* 16 (7), 1351–1352. doi:10.1080/15548627.2020.1760624

Wu, L., Zhang, X., Zheng, L., Zhao, H., Yan, G., Zhang, Q., et al. (2020). RIPK3 Orchestrates Fatty Acid Metabolism in Tumor-Associated Macrophages and Hepatocarcinogenesis. *Cancer Immunol. Res.* 8 (5), 710–721. doi:10.1158/2326-6066.CIR-19-0261

Xie, S., Xie, B., Lee, M. Y., and Dai, W. (2005). Regulation of Cell Cycle Checkpoints by Polo-like Kinases. *Oncogene* 24 (2), 277–286. doi:10.1038/sj.onc.1208218

Xin, S., Mao, J., Duan, C., Wang, J., Lu, Y., Yang, J., et al. (2022). Identification and Quantification of Necroptosis Landscape on Therapy and Prognosis in Kidney Renal Clear Cell Carcinoma. *Front. Genet.* 13, 832046. doi:10.3389/fgene.2022.832046

Yan, J., Wan, P., Choksi, S., and Liu, Z.-G. (2022). Necroptosis and Tumor Progression. *Trends Cancer* 8 (1), 21–27. doi:10.1016/j.trecan.2021.09.003

Yatim, N., Jusforgues-Saklani, H., Orozco, S., Schulz, O., Barreira da Silva, R., Reis e Sousa, C., et al. (2015). RIPK1 and NF-κB Signaling in Dying Cells Determines Cross-Priming of CD8 + T Cells. *Science* 350 (6258), 328–334. doi:10.1126/science.aad0395

Zhang, Z.-Y., Guo, S., Zhao, R., Ji, Z.-P., and Zhuang, Z.-N. (2020). Clinical Significance of SQSTM1/P62 and Nuclear Factor-κB Expression in Pancreatic Carcinoma. *World J. Gastrointest. Oncol.* 12 (7), 719–731. doi:10.4251/wjgo.v12.i7.719

Zhang, X., Yang, L., Kong, M., Ma, J., and Wei, Y. (2021). Development of a Prognostic Signature of Patients with Esophagus Adenocarcinoma by Using Immune-Related Genes. *BMC Bioinform.* 22 (1), 536. doi:10.1186/s12859-021-04456-2

Zhao, J., Jitkaew, S., Cai, Z., Choksi, S., Li, Q., Luo, J., et al. (2012). Mixed Lineage Kinase Domain-like Is a Key Receptor Interacting Protein 3 Downstream Component of TNF-Induced Necrosis. *Proc. Natl. Acad. Sci. U.S.A.* 109 (14), 5322–5327. doi:10.1073/pnas.1200012109

Zhao, X. M., Chen, Z., Zhao, J. B., Zhang, P. P., Pu, Y. F., Jiang, S. H., et al. (2016). Hsp90 Modulates the Stability of MLKL and Is Required for TNF-Induced Necroptosis. *Cell Death Dis.* 7 (2), e2089. doi:10.1038/cddis.2015.390

Conflict of Interest: The authors declare that the research was conducted in the absence of any commercial or financial relationships that could be construed as a potential conflict of interest.

Publisher's Note: All claims expressed in this article are solely those of the authors and do not necessarily represent those of their affiliated organizations, or those of the publisher, the editors, and the reviewers. Any product that may be evaluated in this article, or claim that may be made by its manufacturer, is not guaranteed or endorsed by the publisher.

Copyright © 2022 Ren, Zheng, Cheng, Yang and Fu. This is an open-access article distributed under the terms of the Creative Commons Attribution License (CC BY). The use, distribution or reproduction in other forums is permitted, provided the original author(s) and the copyright owner(s) are credited and that the original publication in this journal is cited, in accordance with accepted academic practice. No use, distribution or reproduction is permitted which does not comply with these terms.

frontiers | Frontiers in Genetics

TYPE Original Research
PUBLISHED 29 August 2022
DOI 10.3389/fgene.2022.939956

Check for updates

OPEN ACCESS

EDITED BY
Jinhui Liu,
Nanjing Medical University, China

REVIEWED BY
Wahafu Alafate,
Guangdong Provincial People's Hospital, China
Zizhao Xu,
The University of the Pacific, United States
Bangjie Chen,
First Affiliated Hospital of Anhui Medical University, China

*CORRESPONDENCE
Wenbin Lu,
14555271@qq.com

†These authors have contributed equally to this work and share first authorship

SPECIALTY SECTION
This article was submitted to Cancer Genetics and Oncogenomics, a section of the journal Frontiers in Genetics

RECEIVED 11 May 2022
ACCEPTED 05 August 2022
PUBLISHED 29 August 2022

CITATION
Liu J, Lu Y, Dai Y, Shen Y, Zeng C, Liu X, Yu H, Deng J and Lu W (2022), A comprehensive analysis and validation of cuproptosis-associated genes across cancers: Overall survival, the tumor microenvironment, stemness scores, and drug sensitivity.
Front. Genet. 13:939956.
doi: 10.3389/fgene.2022.939956

COPYRIGHT
© 2022 Liu, Lu, Dai, Shen, Zeng, Liu, Yu, Deng and Lu. This is an open-access article distributed under the terms of the Creative Commons Attribution License (CC BY). The use, distribution or reproduction in other forums is permitted, provided the original author(s) and the copyright owner(s) are credited and that the original publication in this journal is cited, in accordance with accepted academic practice. No use, distribution or reproduction is permitted which does not comply with these terms.

A comprehensive analysis and validation of cuproptosis-associated genes across cancers: Overall survival, the tumor microenvironment, stemness scores, and drug sensitivity

Jinsong Liu[1†], Yueyao Lu[2†], Yuyang Dai[3†], Ying Shen[1], Cheng Zeng[1], Xiuling Liu[1], Huayi Yu[1], Jianzhong Deng[1] and Wenbin Lu[1,2,4*]

[1]Department of Oncology, Wujin Hospital Affiliated with Jiangsu University, Jiangsu, China, [2]Department of Oncology, The Changzhou Clinical School of Nanjing Medical University, Jiangsu, China, [3]Department of Radiology, Wujin Hospital Affiliated with Jiangsu University, Changzhou, Jiangsu, China, [4]Department of Oncology, The Wujin Clinical College of Xuzhou Medical University, Jiangsu, China

Background: Cuproptosis is a novel type of cell death induced by copper. Cuproptosis-associated genes play a crucial part in oncogenesis and the growth and metastasis of tumors. However, the correlations among cuproptosis-associated genes, overall survival, the tumor microenvironment, and drug sensitivity remain unclear. Therefore, we performed an analysis of cuproptosis-associated genes across cancers.

Methods: We downloaded RNA sequence expression data, clinical and survival data, stemness score data, and immune subtype data of cuproptosis-associated genes from the UCSC Xena. Next, we conducted differential analysis, expression analysis and correlation analysis across cancers with various R packages. Moreover, survival analysis and Cox hazard analysis were conducted to investigate the relationships between cuproptosis-associated genes and survival outcomes in various cancer types. Finally, we also analyzed the relationship among the levels of cuproptosis-associated genes across cancers, immune types, the tumor microenvironment, stemness scores, and drug sensitivity. Expression validation of cuproptosis-associated genes in renal cancer and normal tissues by immunohistochemical staining.

Results: We found that 10 cuproptosis-associated genes (FDX1, LIAS, LIPT1, DLD, DLAT, PDHA1, PDHB, MTF1, GLS, and CDKN2A) were differently expressed in 18 tumors and normal tissues. Survival outcomes showed that cuproptosis-

Abbreviations: TCGA, The Cancer Genome Atlas; DNAss, DNA stemness score; RNAss, RNA stemness score.

associated genes had prognostic value in various cancer types. Moreover, we identified that cuproptosis-associated genes had different levels in six immune subtypes. The study also indicated that the levels of most cuproptosis-associated genes were positively correlated with the RNAss and DNAss. FDX1, LIAS, LIPT1, DLD, DLAT, PDHA1, and PDHB were negatively correlated with immune scores and ESTIMATE scores. In addition, we identified the top 16 drugs strongly sensitivity to cuproptosis-associated genes according to the correlation coefficient. Finally, we also found that cuproptosis-associated genes were significantly correlated with immune subtype, clinical features, the tumor microenvironment, and drug sensitivity in Kidney renal clear cell carcinoma. And the results of immunohistochemical staining analysis was very consistent with the previous analysis.

Conclusion: We performed an overall analysis to uncover the roles of cuproptosis-associated genes in differential expression, survival outcomes, immune subtypes, the tumor microenvironment, stemness scores, and cancer drug sensitivity across cancers.

KEYWORDS

cuproptosis-associated genes, pan-cancer analysis, differential analysis, overall survival, immune subtype, the tumor microenvironment, stemness score, drug sensitivity

Introduction

Previously reported statistics have shown that cancer is the main public health problem globally and the second most common cause of death (Bray et al., 2021). In 2020, there were roughly 19.3 million new cases and 10 million deaths globally (Sung et al., 2021). Although there have been significant advances in diagnosis and therapy techniques, survival time of individuals with cancer remains extremely short. Therefore, it is significant and urgent to explore potential predictive indicators and promising therapeutic strategies.

There are many kinds of cell death, such as necroptosis, pyroptosis, autophagy, and ferroptosis (Tang et al., 2020). Previous study has found that after blocking adenosine triphosphate (ATP) biosynthesis, a high concentration of zinc can induce nonapoptotic cell death (Dineley et al., 2003; Du et al., 2021). Besides, ferroptosis, a unique kind of cell death, is characterized by the production of hazardous membrane lipid peroxides, which is catalyzed by iron (Kagan et al., 2017). Another trace metals, including copper, are necessary for a number of biological activities in living organisms. However, these trace metals should be present in cells in appropriate amounts. Insufficient metal concentrations can cause essential metal-binding enzymes to malfunction, while excessive metal concentrations can increase the cellular burden and cause cell death. In 1928, scientists investigated the role of copper in physiological processes for the first time (Tardito and Marchio, 2009). Cu-TSCs (thiosemicarbazones) were shown to have antitumor activity in the 1960s, pioneering a new era of cancer treatment with copper compounds (Booth and Sartorelli, 1966; Cappuccino et al., 1967). In 2005, scientists found that the production of reactive oxygen and nitrogen species was a fundamental element influencing the toxic effects and carcinogenicity of trace metals, including copper (Valko et al., 2005). In addition, the Fenton reaction, which generates superoxide radicals and hydroxyl radicals, is involved in the influence of copper on living organisms (Singh et al., 2021). Previous studies have shown that unbalanced intracellular copper levels influence tumorigenesis and the growth and metastasis of tumors, causing irreversible damage. In humans, excessive copper accumulation has two sides. On the one hand, it is life-threatening. On the other hand, intracellular copper accumulation can be used to selectively kill cancer cells (Ge et al., 2022).

A major discovery was recently published in *Science*, as an increased concentration of intracellular copper was found to induce the polymerization of mitochondrial lipoylated proteins and the instability of Fe-S cluster proteins, inducing a novel kind of cell death known as cuproptosis (Tsvetkov et al., 2022). Unlike all other known mechanisms that regulate cell death, cuproptosis, which is a recently discovered copper-induced cell death process, has attracted substantial attention and has become a research hotspot in the field of tumor therapy. First, *Tsvetkov* and colleagues identified whether intracellular copper triggered a new type of regulated cell death that was distinct from oxidative stress-associated cell death processes, such as ferroptosis, apoptosis, and necroptosis. They used different cell death inhibitors, including Z-VAD-FMK, ferrostatin-1, liproxstatin-1, and necrostatin-1, to suppress cell death

triggered by copper complexes, but the inhibitors had no effect on the process. Second, it was demonstrated that copper-induced cell death required the involvement of mitochondrial respiration and that ATP produced by glycolysis had a minor effect on copper-induced cell death. Immediately afterward, the authors also found that copper was not directly involved in the electron transport chain (ETC) but played a role in only the tricarboxylic acid (TCA) cycle. Finally, the researchers found that the copper that penetrated into the mitochondria *via* copper carriers bound directly to these lipid-modified proteins, causing them to form long chains and clump together, leading to cell death. These copper molecules also interfered with iron-sulfur clusters, leading to the downregulation of iron-sulfur proteins and resulting in cytotoxic stress and death. This surprising discovery illustrated how copper actually disrupted mitochondrial function and how it caused cell death, which laid a solid foundation for elucidating the pathology of inherited copper overload illnesses and developing novel ways to treat cancer *via* copper toxicity.

In our work, we first downloaded RNA sequence expression data, clinical and survival data, stemness score data, and immune subtype data of cuproptosis-associated genes (FDX1, LIAS, LIPT1, DLD, DLAT, PDHA1, PDHB, MTF1, GLS, and CDKN2A) from the UCSC Xena. Next, we conducted differential analysis, expression analysis and correlation analysis across cancers. Moreover, survival analysis was conducted to identify the connection between the prognostic outcomes of cuproptosis-associated genes and various cancer types from TCGA. Additionally, we examined the relationship among the levels of cuproptosis-associated genes and immune types, the tumor microenvironment and tumor stem cells across cancers. We further explored the association between drug sensitivity and cuproptosis-associated genes. Finally, the relationship between cuproptosis-associated genes in Kidney renal clear cell carcinoma and tumor features was further analyzed in our work. And we also validated the protein expression by immunohistochemical staining. The above thorough research paved a path for discovering new functions of cuproptosis-associated genes and potential chemotherapy methods in pan-cancer research.

Materials and methods

Data downloading

RNA sequence expression data, clinical and survival data, stemness score data (based on DNA methylation and RNA expression), and immune subtype data of 33 TCGA tumors were abstracted from UCSC Xena (http://xena.ucsc.edu/) (Goldman et al., 2020; Miao et al., 2020). The abbreviations and full names of 33 tumors are listed in the Supplementary Table S1. Because the data from TCGA are open access, this study does not need the approval of the clinical ethics committee. The study complied with the access policies and publication rules of TCGA.

Differential expression analysis and correlation analysis of various cancer types

We obtained 10 cuproptosis-associated genes (FDX1, LIAS, LIPT1, DLD, DLAT, PDHA1, PDHB, MTF1, GLS, and CDKN2A) from the article: copper induces cell death by targeting lipoylated TCA cycle proteins, which was recently published in *Science* (Tsvetkov et al., 2022). These 10 genes were abstracted from Figure 3A in the above article. The team used a genome-wide CRISPR-Cas9 to ensure the scientific and accurate screening and the final screen yielded only 10 genes. These 10 genes were involved in the direct regulation of the vital activity of copper death. Therefore, we selected 10 cuproptosis-associated genes for the following analysis. To study the overall expression of 10 cuproptosis-associated genes across cancers, we first generated a boxplot graph of the expression levels of cuproptosis-associated genes in 33 cancers. Moreover, we visualized the differential expression levels of 10 cuproptosis-associated genes in 18 tumor types, which contained over five normal samples. A heatmap was constructed utilizing the R package "pheatmap". The Wilcoxon test was also used to explore the differences between normal and tumor tissues. Besides, the correlations of cuproptosis-associated genes with other parameters in 33 cancers were analyzed utilizing the R package "corrplot". Finally, we performed Spearman's test to analyze the differential levels of cuproptosis-associated genes in 18 tumors, which contained over five normal samples. Differential expression analysis was visualized with the R package "ggpubr". $^{*}p < 0.05$, $^{**}p < 0.01$, and $^{***}p < 0.001$. $p < 0.05$ was considered statistically significant.

Clinical correlation

To analyze the survival value of patients who had different levels of cuproptosis-associated genes, we performed survival analysis with the R packages "survival" and "survminer". Additionally, Cox proportional hazard regression was also conducted to identify the connection between cuproptosis-associated genes and survival outcomes in various cancer types.

Correlation analysis of six immune subtypes

We visualized the immune subtype analysis of cuproptosis-associated genes using the R packages "limma", "ggplot2", and "reshape2". The Kruskal test was conducted to analyze the differential expression of cuproptosis-associated genes in six

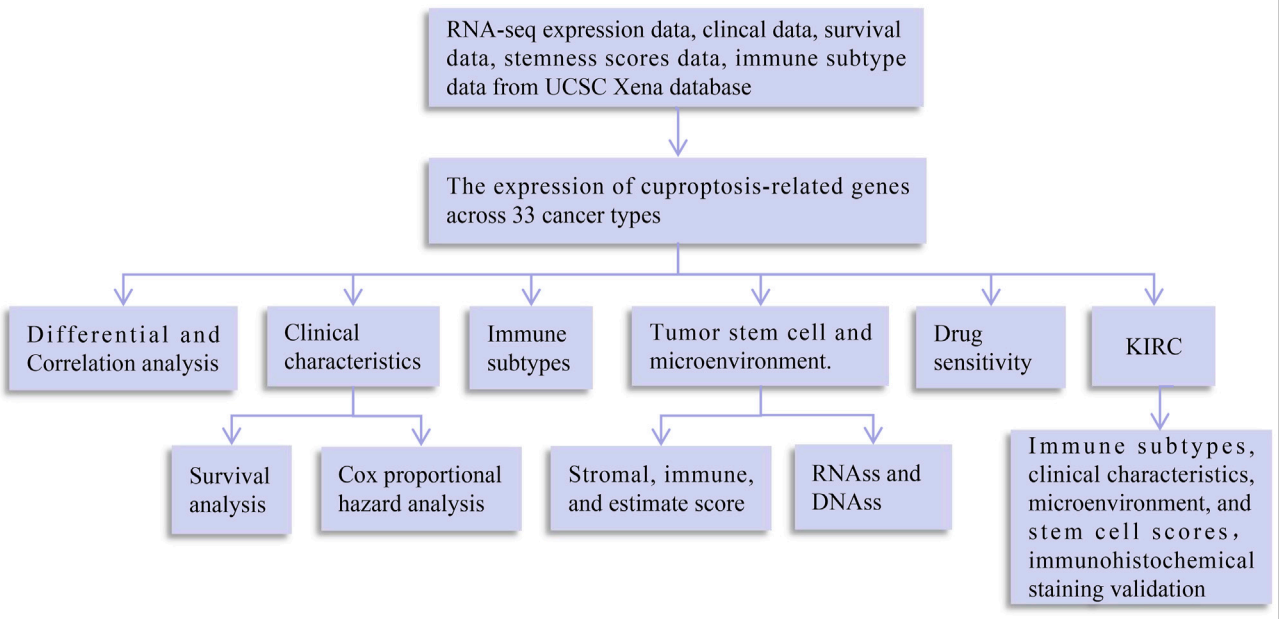

FIGURE 1
Flowchart of pan-cancer analysis in cuproptosis-associated genes. DNAss, DNA stemness score; RNAss, RNA stemness score.

immune subtypes (C1: wound healing, C2: IFN-γ dominant, C3: inflammatory, C4: lymphocyte depleted, C5: immunologically quiet, and C6: TGF-β dominant) (Thorsson et al., 2018).

Correlation analysis of the tumor microenvironment and tumor stem cells

To predict tumor purity and the infiltration of stromal and immune cells in various cancer types, we used the R packages "limma", "estimate", and "corrplot" to visualize the correlations between cuproptosis-associated genes and the tumor microenvironment (Diboun et al., 2006). Spearman's test was used during the process. To analyze the features of tumor stem cells, we downloaded RNA expression data and DNA methylation data for various cancers from TCGA. RNA stemness score (RNAss) and DNA stemness score (DNAss) of cuproptosis-associated genes were presented using the R packages "limma" and "corrplot". Spearman's test was also used during the process.

Drug sensitivity

The CellMiner database (https://discover.nci.nih.gov/cellminer/home.do) is a large database for collecting, processing, and integrating molecular data on NCI-60 and other tumor cells (Shankavaram et al., 2009; Reinhold et al., 2012). We first abstracted gene data and drug sensitivity data from the CellMiner. Drug sensitivity data were validated after a clinical trial and certified with FDA standards. Next, we conducted Pearson test to identify the connections between cuproptosis-associated genes and drug sensitivity. The process was visualized by using the R packages "impute", "limma", "ggplot2", and "ggpubr".

Immune subtypes, clinical characteristics, stem cell scores and the tumor microenvironment in kidney renal clear cell carcinoma

To further identify the relationship between cuproptosis-associated genes and a specific cancer type (KIRC), we explored the levels of cuproptosis-associated genes in six immune subtypes using the Kruskal test. Moreover, we also identified the relationships between cuproptosis-associated genes and clinical characteristics, including stage, grade, age, and sex. Differential expression analysis of cuproptosis-associated genes and clinical characteristics was conducted with the R packages "limma", "ggplot2", and "reshape2". The Kruskal test was also used in the process. Additionally, the correlations between stem cell stores and cuproptosis-associated genes were visualized by utilizing the R packages "limma", "ggplot2", "ggpubr", and "reshape2". Finally, we identified the connection between cuproptosis-associated genes and the tumor microenvironment with Spearman's test.

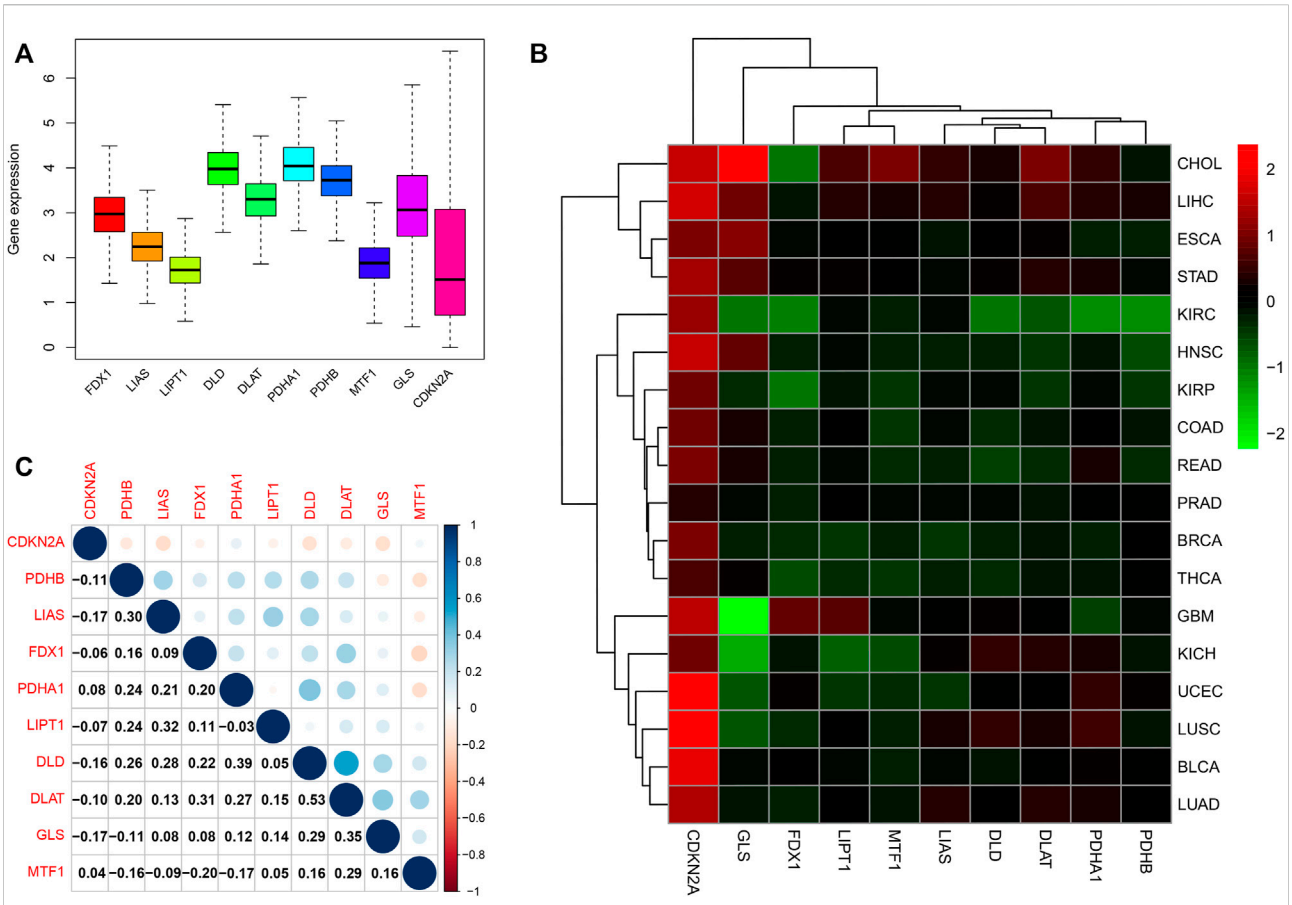

FIGURE 2
Differential expression and correlation analysis of 10 cuproptosis-associated genes in various cancer types. **(A)** Different levels of cuproptosis-associated genes in 33 cancers. Different colors in the bar chart represent different genes. The Y-axis in boxplot means the relative gene expression level in pan-cancer. **(B)** The differential expression of cuproptosis-associated genes in 18 cancers. The red boxes indicate high expression, and the green boxes indicate low expression. **(C)** Correlation analysis of cuproptosis-associated genes. Blue and red dots indicate positive and negative correlations, respectively.

Validation analysis of the human protein atlas

The Human Protein Atlas (http://www.proteinatlas.org/) could be performed to map all the human proteins in tissues using an integration of antibody-based imaging. The tissue section and the pathology section show the distribution of the proteins across major normal tissues and cancer tissues, respectively. We verified the differences in gene expression at the protein level by comparing these two parts. There four degrees of staining: high, medium, low, and not detected.

Statistical analysis

Statistical analyses were processed using the R package v. 3.6.3. The Wilcoxon test was used to explore the differences between normal and tumor tissues. The Kruskal test was conducted to analyze the differential expression of cuproptosis-associated genes in six immune subtypes. The connection between cuproptosis-associated genes and the tumor microenvironment with Spearman's test. Pearson test was used in drug sensitivity analysis. $^{*}p < 0.05$, $^{**}p < 0.01$, and $^{***}p < 0.001$. $p < 0.05$ was considered statistically significant.

Results

The expression of cuproptosis-associated genes across cancers

A flowchart of pan-cancer analysis in cuproptosis-associated genes is shown in Figure 1. We first visualized the levels of 10 cuproptosis-associated genes in 33 cancers (Figure 2A). The boxplot shows that cuproptosis-associated genes, including FDX1, LIAS, DLD, DLAT, PDHA1, PDHB, GLS, LIPT1, MTF1, and CDKN2A had high expression in 33 cancers.

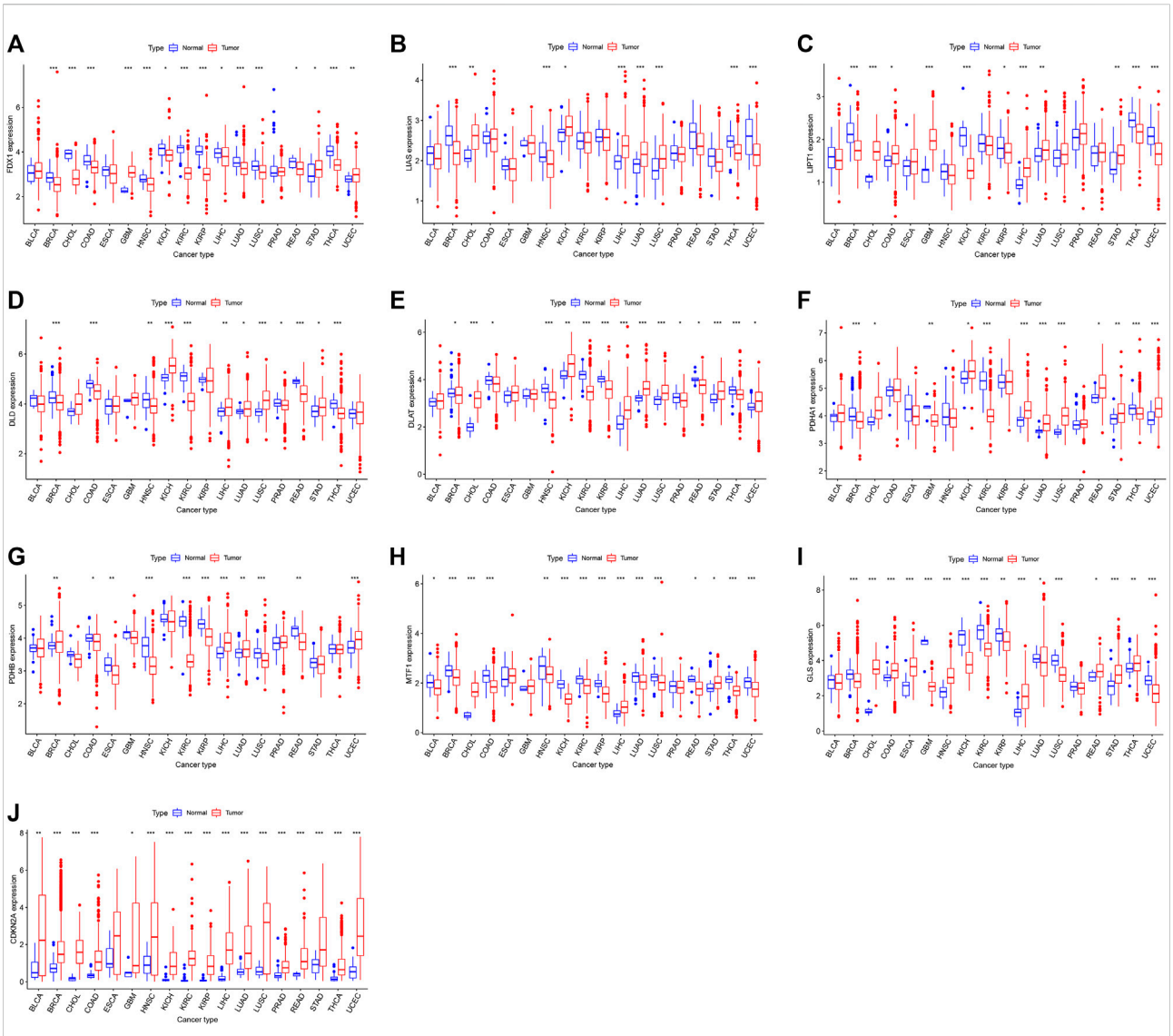

FIGURE 3
(A–J) The levels of cuproptosis-associated genes in various tumor and normal tissues. The blue box plot indicates normal tissue. The red box plot indicates tumor tissue. *$p < 0.05$, **$p < 0.01$, and ***$p < 0.001$.

Gene expression >1 means high expression level and Gene expression <1 means low expression level. Figure 2B shows the differential expression levels of cuproptosis-associated genes in 18 tumor types compared with adjacent non-tumor tissues. The heatmap shows that the fold change in cuproptosis-associated gene was greater than 1, which indicated that the level of cuproptosis-associated gene was higher in tumor tissue than corresponding normal tissue. It was surprise findings that CDKN2A had higher expression levels in 18 tumor types, which indicated that CDKN2A could be a novel biomarker in various cancers. Figure 2C presents the correlation analysis of cuproptosis-associated genes in 33 cancers. DLD and DLAT shared the strongest positive correlation (correlation coefficient = 0.53). However, FDX1 and MTF1 had the strongest negative correlation (correlation coefficient = −0.20). The expression of cuproptosis-associated genes in different tumors and normal tissues is presented in Figure 3. The boxplots indicates that CDKN2A had higher levels in various cancers, in accordance with the outcomes in Figure 2B.

Prognostic value of cuproptosis-associated genes across cancers

Figure 4; Supplementary Figure S1 show the survival analysis of cuproptosis-associated genes in various cancers. A large majority of

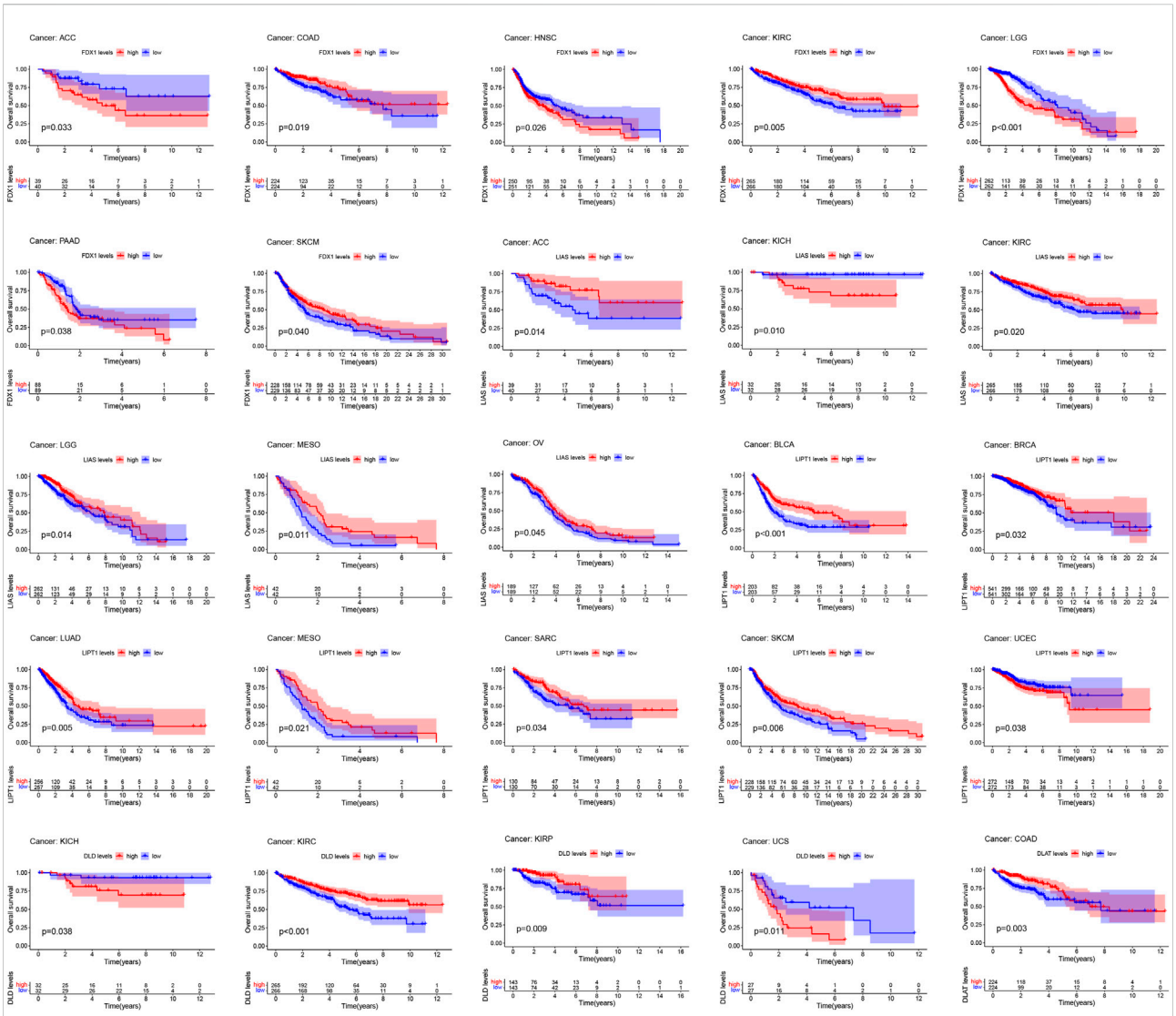

FIGURE 4
Survival analysis of cuproptosis-associated genes in various cancers. The red and blue lines of the picture indicate high and low level, respectively.

cuproptosis-associated genes including FDX1, LIAS, DLD, DLAT, MTF1, and CDKN2A had significant overall survival ($p < 0.05$), which indicated that cuproptosis-associated genes could be prognosis factors in Kidney renal clear cell carcinoma (KIRC). The above results also indicated that cuproptosis could play a crucial part in the occurrence and development of KIRC, paving the way for the following analysis. We also discovered that cuproptosis-associated genes including FDX1, LIAS, PDHA1, MTF1, CDKN2A had significant overall survival ($p < 0.05$), which indicated that cuproptosis-associated genes could be prognosis factors in Adrenocortical carcinoma (ACC). Similarly, cuproptosis-associated genes including LIAS, LIPT1, PDHB, GLS, and CDKN2A had significant overall survival in Mesothelioma (MESO) ($p < 0.05$). Cox proportional hazard analysis indicated the overall survival rates associated with cuproptosis-associated gene expression in various cancer types, as shown in Figure 5. And explicit HR and p-value in the Cox risk model were found in the Supplementary Table S2. A hazard ratio <1 indicated that cuproptosis-associated genes could be low risk factors; however, a hazard ratio >1 indicated that cuproptosis-associated genes could be high risk factors. As shown in the figure, all cuproptosis-associated genes were high risk factors in Prostate adenocarcinoma (PRAD). However, a large majority of cuproptosis-associated genes including FDX1, LIAS, LIPT1, DLD, DLAT, and PDHB acted as a low-risk indicator in Lymphoid neoplasm diffuse large B-cell lymphoma (DLBC). The above results indicated that cuproptosis-associated genes played a vital role in the survival of the patients with PRAD or DLBC.

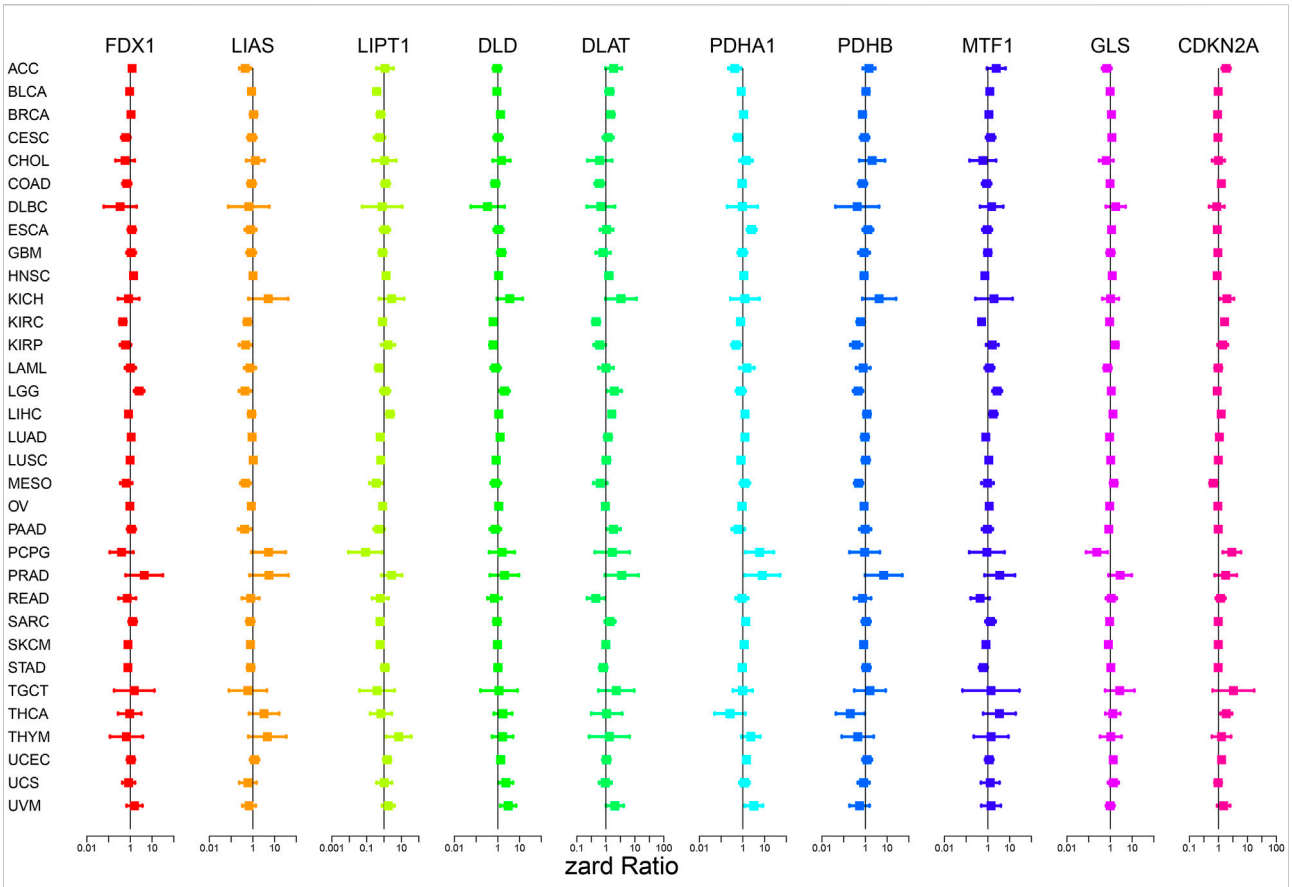

FIGURE 5
Cox proportional hazard analysis indicates the overall survival rate associated with cuproptosis-associated gene expression in various cancer types. A hazard ratio <1 indicates low risk, and a hazard ratio >1 indicates high risk.

Correlation analysis of cuproptosis-associated genes and different immune subtypes

Figure 6 shows the different levels of cuproptosis-associated genes in six different immune subtypes. Cuproptosis-associated genes, including FDX1, LIAS, LIPT1, DLD, DLAT, PDHA1, PDHB, MTF1, and GLS were highly expressed in different immune subtypes. The levels of CDKN2A were higher in C1, C2, C4, C5, and C6, and lower in C3. *p*-value is labeled as the comparison of six different immune subtypes.

Correlation analysis among cuproptosis-associated genes, stem cell scores and the tumor microenvironment

Tumor cells can lose their differentiated phenotype and develop precursor and stem cell-like characteristics as they develop. RNAss and DNAss were calculated to assess the features of tumor stem cells (Malta et al., 2018). Correlation analysis of cuproptosis-associated gene and stemness scores is shown in Figures 7A,B. As shown in the picture, the expression of a large majority of cuproptosis-associated genes including FDX1, LIAS, LIPT1, DLD, DLAT, PDHA1, and PDHB was positively correlated with RNAss and DNAss, which indicated that the higher the levels of cuproptosis-associated genes are, the higher the levels of stem cell scores, the more vigorous the tumor stem cells, and the lower the levels of tumor differentiation. However, MTF1 and GLS were negatively correlated with RNAss and DNAss. Figures 7C–E shows the associations among the expression of cuproptosis-associated genes and stromal, immune, and ESTIMATE scores. As shown in the picture, a large majority of cuproptosis-associated genes, including FDX1, LIAS, LIPT1, DLD, DLAT, PDHA1, and PDHB were negatively associated with immune, stromal, and estimated scores, which implies that the levels of immune and stromal cells are low across cancers and that tumor purity is high. However, some cuproptosis-associated genes, including MTF1, GLS, and CDKN2A, were positively associated with immune, stromal, and ESTIMATE scores, and the levels of immune and stromal cells were high across cancers, with low tumor purity.

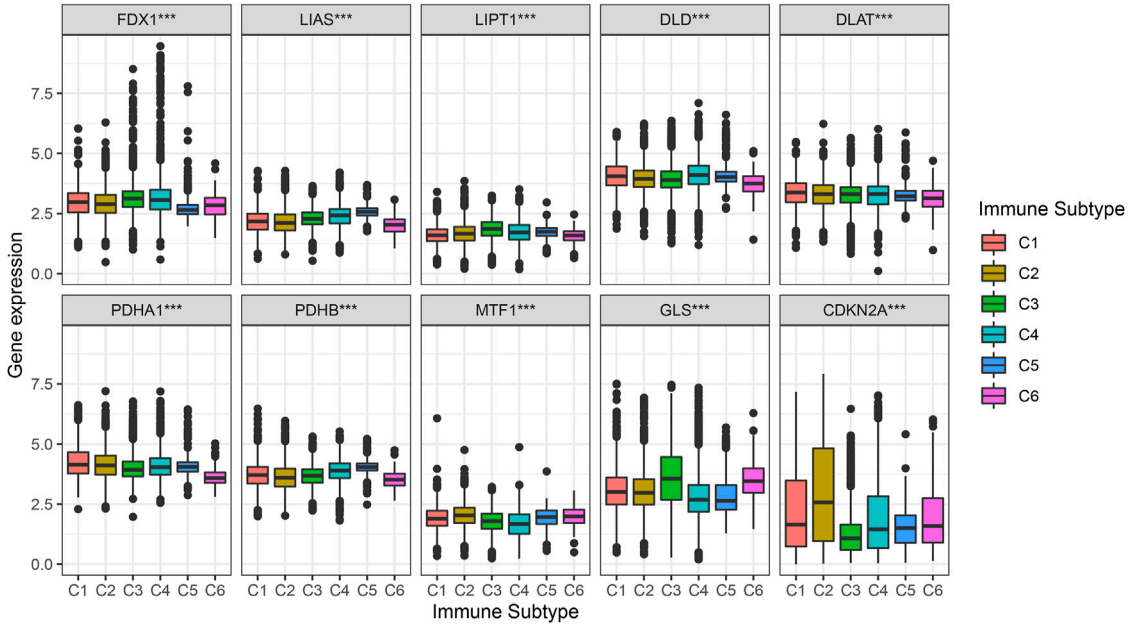

FIGURE 6
Correlation analysis between cuproptosis-associated genes and six immune subtypes. C1, wound healing, C2, IFN-γ dominant, C3, inflammatory, C4, lymphocyte depleted, C5, immunologically quiet, and C6, TGF-β dominant.

The relationship between cuproptosis-associated genes and drug sensitivity

To explore the correlation between drug sensitivity and cuproptosis-associated genes, we conducted Pearson correlation analysis to address the expression data of cuproptosis-associated genes and drug sensitivity data. Figure 8 shows the top 16 drugs strongly sensitivity to cuproptosis-associated genes according to the correlation coefficient. As shown in the picture, GLS was negatively associated with sensitivity to bisacodyl, active ingredient of viraplex (cor = −0.372, p = 0.003), Actinomycin D (cor = −0.372, p = 0.003), Paclitaxel (cor = −0.366, p = 0.004) and positively associated with sensitivity to Midostaurin (cor = 0.340, p = 0.008). The higher the level of LIAS is, the stronger the sensitivity to drugs, including Hydroxyurea (cor = 0.348, p = 0.006), Asparaginase (cor = 0.332, p = 0.010), Acrichine (cor = 0.315, p = 0.014), RH1 (cor = 0.307, p = 0.017), and Nitrogen mustard (cor = 0.301, p = 0.020). PDHA1 was positively associated with Carmustine (cor = 0.370, p = 0.004), PX-316 (cor = 0.324, p = 0.012), and Hypothemycin (cor = 0.322, p = 0.012). The increased expression of CDKN2A resulted in less sensitivity to Mitoxantrone (cor = −0.360, p = 0.005) and stronger sensitivity to bisacodyl, active ingredient of viraplex (cor = 0.302, p = 0.019). DLAT and Methotrexate had positive correlation (cor = 0.322, p = 0.012). Cor means correlation coefficient.

Correlation analysis of cuproptosis-associated genes, immune subtypes, and clinical features in kidney renal clear cell carcinoma

From previous survival analysis, we found that the number of cuproptosis-associated genes with survival statistical significance was the highest in KIRC, compared with other cancers, which indicated that cuproptosis could play a crucial part in the occurrence and development of KIRC. Therefore, we further analyzed the connection of cuproptosis-associated genes, immune subtypes and clinical features. Figure 9 shows the correlation of cuproptosis-associated genes and different immune subtypes in KIRC. All cuproptosis-associated genes except for PDHB, were associated with six immune subtypes, with statistical significance, and most of them had high expression in various immune subtypes. The correlation between cuproptosis-associated gene expression and clinical characteristics in KIRC is shown (Figure 10). Clinical features, including age, sex, stage, and grade, were studied in our work. Figure 10A shows that the expression levels of all cuproptosis-associated genes except for GLS were significantly different in different grades. Most of cuproptosis-associated genes including LIAS, DLD, DLAT, PDHA1, PDHB, MTF1, and CDKN2A had significantly differential expression according to stage (Figure 10B). The above results indicated cuproptosis had strong guidance value in clinical features of the patients with KIRC. The expression levels of FDX1, MTF1, and GLS varied significantly in different genders

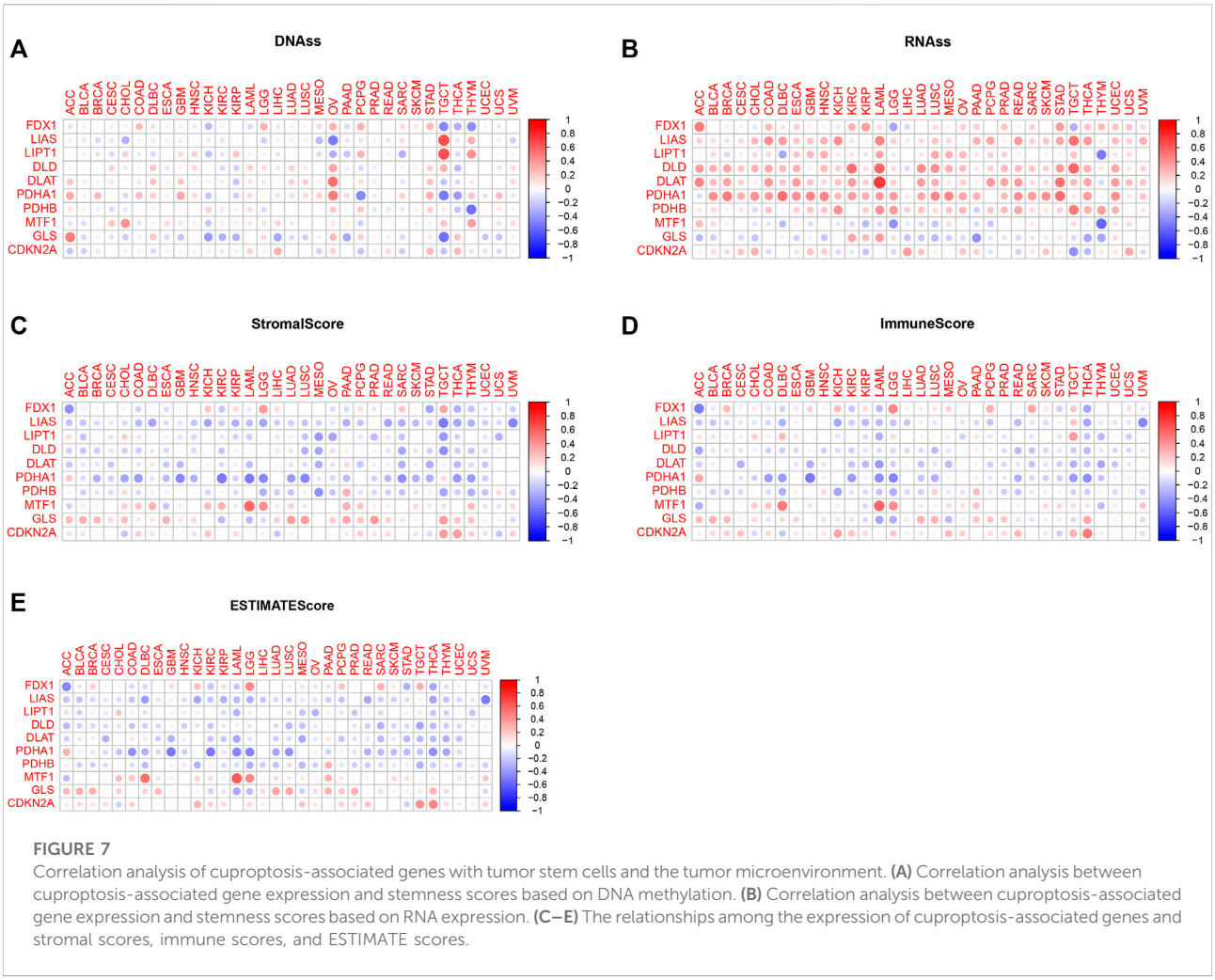

FIGURE 7
Correlation analysis of cuproptosis-associated genes with tumor stem cells and the tumor microenvironment. **(A)** Correlation analysis between cuproptosis-associated gene expression and stemness scores based on DNA methylation. **(B)** Correlation analysis between cuproptosis-associated gene expression and stemness scores based on RNA expression. **(C–E)** The relationships among the expression of cuproptosis-associated genes and stromal scores, immune scores, and ESTIMATE scores.

(Figure 10C). Figure 10D shows that only PDHA1 was associated with ages. *p*-value was the result of an inter-group comparison.

The relationship of cuproptosis-associated genes, stem cell scores and the tumor microenvironment in kidney renal clear cell carcinoma

Figure 11 indicates the correlations of cuproptosis-associated genes, the KIRC microenvironment, and stem cell scores. Cuproptosis-associated genes, including DLD and GLS, were significantly associated with stemness scores (DNAss and RNAss) ($p < 0.05$). The scatter plot shows that the levels of DLD and GLS were positively associated with the DNAss and RNAss, which indicated that the higher the levels of DLD and GLS were, the higher the levels of stem cell scores, the more vigorous the tumor stem cells, and the lower the levels of tumor differentiation. Meanwhile, a large majority of cuproptosis-associated genes including FDX1, LIAS, DLD, DLAT, PDHA1, and GLS, were significantly associated with the tumor microenvironment (immune, stromal, and estimate scores) ($p < 0.05$). We surprisingly found that the levels of most of cuproptosis-associated genes were negatively associated with immune, stromal, and ESTIMATE scores, which implied that the lower the expression of cuproptosis-associated genes was, the higher the tumor purity. The above results implied that cuproptosis acted as a crucial role in the occurrence and development, which indicated that cuproptosis-associated genes could serve as a potential novel target for KIRC therapy.

Validation of cuproptosis-associated genes in renal cancer tissues compared with normal tissues by immunohistochemical staining

The above results showed that differential expression levels of cuproptosis-associated genes played a crucial in survival

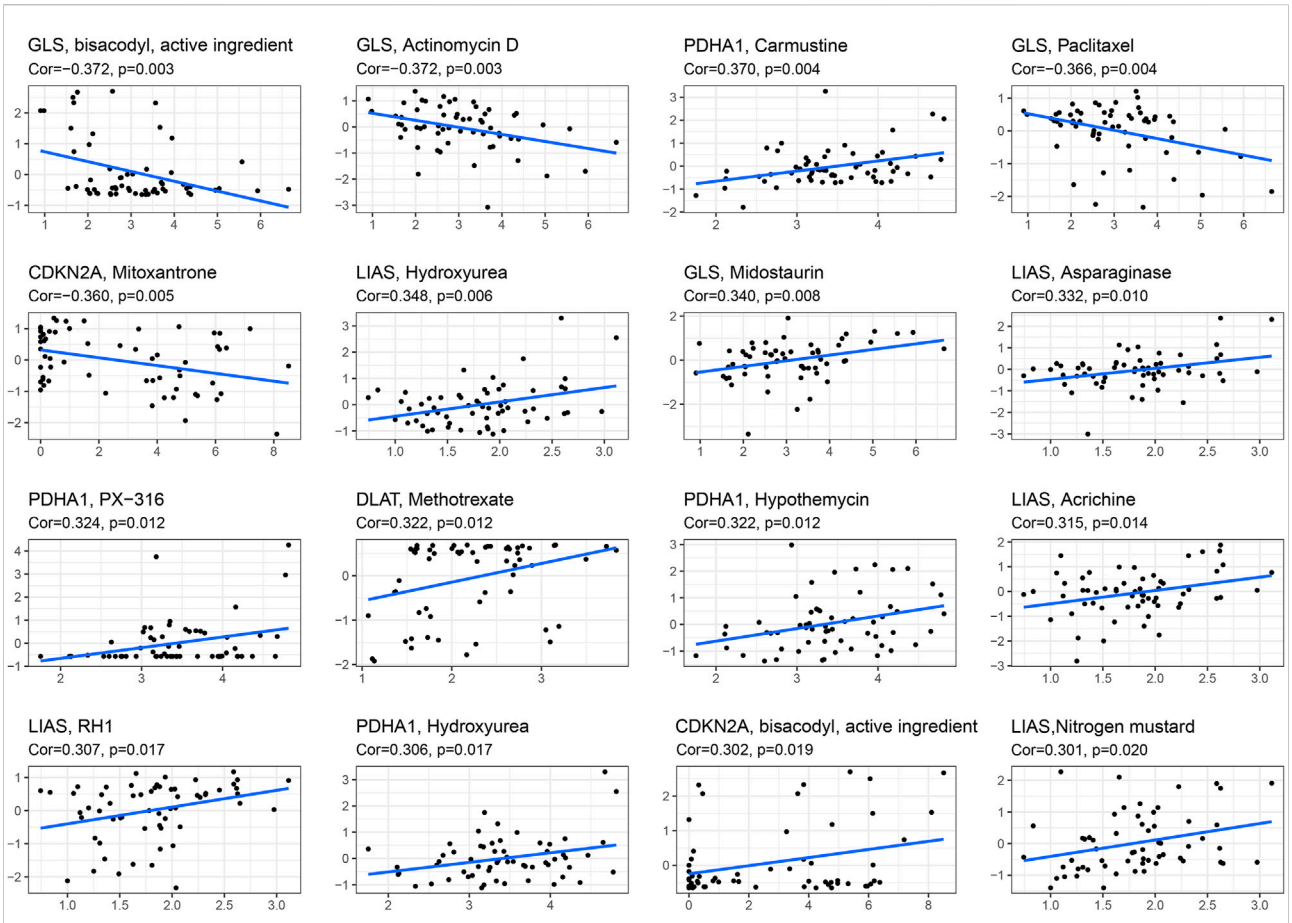

FIGURE 8
The relationship between cuproptosis-associated genes and drug sensitivity.

outcomes, immune subtypes, clinical features, stem cell scores and the tumor microenvironment of patients. Next, by immunohistochemical staining, we identified protein expression levels of cuproptosis-associated genes in renal cancer tissues and normal tissues. The results demonstrated that a large majority of cuproptosis-associated genes including FDX1, LIAS, LIPT1, DLD, DLAT, PDHA1, PDHB, MTF1, and GLS had higher expression in normal tissues compared with renal cancer tissues, whereas CDKN2A was highly expressed in renal cancer tissues, which was very consistent with the results of our previous analysis (Figure 12).

Discussion

Previous studies have shown that copper can induce various cell death pathways, such as apoptosis and autophagy, through different mechanisms, including an increase in reactive oxygen species, proteasome suppression, and antiangiogenesis (Jiang et al., 2022). The first mechanism is oxidative stress: Increased levels of ROS are triggered by the copper-regulated Fenton reaction or a deficiency of antioxidant suppression, which leads to mitochondrial malfunction and cell death. Second, copper bound to proteasome subunits, leading to the accumulation of ubiquitinated proteins. Third, copper deficiency restricted the creation of new blood vessels, reducing nutrient access in tumor tissues. A major discovery was recently published in *Science*: Copper induces cell death by targeting lipoylated TCA cycle proteins (Tsvetkov et al., 2022). This significant discovery fully illuminated how copper caused mitochondrial dysfunction and how this led to cell death (Zischka et al., 2011; Bock and Tait, 2020). These findings could imply that it is of great significance to maintain the dynamic balance of copper in the organism. Most importantly, these new outcomes could lay a solid foundation for investigating the usage of copper to treat cancer. Despite these significant advancements, scientists must increase awareness of the detailed mechanisms and effects of cuproptosis in the future (Kahlson and Dixon, 2022).

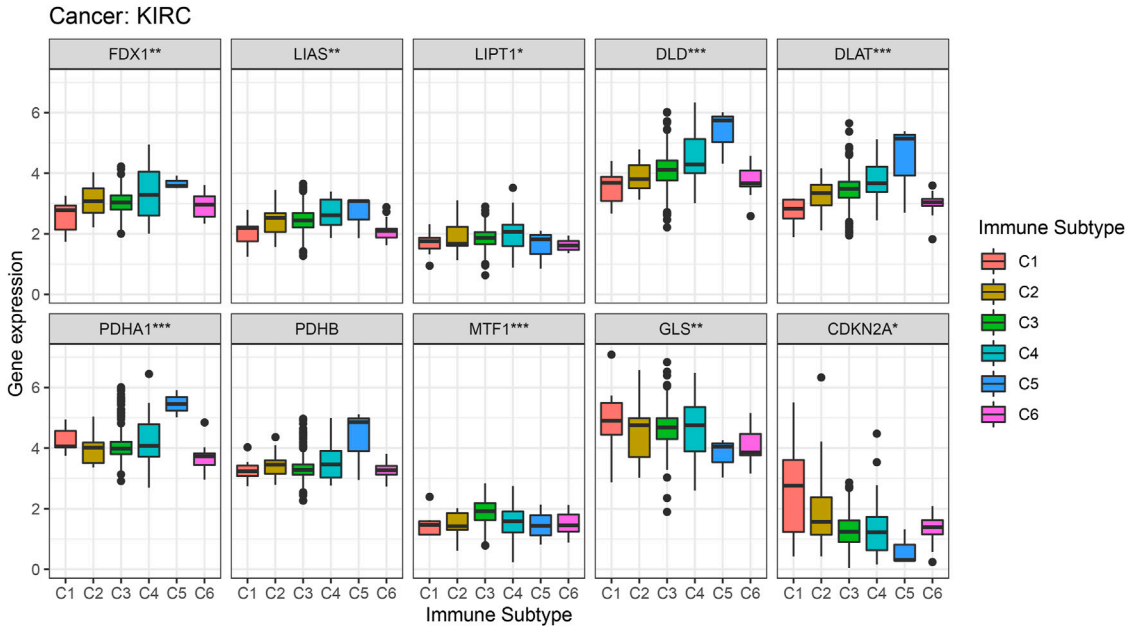

FIGURE 9
Correlation analysis between the expression of cuproptosis-associated genes and different immune subtypes in Kidney renal clear cell carcinoma (KIRC).

Cuproptosis-associated genes play a key part in the oncogenesis, progression and metastasis of tumors (Tang et al., 2022). Therefore, we performed an overall analysis to uncover the value of cuproptosis-associated genes across cancers. We obtained 10 cuproptosis-associated genes (FDX1, LIAS, LIPT1, DLD, DLAT, PDHA1, PDHB, MTF1, GLS, and CDKN2A) from the article: copper induces cell death by targeting lipoylated TCA cycle proteins, which was recently published in *Science* (Tsvetkov et al., 2022). Tsvetkov et al. firstly demonstrated that cuproptosis, a novel cell death path induced by copper ionophore, was distinguish from apoptotic, ferroptotic, necroptotic. Moreover, the research identified that copper-induced cell death was closely associated with mitochondrial metabolism, further elucidating the precise relationship between copper and the TCA cycle. Next, the team used a genome-wide CRISPR-Cas9 screen in order to clarify the specific metabolic pathway of this cell death and treated with different structures of copper ion vectors to improve the generality of the screen. The final screen yielded 10 genes, and the knockdown of each of these 10 genes significantly inhibited both types of copper ion vector-mediated cell killing. They further demonstrated that FDX1, the key gene for copper death, was also an upstream regulator of protein lipoic acidification. Besides, FDX1, LIAS, LIPT1, and DLD was involved in the lipoic acid pathway, and DLAT, PDHA1, PDHB, MTF1, GLS, and CDKN2A was involved in forming the Pyruvate dehydrogenase complex. The above genes were involved in the direct regulation of the vital activity of copper death. A genome-wide CRISPR-Cas9 screen is superior to other screening routes including correlation coefficients, Reason is that based only on correlation coefficients, the above genes are not representative and also not involved in the direct regulation of cuproptosis. Therefore, we selected 10 cuproptosis-associated genes from a genome-wide CRISPR-Cas9 screen for the following analysis.

Our work aimed to explore the relationships between cuproptosis-associated genes and tumor features, including clinical characteristics, survival outcome, immune subtype, tumor microenvironment, stemness score, and drug sensitivity. We found that all cuproptosis-associated genes, including FDX1, LIAS, LIPT1, DLD, DLAT, PDHA1, PDHB, MTF1, GLS, and CDKN2A had higher expression in various cancers. Our research revealed the differential expression levels of cuproptosis-associated genes in 18 cancer types compared with adjacent non-tumor tissues. Moreover, survival analysis showed that cuproptosis-associated genes had prognostic value in various cancer types. Cox proportional hazard analysis showed the overall survival rate of cuproptosis-associated genes in various cancer types, which indicated whether cuproptosis-associated genes were low- or high-risk factors. These outcomes strongly suggested that cuproptosis-associated genes could

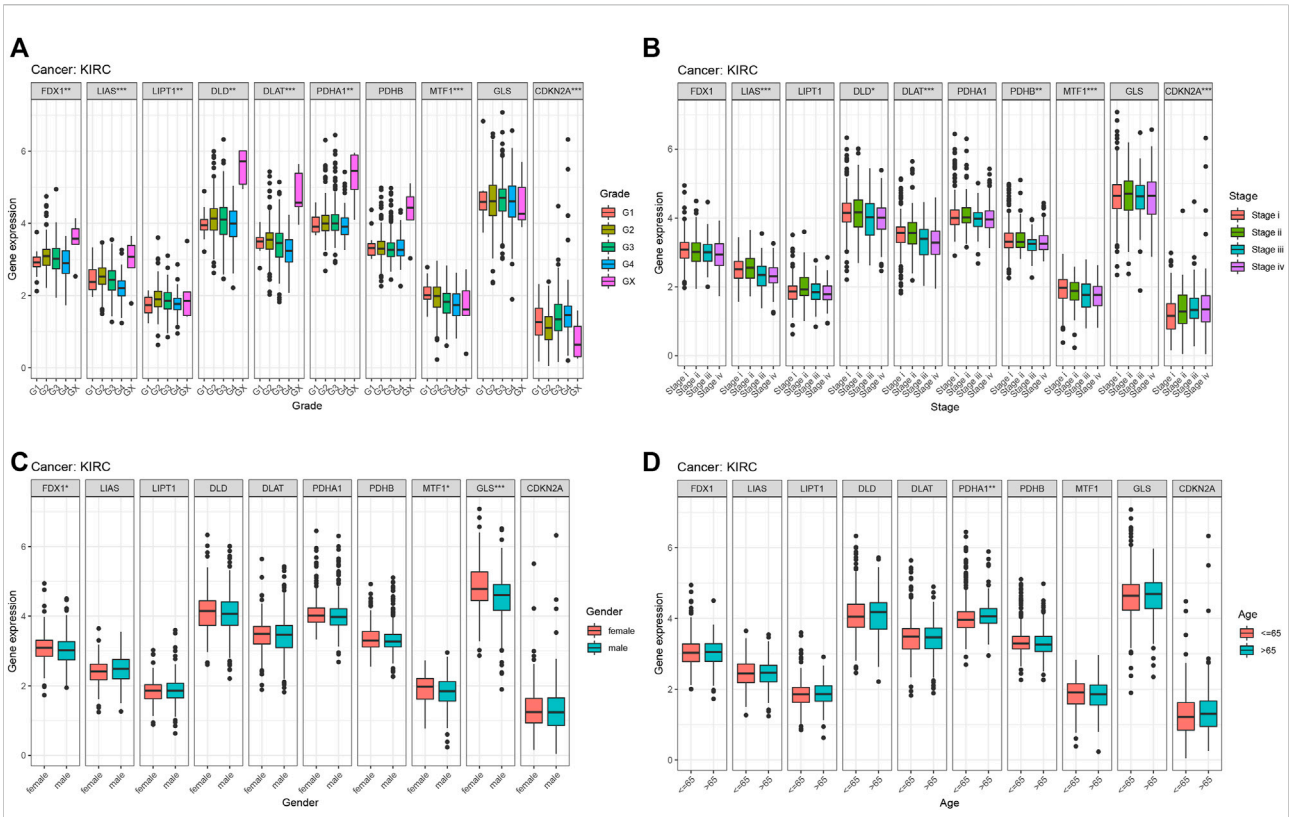

FIGURE 10
The relationship between cuproptosis-associated genes and clinical characteristics in KIRC. **(A)** Stage, **(B)** grade, **(C)** age, and **(D)** sex.

be significant diagnostic or prognostic markers across cancers, thereby contributing to research on targeted therapy.

The immune subtypes of cancers differ from one another, and each immune subtype has distinct biological and clinical characteristics that influence anticancer therapy to some extent. Our study also investigated the associations of cuproptosis-associated genes, immune subtype and clinical features. The findings showed that most of cuproptosis-associated genes, including FDX1, LIAS, LIPT1, DLD, DLAT, PDHA1, PDHB, MTF1, and GLS were highly expressed in different immune subtypes. The levels of CDKN2A were higher in C1, C2, C4, C5, and C6, and lower in C3. Previous research showed that tumors with the C4 and C6 subtypes had the worst prognosis, presenting with mainly macrophages, low lymphocyte infiltration, and a large number of M2 macrophages. In contrast, tumors consisting of the C2 and C3 subtypes had better survival outcomes. These findings implied that neoantigen could provide more prognostic signals in immune subtypes compared with tissue-based sources and highlight the significance of immune information for the response to tumor neoantigens.

The tumor microenvironment has a close relationship with oncogenesis and the growth and metastasis of tumors, and it is not only associated with the intrinsic environment of the tumor cells themselves (nuclear and cytoplasmic) but also includes various normal cells, including fibroblasts, vascular endothelial cells, stromal and immune cells (Neal et al., 2018; Jiao et al., 2019). We demonstrated that cuproptosis-associated genes were differentially associated with immune, stromal, and ESTIMATE scores, which revealed the effects of different tumor purities and infiltration of immune and stromal cells (Yoshihara et al., 2013). More importantly, the infiltration of immune and stromal cells was strongly associated with clinical outcomes and provided crucial clues for the diagnosis and prognosis of tumors. This infiltration was used to identify an effective drug target, further improving the survival outcome of patients (Malta et al., 2018). In addition, we also paid attention to the tumor stemness score. A higher stemness score was associated with stronger biological activity and weaker tumor dedifferentiation ability in tumor stem cells. Our work showed that a large majority of cuproptosis-associated genes was positively associated with RNAss and DNAss. These findings showed that the expression of

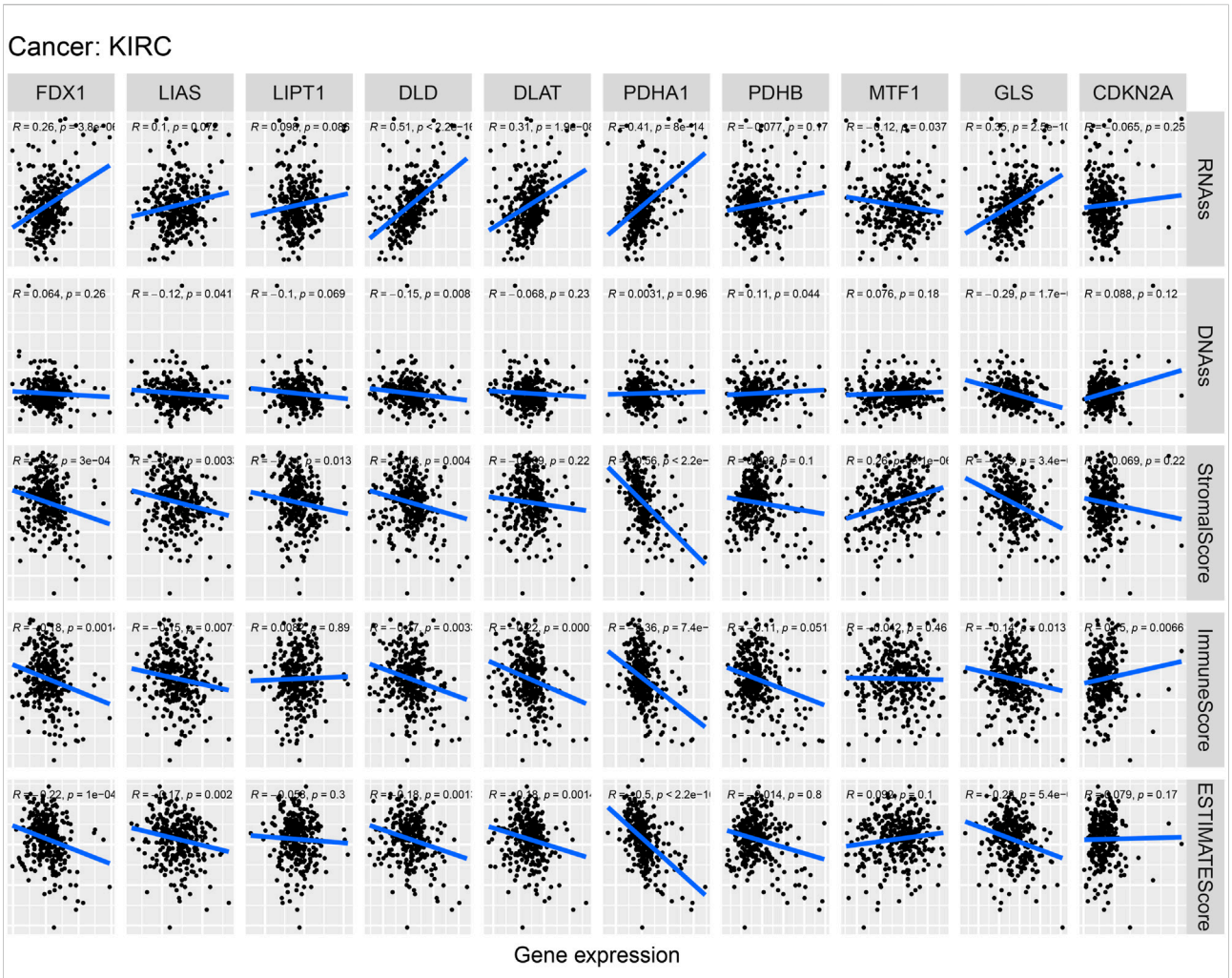

FIGURE 11
Correlation analysis of cuproptosis-associated gene expression, the tumor microenvironment, and stem cell scores in KIRC.

cuproptosis-associated genes and the stemness score could predict the effectiveness of stem cell-associated immunotherapy, further improving the survival outcome of patients.

Finally, we investigated the interaction between drug sensitivity and cuproptosis-associated genes. The expression data of cuproptosis-associated genes and drug sensitivity data were abstracted from CellMiner, which included 108 FDA-approved and 70 clinical trial drugs and genomic data. Across numerous cancer types, this database provided a resource for pharmacologic data that could be used to strengthen existing therapeutic strategies and find new medications and pharmacological targets. Our findings revealed that cuproptosis-associated genes were closely associated with sensitivity to FDA-approved and clinical trial drugs. For example, both LIAS and PDHA1 were positively associated with sensitivity to Hydroxyurea. A recent study showed that some drugs, including Hydroxyurea, have shown promising anticancer efficacy *in vitro*, *in vivo*, and in clinical trials, making them potential candidates for therapeutic repurposing in oncology. These findings showed that cuproptosis-associated genes were associated with sensitivity to drugs and that their expression is important in the clinic for the selection of anticancer drugs. For certain cancers (KIRC), we also found that cuproptosis-associated genes were tightly associated with immune subtype, clinical features, the tumor microenvironment, and stem cell scores. And we also validated the protein expression by immunohistochemical staining.

We performed a pan-cancer analysis of cuproptosis-associated genes, which included differential expression,

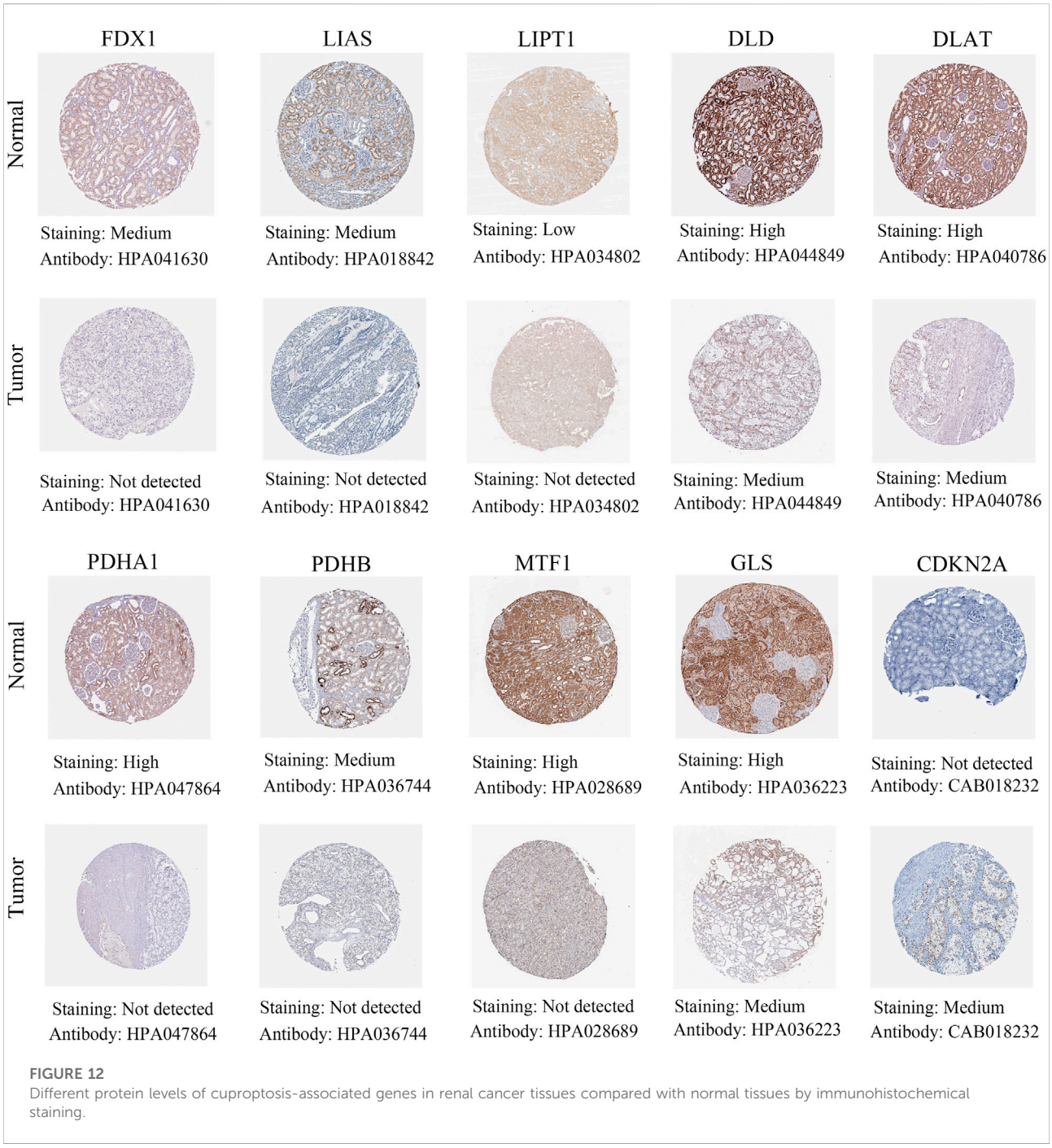

FIGURE 12
Different protein levels of cuproptosis-associated genes in renal cancer tissues compared with normal tissues by immunohistochemical staining.

survival outcomes, immune subtypes, clinical features, the tumor microenvironment, stemness scores, and drug sensitivity. There was still some work to be done. First, we should further explore the mechanism of copper death in depth, and how cell respiration promotes cuproptosis. Second, we also should conduct a pan-cancer analysis of cuproptosis-associated genes with corresponding experiments for validation.

Conclusion

In conclusion, this is the first and most comprehensive work to investigate the correlations between cuproptosis-associated genes and tumor features, including differential expression, survival outcomes, immune subtypes, the tumor immune microenvironment, stemness scores, and cancer drug sensitivity, which provides new insight into the

mechanism of cuproptosis-associated genes across cancers and lays a solid foundation for the discovery of novel therapeutic targets.

Data availability statement

The original contributions presented in the study are included in the article/Supplementary Material, further inquiries can be directed to the corresponding author.

Ethics statement

The data from public database are open access, this study does not need the approval of the clinical ethics committee. The study complied with the access policies and publication rules of public database.

Author contributions

JL and WL designed the study; YL, YD, and CZ collected the data; JL, YS, and XL analyzed the data; JL wrote the manuscript; WL, HY, and JD revised the manuscript. All authors approved the submitted version.

Funding

Our study received funding from Changzhou High-Level Medical Talents Training Project (No: 2016CZBJ054) and Clinical Medical Science and Technology Development Fund by the Changzhou Sci & Tech Program (Nos: CJ20210015 and CJ20220006).

Acknowledgments

This is an acknowledgment to the contributions of all colleagues, public database that aided the authors.

Conflict of interest

The authors declare that the research was conducted in the absence of any commercial or financial relationships that could be construed as a potential conflict of interest.

Publisher's note

All claims expressed in this article are solely those of the authors and do not necessarily represent those of their affiliated organizations, or those of the publisher, the editors and the reviewers. Any product that may be evaluated in this article, or claim that may be made by its manufacturer, is not guaranteed or endorsed by the publisher.

Supplementary material

The Supplementary Material for this article can be found online at: https://www.frontiersin.org/articles/10.3389/fgene.2022.939956/full#supplementary-material

References

Bock, F. J., and Tait, S. W. G. (2020). Mitochondria as multifaceted regulators of cell death. *Nat. Rev. Mol. Cell Biol.* 21 (2), 85–100. doi:10.1038/s41580-019-0173-8

Booth, B. A., and Sartorelli, A. C. (1966). Synergistic interaction of kethoxal bis(thiosemicarbazone) and cupric ions in sarcoma 180. *Nature* 210 (5031), 104–105. doi:10.1038/210104b0

Bray, F., Laversanne, M., Weiderpass, E., and Soerjomataram, I. (2021). The ever-increasing importance of cancer as a leading cause of premature death worldwide. *Cancer* 127 (16), 3029–3030. doi:10.1002/cncr.33587

Cappuccino, J. G., Banks, S., Brown, G., George, M., and Tarnowski, G. S. (1967). The effect of copper and other metal ions on the antitumor activity of pyruvaldehyde bis(thiosemicarbazone). *Cancer Res.* 27 (5), 968–973.

Diboun, I., Wernisch, L., Orengo, C. A., and Koltzenburg, M. (2006). Microarray analysis after RNA amplification can detect pronounced differences in gene expression using limma. *BMC Genomics* 7, 252. doi:10.1186/1471-2164-7-252

Dineley, K. E., Votyakova, T. V., and Reynolds, I. J. (2003). Zinc inhibition of cellular energy production: implications for mitochondria and neurodegeneration. *J. Neurochem.* 85 (3), 563–570. doi:10.1046/j.1471-4159.2003.01678.x

Du, W., Gu, M., Hu, M., Pinchi, P., Chen, W., Ryan, M., et al. (2021). Lysosomal Zn(2+) release triggers rapid, mitochondria-mediated, non-apoptotic cell death in metastatic melanoma. *Cell Rep.* 37 (3), 109848. doi:10.1016/j.celrep.2021.109848

Ge, E., Bush, A., Casini, A., Cobine, P., Cross, J., DeNicola, G., et al. (2022). Connecting copper and cancer: from transition metal signalling to metalloplasia. *Nat. Rev. Cancer* 22 (2), 102–113. doi:10.1038/s41568-021-00417-2

Goldman, M. J., Craft, B., Hastie, M., Repecka, K., McDade, F., Kamath, A., et al. (2020). Visualizing and interpreting cancer genomics data via the Xena platform. *Nat. Biotechnol.* 38 (6), 675–678. doi:10.1038/s41587-020-0546-8

Jiang, Y., Huo, Z., Qi, X., Zuo, T., and Wu, Z. (2022). Copper-induced tumor cell death mechanisms and antitumor theragnostic applications of copper complexes. *Nanomedicine (Lond)* 17 (5), 303–324. doi:10.2217/nnm-2021-0374

Jiao, S., Subudhi, S. K., Aparicio, A., Ge, Z., Guan, B., Miura, Y., et al. (2019). Differences in tumor microenvironment dictate T helper lineage polarization and response to immune checkpoint therapy. *Cell* 179 (5), 1177–1190.e13. doi:10.1016/j.cell.2019.10.029

Kagan, V. E., Mao, G., Qu, F., Angeli, J. P., Doll, S., Croix, C. S., et al. (2017). Oxidized arachidonic and adrenic PEs navigate cells to ferroptosis. *Nat. Chem. Biol.* 13 (1), 81–90. doi:10.1038/nchembio.2238

Kahlson, M. A., and Dixon, S. J. (2022). Copper-induced cell death. *Science* 375 (6586), 1231–1232. doi:10.1126/science.abo3959

Malta, T. M., Sokolov, A., Gentles, A. J., Burzykowski, T., Poisson, L., Weinstein, J. N., et al. (2018). Machine learning identifies stemness features associated with oncogenic dedifferentiation. *Cell* 173 (2), 338–354.e15. doi:10.1016/j.cell.2018.03.034

Miao, Y., Wang, J., Li, Q., Quan, W., Wang, Y., Li, C., et al. (2020). Prognostic value and immunological role of PDCD1 gene in pan-cancer. *Int. Immunopharmacol.* 89, 107080. doi:10.1016/j.intimp.2020.107080

Neal, J. T., Li, X., Zhu, J., Giangarra, V., Grzeskowiak, C. L., Ju, J., et al. (2018). Organoid modeling of the tumor immune microenvironment. *Cell* 175 (7), 1972–1988. doi:10.1016/j.cell.2018.11.021

Reinhold, W. C., Sunshine, M., Liu, H., Varma, S., Kohn, K. W., Morris, J., et al. (2012). CellMiner: a web-based suite of genomic and pharmacologic tools to explore transcript and drug patterns in the NCI-60 cell line set. *Cancer Res.* 72 (14), 3499–3511. doi:10.1158/0008-5472.CAN-12-1370

Shankavaram, U. T., Varma, S., Kane, D., Sunshine, M., Chary, K. K., Reinhold, W. C., et al. (2009). CellMiner: a relational database and query tool for the NCI-60 cancer cell lines. *BMC Genomics* 10, 277. doi:10.1186/1471-2164-10-277

Singh, P., Youden, B., Yang, Y., Chen, Y., Carrier, A., Cui, S., et al. (2021). Synergistic multimodal cancer therapy using glucose oxidase@CuS nanocomposites. *ACS Appl. Mat. Interfaces* 13 (35), 41464–41472. doi:10.1021/acsami.1c12235

Sung, H., Ferlay, J., Siegel, R. L., Laversanne, M., Soerjomataram, I., Jemal, A., et al. (2021). Global cancer statistics 2020: GLOBOCAN estimates of incidence and mortality worldwide for 36 cancers in 185 countries. *CA. Cancer J. Clin.* 71 (3), 209–249. doi:10.3322/caac.21660

Tang, R., Xu, J., Zhang, B., Liu, J., Liang, C., Hua, J., et al. (2020). Ferroptosis, necroptosis, and pyroptosis in anticancer immunity. *J. Hematol. Oncol.* 13 (1), 110. doi:10.1186/s13045-020-00946-7

Tang, D., Chen, X., and Kroemer, G. (2022). Cuproptosis: a copper-triggered modality of mitochondrial cell death. *Cell Res.* 32 (5), 417–418. doi:10.1038/s41422-022-00653-7

Tardito, S., and Marchio, L. (2009). Copper compounds in anticancer strategies. *Curr. Med. Chem.* 16 (11), 1325–1348. doi:10.2174/092986709787846532

Thorsson, V., Gibbs, D. L., Brown, S. D., Wolf, D., Bortone, D. S., Ou Yang, T. H., et al. (2018). The immune landscape of cancer. *Immunity* 48 (4), 812–830.e814. doi:10.1016/j.immuni.2018.03.023

Tsvetkov, P., Coy, S., Petrova, B., Dreishpoon, M., Verma, A., Abdusamad, M., et al. (2022). Copper induces cell death by targeting lipoylated TCA cycle proteins. *Science* 375 (6586), 1254–1261. doi:10.1126/science.abf0529

Valko, M., Morris, H., and Cronin, M. T. (2005). Metals, toxicity and oxidative stress. *Curr. Med. Chem.* 12 (10), 1161–1208. doi:10.2174/0929867053764635

Yoshihara, K., Shahmoradgoli, M., Martinez, E., Vegesna, R., Kim, H., Torres-Garcia, W., et al. (2013). Inferring tumour purity and stromal and immune cell admixture from expression data. *Nat. Commun.* 4, 2612. doi:10.1038/ncomms3612

Zischka, H., Lichtmannegger, J., Schmitt, S., Jagemann, N., Schulz, S., Wartini, D., et al. (2011). Liver mitochondrial membrane crosslinking and destruction in a rat model of Wilson disease. *J. Clin. Invest.* 121 (4), 1508–1518. doi:10.1172/JCI45401

frontiers | Frontiers in Genetics

TYPE Original Research
PUBLISHED 26 September 2022
DOI 10.3389/fgene.2022.969856

Check for updates

OPEN ACCESS

EDITED BY
Jiayi Wang,
Shanghai Jiao Tong University, China

REVIEWED BY
Yutong Chen,
China Medical University, China
Ping Yue,
First Hospital of Lanzhou University, China
Lifang Ma,
Shanghai Jiao Tong University, China
Hongyu Wang,
Dalian University of Technology, China

*CORRESPONDENCE
Hongxin Cao,
caohongxin@sdu.edu.cn

SPECIALTY SECTION
This article was submitted to Cancer Genetics and Oncogenomics, a section of the journal Frontiers in Genetics

RECEIVED 21 June 2022
ACCEPTED 05 September 2022
PUBLISHED 26 September 2022

CITATION
Li X, Dai Z, Liu J, Sun Z, Li N, Jiao G and Cao H (2022), Characterization of the functional effects of ferredoxin 1 as a cuproptosis biomarker in cancer. *Front. Genet.* 13:969856. doi: 10.3389/fgene.2022.969856

COPYRIGHT
© 2022 Li, Dai, Liu, Sun, Li, Jiao and Cao. This is an open-access article distributed under the terms of the Creative Commons Attribution License (CC BY). The use, distribution or reproduction in other forums is permitted, provided the original author(s) and the copyright owner(s) are credited and that the original publication in this journal is cited, in accordance with accepted academic practice. No use, distribution or reproduction is permitted which does not comply with these terms.

Characterization of the functional effects of ferredoxin 1 as a cuproptosis biomarker in cancer

Xiang Li[1], Zihan Dai[1], Jincheng Liu[1], Zhenqian Sun[1], Na Li[2], Guangjun Jiao[3] and Hongxin Cao[4]*

[1]Cheeloo College of Medicine, Shandong University, Jinan, China, [2]Mechanics Laboratory, Binzhou Medical University, Yantai, China, [3]Department of Orthopedics, Qilu Hospital, Shandong University, Jinan, China, [4]Department of Medical Oncology, Qilu Hospital, Shandong University, Jinan, China

Background: Cuproptosis is a recently discovered form of programmed cell death. Ferredoxin 1 (FDX1) is a key gene that mediates this process. However, the role of FDX1 in human tumors is not clear.

Methods: We comprehensively analyzed the differential expression and genetic alterations of FDX1 using multiomics data from The Cancer Genome Atlas (TCGA) and the Genotype-Tissue Expression (GTEx) database. Subsequently, we explored the association between FDX1 and tumor parameters such as genomic instability, RNA methylation modifications, immune infiltration and pathway activity. In addition, we performed functional enrichment analysis and assessed the sensitivity potential of FDX1-related drugs. Finally, we experimentally verified the functional effects of FDX1.

Results: The analysis revealed differential expression of FDX1 in a variety of tumors. By analyzing the association of FDX1 expression with genomic instability, immune cell infiltration, signaling pathway *etc.* We explored the role of FDX1 in regulating cell activity. Also, we evaluated the function of FDX1 in biologic process and drug sensitivity. Our experimental results demonstrated that FDX1 exerts its antitumor effects through cuproptosis in liver hepatocellular carcinoma and non-small cell lung cancer cell lines.

Conclusion: Our study reveals the functional effects of FDX1 in tumors and deepens the understanding of the effects of FDX1. We validated the inhibitory effect of FDX1 in copper induced cell-death, confirming the role of FDX1 as a cuproptosis biomarker.

KEYWORDS

tumor, cuproptosis, ferredoxin 1, pan-cancer analysis, biomarker

Introduction

Cancer is one of the most important public health problems in the world and has become a major impediment to increasing human life expectancy (Siegel et al., 2022). However, the prognosis of many tumors remains poor and patient survival rates are low due to factors such as drug resistance. Some of the main mechanisms leading to the emergence of this drug resistance are tumor evasion and resistance to programmed cell death (PCD) (Johnstone et al., 2002). PCD includes necroptosis, pyroptosis, ferroptosis, and cuproptosis (Bertheloot et al., 2021). As a recently discovered mode of cell death, cuproptosis undoubtedly has great potential in the treatment of tumors.

Unlike other types of PCD, ferredoxin 1 (FDX1) and protein lipoylation are the key regulators of copper ionophore induced cell death (Tang et al., 2022). Copper is an essential nutrient, but it is both beneficial and toxic to cells. The link between copper and disease has been observed in previous studies, and some studies have reported that dysregulation of copper homeostasis played an important role in tumors (Oliveri, 2022). However, it is not certain whether copper is a cause or a consequence of tumorigenesis (Ge et al., 2022). An in-depth analysis of the mechanism of cuproptosis was carried out in the pioneering work of Tsvetkov *et al.* FDX1 was a direct target of copper ion carriers, and the researchers found that knockdown of FDX1 could protect cells from copper toxicity (Tsvetkov et al., 2022). In terms of biological function, FDX1 is a protein-coding gene. It is deeply involved in mitochondrial respiration and steroid metabolism (Sheftel et al., 2010; Strushkevich et al., 2011). And mitochondrial respiration regulates copper ionophore induced cell death. Thus, FDX1 is the main molecule that mediates cuproptosis (Tsvetkov et al., 2022). These work reveals the biological significance of copper and inspires a new strategy for tumor treatment: targeting cuproptosis. And FDX1 is the key gene related to such strategies.

The role of FDX1 in human diseases including tumors is not well known, and the effect of FDX1 mediated cuproptosis in tumors is not clear (Zhang et al., 2021). Therefore, a large-scale pan-cancer analysis of FDX1 is necessary to explore the therapeutic potential of strategies targeting cuproptosis for tumor treatment. In this study, we investigated FDX1 expression and its association with RNA methylation modifications, genomic instability, immune status, pathway activity and prognosis. Furthermore, we predicted immunotherapeutic responses and effective small molecule drugs based on the expression of FDX1 with public datasets. Finally, a series of molecular experiments such as CCK8, ethynyldeoxyuridine (EdU) staining and colony formation assay were performed to validate the role of FDX1 and cuproptosis in tumors.

Methods and materials

Expression alteration and survival analysis

We used ProteomicsDB to investigate the gene and protein expression of FDX1 in normal tissues (Schmidt et al., 2018). Clinical features and mRNA expression profiles of 33 human tumors were downloaded from TCGA (Weinstein et al., 2013). The mRNA expression matrix of normal tissues was obtained from GTEx (GTEx Consortium, 2017). UALCAN was used to assess the protein expression level of FDX1 (Chandrashekar et al., 2022).

Cox regression analysis was used to analyze the relationship between FDX1 expression and patient survival. Parameters for the survival analysis included overall survival (OS), progression-free survival (PFS), disease -specific survival (DSS) and disease-free interval (DFI).

Genetic alteration and RNA methylation modification analyses

We performed genetic alteration analysis with cBioPortal and GSCA (Cerami et al., 2012; Liu et al., 2018). Genetic alteration parameters included FDX1 mutation type, spectrum and frequency in tumors, and the relationship between mutations and patient survival was analyzed. In addition, the copy number variations (CNVs), single nucleotide variations (SNVs) and methylation level of FDX1 were analyzed.

RNA methylation modifications mainly include N1-methyladenosine (m1A), 5-methylcytidine (m5C) and N6-methyladenosine (m6A). Modification-related genes are classified as writers, readers and erasers. We explored the relationship between FDX1 expression and genes related to RNA methylation modifications in different tumor types.

Genomic instability and immune infiltration analyses

Here, genomic instability was assessed based on tumor mutation burden (TMB), microsatellite instability (MSI), DNA stemness score (DNAss), RNA stemness score (RNAss), homologous recombination deficiency (HRD) status, loss of heterozygosity (LOH) status, mutant-allele tumor heterogeneity (MATH) score and neoantigen (NEO) levels. Sangerbox, an online data analysis platform, was used to assess the relationship of FDX1 expression with genomic instability in tumors.

For immune infiltration analysis, expression data of common immune checkpoints were extracted from TCGA. CIBERSORT, MCPcounter and TIMER were used to assess the levels of immune cell infiltration in TCGA. The correlations between

the levels of infiltrating immune cells and FDX1 expression were calculated using Spearman correlation analysis.

Evaluation of the effect of FDX1 on biological processes in tumors

We evaluated the effect of FDX1 on pathway activity based on previous studies (Akbani et al., 2014; Ye et al., 2018). The pathways involved in this analysis included well-known cancer-related pathways such as the apoptosis, cell cycle, and DNA damage pathways. The pathway score was defined as the sum of the relative protein levels of all positively regulated genes minus the sum of the relative protein levels of all negatively regulated genes. A score greater than zero indicated that FDX1 activated the pathway, and a score less than zero indicated that FDX1 inhibited the pathway.

The tumor microenvironment (TME) scores were calculated by the ESTIMATE method using TCGA data (Yoshihara et al., 2013). In the TCGA cohort, the effect of FDX1 on tumor proliferation was assessed by analyzing the correlation between FDX1 expression and the Ki67 level.

FDX1-associated gene enrichment analysis

We used STRING to obtain genes associated with FDX1 and constructed a protein–protein interaction network (Szklarczyk et al., 2021). The parameters were set to the default values. GEPIA2 was used to obtain the top 30 genes associated with FDX1 in tumors (Tang et al., 2017). A gene co-expression network was generated by GeneMANIA (Warde-Farley et al., 2010). In addition, we obtained genes associated with cuproptosis from Tsvetkov's work (Tsvetkov et al., 2022). We pooled the genes obtained from the four approaches and removed the duplicates. Then, Gene Ontology (GO) and Kyoto Encyclopedia of Genes and Genomes (KEGG) enrichment analyses of these genes were performed. The GO analysis included analysis of biological process (BP), cellular component (CC) and molecular function (MF) terms. Finally, the OPENTARGET platform was used to identify the relationship between FDX1 and diseases.

Drug sensitivity analysis

GSCA was used to analyze the relationship between drug sensitivity and gene expression using data from cancer cell lines in GDSC and CTRP (Yang et al., 2013; Rees et al., 2016; Liu et al., 2018). Pearson correlation analysis was used to assess the relationship between the expression of FDX1 in and small molecule drug sensitivity (IC50 values). In addition, the Tumor Immune Dysfunction and Exclusion (TIDE) algorithm was applied to assess the association of FDX1 expression with immunotherapy response (Fu et al., 2020).

Cell culture and transfection

Two human tumor cell lines were used in this study: HepG2 (liver hepatocellular carcinoma) and H1299 (non-small cell lung cancer). The cell lines were purchased from Procell Biotechnology Co., Ltd. (Wuhan, China) and cultured according to the instructions. The identity of the cell lines was confirmed by short tandem repeat (STR) analysis.

Small interfering RNAs were purchased from Gene Pharma (Shanghai, China). The following siRNA sequences were used: FDX1-1-F: GUGAUUCUCUGCUAGAUGUTT; FDX1-1-R: ACAUCUAGCAGAGAAUCACTT; FDX1-2-F: CCUGUC ACCUCAUCUUUGATT; FDX1-2-R: UCAAAGAUGAGG UGACAGGTT; FDX1-3-F: CUAACAGACAGAUCACGG UTT; FDX1-3-R: ACCGUGAUCUGUCUGUUAGTT.

We transfected the cells according to the manufacturer's protocol. After that, PCR was used to confirm the transfection effect. β-Actin was set as internal control and relative gene expression was calculated by the $2^{-\Delta\Delta Ct}$ method. The primers were as follows: FDX1-F, TTCAACCTGTCACCTCATCTTTG; FDX1-R, TGCCAGATCGAGCATGTCATT.

Analysis of cell proliferation

After 48 h of transfection, we added $CuSO_4$ (1 μM), elesclomol (ELE) (100 nM) and tetrathiomolybdate (TTM) (100 nM) to the culture medium to trigger FDX1-mediated cuproptosis. ELE is a copper ion carrier, while TTM is a copper ion chelator. Cell proliferation was detected by CCK-8, ethynyldeoxyuridine (EdU) staining and colony formation assay.

For CCK-8, the cell lines and controls were first inoculated separately in 96-well plates. 10 μL of CCK-8 reagent was added to each well at the specified time points. The optical density (OD) was measured at 450 nm after incubation for 1 h at 37°C.

The fraction of DNA-replicating cells, which represents cell proliferation status, was assessed using EdU detection kit (RiboBio, Guangzhou, China).

For colony formation assay, cells were incubated in a 6-well plate at 37°C for 1 week, followed by fixation in methanol and staining in a 0.1% crystal violet solution for 15 min before colony counting.

Statistics analysis

In bioinformatics analysis, we used flexible methods to process data. For molecular biology experiments, two-sided

10.3389/fgene.2022.969856

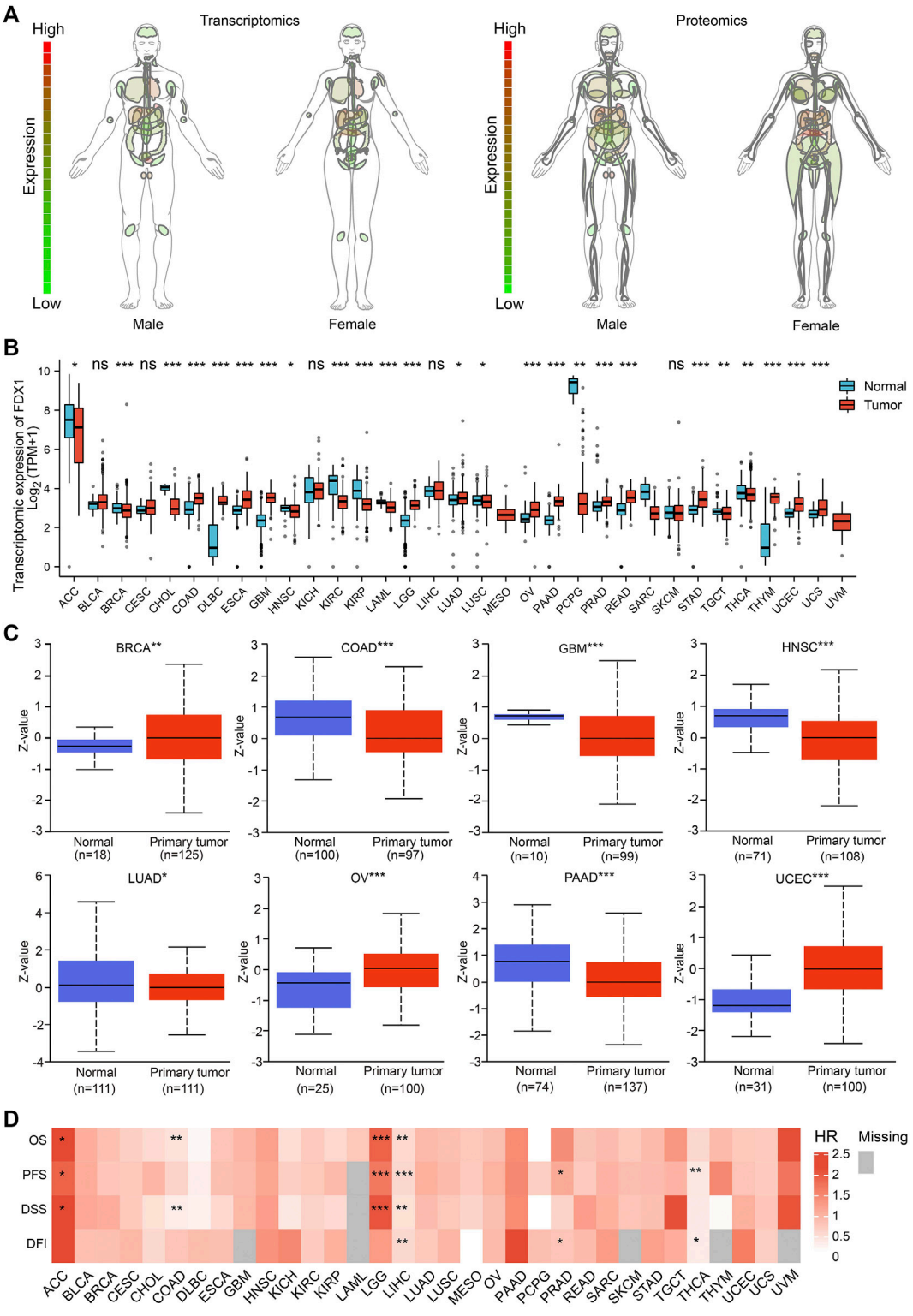

FIGURE 1
FDX1 expression profile and survival analysis. **(A)** Anatomy plot of the transcriptomic and proteomic expression of FDX1 across normal tissues in males and females. **(B)** Combining the data from TCGA and GTEx, transcriptomic expression differences of FDX1 between tumor and normal tissues. (ns: not significant; *$p < 0.05$; **$p < 0.01$; ***$p < 0.001$). **(C)** Data from UALCAN revealed proteomic expression differences of FDX1 between tumor and normal tissues. (*$p < 0.05$; **$p < 0.01$; ***$p < 0.001$). **(D)** Survival analysis across tumors revealed FDX1 was associated with prognosis. (HR, hazard ratio; OS, overall survival; PFS, progression free survival; DSS, disease specific survival; DFI, disease free interval; *$p < 0.05$; **$p < 0.01$; ***$p < 0.001$).

TABLE 1 Abbreviations and full names of cancer types used in this study.

Abbreviation	Full name	Abbreviation	Full name
ACC	Adrenocortical carcinoma	MNT	Miscellaneous neuroepithelial tumor
BLCA	Bladder urothelial carcinoma	NSCLC	Non-small cell lung cancer
BRCA	Breast invasive carcinoma	NSGCT	Non-seminomatous germ cell tumor
CEAD	Cervical adenocarcinoma	OET	Ovarian epithelial tumor
CESC	Cervical squamous cell carcinoma and endocervical adenocarcinoma	OM	Ocular melanoma
CHOL	Cholangiocarcinoma	OV	Ovarian serous cystadenocarcinoma
COAD	Colon adenocarcinoma	PAAD	Pancreatic adenocarcinoma
COADREAD	Colon adenocarcinoma/Rectum adenocarcinoma Esophageal carcinoma	PCPG	Pheochromocytoma and paraganglioma
DG	Diffuse glioma	PRAD	Prostate adenocarcinoma
DLBC	Lymphoid neoplasm diffuse large B-cell lymphoma	READ	Rectum adenocarcinoma
EA	Esophagogastric Adenocarcinoma	RNCCC	Renal non-clear cell carcinoma
ESCA	Esophageal carcinoma	SARC	Sarcoma
GBM	Glioblastoma multiforme	SEMI	Seminoma
HNSC	Head and neck squamous cell carcinoma	SKCM	Skin cutaneous melanoma
KICH	Kidney chromophobe	STAD	Stomach adenocarcinoma
KIRC	Kidney renal clear cell carcinoma	STES	Stomach and esophageal carcinoma
KIRP	Kidney renal papillary cell carcinoma	TET	Thymic epithelial tumor
LAML	Acute myeloid leukemia	TGCT	Testicular germ cell tumors
LGG	Brain lower grade glioma	THCA	Thyroid carcinoma
LIHC	Liver hepatocellular carcinoma	THYM	Thymoma
LUAD	Lung adenocarcinoma	UCEC	Uterine corpus endometrial carcinoma
LUSC	Lung squamous cell carcinoma	UCS	Uterine carcinosarcoma
MBCN	Mature B-cell neoplasms	UVM	Uveal melanoma
MESO	Mesothelioma		

student's t-test was used to compare the difference between two groups. Mean ± standard deviation was used to represent quantitative data. In correlation tests, the absolute value of the correlation coefficient ≥0.7 would be regarded as "strong" correlation, values between 0.50 and 0.70 would be interpreted as "good" correlation, between 0.3 and 0.5 would be treated as "fair" or "moderate" correlation, and any value ≤0.30 would be poor correlation (Hazra and Gogtay, 2016). Difference with $p < 0.05$ was considered statistically significant.

Results

Dysregulation and prognostic value of FDX1 in tumors

First, analysis of normal tissues showed that the gene and protein expression of FDX1 varies in different organs and tissues, with the highest expression level in adrenal gland in both males and females (Figure 1A). As shown in Figure 1B, the RNA expression of FDX1 differed significantly in 25 of the 33 tumor types studied. Analysis of proteomic data also revealed differential expression of FDX1 in the tumors, among which FDX1 expression level was lower in colon adenocarcinoma (COAD), glioblastoma multiforme (GBM), head and neck squamous cell carcinoma (HNSC), lung adenocarcinoma (LUAD) and pancreatic adenocarcinoma (PAAD) compared with normal tissues; while higher in breast invasive carcinoma (BRCA), ovarian serous (OV) and uterine corpus endometrial carcinoma (UCEC) (Figure 1C).

As shown in Figure 1D, Cox regression analysis showed that the expression of FDX1 was positively correlated with the prognosis of adrenocortical carcinoma (ACC) and lower grade glioma (LGG); and negatively correlated with the prognosis of colon adenocarcinoma (COAD), liver hepatocellular carcinoma (LIHC) and thyroid carcinoma (THCA). The abbreviations and full names of all the tumors mentioned in this study are presented in Table 1. Taken together, our data indicated that the expression of FDX1 was dysregulated in tumors and that this dysregulation had prognostic implications in some tumors.

Genetic alterations of FDX1

Genetic alterations are now known to be strongly associated with tumorigenesis and progression. Our analysis revealed that

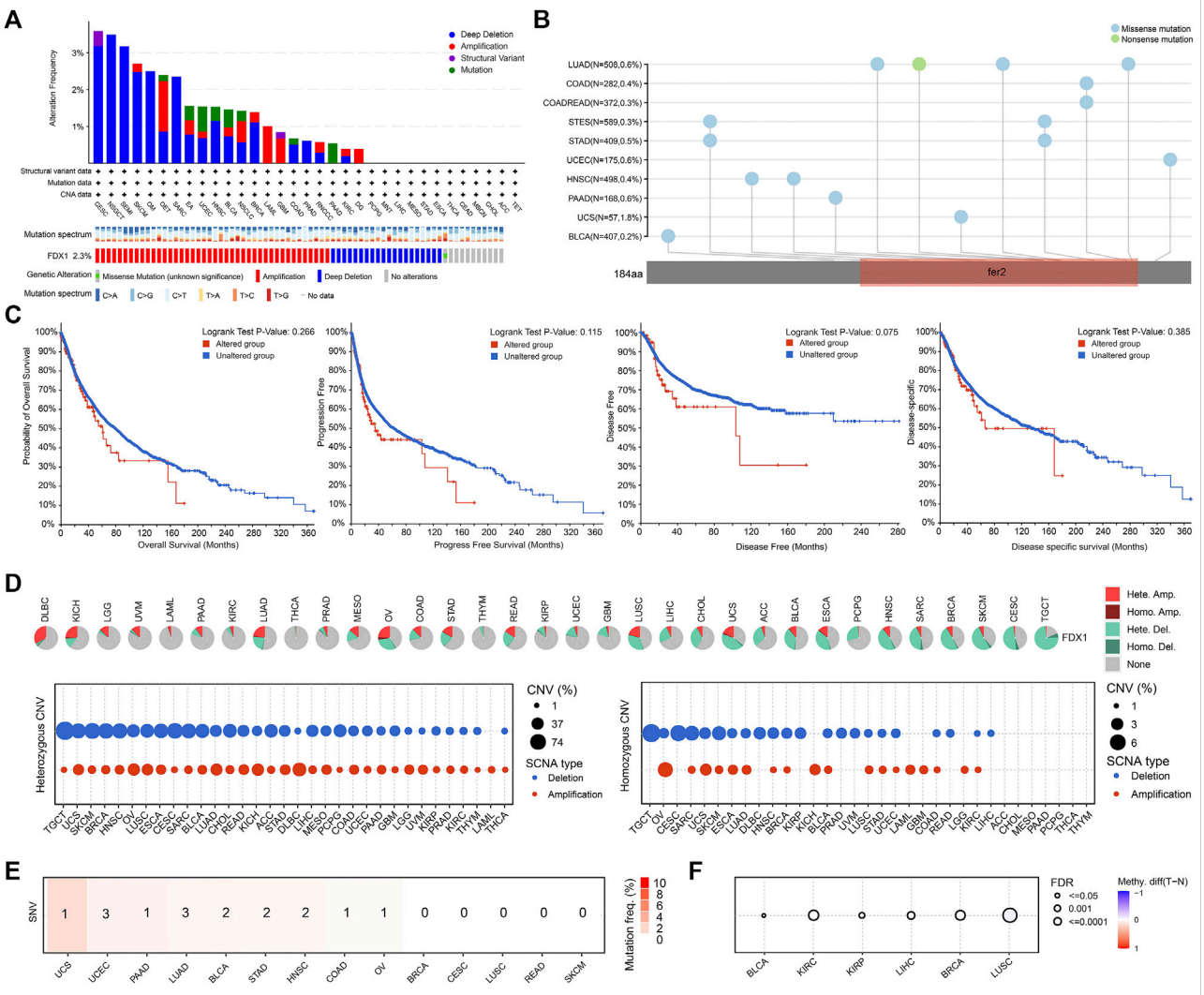

FIGURE 2
Genetic alteration of FDX1 in tumors. **(A)** The FDX1 genetic alteration frequencies of different types of tumors. **(B)** Mutation diagram of FDX1 in different tumor types across protein domains. **(C)** The survival analysis of patients with or without FDX1 genetic alterations. **(D)** Copy number variation (CNV) pie chart showed the combined heterozygous/homozygous CNV ratio of FDX1 in each tumor. The CNV profile showed the percentage of heterozygous CNV and the percentage of homozygous CNV. **(E)** The profile of single nucleotide variant (SNV) of FDX1 and number of cases with deleterious mutations in tumors **(F)** Differential methylation in FDX1 between tumor and normal samples in tumors. Red dots represented increased methylation in tumors and blue dots represented decreased methylation in tumors.

the average frequency of FDX1 alterations was 2.3% in all tumors, with deep deletion and amplification as the predominant types. The highest frequency of FDX1 alterations (>3%) was observed in cervical squamous cell carcinoma and endocervical adenocarcinoma (CESC), followed by nonseminomatous testicular tumor (NSGCT) and seminoma (SEMI) (Figure 2A). Further analysis showed that the main type of amino acid alteration in FDX1 was missense mutation, and most mutations affected the fer2 region. The mutation frequency was highest in LUAD, COAD and rectum adenocarcinoma (READ) (Figure 2B). However, in the pooled survival analysis of all tumor types, although the survival curves were separated, there was no statistical significance between FDX1 altered group and the unaltered group ($p > 0.05$) (Figure 2C).

To further identify FDX1 changes at the chromosomal level, we analyzed copy number variation (CNV), single nucleotide variation (SNV)and methylation level data from TCGA. As shown in Figure 2D, the major CNV types of FDX1 in 33 tumors were heterozygous amplification and deletion. In diffuse large B-cell lymphoma (DLBCL), LGG, acute myeloid leukemia (LAML), and uveal melanoma (UVM), heterozygous amplification was the main type. In pheochromocytoma and paraganglioma (PCPG), sarcoma (SARC), breast invasive carcinoma (BRCA), skin cutaneous melanoma (SKCM), CESC

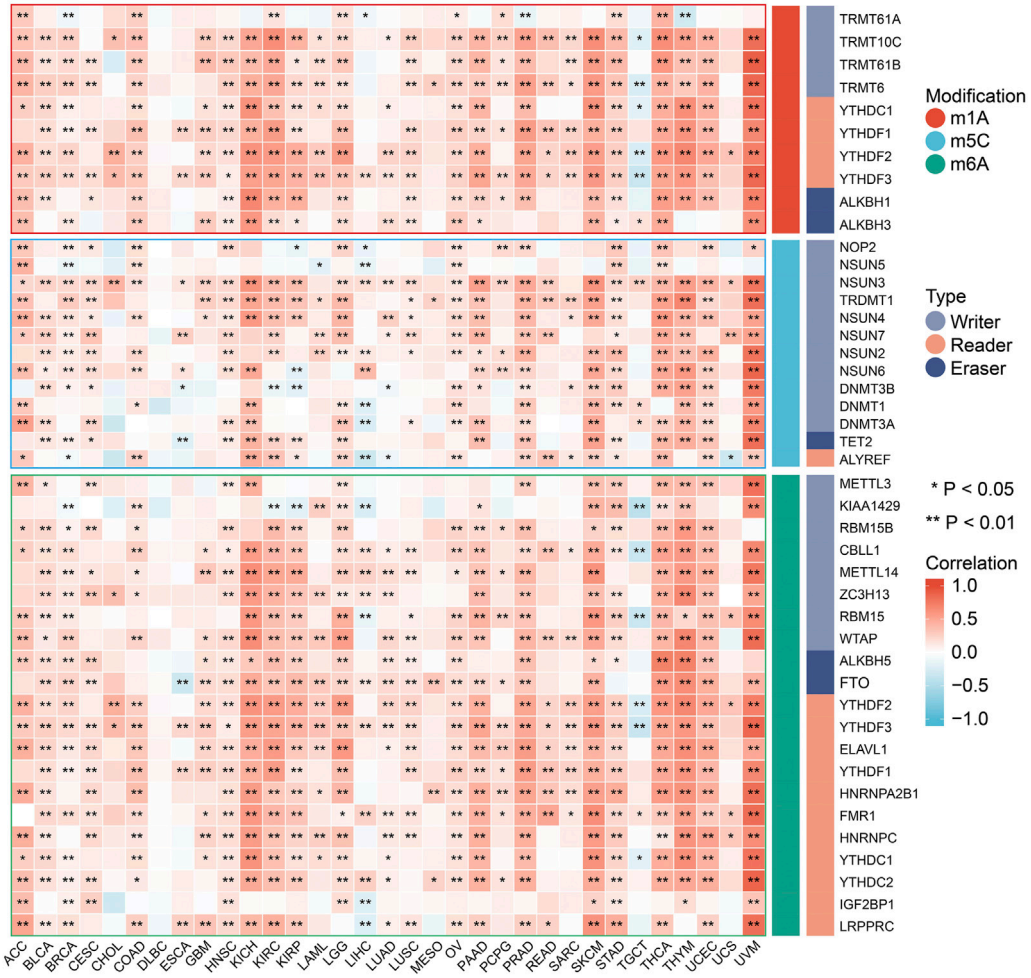

FIGURE 3
Spearman correlation of FDX1 expression with RNA methylation modifications including m1A, m5C and m6A in pan-cancer. (*$p < 0.05$; **$p < 0.01$).

and testicular germ cell tumor (TGCT), the predominant type was heterozygous deletion. In addition, the proportion of homozygous FDX1 CNVs in tumors was much lower than that of heterozygous FDX1 CNVs. We also found that SNVs of FDX1 did not occur frequently in tumors, affecting no more than 4% of cases (Figure 2E). Finally, we detected differences in the methylation levels of FDX1 in only a few tumors (Figure 2F).

RNA methylation modification-related gene analysis

Positive correlations were found between FDX1 expression and most RNA methylation modification-related genes in the vast majority of tumors (Figure 3). Only in specific tumor types, such as TGCT, did we primarily find negative correlations. In addition, FDX1 expression was not associated with any modification-related genes in DLBCL. In short, our analysis revealed that there were likely profound effects of FDX1 expression on RNA methylation modifications in tumors.

Genomic instability analysis

The results of the genomic instability analysis were shown in Figure 4. The data showed significant association of FDX1 expression with genomic instability in a variety of tumors. This association was stronger in ACC, kidney renal clear cell carcinoma (KIRC) and stomach adenocarcinoma (STAD). However, in a few tumors (bladder urothelial carcinoma (BLCA), cholangiocarcinoma (CHOL), mesothelioma (MESO) and rectum adenocarcinoma (READ), FDX1 expression was not correlated with

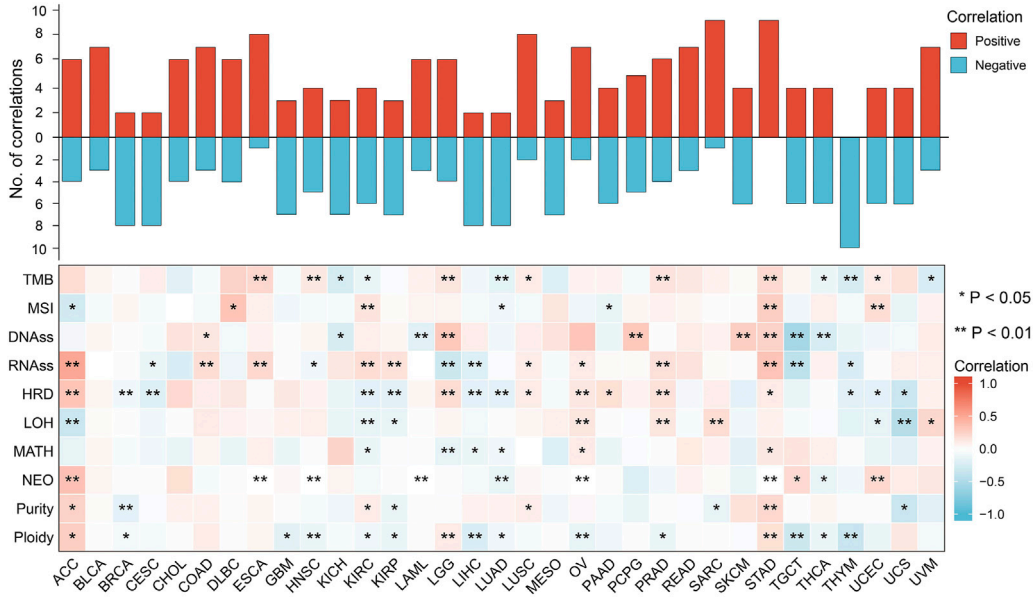

FIGURE 4
Spearman correlation of FDX1 expression with genomic instability in pan-cancer. Red indicated positive correlation, blue indicated negative correlation. And the darker the color, the stronger the correlation. (TMB, tumor mutation burden; MSI, microsatellite instability; DNAss, DNA stemness; RNAss, RNA stemness; HRD, homologous recombination deficiency; LOH, loss of heterozygosity; MATH, mutant-allele tumor heterogeneity; NEO, neoantigens; *$p < 0.05$; **$p < 0.01$).

genomic instability. We found negative correlation between FDX1 expression and genomic instability parameters such as tumor mutation burden (TMB), microsatellite instability (MSI), homologous recombination deficiency (HRD), loss of heterozygosity (LOH) and neo-antigen (NEO) *etc.* in CRCA, CESC, LIHC, LUAD, TGCT, THCA and THYM. While positive correlation of FDX1 and genomic instability parameters was found in STAD, ACC, OV and PRAD. As we known, MSI and TMB are important biomarkers in immunotherapy of COAD, but there was no statistical relevance between FDX1 and TMB and MSI in COAD in our analysis.

Associations of FDX1 expression with the levels of infiltrating immune cells in tumors

FDX1 is a key molecule in cuproptosis. To determine whether cuproptosis has an effect on the immune environment of tumors, we explored the link between FDX1 expression and immune infiltration in each tumor. As shown in Figure 5A, FDX1 expression was negatively correlated with the expression of immune checkpoints such as CD274 (PD-L1), CTLA-4, TIGIT *etc.* In most tumors including ACC, BLCA, LAML, STAD and THCA *etc.*; while the expression of FDX1 was positively correlated with the expression of immune checkpoints in BRCA, KICH, LGG and PCPG *etc.*

Subsequently, we evaluated the relationship between FDX1 expression and immune cell infiltration using three algorithms. As shown in Figures 5B–D, FDX1 expression was negatively correlated with tumor infiltrating immune cells including $CD8^+$ T cells, $CD4^+$ T cells, macrophage *etc.* In a large part of tumor types we analyzed such as ACC, COAD, KIRC, LAML, LUAD, STAD, THCA. In most tumors, the relationship of FDX1 and immune checkpoints was consistent with its relationship with the infiltrating immune cells. However, our data showed that there were positive correlations of FDX1 and immune cells infiltration in some tumors such as LGG, SARC and TGCT etc. Also, we noted that FDX1 expression was not correlated with the expression of any immune checkpoint genes in CHOL and uterine carcinosarcoma (UCS), and the levels of infiltrating immune cells in these two tumors were also almost completely independent of FDX1 expression. These data indicating that the effect of FDX1 in tumor microenvironment varies in different type of tumors.

In the view of immune cell functions, our data showed logical results in most tumors. For example, in ACC and STAD, FDX1 expression was positively correlated with the immune effector cell $CD8^+$ T cells, while it was negatively correlated with the immunosuppressive cell Tregs (Figure 5B). In ACC, COAD, LIHC and STAD, the relative consistent negative correlation of FDX1 and immune checkpoints and tumor infiltrating cells indicated the negative regulating function of FDX1 in these tumors.

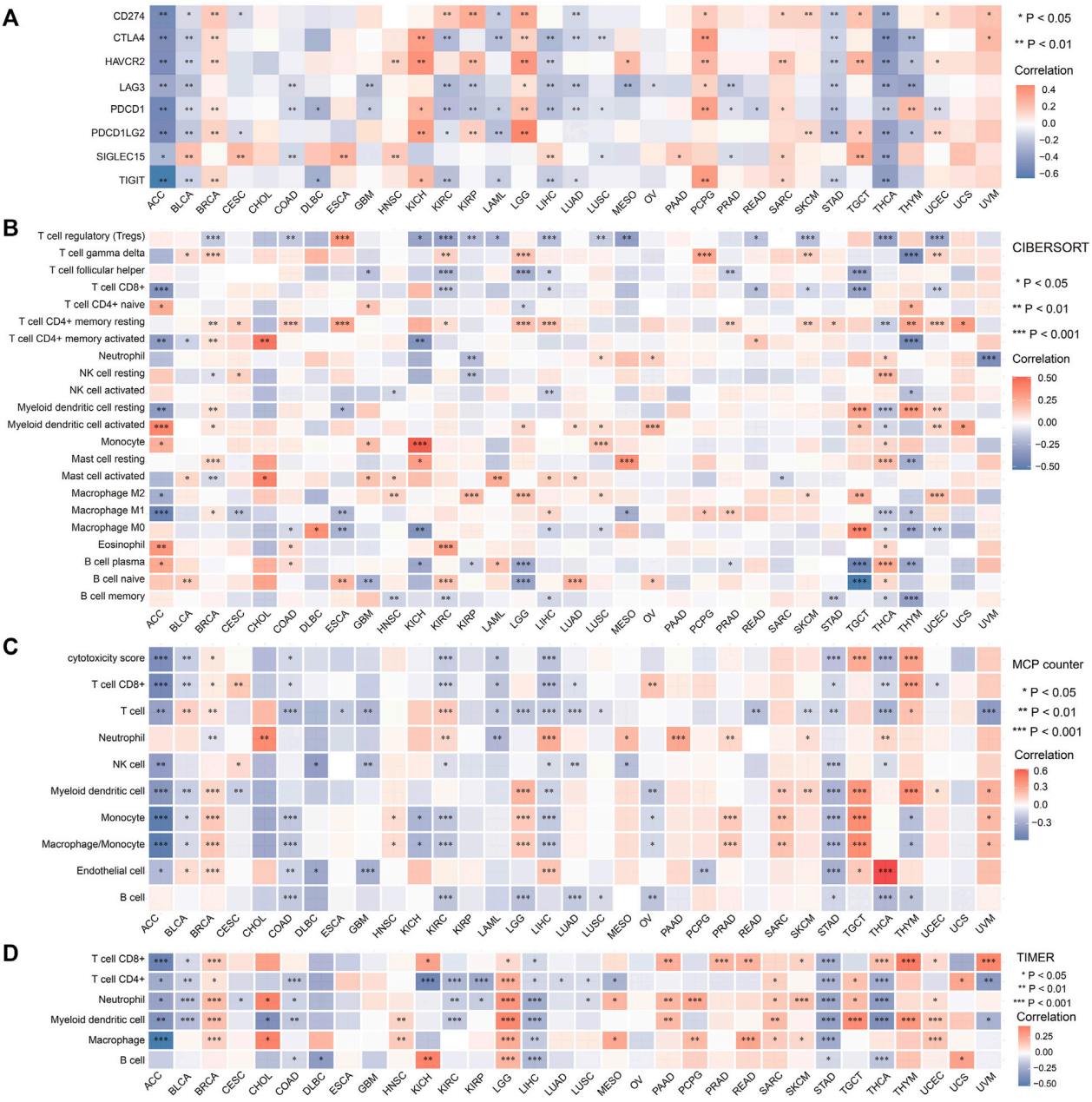

FIGURE 5
Relationship between FDX1 expression and immune checkpoints and immune cells across tumors. **(A)** Correlation of FDX1 expression and common immune checkpoint genes in pan-cancer. (*$p < 0.05$; **$p < 0.01$). Immune cell infiltration analyzed by the CIBERSORT **(B)**, MCP counter **(C)** and TIMER **(D)**. (*$p < 0.05$, **$p < 0.01$, ***$p < 0.001$).

Biological process analysis

We first analyzed the association of FDX1 with multiply pathway activity which play important role in regulating tumor behavior in tumors. The data showed that FDX1 affected well-known tumor-associated pathways in only a small number of tumors. The effect of FDX1 was more pronounced in specific tumors, such as THCA and LIHC. In THCA and LIHC, FDX1 was positively correlated with the activity of growth promoting signaling pathways including RTK, RAS/MAPK and PI3K/AKT pathways; and was negatively correlated with DNA damage (Figure 6A). We found that FDX1 was negatively correlated with Ki-67 in LIHC and THCA (Figure 6B), and this was consisted with its role in signaling pathway. While FDX1 was

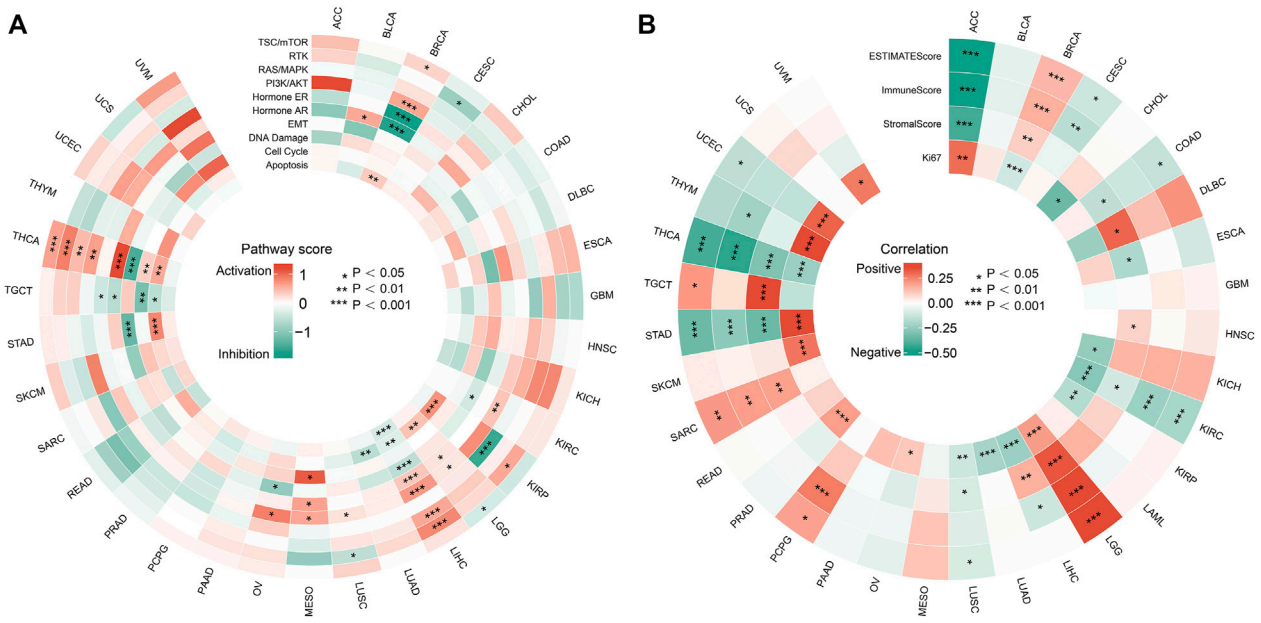

FIGURE 6
Effects of FDX1 on biological processes in tumors. **(A)** Relationship between FDX1 expression and famous cancer related pathways. (*$p < 0.05$; **$p < 0.01$; ***$p < 0.001$). **(B)** Correlation of FDX1 expression with tumor microenvironment scores and Ki67 in pan-cancer. (*$p < 0.05$; **$p < 0.01$; ***$p < 0.001$).

positively correlated with proliferation index Ki-67 in some other tumors including ACC, LGG, PRAD, STAD, THYM and UCEC.

The tumor microenvironment (TME) has a profound impact on the biological behavior of tumors, and ESTIMATEScore, Immune Score and Stroma Score are important index to evaluate the immune state of tumors. Therefore, we investigated the correlation between FDX1 and TME parameters using the ESTIMATE algorithm. As shown in Figure 6B, FDX1 was negatively correlated with the TME scores of ACC, KIRC, THCA and STAD, while it was positively correlated with the scores of LGG and SARC. Also, the relationship of FDX1 with TME parameters and Ki-67 was in accordance in LGG, KIRC and THCA, while its role was opposite in some other tumors such as ACC, BRCA, STAD, TYHM and UCEC. All above, we can see the complexity of tumor activity and microenvironment. The specific mechanisms need to be further clarified in future studies.

Potential functions of FDX1 in tumors

To predict the function of FDX1 in tumors, we identified genes associated with FDX1. As shown in Supplementary Figure S1A, a protein–protein interaction network based on FDX1 and ten related genes was generated by STRING. Supplementary Figure S1B shows a co-expression network consisting of FDX1 and 20 related genes. Ultimately, we obtained a total of 58 FDX1-related genes (Supplementary Figure S1C). In Supplementary Figure S1D, we present the results of functional enrichment analysis of these 58 genes and FDX1. The genes were mainly enriched in the BP terms synthesis and metabolic processes of steroids and hormones (Supplementary Figure S1E). In the CC analysis, the genes were found to be mainly located in mitochondria (Supplementary Figure S1F). The significantly enriched MF terms were iron ion binding, iron-sulfur cluster binding and metal cluster binding (Supplementary Figure S1G). As seen in Supplementary Figure S1H, the KEGG enrichment analysis revealed significant enrichment of FDX1 and FDX1-related genes in steroid hormone synthesis and secretion. The results of the functional enrichment analysis were in line with the mechanisms by which cuproptosis occurs.

In addition, we used the OPENTARGET platform to explore the diseases associated with FDX1. The results showed that in addition to its involvement in tumors, FDX1 was also involved in cardiovascular diseases, respiratory diseases, and endocrine system diseases (Supplementary Figure S1I).

Drug sensitivity analysis

As shown in Figure 7A, FDX1 expression was negatively correlated with sensitivity to drugs such as AT-7519, PIK-93, phenformin and YM201636 and positively correlated with sensitivity to 17-AAG. In the CTRP database,

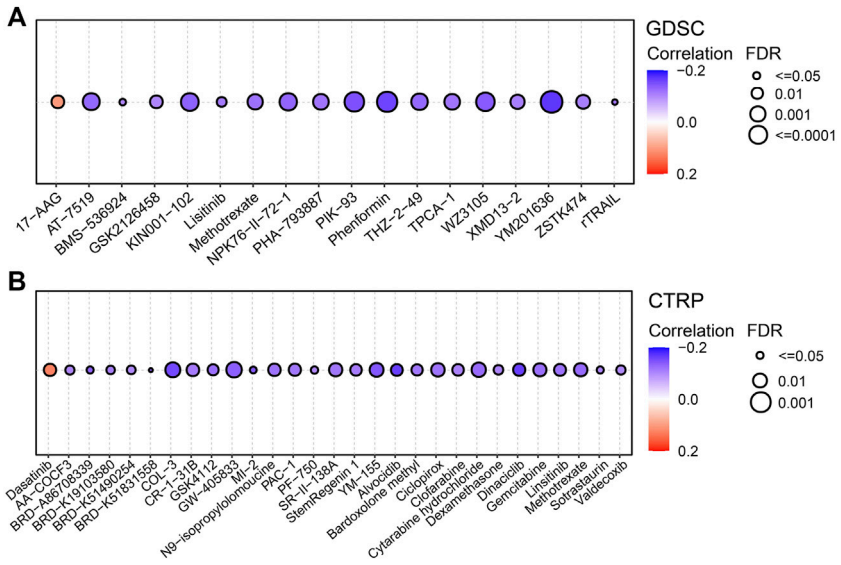

FIGURE 7
Predictive drugs based on the FDX1 expression in pan-cancer from the GDSC **(A)** and CTRP **(B)** datasets.

TABLE 2 Association between gene expression and therapy outcome in clinical studies of immune checkpoint blockade.

Cohort	Cancer	Survival	Risk	Count	*p*
Liu2019_PD1	Melanoma	OS	2.209	47	0.027
Riaz2017_PD1	Melanoma	PFS	1.963	25	0.049
Liu2019_PD1	Melanoma	PFS	1.933	47	0.053
Miao2018_ICB	Kidney	PFS	1.892	33	0.059
VanAllen2015_CTLA4	Melanoma	OS	1.803	42	0.071
VanAllen2015_CTLA4	Melanoma	PFS	1.752	42	0.080
Gide2019_PD1+CTLA4	Melanoma	OS	1.230	32	0.219
Gide2019_PD1+CTLA4	Melanoma	PFS	1.016	32	0.310
Lauss2017_ACT	Melanoma	PFS	−1.127	25	0.260
Nathanson2017_CTLA4	Melanoma	OS	−1.336	9	0.181
Lauss2017_ACT	Melanoma	OS	−1.375	25	0.169
Nathanson2017_CTLA4	Melanoma	OS	−1.444	15	0.149
Braun2020_PD1	Kidney	OS	−2.894	295	0.038

OS, overall survival; PFS, progression free survival.

FDX1 expression was negatively correlated with sensitivity to drugs such as ciclopirox, dinaciclib and linsitinib and positively correlated with sensitivity to dasatinib (Figure 7B). The results of TIDE analysis showed that FDX1 expression was correlated with the response to PD1 immunotherapy in a cohort of patients with melanoma and kidney tumors. More detailed data is presented in Table 2. Our analysis indicated that FDX1 had potential value for predicting chemotherapy sensitivity, but its relationship with drug sensitivity varied by cancer types.

Effects of FDX1 in tumor proliferation

As shown in Figures 8A,E, we successfully knocked down FDX1 in HepG2 and H1299 cell lines. And the cells with the highest transfection efficiency were selected for the subsequent experiments.

The CCK-8 showed that FDX1 inhibited the proliferation of tumor cells when copper ions were present. This inhibitory effect was significantly diminished by using TTM to chelate copper

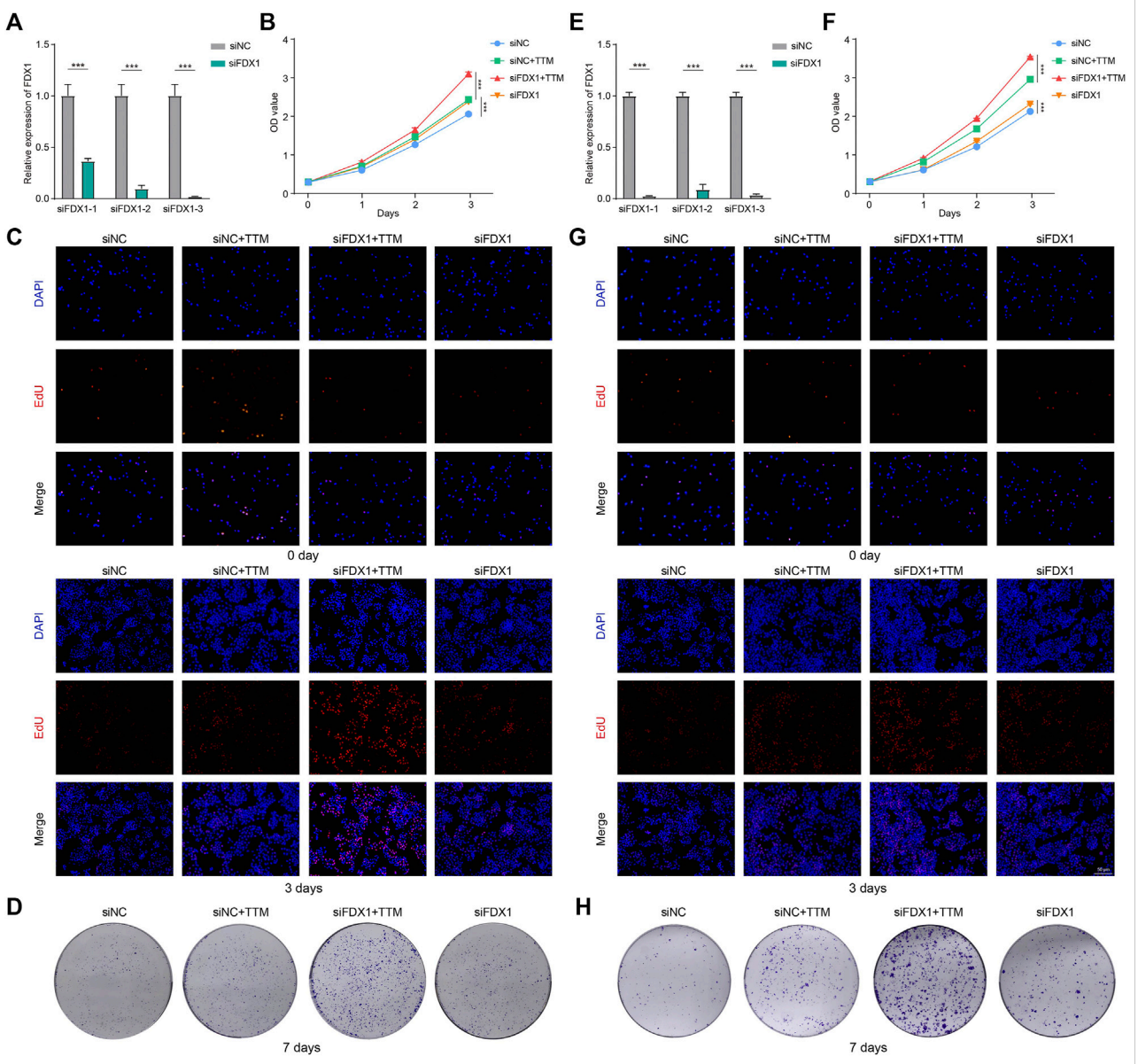

FIGURE 8
Effects of FDX1 in tumor proliferation. **(A)** PCR was performed to confirm knockdown of FDX1 in HepG2 **(A)** and H1299 **(E)** (***$p < 0.001$). CCK-8, EdU staining and colony formation assays were used to assess the proliferation of HepG2 **(B–D)** and H1299 **(F–H)** at specific time points (***$p < 0.001$).

ions (Figures 8B,F). EdU staining and colony formation assays further confirmed our findings (Figures 8C,D,G,H). These results indicated that FDX1 exerted anti-tumor effects through cuproptosis.

Discussion

FDX1 is a key molecule mediating cuproptosis. Herein, we performed the pan-cancer analysis of FDX1. First, we conducted expression analysis of FDX1 although different organs and compared the expression difference of FDX1 between normal tissues and tumor tissues. Our data showed that FDX1 expression various in different organs and tumors, indicating the heterogeneity of different organs and tumors. It is worth noticing that FDX1 protein expression was lower in COAD, GBM, HNSC, LUAD and PAAD compared with normal tissues. Together with the data in survival analysis, FDX1 expression positively correlated with survival parameters in ACC, LGG, LIHC *etc.* Also, although without statistical difference, HR was

greater than one in some other tumors. We may deduce the "anti-tumor" effect of FDX1 in those tumors. This is in consistent with the study that demonstrated FDX1 was lower expressed in HCC, and FDX1 expression level was positively correlated with overall survival (Zhang et al., 2022).

In the present study, the analysis of parameters such as genomic instability and pathway activity of tumors demonstrated that FDX1 expression was closely associated with tumor biological behavior. Our data showed that the most common mutation of FDX1 was deep deletion and amplification and main type of amino acid alteration was missense mutation. Patients with genomic instability of FDX1 had the disposition to poor survival in cancer patients. There has been a research on single-nucleotide polymorphisms (SNPs) in cuproptosis-related genes demonstrating that *FDX1-rs10488764* was associated with an increased risk of lung cancer (Yun et al., 2022). Further study is needed to explore the effect of FDX1 in different tumors. Moreover, our data showed that FDX1 expression level was positively associated with cell proliferative cell pathway such as RTKs, RAS/MAPK and PI3k/AKT pathway in LIHC and THCA, while there was no significant correlation in other tumor types. Copper was reported to be a dynamic signaling metal to regulate cell behavior, for example, it was involved in mitogen-activated protein kinase 1 (MEK1) and MEK2 pathway (Smith et al., 2022). The role and mechanisms of FDX1 in cell signaling needed to explored in further studies.

Tumor microenvironment (TME) is composed of cancer cells, stromal cells, fibroblasts and innate and adaptive immune cells, producing marked effect in tumorigenesis, development and anti-tumor therapy (Hui and Chen, 2015). Previous studies have shown that cross-talk between cancer cells, stromal cells and the infiltrating immune cells made TME complex and evolving (Hinshaw and Shevde, 2019). Our study analyzed the correlation of FDX1 and tumor immune status including tumor infiltrating immune cells, immunoscore, TMB and MSI *etc*. Clinical studies have confirmed the important role of CD274 (PD-L1) expression level in immune checkpoint inhibitor (ICI) therapy in lung cancer including LUAD. Patients with higher PD-L1 expression may have better response to ICIs and tend to have better prognosis (Yang et al., 2021). In our study, PD-L1 expression was negatively correlated with FDX1 in LUAD, together with the relative lower expression of FDX1 in LUAD, inferred that PD-L1 expression might higher in FDX1 low expressed LUAD. This is an interesting project needed further validation in following researches. The effect of FDX1 to infiltrating immune cells such as $CD8^+$ T cells, $CD4^+$ T cells, macrophage *etc*. various in different tumors and was not exactly consistent throughout different databases. We analyze that heterogeneity may partially explain this result. On the other hand, the difference of inclusion criteria, limited sample size and lack of validation may also cause the inconsistence. And those are also the limitation of bioinformatics analysis studies.

Finally, we validated the function of FDX1 in liver hepatocellular carcinoma and non-small cell lung cancer cell lines. According to our results, knockdown of FDX1 promoted the proliferation of tumor cell lines, verifying the inhibitory effect of FDX1 in those tumors. Our result is consistent with previous studies (Tsvetkov et al., 2022; Zhang et al., 2022). It is noteworthy that Duan *et al.* declared that simply knockdown of FDX1 in LUAD neither inhibited tumor cell growth nor did it induce apoptosis (Zhang et al., 2021). Tsvetkov *et al.* reported that FDX1 knockdown partially rescued from copper induced cell-death, clarifying the important role of FDX1 in cuproptosis. We conducted our experiment with $CuSO_4$, ELE and TTM, and we successfully validated the inhibitory effect of FDX1 and explored that FDX1 played its role through copper induced cell-death. In addition, there were sensitive and resistant cell lines in FDX1 mediated copper induced cell-death in Tsvetkov's work, indicating the heterogeneity of different cell lines and the complexity of FDX1 mediated cell activity. Further studies are needed to illustrate the precise mechanism.

Conclusion

We conducted pan-cancer analysis to explore the association between FDX1 and prognosis, genomic instability, RNA methylation modifications, immune infiltration and signaling pathway activity *etc*. Our experimental result validated the inhibitory effect of FDX1 in copper induced cell-death in liver hepatocellular carcinoma and non-small cell lung cancer cell lines. Our study reveals the functional effects of FDX1 in tumors and deepens the understanding of the effects of FDX1.

Data availability statement

The original contributions presented in the study are included in the article/Supplementary Materials, further inquiries can be directed to the corresponding author.

Author contributions

XL: Conceptualization; Data curation; Formal analysis; Writing; Visualization ZD: Methodology JL: Manuscript revison, Experiments; ZS: Methodology NL: Manuscript revison, GJ: Validation HC: Supervision, Manuscript writing.

Funding

This research was supported by The National Natural Science Foundation of China (Grant No. 81702261).

Conflicts of interest

The authors declare that the research was conducted in the absence of any commercial or financial relationships that could be construed as a potential conflict of interest.

Publisher's note

All claims expressed in this article are solely those of the authors and do not necessarily represent those of their affiliated organizations, or those of the publisher, the editors and the reviewers. Any product that may be evaluated in this article, or claim that may be made by its manufacturer, is not guaranteed or endorsed by the publisher.

Supplementary material

The Supplementary Material for this article can be found online at: https://www.frontiersin.org/articles/10.3389/fgene.2022.969856/full#supplementary-material

SUPPLEMENTARY FIGURE S1
Potential functions of RAD51 in tumors. **(A)** FDX1-interacting proteins network analysis in the STRING database. **(B)** A co-expression network of FDX1. **(C)** The union of FDX1-related genes. **(D)** Functional enrichment analysis of FDX1 and FDX1-related genes in GO and KEGG. (E–H) GO and KEGG cnetplot plot showed the top 5 enriched pathways and functions. **(I)** The OPENTARGET platform was used to conduct a gene-disease network analysis of FDX1.

References

Akbani, R., Ng, P. K. S., Werner, H. M. J., Shahmoradgoli, M., Zhang, F., Ju, Z., et al. (2014). A pan-cancer proteomic perspective on the Cancer Genome Atlas. *Nat. Commun.* 5, 3887. doi:10.1038/ncomms4887

Bertheloot, D., Latz, E., and Franklin, B. S. (2021). Necroptosis, pyroptosis and apoptosis: An intricate game of cell death. *Cell. Mol. Immunol.* 18 (5), 1106–1121. doi:10.1038/s41423-020-00630-3

Cerami, E., Gao, J., Dogrusoz, U., Gross, B. E., Sumer, S. O., Aksoy, B. A., et al. (2012). The cBio cancer genomics portal: An open platform for exploring multidimensional cancer genomics data. *Cancer Discov.* 2 (5), 401–404. doi:10.1158/2159-8290.CD-12-0095

Chandrashekar, D. S., Karthikeyan, S. K., Korla, P. K., Patel, H., Shovon, A. R., Athar, M., et al. (2022). Ualcan: An update to the integrated cancer data analysis platform. *Neoplasia (New York, N.Y.)* 25, 18–27. doi:10.1016/j.neo.2022.01.001

Fu, J., Li, K., Zhang, W., Wan, C., Zhang, J., Jiang, P., et al. (2020). Large-scale public data reuse to model immunotherapy response and resistance. *Genome Med.* 12 (1), 21. doi:10.1186/s13073-020-0721-z

Ge, E. J., Bush, A. I., Casini, A., Cobine, P. A., Cross, J. R., DeNicola, G. M., et al. (2022). Connecting copper and cancer: From transition metal signalling to metalloplasia. *Nat. Rev. Cancer* 22 (2), 102–113. doi:10.1038/s41568-021-00417-2

GTEx Consortium (2017). Genetic effects on gene expression across human tissues. *Nature* 550 (7675), 204–213. doi:10.1038/nature24277

Hazra, A., and Gogtay, N. (2016). Biostatistics series module 6: Correlation and linear regression. *Indian J. dermatol.* 61 (6), 593–601. doi:10.4103/0019-5154.193662

Hinshaw, D. C., and Shevde, L. A. (2019). The tumor microenvironment innately modulates cancer progression. *Cancer Res.* 79 (18), 4557–4566. doi:10.1158/0008-5472.CAN-18-3962

Hui, L., and Chen, Y. (2015). Tumor microenvironment: Sanctuary of the devil. *Cancer Lett.* 368 (1), 7–13. doi:10.1016/j.canlet.2015.07.039

Johnstone, R. W., Ruefli, A. A., and Lowe, S. W. (2002). Apoptosis: A link between cancer genetics and chemotherapy. *Cell* 108 (2), 153–164. doi:10.1016/s0092-8674(02)00625-6

Liu, C.-J., Hu, F. F., Xia, M. X., Han, L., Zhang, Q., and Guo, A. Y. (2018). GSCALite: A web server for gene set cancer analysis. *Bioinforma. Oxf. Engl.* 34 (21), 3771–3772. doi:10.1093/bioinformatics/bty411

Oliveri, V. (2022). Selective targeting of cancer cells by copper ionophores: An overview. *Front. Mol. Biosci.* 9, 841814. doi:10.3389/fmolb.2022.841814

Rees, M. G., Seashore-Ludlow, B., Cheah, J. H., Adams, D. J., Price, E. V., Gill, S., et al. (2016). Correlating chemical sensitivity and basal gene expression reveals mechanism of action. *Nat. Chem. Biol.* 12 (2), 109–116. doi:10.1038/nchembio.1986

Schmidt, T., Samaras, P., Frejno, M., Gessulat, S., Barnert, M., Kienegger, H., et al. (2018). ProteomicsDB. *Nucleic Acids Res.* 46 (D1), D1271–D1281. doi:10.1093/nar/gkx1029

Sheftel, A. D., Stehling, O., Pierik, A. J., Elsasser, H. P., Muhlenhoff, U., Webert, H., et al. (2010). Humans possess two mitochondrial ferredoxins, Fdx1 and Fdx2, with distinct roles in steroidogenesis, heme, and Fe/S cluster biosynthesis. *Proc. Natl. Acad. Sci. U. S. A.* 107 (26), 11775–11780. doi:10.1073/pnas.1004250107

Siegel, R. L., Miller, K. D., Fuchs, H. E., and Jemal, A. (2022). Cancer statistics, 2022. *Ca. A Cancer J. Clin.* 72, 7–33. doi:10.3322/caac.21708

Smith, J. D., Hill, A. J., Reeder, L. E., Franke, B. C., Lehoucq, R. B., Parekh, O., et al. (2022). Neuromorphic scaling advantages for energy-efficient random walk computations. *Nat. Electron.* 5 (2), 102–112. doi:10.1038/s41928-021-00705-7

Strushkevich, N., MacKenzie, F., Cherkesova, T., Grabovec, I., Usanov, S., and Park, H. W. (2011). Structural basis for pregnenolone biosynthesis by the mitochondrial monooxygenase system. *Proc. Natl. Acad. Sci. U. S. A.* 108 (25), 10139–10143. doi:10.1073/pnas.1019441108

Szklarczyk, D., Gable, A. L., Nastou, K. C., Lyon, D., Kirsch, R., Pyysalo, S., et al. (2021). The STRING database in 2021: Customizable protein-protein networks, and functional characterization of user-uploaded gene/measurement sets. *Nucleic Acids Res.* 49, D605–D612. doi:10.1093/nar/gkaa1074

Tang, D., Chen, X., and Kroemer, G. (2022). Cuproptosis: A copper-triggered modality of mitochondrial cell death. *Cell Res.* 32 (5), 417–418. doi:10.1038/s41422-022-00653-7

Tang, Z., Li, C., Kang, B., Gao, G., Li, C., and Zhang, Z. (2017). Gepia: A web server for cancer and normal gene expression profiling and interactive analyses. *Nucleic Acids Res.* 45, W98–W102. doi:10.1093/nar/gkx247

Tsvetkov, P., Coy, S., Petrova, B., Dreishpoon, M., Verma, A., Abdusamad, M., et al. (2022). Copper induces cell death by targeting lipoylated TCA cycle proteins. *Sci. (New York, N.Y.)* 375 (6586), 1254–1261. doi:10.1126/science.abf0529

Warde-Farley, D., Donaldson, S. L., Comes, O., Zuberi, K., Badrawi, R., Chao, P., et al. (2010). The GeneMANIA prediction server: Biological network integration for gene prioritization and predicting gene function. *Nucleic Acids Res.* 38, W214–W220. Web Server issue. doi:10.1093/nar/gkq537

Weinstein, J. N., Collisson, E. A., Mills, G. B., Shaw, K. R. M., Ozenberger, B. A., Ellrott, K., et al. (2013). The cancer genome Atlas pan-cancer analysis project. *Nat. Genet.* 45 (10), 1113–1120. doi:10.1038/ng.2764

Yang, F., Wang, J. F., Wang, Y., Liu, B., and Molina, J. R. (2021). Comparative analysis of predictive biomarkers for PD-1/PD-L1 inhibitors in cancers: Developments and challenges. *Cancers (Basel)* 14 (1), 109. doi:10.3390/cancers14010109

Yang, W., Soares, J., Greninger, P., Edelman, E. J., Lightfoot, H., Forbes, S., et al. (2013). Genomics of drug sensitivity in cancer (GDSC): A resource for therapeutic biomarker discovery in cancer cells. *Nucleic Acids Res.* 41, D955–D961. Database issue. doi:10.1093/nar/gks1111

Ye, Y., Xiang, Y., Ozguc, F. M., Kim, Y., Liu, C. J., Park, P. K., et al. (2018). The genomic landscape and pharmacogenomic interactions of clock genes in cancer chronotherapy. *Cell Syst.* 6, 314–328. doi:10.1016/j.cels.2018.01.013

Yoshihara, K., Shahmoradgoli, M., Martinez, E., Vegesna, R., Kim, H., Torres-Garcia, W., et al. (2013). Inferring tumour purity and stromal and immune cell admixture from expression data. *Nat. Commun.* 4, 2612. doi:10.1038/ncomms3612

Yun, Y., Wang, Y., Yang, E., and Jing, X. (2022). Cuproptosis-related gene - SLC31A1, FDX1 and ATP7B - polymorphisms are associated with risk of lung cancer. *Pharmgenomics. Pers. Med.* 15, 733–742. doi:10.2147/PGPM.S372824

Zhang, Z., Ma, Y., Guo, X., Du, Y., Zhu, Q., Wang, X., et al. (2021). FDX1 can impact the prognosis and mediate the metabolism of lung adenocarcinoma. *Front. Pharmacol.* 12, 749134. doi:10.3389/fphar.2021.749134

Zhang, Z., Zeng, X., Wu, Y., Liu, Y., Zhang, X., and Song, Z. (2022). Cuproptosis-related risk score predicts prognosis and characterizes the tumor microenvironment in hepatocellular carcinoma. *Front. Immunol.* 13, 925618. doi:10.3389/fimmu.2022.925618

frontiers | Frontiers in Genetics

TYPE Original Research
PUBLISHED 28 September 2022
DOI 10.3389/fgene.2022.942166

Check for updates

OPEN ACCESS

EDITED BY
Mukesh Kumar Gupta,
National Institute of Technology Rourkela, India

REVIEWED BY
Tung Nguyen-Thanh,
Hue University of Medicine and Pharmacy, Vietnam
Kangkang Yu,
Fudan University, China

*CORRESPONDENCE
Dan-Li Shi,
jasonmob@sina.com
Meng Luo,
luosh9hospital@sina.com

†These authors have contributed equally to this work

SPECIALTY SECTION
This article was submitted to Cancer Genetics and Oncogenomics, a section of the journal Frontiers in Genetics

RECEIVED 12 May 2022
ACCEPTED 02 September 2022
PUBLISHED 28 September 2022

CITATION
Chen M, Wu G-B, Xie Z-W, Shi D-L and Luo M (2022), A novel diagnostic four-gene signature for hepatocellular carcinoma based on artificial neural network: Development, validation, and drug screening.
Front. Genet. 13:942166.
doi: 10.3389/fgene.2022.942166

COPYRIGHT
© 2022 Chen, Wu, Xie, Shi and Luo. This is an open-access article distributed under the terms of the Creative Commons Attribution License (CC BY). The use, distribution or reproduction in other forums is permitted, provided the original author(s) and the copyright owner(s) are credited and that the original publication in this journal is cited, in accordance with accepted academic practice. No use, distribution or reproduction is permitted which does not comply with these terms.

A novel diagnostic four-gene signature for hepatocellular carcinoma based on artificial neural network: Development, validation, and drug screening

Min Chen[1,2†], Guang-Bo Wu[1†], Zhi-Wen Xie[2†], Dan-Li Shi[1*] and Meng Luo[1*]

[1]Department of General Surgery, Shanghai Ninth People's Hospital Affiliated to Shanghai Jiao Tong University School of Medicine, Shanghai, China, [2]Department of Urology, Shanghai General Hospital, Shanghai Jiao Tong University School of Medicine, Shanghai, China

Background: Hepatocellular carcinoma (HCC) is one of the most common cancers with high mortality in the world. HCC screening and diagnostic models are becoming effective strategies to reduce mortality and improve the overall survival (OS) of patients. Here, we expected to establish an effective novel diagnostic model based on new genes and explore potential drugs for HCC therapy.

Methods: The gene expression data of HCC and normal samples (GSE14811, GSE60502, GSE84402, GSE101685, GSE102079, GSE113996, and GSE45436) were downloaded from the Gene Expression Omnibus (GEO) dataset. Bioinformatics analysis was performed to distinguish two differentially expressed genes (DEGs), diagnostic candidate genes, and functional enrichment pathways. QRT-PCR was used to validate the expression of diagnostic candidate genes. A diagnostic model based on candidate genes was established by an artificial neural network (ANN). Drug sensitivity analysis was used to explore potential drugs for HCC. CCK-8 assay was used to detect the viability of HepG2 under various presentative chemotherapy drugs.

Results: There were 82 DEGs in cancer tissues compared to normal tissue. Protein–protein interaction (PPI), Gene Ontology (GO), and Kyoto Encyclopedia of Genes and Genomes (KEGG) enrichment analyses and infiltrating immune cell analysis were administered and analyzed. Diagnostic-related genes of *MT1M*, *SPINK1*, *AKR1B10*, and *SLCO1B3* were selected from DEGs and used to construct a diagnostic model. The receiver operating characteristic (ROC) curves were 0.910 and 0.953 in the training and testing cohorts, respectively. Potential drugs, including vemurafenib, LOXO-101, dabrafenib, selumetinib, Arry-162, and NMS-E628, were found as well. Vemurafenib, dabrafenib, and selumetinib were observed to significantly affect HepG2 cell viability.

Conclusion: The diagnostic model based on the four diagnostic-related genes by the ANN could provide predictive significance for diagnosis of HCC patients,

which would be worthy of clinical application. Also, potential chemotherapy drugs might be effective for HCC therapy.

KEYWORDS

hepatocellular carcinoma, diagnostic model, artificial neural network, MT1M, SPINK1, AKR1B10, SLCO1B3

Introduction

Hepatocellular carcinoma (HCC) is an increasingly serious public health problem, and it is gradually becoming one of the main causes of cancer mortality in the world (Villanueva, 2019). As most cases of HCC occur in patients with underlying chronic liver diseases like hepatitis B virus (HBV) infection and varying degrees of cirrhosis, the diagnosis of HCC in humans is challenging (Vogel and Saborowski, 2020; Yang and Heimbach, 2020). Most HCC patients are diagnosed when they have obvious clinical symptoms appear or are at advanced stages of the disease, which reduces or even precludes the effective use of curative therapy (Ayuso et al., 2018; Rastogi, 2018). Therefore, identifying candidate biomarkers and constructing novel diagnostic models could be useful in distinguishing HCC patients from normal people, which would improve the overall survival (OS) of HCC patients.

In the clinic, the detection of serum tumor markers has been widely used for its advantages of the noninvasive method (Han et al., 2020). However, the information provided by the conventional assays for carcinoembryonic antigen (CEA) and carbohydrate antigen 19-9 (CA19-9) is not specific or sensitive enough (Cui et al., 2016; Edoo et al., 2019). Thus, developing novel diagnostic biomarkers is necessary for early detection of HCC. Meanwhile, HCC patients could not get timely treatment because of multidrug resistance or might have suffered from severe drug-related adverse effects from chemotherapy (Zhang et al., 2016). Calling for novel and effective drugs for HCC patients is an eternal theme of the times.

With the improvement of bioinformatics technology, differentially expressed genes (DEGs) by systematic bioinformatics analysis could be employed to select candidate genes and underlying pathways that were related to the occurrence and progression of HCC for diagnosis (Wang et al., 2018; Li et al., 2021). Moreover, an artificial neural network (ANN) is a classic machine learning method, which is often used for modeling construction (Zhong et al., 2019; Mai et al., 2020). In this study, we first retrieved transcriptional expression data of patients with HCC patients from GEO datasets and found 82 DEGs between normal and HCC tissues. Next, the possible functional mechanisms were explored by protein–protein interaction (PPI), Kyoto Encyclopedia of Genes and Genomes (KEGG), and Gene Ontology (GO) enrichment analyses. Then, metallothionein 1M (MT1M), solute carrier organic anion transporter family member 1B3 (SLCO1B3), serine protease inhibitor Kazal type 1 gene (SPINK1), and aldo–keto reductase family 1B10 (AKR1B10) were found and used as candidate biomarkers to construct an artificial neural network (ANN) model. Further validation of diagnostic-related genes was performed by QRT-PCR in HepG2 and HL7702 cell lines. The potential drug for HCC therapy, including vemurafenib, LOXO-101, dabrafenib, selumetinib, Arry-162, and NMS-E628, were found based on four diagnostic-related genes. Vemurafenib, dabrafenib, and selumetinib might have a broad application prospect in HCC.

Methods

Datasets

The RNA microarray data of HCC samples and corresponding normal liver tissue were retrieved from the GEO dataset (https://www.ncbi.nlm.nih.gov/geo/). The datasets of GSE14811, GSE60502, GSE84402, GSE101685, GSE102079, GSE113996, and GSE45436 were downloaded and divided into training and testing cohorts. The "sva" package of R was used to ensure that the GEO datasets were batch effects-corrected before bioinformatics analysis to avoid generating less reliable results (Leek et al., 2012). The first six datasets were classified as training cohorts and used for diagnostic model construction. The latter was classified as a testing cohort and used for validation.

Identification of differentially expressed genes

Normalization of the count matrix was performed with the trimmed mean of the M-values normalization method of the edgeR (R package). The limma R package was used to identify differentially expressed genes (DEGs) in the construction cohort. The screening standards of DEGs for functional enrichment analysis were $|\log_2 FC| > 1$ and FDR<0.05. The screening standards of DEGs for diagnostic-related genes used for ANN model establishment and drug-sensitive analysis were $|\log_2 FC| > 2$ and FDR<0.05.

Functional enrichment analysis

For protein–protein interaction (PPI), we used the String (Protein–Protein Interaction Networks, V: 10.5) database (https://string-db.org/). Kyoto Encyclopedia of Genes and Genomes

(KEGG) and Gene Ontology (GO) enrichment analyses of the DEGs were performed by using the R clusterProfiler package, including the packages of "GOplot," "ggplot2," "stringi," "colorspace," and "digest". Then, the pathway and process enrichment analyses were carried out using Metascape (Metascape, http://metascape.org). As for infiltrating immune cell analysis, the R package of "e1071," "corrplot," and "vioplot" were used for analysis and depicting differences. The 22 representative immune cells and gene expressions in every kind of immune cell to distinguish immune cells from each other are shown in Supplementary Table S1.

Construction and validation of the diagnostic model

The artificial neural network (ANN) classifier was a feed-forward neural network with three layers, which included input nodes, a hidden layer, and output nodes. The multi-layer perceptron method was incorporated, and training of the network was based on the feed-forward back propagation method to adjust the internal factors of the network, which reduced the overall errors during the repeated development cycles. The ANN model learned to connect the relations between the input and output layers by adjusting the weights and biases of the hidden layer. Here, we used the training cohort (GSE14811, GSE60502, GSE84402, GSE101685, GSE102079, and GSE113996) to establish the ANN diagnostic model, and the testing cohort (GSE45436) was used as the validation one. There were 221 normal tissues and 284 HCC tissues in the training cohort, while 41 normal tissues and 93 HCC tissues were in the testing cohort.

Cells and cell culture

The HepG2 cell line (Human HCC) and HL7702 (human normal cells) were purchased from the Chinese Academy of Medical Sciences (Beijing, China). The HepG2 cells were grown in Dulbecco's modified Eagle's medium (DMEM) supplemented with 10% fetal bovine serum (Life Technologies, Inc., Carlsbad, CA, United States), 1 mM sodium pyruvate, 0.1 mM non-essential amino acids, and 2 mM L-glutamine at 37°C and in 5% CO_2 in a humidified incubator. The HL7702 cells were cultured in RPMI-1640 medium (Gibco, Rockville, MD, United States) supplemented with 10% Fetal Bovine Serum (Life Technologies, Inc., Carlsbad, CA, United States) at 37°C in a humidified 5% CO_2 atmosphere.

Quantitative real-time PCR

Here, we used HepG2 and HL7702 to verify the expression of diagnostic genes. The total RNA was isolated by TRIzol reagent (Life Technologies Corporation, Carlsbad, CA, United States) under the manufacturer's s directions. Then, 0.8 μg mRNA was used for synthesis of 20 μL cDNA using Superscript II reverse transcriptase and random hexamers (Invitrogen, Carlsbad, CA, United States). Q-RT PCR was further performed on an ABI PRISM 7300 Sequence Detection System with SYBR Green PCR Master Mix (Applied Biosystems). The primers used in this study were *MT1M* (forward 5′-ATTGAATTCGGATGGACCCCAACTGCTC-3′, reverse 5′-ATTCTCGAGTCAGGCACAGCAGCTG-3′), *SLCO1B3*(forward 5′-TCATAAACTCTTTGTTCTCTG CAA-3′, reverse 5′-GTTGGCAGGCATTGTCTTG-3′), *SPINK1* (forward 5′-AACACTGGAGCTGACTCCCT-3′, reverse 5′-ATCAGTCCCACAGACAGGGT-3′), and *AKR1B10* (forward 5′-CATATCCAGAGGAATGTGATT GTCA-3′, reverse 5′- AGACCTGAATGTTCTCAACAA TGC-3′). GAPDH was the internal comparison. The mRNA expression of relative genes was calculated using the 2−ΔΔCt method with normalization to GAPDH expression.

Drug-sensitive analysis of the gene signatures

The transcriptional expression of NCI-60 human cancer cell lines was downloaded from the CellMiner project page (https://discover.nci.nih.gov/cellminer). Pearson's correlation analysis was performed to determine the association between diagnostic genes and drug sensitivity.

Cell counting kit-8 (CCK-8 assay)

CCK-8 assay was used to detect the viability of HepG2 under various presentative chemotherapy drugs. The cells were resuspended, seeded in a 96-well plate (6 × 104 cells/well), cultured at an appropriate environment (37°C, 5% CO_2.), and continually incubated for 2 h with 10 ul CCK-8 solution (Yeasen, Shanghai, China) added to each well. The absorbance of each well was measured at 450 nm and tested by a microplate reader (Bio-Rad, Hercules, CA). The calculation of cell viability was processed as follows: (Experimental group - blank control)/(Negative control - blank control) ×100%. The blank groups contained DMEM medium only, while the negative groups were set up with HepG2 and HL7702 cultured in DMEM-F12 without drugs. Vemurafenib (S1267) and Selumetinib (S1008) were obtained from Selleck Chemicals (Houston, TX, United States). Dabrafenib was purchased from Merck (Kenilworth, NJ, United States). Binimetinib and larotrectinib were provided by Med Chem Express (Shanghai, China).

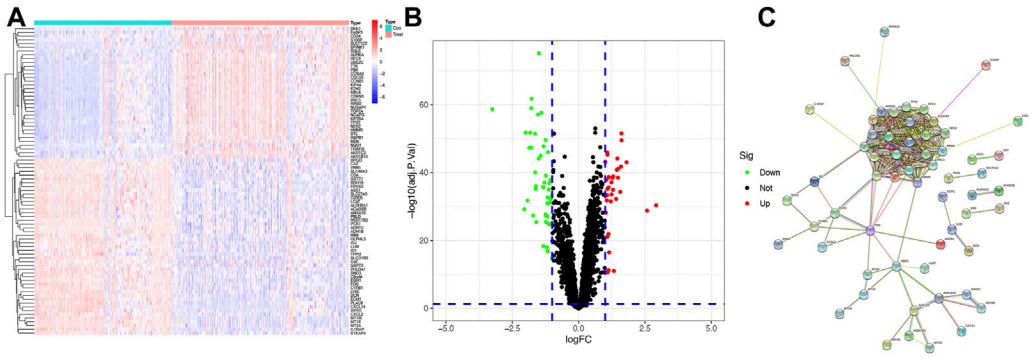

FIGURE1
Identification of candidate genes **(A)** Heatmap of differential gene expression between normal and HCC samples in the training cohort, log_2FC = 1. **(B)** Volcano map of differential gene expression between normal and HCC samples in the training cohort. **(C)** PPI network between these genes (cutoff = 0.4).

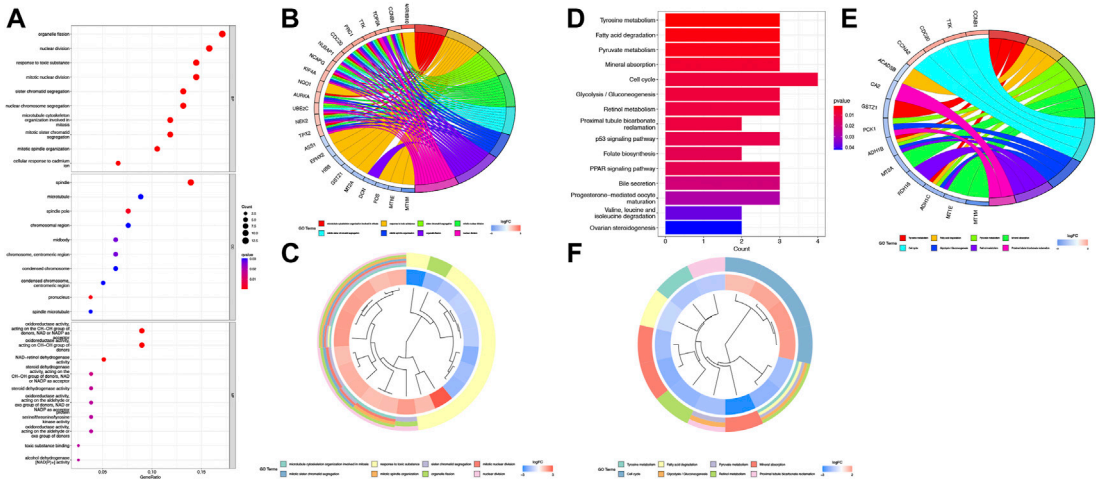

FIGURE 2
Function analysis based on the DEGs **(A)** Heatmap of GO analysis. **(B)** Circos plot of GO terms based on DEGs. **(C)** Cluster profiler analysis of the GO based on DEGs. **(D)** Barplot of KEGG terms based on DEGs. **(E)** Circos plot of KEGG terms based on DEGs. **(F)** Cluster profiler analysis of the KEGG based on DEGs.

Results

Identification of DEGs

A total of 221 normal samples and 284 tumor samples obtained from the GEO dataset formed the training cohort and participated in the identification of DEGs. The differential expression of 82 genes between the normal and HCC samples was identified by building a difference comparison matrix. A heatmap and volcano map showed 47 downregulated genes and 35 upregulated genes (Figures 1A and B). The protein–protein interaction (PPI) network and co-expression among these genes are presented in Figure 1C.

Functional enrichment and pathway analyses

KEGG and GO function enrichment analyses were performed here. As for GO function analysis, three GO terms were selected: molecular function (MF), cellular component (CC), and biological process (BP). Expression analysis showed that DEGs had the most uniquely enriched terms for organelle

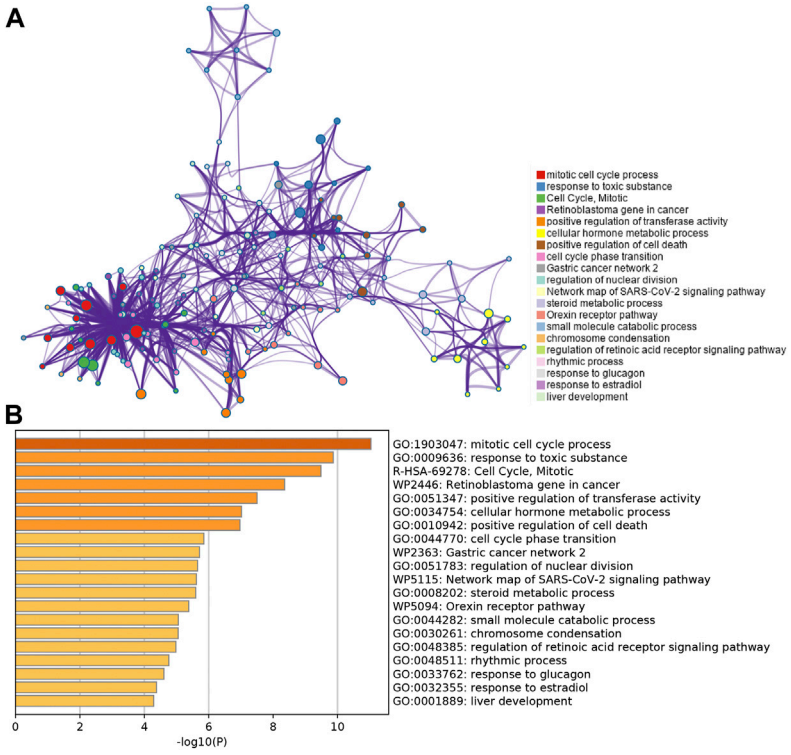

FIGURE 3
Functional pathway analysis using Metascape. **(A)** Network of enriched terms colored by the cluster identified in DEGs using the Metascape tool. **(B)** Top 20 clusters of enriched biological processes identified in DEGs using the Metascape tool.

fission, (mitotic) nuclear division, and spindle, which were related to cell proliferation, cell division, and cell cycling. The processes mentioned were substantially over-represented during cancer transformation. Also, "oxidoreductase activity, acting on the CH–CH group of donors" was enriched in the list (Figure 2A). In Figures 2B, C, several up-regulated DEGs were mainly enriched in processes of "nuclear division," "organelle fission," etc., while down-regulated ones were mainly gathered in "response to toxic substance".

Furthermore, KEGG pathway enrichment analysis indicated that DEGs were significantly enriched in "Cell cycle", "Tyrosine metabolism", etc (Figure 2D). In Figures 2E and F, upregulated DEGs were mainly enriched in the "Cell cycle" while downregulated DEGs were gathered in several cancer-related metabolism pathways.

To further validate and organize the results of KEGG and GO function, the DEGs were functionally annotated using Metascape. Metascape analysis showed the top 20 clusters of enriched biological processes like "mitotic cell cycle process," "response to toxic substance," etc (Figures 3A and B).

Identification and validation of diagnostic-related genes

Further comparison analysis between liver tissues from HCC and normal samples was identified by improving the screening criteria of logFC into $|\log_2 FC|>2$, and we got four genes as candidate genes (Supplementary Figure S1). Next, a random forest analysis was performed, and four diagnostic-related genes (*MT1M*, *SPINK1*, *AKR1B10*, and *SLCO1B3*) were ensured, which showed that two genes were upregulated and two genes were downregulated (Figures 4A, B). The mean decrease in the Gini coefficient was a measure of how each variable contributed to the homogeneity of the nodes in the resulting random forest. The values were all over 40, which meant the four genes were of great importance in the development of the ANN model (Figure 4B). The diagnostic-related genes identified were shown in heatmap and could divide the training cohort into two groups (Figure 4C). Further validation of the diagnostic-related genes was performed by QRT-PCR (Figure 4D).

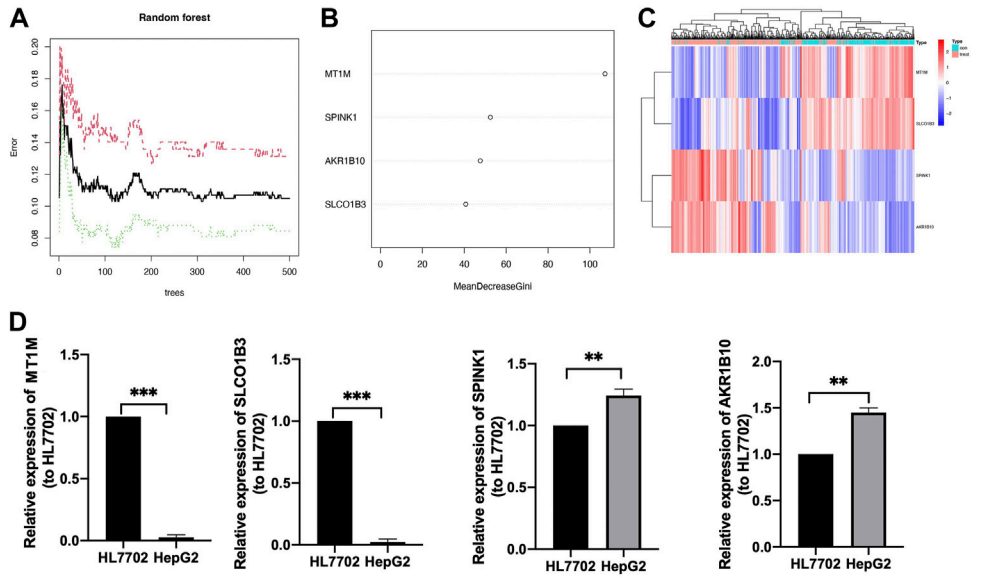

FIGURE 4
Identification of target genes. **(A)** Decision tree random forest tree. **(B)** Mean decrease in Gini coefficient of four target genes. **(C)** Heatmap of diagnostic candidate DEGs **(D)** QRT-PCR of four target genes, $^{**}p < 0.01$, $^{***}p < 0.001$.

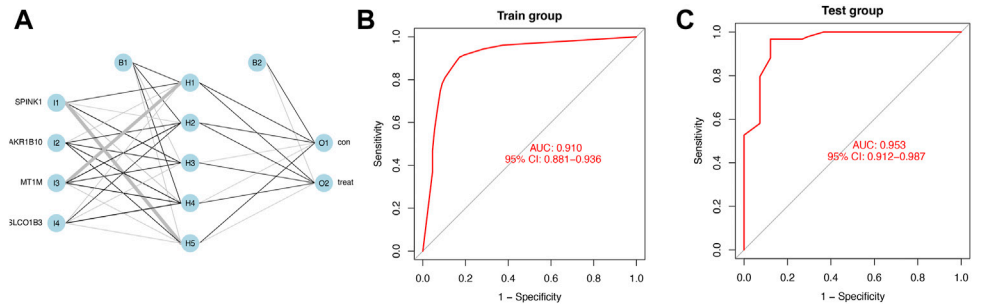

FIGURE 5
Diagnostic model constructed by the ANN **(A)** Schematic representation of the ANN model developed to predict the risk of HCC and normal samples. Thin lines represented synaptic weight <0; the thicker lines represented synaptic weight >0. **(B)** AUC of ROC curves verified the diagnostic performance of the ANN model in the training cohort. **(C)** AUC of ROC curves verified the diagnostic performance of the ANN model in the testing cohort.

Construction and validation of the diagnostic model built on an artificial neural network

We calculated the risk gene scores of the four genes in each sample to get the median cutoff value and defined the upregulated gene as "1" and the downregulated gene as "0" in each sample in the training and testing cohorts (Supplementary Table S2). The approximate ratio of the sample number in the training cohort (Normal:221; HCC:284) and the testing cohort (Normal:41; HCC:93) is 4 to 1. Then, the ANN method was performed to construct a diagnostic model based on gene scores of *MT1M, SPINK1, AKR1B10, and SLCO1B3* in each sample. The ANN model included three layers (input, hidden, and output) in which the number of nodes in the input layer and output layer was equal to 4 (number of input genes) and 2 (control and treatment), respectively (Figure 5A). An ROC curve was performed to detect whether the model could distinguish the HCC sample from the normal sample, and the area under the curve (AUC) was 0.910 (Figure 5B). In addition, the model worked well in the testing cohort as the AUC of ROC was 0.953 (Figure 5C).

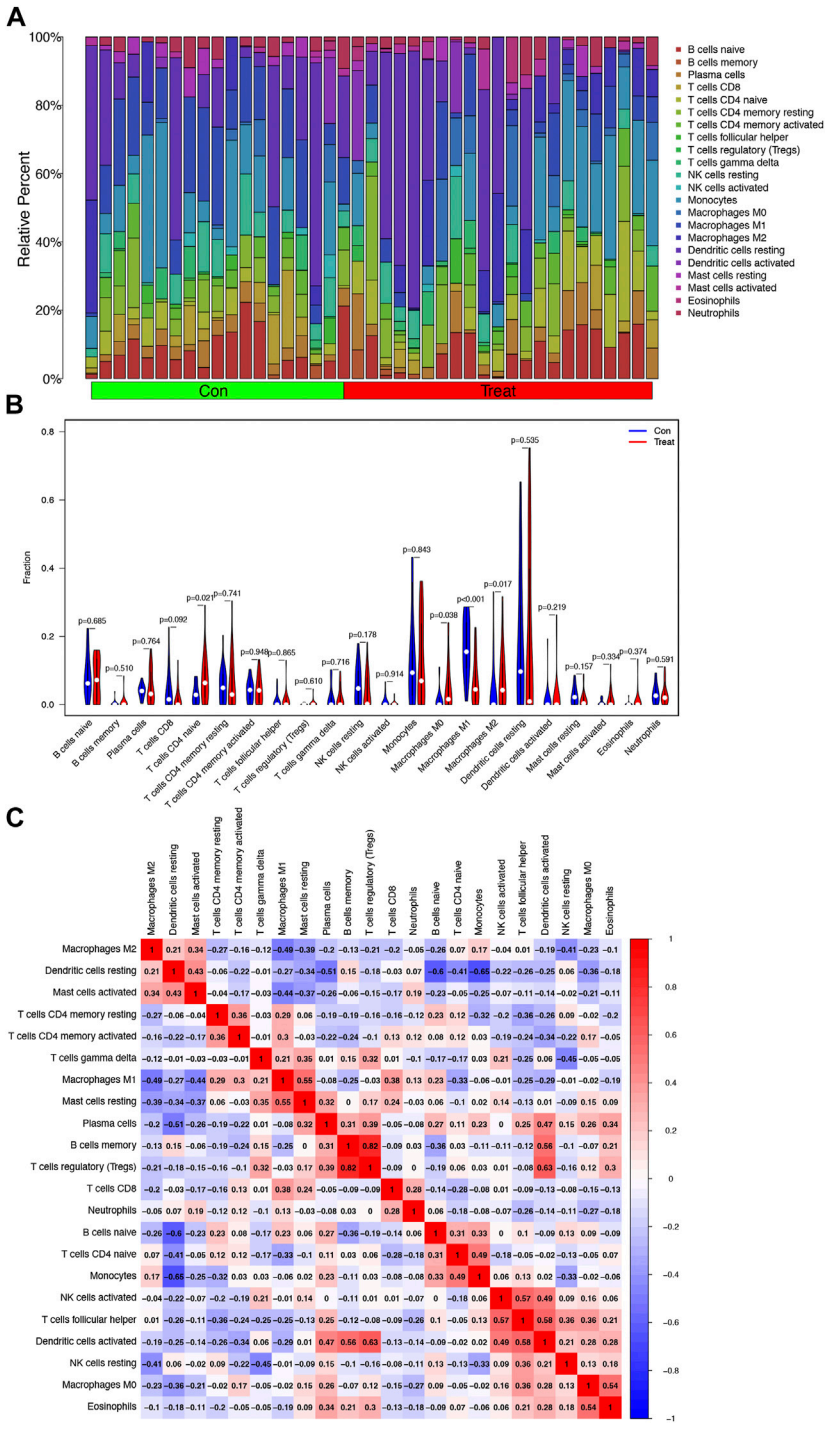

FIGURE 6
Analysis of infiltrating immune cells in the training cohort. **(A)** Heatmap of relative fraction of 22 representative immune cell population in the Con (normal) and Treat (HCC) cohorts was displayed. **(B)** Boxplots showed the cores of 22 immune cells between the Con (normal) and Treat (tumor) cohorts. **(C)** Heatmap of correlation between 22 immune cells.

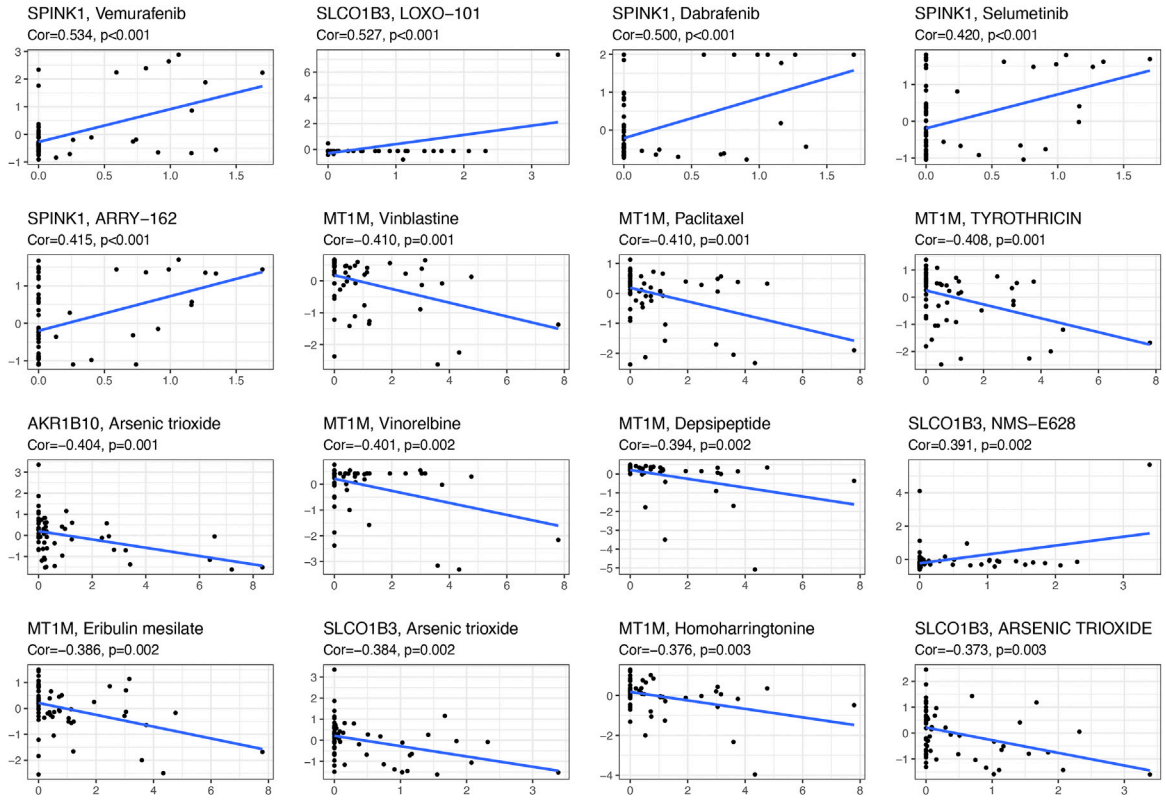

FIGURE 7
Scatter plot of the relationship between diagnostic-related gene expression and drug sensitivity.

Infiltrating immune cell analysis

The relative percent of 22 representative immune cells in the normal and HCC samples is presented in Figure 6A to show the approximate change in the proportion of immune cells in the training cohort. In Figure 6B, only "T cells CD4 naive", "Macrophages M0", "Macrophages M1", and "Macrophages M2" displayed a substantial difference between the two groups (Figure 6B). "Macrophages M1" was the most significant one ($p < 0.001$) compared to "T cells CD4 naïve" ($p = 0.021$), "Macrophages M0" ($p = 0.038$), and "Macrophages M2" ($p = 0.017$). Furthermore, Macrophages M2 showed a significant negative correlation with Macrophages M1 and M0, while Macrophages M0 and M2 were both upregulated in the HCC group (Figures 6B, C).

The sensitivity of diagnostic-related gene expression to presentative chemotherapy drug

With the help of NCI-60, a public database of human cancer cell lines, we determined the relationship between these diagnostic genes and drug sensitivity and showed the top 16 correlation analyses according to the *p*-value. Figure 7 demonstrated that *SPINK1* was sensitive to vemurafenib, dabrafenib, selumetinib, ARRY-162 (binimetinib) ($p < 0.001$), and *SLCO1B3* was sensitive to LOXO-101(larotrectinib) ($p < 0.001$) and NMS-E628 ($p = 0.002$), while it was insensitive to arsenic trioxide. In addition, the expression of *MT1M* was insensitive to vinblastine, paclitaxel, and tyrothricin ($p < 0.001$). Moreover, *AKR1B10* was insensitive to arsenic trioxide ($p = 0.001$).

The cell viability under various presentative chemotherapy agents

Here, we further validate the HepG2 under various presentative chemotherapy drugs, including vemurafenib, dabrafenib, selumetinib, binimetinib, and larotrectinib, for they were sensitive to *SPINK1* and *SLCO1B3*. We found that the former three kinds of drugs could significantly inhibit the cell viability of HepG2, while the latter two could also work slightly without significant differences observed (Figure 8).

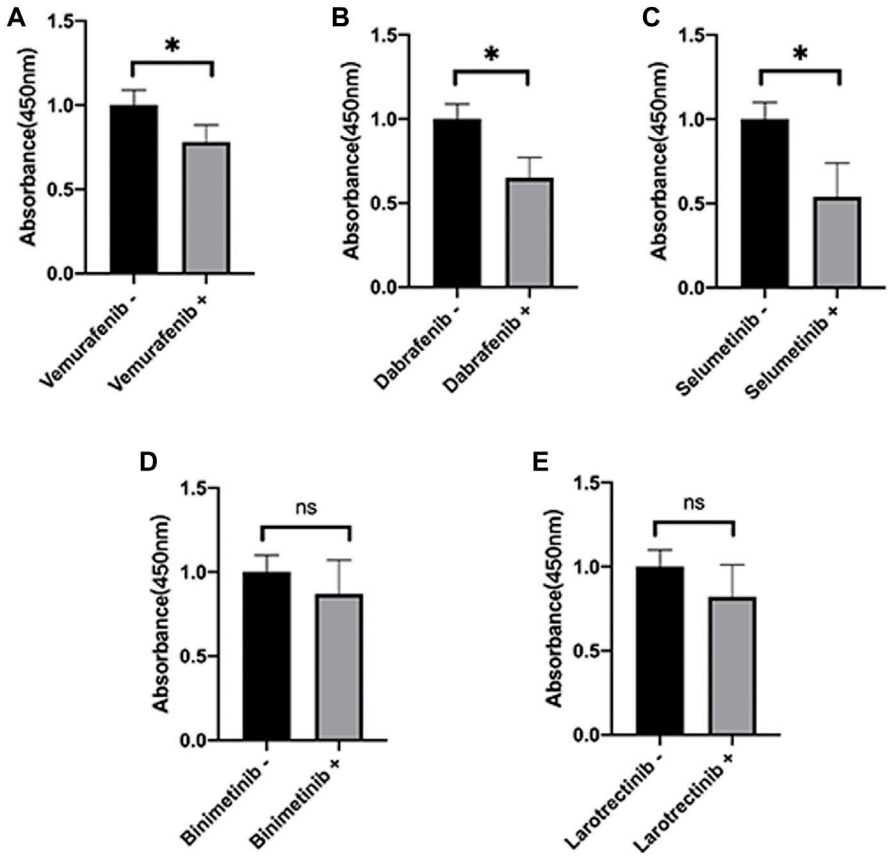

FIGURE 8
Cell viability of HepG2 under various presentative chemotherapy agent treatment in 24 h. The absorbance of HepG2 under treatment of **(A)** vemurafenib (5 μM), **(B)** dabrafenib (5 μM), **(C)** selumetinib (5 μM), **(D)** binimetinib (5 μM), and **(E)** larotrectinib (5 μM). *$p < 0.05$, ns = not significant.

Discussion

HCC is one of the most widespread problems facing by society today, which still has a high mortality rate in China (Xie et al., 20192020). Although comprehensive treatments have been adopted, HCC is associated with poor OS due to late diagnosis and high metastasis rate (Liu et al., 2020; Zhang et al., 2020). Early diagnosis, reasonable assessment of prognosis, and timely intervention are important for HCC patients, which encouraged us to explore better relevant biomarkers and diagnostic models (Beumer et al., 2021). Advancing molecular biology research methods brought diagnostic evaluation based on new types of biomarkers into reality. In this study, we observed 82 DEGs between HCC and normal samples. Based on DEGs, we explored the functional enrichment and pathway analyses and found that they were likely to be involved in mitosis and oxidative stress, which is consistent with the current latest research about cancer proliferation, metastasis, and treatment resistance. Moreover, in the infiltrating immune cell analysis, the unbalance of Macrophage M1/M2 was observed in this study. Macrophage M1 exerted cytotoxic function and eliminated early HCC, while macrophage M2 exerted anti-inflammatory activities and promoted cancer cell proliferation and invasion (Tian et al., 2019). However, Macrophage M0 and Naive T cell amounts were upregulated in the HCC cohort, while not all of them would differentiate to maturity and interfere with HCC proliferation or immigration. Thus, increasing the ratio of M1/M2 and the number of mature T cells might be a potential treatment for HCC (Dou et al., 2019; Yan et al., 2021).

To better select the candidate gene from DEGs for diagnostic model construction, we employed a random forest algorithm and found *MT1M*, *SLCO1B3*, *SPINK1*, and *AKR1B10* were the chosen ones. The mean decrease in the Gini coefficient of the four target genes was all above 40, which meant they had obvious specificity in DEGs. *MT1M*, *SLCO1B3*, *SPINK1*, and *AKR1B10* were cancer-related genes that were associated with different human diseases, especially in HCC. The specific biological functions of the four diagnostic-related genes (*MT1M*, *SLCO1B3*, *SPINK1*, and *AKR1B10*) in HCC in the recent 10 years are presented in Table 1.

TABLE 1 Various biological functions of four diagnostic-related genes in HCC.

Gene	Biological function	References
MT1M	Inhibiting proliferation, migration, invasion, and inducing apoptosis as well in HepG2 and Hep3B	(Changjun et al., 2018; Zhang et al., 2018)
	Promoter methylation of it could be regarded as serum biomarkers for noninvasive detection of HCC.	Ji et al. (2014)
SLCO1B3	It participated in drug absorption, distribution, metabolism, and excretion and was downregulated in HCC patients	Hu et al. (2019)
	Low expression of it might be a potential diagnostic, prognostic marker, targeted treatment in HCC patients and multistep hepatocarcinogenesis	(Yamashita et al., 2014; Chen et al., 2020; Kitao et al., 2020)
	However, SLCO1B3-mediated up-taking of indocyanine green was essential for HCC resection. It might also be related to poor prognosis of specific subclass of Wnt/β-catenin-activated HCC.	(Ueno et al., 2014; Shibasaki et al., 2015)
SPINK1	Promoting HCC cell proliferation, cell cycle, and invasion *in vitro*	(Huang et al., 2021; Lin et al., 2021)
	Downregulating E-cadherin and inducing EMT of HCC to promote metastasis	Ying et al. (2017)
	It could be regarded as a potential biomarker for early detection and targeted therapy of HCC.	(Marshall et al., 2013; Li et al., 2015; Jia et al., 2022)
	It was a downstream effector of the CDH17/β-catenin axis in HCC.	Shek et al. (2017)
AKR1B10	It might be a potential diagnostic biomarker for HCC development, metastasis, and a target for HCC-directed drug development	(DiStefano and Davis, 2019; Zhu et al., 2019)
		(Han et al., 2018; Ye et al., 2019)
	Inhibiting AKR1B10 expression elevated sorafenib's anti-HCC effects via blocking the mTOR pathway, leading apoptosis and autophagy in HCC	Geng et al. (2020)
	It participated in the IRAK4/IRAK1/AP-1/AKR1B10 signaling pathway and AUF1-mediated post-transcriptional regulation of AKR1B10 expression to regulate cancer stemness and drug resistance in HCC.	(Cheng et al., 2018; Zhang et al., 2022)
	AKR1B10 expression was downregulated by fidarestat in NK cells, which promoted NK cell glycolysis to enhance killing ability to fight against HCC cells	Wu et al. (2021)
	The alteration rate of it increased significantly with the age of HCC patients	Atyah et al. (2018)
	Meanwhile, it played an important role in protecting hepatocytes from damage induced by ROS.	Liu et al. (2019)

In this study, we found the four target genes could divide the training cohort into two groups and have the same trend as in previous research. We also confirmed the expression trend of the four genes in HepG2 and HL7702 cell lines by QRT-PCR. Based on the four diagnostic-related genes, the ANN diagnostic model was developed and validated in GEO datasets. The ANN model obtained the highest prediction performance and has been widely used in various diseases to predict the population with high risk (Kourou et al., 2015; Zhong et al., 2019; Li et al., 2020). Based on the four diagnostic candidate genes, we successfully established a diagnostic model as for AUC of ROC was 0.910 and 0.953 in the training and testing cohorts, respectively, which meant it served as a reliable prediction model in our study.

According to the four diagnostic-related genes, we screened the potential drug that has a connection with diagnostic genes by NCI-60. We found that *SPINK1* was sensitive to vemurafenib, dabrafenib, selumetinib, and ARRY-162, and *SLCO1B3* was sensitive to LOXO-101 and NMS-E628. In addition, we further validated the cell viability of HepG2 under various presentative chemotherapy drugs, including vemurafenib, dabrafenib, selumetinib, binimetinib, and larotrectinib and observed vemurafenib, dabrafenib, and selumetinib might have a broad application prospect in HCC. Vemurafenib was a small-molecule inhibitor of the oncogenic v-raf murine sarcoma viral oncogene homolog B (BRAF) kinase that was used for treatment of melanoma (Hyman et al., 2015). However, increased *SPINK1* secretion was reported to be related to vemurafenib resistance in BRAF V600E-mutant colorectal cancers, indicating the need to target different gene variant subtypes of HCC during chemotherapy (29193645). Vemurafenib was also noticed to be the substrate of *SLCO1B3,* which might influence the absorption and elimination of the HCC chemotherapy drug (23340295). Nevertheless, BRAF gene polymorphisms were associated with capsule formation in HCC (Sun et al., 2021). BRAF-mutation-mediated MAPK pathway downstream was often constitutively activated and led to cancer cell differentiation, proliferation, angiogenesis, and anti-apoptosis, suggesting targeting the BRAF pathway might inhibit HCC progression in the future (Gnoni et al., 2019). Dabrafenib was also a selective inhibitor of BRAF kinase for patients suffering from BRAF-mutated melanoma, advanced non-small cell lung cancer, and anaplastic thyroid cancer harboring the $BRAF^{V600E}$ mutation (Puszkiel et al., 2019). Until now, no association between dabrafenib and expression of *SPINK1* was reported in cancer treatment. Also, dabrafenib was found to inhibit the activation of OATP1B3 (*SLCO1B3*), which might contribute to increasing OATP1B3-substrate-sensitive drug during the absorption phase (Nebot et al., 2021). Considering the pharmacological mechanisms of dabrafenib and vemurafenib were similar, we also expected that dabrafenib

might have prospects in the treatment of HCC. Selumetinib was a mitogen-activated protein kinase 1 and 2 (MEK1/2) inhibitor for treatment of neurofibromatosis, pediatric low-grade glioma, non-small cell lung cancer, and melanoma (Campagne et al., 2021). Selumetinib could be delivered by a novel delivery nanosystem in HCC and showed a well-targeted therapeutic strategy for HCC (Farinha et al., 2021). In addition, a combination of sorafenib and selumetinib could inhibit the growth of naïve and sorafenib-resistant HCC tumors via suppression of β-catenin signaling (Huynh et al., 2019). No specific research reported the direct connection among selumetinib, *SPINK1*, and *SLCO1B3*. However, *SPINK1* promoted HCC metastasis *via* the MEK/ERK signaling pathway (Ying et al., 2017). Similar research also reported that *SPINK1* expression in HCC cells was associated with HCC *via* activating the c-Raf/MEK/ERK pathway, which suggested that inhibiting the MEK pathway and usage of selumetinib could be a potential treatment strategy for HCC(37). In addition, the potential chemotherapy drug mentioned above mainly participated in cell proliferation, cell division, and cell cycling, which was consistent with our functional analysis and has not been fully used for HCC treatment in clinics (Davies et al., 2002; Yuan et al., 2020). Moreover, combined inhibition of BRAF and CSF-1R, which recruits M2-polarized macrophages in a tumor, resulted in superior antitumor responses (Mok et al., 2015). Although the potential drugs for chemotherapy were with broad application foreground, the diagnostic genes not only could enhance the drug sensitivity but also increased the resistance of chemotherapy drugs approved by the Food and Drug Administration (FDA). Thus, further research is needed for accurate application of these drugs in HCC.

Conclusion

In conclusion, we constructed a novel diagnostic model based on four genes by the ANN model to predict the diagnosis of HCC patients. The model could provide useful insights into the potential prediction of HCC diagnosis. Several potential chemotherapy drugs came into view, although further research is required.

Data availability statement

The original contributions presented in the study are included in the article/Supplementary Material; further inquiries can be directed to the corresponding authors.

Author contributions

MC: writing—original draft. G-BW: writing—reviewing and editing. Z-WX: data curation. D-LS: supervision. ML: funding acquisition.

Funding

This work was supported by The National Natural Science Foundation of China (Nos. 81771564, 81901463, and 81970526).

Conflict of interest

The authors declare that the research was conducted in the absence of any commercial or financial relationships that could be construed as a potential conflict of interest.

Publisher's note

All claims expressed in this article are solely those of the authors and do not necessarily represent those of their affiliated organizations, or those of the publisher, the editors, and the reviewers. Any product that may be evaluated in this article, or claim that may be made by its manufacturer, is not guaranteed or endorsed by the publisher.

Supplementary material

The Supplementary Material for this article can be found online at: https://www.frontiersin.org/articles/10.3389/fgene.2022.942166/full#supplementary-material

References

Atyah, M., Yin, Y. R., Zhou, C. H., Zhou, Q., Chen, W. Y., Dong, Q. Z., et al. (2018). Integrated analysis of the impact of age on genetic and clinical aspects of hepatocellular carcinoma. *Aging (Albany NY)* 10 (8), 2079–2097. PubMed PMID: 30125264; PubMed Central PMCID: PMCPMC6128442. doi:10.18632/aging.101531

Ayuso, C., Rimola, J., Vilana, R., Burrel, M., Darnell, A., Garcia-Criado, A., et al. (2018). Diagnosis and staging of hepatocellular carcinoma (HCC): Current guidelines. *Eur. J. Radiol.* 101, 72–81. PubMed PMID: 29571804. doi:10.1016/j.ejrad.2018.01.025

Beumer, B. R., Buettner, S., Galjart, B., van Vugt, J. L. A., de Man, R. A., Ijzermans, J. N. M., et al. (2021). Systematic review and meta-analysis of validated prognostic models for resected hepatocellular carcinoma patients. *Eur. J. Surg. Oncol.* 48, 492–499. PubMed PMID: 34602315. doi:10.1016/j.ejso.2021.09.012

Campagne, O., Yeo, K. K., Fangusaro, J., and Stewart, C. F. (2021). Clinical pharmacokinetics and pharmacodynamics of selumetinib. *Clin. Pharmacokinet.* 60 (3), 283–303. PubMed PMID: 33354735. doi:10.1007/s40262-020-00967-y

Changjun, L., Feizhou, H., Dezhen, P., Zhao, L., and Xianhai, M. (2018). MiR-545-3p/MT1M axis regulates cell proliferation, invasion and migration in hepatocellular carcinoma. *Biomed. Pharmacother.* 108, 347–354. PubMed PMID: 30227328. doi:10.1016/j.biopha.2018.09.009

Chen, S., Li, K., Jiang, J., Wang, X., Chai, Y., Zhang, C., et al. (2020). Low expression of organic anion-transporting polypeptide 1B3 predicts a poor prognosis in hepatocellular carcinoma. *World J. Surg. Oncol.* 18 (1), 127. PubMed PMID: 32534581; PubMed Central PMCID: PMCPMC7293789. doi:10.1186/s12957-020-01891-y

Cheng, B. Y., Lau, E. Y., Leung, H. W., Leung, C. O., Ho, N. P., Gurung, S., et al. (2018). IRAK1 augments cancer stemness and drug resistance via the AP-1/AKR1B10 signaling cascade in hepatocellular carcinoma. *Cancer Res.* 78 (9), 2332–2342. PubMed PMID: 29483095. doi:10.1158/0008-5472.CAN-17-2445

Cui, L-H., Quan, Z-Y., Piao, J-M., Zhang, T-T., Jiang, M-H., Shin, M-H., et al. (2016). Plasma folate and vitamin B12 levels in patients with hepatocellular carcinoma. *Int. J. Mol. Sci.* 17 (7), E1032. PubMed PMID: 27376276. doi:10.3390/ijms17071032

Davies, H., Bignell, G. R., Cox, C., Stephens, P., Edkins, S., Clegg, S., et al. (2002). Mutations of the BRAF gene in human cancer. *Nature* 417 (6892), 949–954. PubMed PMID: 12068308. doi:10.1038/nature00766

DiStefano, J. K., and Davis, B. (2019). Diagnostic and prognostic potential of AKR1B10 in human hepatocellular carcinoma. *Cancers (Basel)* 11 (4), E486. PubMed PMID: 30959792; PubMed Central PMCID: PMCPMC6521254. doi:10.3390/cancers11040486

Dou, L., Shi, X., He, X., and Gao, Y. (2019). Macrophage phenotype and function in liver disorder. *Front. Immunol.* 10, 3112. PubMed PMID: 32047496. doi:10.3389/fimmu.2019.03112

Edoo, M. I. A., Chutturghoon, V. K., Wusu-Ansah, G. K., Zhu, H., Zhen, T. Y., Xie, H. Y., et al. (2019). Serum biomarkers AFP, CEA and CA19-9 combined detection for early diagnosis of hepatocellular carcinoma. *Iran. J. Public Health* 48 (2), 314–322. PubMed PMID: 31205886.

Farinha, D., Migawa, M., Sarmento-Ribeiro, A., and Faneca, H. (2021). A combined antitumor strategy mediated by a new targeted nanosystem to hepatocellular carcinoma. *Int. J. Nanomedicine* 16, 3385–3405. PubMed PMID: 34040370; PubMed Central PMCID: PMCPMC8141275. doi:10.2147/IJN.S302288

Geng, N., Jin, Y., Li, Y., Zhu, S., and Bai, H. (2020). AKR1B10 inhibitor epalrestat facilitates sorafenib-induced apoptosis and autophagy via targeting the mTOR pathway in hepatocellular carcinoma. *Int. J. Med. Sci.* 17 (9), 1246–1256. PubMed PMID: 32547320; PubMed Central PMCID: PMCPMC7294918. doi:10.7150/ijms.42956

Gnoni, A., Licchetta, A., Memeo, R., Argentiero, A., Solimando, A. G., Longo, V., et al. (2019). Role of BRAF in hepatocellular carcinoma: A rationale for future targeted cancer therapies. *Med. Kaunas.* 55 (12), E754. PubMed PMID: 31766556; PubMed Central PMCID: PMCPMC6956203. doi:10.3390/medicina55120754

Han, C., Gao, L., Bai, H., and Dou, X. (2018). Identification of a role for serum aldo-keto reductase family 1 member B10 in early detection of hepatocellular carcinoma. *Oncol. Lett.* 16 (6), 7123–7130. PubMed PMID: 30546447; PubMed Central PMCID: PMCPMC6256343. doi:10.3892/ol.2018.9547

Han, J., Han, M-L., Xing, H., Li, Z-L., Yuan, D-Y., Wu, H., et al. (2020). Tissue and serum metabolomic phenotyping for diagnosis and prognosis of hepatocellular carcinoma. *Int. J. Cancer* 146 (6), 1741–1753. PubMed PMID: 31361910. doi:10.1002/ijc.32599

Hu, D. G., Marri, S., McKinnon, R. A., Mackenzie, P. I., and Meech, R. (2019). Deregulation of the genes that are involved in drug absorption, distribution, metabolism, and excretion in hepatocellular carcinoma. *J. Pharmacol. Exp. Ther.* 368 (3), 363–381. PubMed PMID: 30578287. doi:10.1124/jpet.118.255018

Huang, K., Xie, W., Wang, S., Li, Q., Wei, X., Chen, B., et al. (2021). High SPINK1 expression predicts poor prognosis and promotes cell proliferation and metastasis of hepatocellular carcinoma. *J. Invest. Surg.* 34 (9), 1011–1020. PubMed PMID: 32066292. doi:10.1080/08941939.2020.1728443

Huynh, H., Ong, R., Goh, K. Y., Lee, L. Y., Puehler, F., Scholz, A., et al. (2019). Sorafenib/MEK inhibitor combination inhibits tumor growth and the Wnt/β-catenin pathway in xenograft models of hepatocellular carcinoma. *Int. J. Oncol.* 54 (3), 1123–1133. PubMed PMID: 30747223. doi:10.3892/ijo.2019.4693

Hyman, D. M., Puzanov, I., Subbiah, V., Faris, J. E., Chau, I., Blay, J-Y., et al. (2015). Vemurafenib in multiple nonmelanoma cancers with BRAF V600 mutations. *N. Engl. J. Med.* 373 (8), 726–736. PubMed PMID: 26287849. doi:10.1056/NEJMoa1502309

Ji, X. F., Fan, Y. C., Gao, S., Yang, Y., Zhang, J. J., and Wang, K. (2014). MT1M and MT1G promoter methylation as biomarkers for hepatocellular carcinoma. *World J. Gastroenterol.* 20 (16), 4723–4729. PubMed PMID: 24782625; PubMed Central PMCID: PMCPMC4000509. doi:10.3748/wjg.v20.i16.4723

Jia, J., Ga, L., Liu, Y., Yang, Z., Wang, Y., Guo, X., et al. (2022). Serine protease inhibitor kazal type 1, A potential biomarker for the early detection, targeting, and prediction of response to immune checkpoint blockade therapies in hepatocellular carcinoma. *Front. Immunol.* 13, 923031. PubMed PMID: 35924241; PubMed Central PMCID: PMCPMC9341429. doi:10.3389/fimmu.2022.923031

Kitao, A., Matsui, O., Yoneda, N., Kozaka, K., Kobayashi, S., Koda, W., et al. (2020). Gadoxetic acid-enhanced MR imaging for hepatocellular carcinoma: Molecular and genetic background. *Eur. Radiol.* 30 (6), 3438–3447. PubMed PMID: 32064560. doi:10.1007/s00330-020-06687-y

Kourou, K., Exarchos, T. P., Exarchos, K. P., Karamouzis, M. V., and Fotiadis, D. I. (2015). Machine learning applications in cancer prognosis and prediction. *Comput. Struct. Biotechnol. J.* 13, 8–17. PubMed PMID: 25750696. doi:10.1016/j.csbj.2014.11.005

Leek, J. T., Johnson, W. E., Parker, H. S., Jaffe, A. E., and Storey, J. D. (2012). The sva package for removing batch effects and other unwanted variation in high-throughput experiments. *Bioinformatics* 28 (6), 882–883. PubMed PMID: 22257669; PubMed Central PMCID: PMCPMC3307112. doi:10.1093/bioinformatics/bts034

Li, F., Liu, T., Xiao, C. Y., Yu, J. X., Lu, L. G., and Xu, M. Y. (2015). FOXP1 and SPINK1 reflect the risk of cirrhosis progression to HCC with HBV infection. *Biomed. Pharmacother.* 72, 103–108. PubMed PMID: 26054682. doi:10.1016/j.biopha.2015.04.006

Li, Z., Lin, Y., Cheng, B., Zhang, Q., and Cai, Y. (2021). Identification and analysis of potential key genes associated with hepatocellular carcinoma based on integrated bioinformatics methods. *Front. Genet.* 12, 571231. PubMed PMID: 33767726. doi:10.3389/fgene.2021.571231

Li, Z., Wu, X., Gao, X., Shan, F., Ying, X., Zhang, Y., et al. (2020). Development and validation of an artificial neural network prognostic model after gastrectomy for gastric carcinoma: An international multicenter cohort study. *Cancer Med.* 9 (17), 6205–6215. PubMed PMID: 32666682. doi:10.1002/cam4.3245

Lin, S., Lin, Y., Wu, Z., Xia, W., Miao, C., Peng, T., et al. (2021). circRPS16 promotes proliferation and invasion of hepatocellular carcinoma by sponging miR-876-5p to upregulate SPINK1. *Front. Oncol.* 11, 724415. PubMed PMID: 34595116; PubMed Central PMCID: PMCPMC8476860. doi:10.3389/fonc.2021.724415

Liu, Y., Zhang, J., Liu, H., Guan, G., Zhang, T., Wang, L., et al. (2019). Compensatory upregulation of aldo-keto reductase 1B10 to protect hepatocytes against oxidative stress during hepatocarcinogenesis. *Am. J. Cancer Res.* 9 (12), 2730–2748. Epub 20191201. PubMed PMID: 31911858; PubMed Central PMCID: PMCPMC6943354.

Liu, Y-C., Yeh, C-T., and Lin, K-H. (2020). Cancer stem cell functions in hepatocellular carcinoma and comprehensive therapeutic strategies. *Cells* 9 (6), E1331. PubMed PMID: 32466488. doi:10.3390/cells9061331

Mai, R-Y., Zeng, J., Mo, Y-S., Liang, R., Lin, Y., Wu, S-S., et al. (2020). Artificial neural network model for liver cirrhosis diagnosis in patients with hepatitis B virus-related hepatocellular carcinoma. *Ther. Clin. Risk Manag.* 16, 639–649. PubMed PMID: 32764948. doi:10.2147/TCRM.S257218

Marshall, A., Lukk, M., Kutter, C., Davies, S., Alexander, G., and Odom, D. T. (2013). Global gene expression profiling reveals SPINK1 as a potential hepatocellular carcinoma marker. *PLoS One* 8 (3), e59459. PubMed PMID: 23527199; PubMed Central PMCID: PMCPMC3601070. doi:10.1371/journal.pone.0059459

Mok, S., Tsoi, J., Koya, R. C., Hu-Lieskovan, S., West, B. L., Bollag, G., et al. (2015). Inhibition of colony stimulating factor-1 receptor improves antitumor efficacy of BRAF inhibition. *BMC Cancer* 15, 356. PubMed PMID: 25939769. doi:10.1186/s12885-015-1377-8

Nebot, N., Won, C. S., Moreno, V., Munoz-Couselo, E., Lee, D. Y., Gasal, E., et al. (2021). Evaluation of the effects of repeat-dose Dabrafenib on the single-dose pharmacokinetics of rosuvastatin (OATP1B1/1B3 substrate) and midazolam (CYP3A4 substrate). *Clin. Pharmacol. Drug Dev.* 10 (9), 1054–1063. PubMed PMID: 33932130; PubMed Central PMCID: PMCPMC8453865. doi:10.1002/cpdd.937

Puszkiel, A., Noé, G., Bellesoeur, A., Kramkimel, N., Paludetto, M-N., Thomas-Schoemann, A., et al. (2019). Clinical pharmacokinetics and pharmacodynamics of Dabrafenib. *Clin. Pharmacokinet.* 58 (4), 451–467. PubMed PMID: 30094711. doi:10.1007/s40262-018-0703-0

Rastogi, A. (2018). Changing role of histopathology in the diagnosis and management of hepatocellular carcinoma. *World J. Gastroenterol.* 24 (35), 4000–4013. PubMed PMID: 30254404. doi:10.3748/wjg.v24.i35.4000

Shek, F. H., Luo, R., Lam, B. Y. H., Sung, W. K., Lam, T. W., Luk, J. M., et al. (2017). Serine peptidase inhibitor Kazal type 1 (SPINK1) as novel downstream effector of the cadherin-17/β-catenin axis in hepatocellular carcinoma. *Cell. Oncol.* 40 (5), 443–456. PubMed PMID: 28631187. doi:10.1007/s13402-017-0332-x

Shibasaki, Y., Sakaguchi, T., Hiraide, T., Morita, Y., Suzuki, A., Baba, S., et al. (2015). Expression of indocyanine green-related transporters in hepatocellular carcinoma. *J. Surg. Res.* 193 (2), 567–576. PubMed PMID: 25173835. doi:10.1016/j.jss.2014.07.055

Sun, W., Zhang, Y., Liu, B., Duan, Y., Li, W., and Chen, J. (2021). Gene polymorphism of MUC15, MMP14, BRAF, and COL1A1 is associated with capsule formation in hepatocellular carcinoma. *Can. J. Gastroenterol. Hepatol.* 2021, 9990305. PubMed PMID: 34007838; PubMed Central PMCID: PMCPMC8100414. doi:10.1155/2021/9990305

Tian, Z., Hou, X., Liu, W., Han, Z., and Wei, L. (2019). Macrophages and hepatocellular carcinoma. *Cell. Biosci.* 9, 79. PubMed PMID: 31572568. doi:10.1186/s13578-019-0342-7

Ueno, A., Masugi, Y., Yamazaki, K., Komuta, M., Effendi, K., Tanami, Y., et al. (2014). OATP1B3 expression is strongly associated with Wnt/β-catenin signalling and represents the transporter of gadoxetic acid in hepatocellular carcinoma. *J. Hepatol.* 61 (5), 1080–1087. PubMed PMID: 24946283. doi:10.1016/j.jhep.2014.06.008

Villanueva, A. (2019). Hepatocellular carcinoma. *N. Engl. J. Med.* 380 (15), 1450–1462. doi:10.1056/NEJMra1713263

Vogel, A., and Saborowski, A. (2020). Current strategies for the treatment of intermediate and advanced hepatocellular carcinoma. *Cancer Treat. Rev.* 82, 101946. PubMed PMID: 31830641. doi:10.1016/j.ctrv.2019.101946

Wang, A., Wu, L., Lin, J., Han, L., Bian, J., Wu, Y., et al. (2018). Whole-exome sequencing reveals the origin and evolution of hepato-cholangiocarcinoma. *Nat. Commun.* 9 (1), 894. PubMed PMID: 29497050. doi:10.1038/s41467-018-03276-y

Wu, T., Ke, Y., Tang, H., Liao, C., Li, J., and Wang, L. (2021). Fidarestat induces glycolysis of NK cells through decreasing AKR1B10 expression to inhibit hepatocellular carcinoma. *Mol. Ther. Oncolytics* 23, 420–431. PubMed PMID: 34853813; PubMed Central PMCID: PMCPMC8605295. doi:10.1016/j.omto.2021.06.005

Xie, D-Y., Ren, Z-G., Zhou, J., Fan, J., and Gao, Q. (20192020). 2019 Chinese clinical guidelines for the management of hepatocellular carcinoma: Updates and insights. *Hepatobiliary Surg. Nutr.* 9 (4), 452–463. PubMed PMID: 32832496. doi:10.21037/hbsn-20-480

Yamashita, T., Kitao, A., Matsui, O., Hayashi, T., Nio, K., Kondo, M., et al. (2014). Gd-EOB-DTPA-enhanced magnetic resonance imaging and alpha-fetoprotein predict prognosis of early-stage hepatocellular carcinoma. *Hepatology* 60 (5), 1674–1685. PubMed PMID: 24700365; PubMed Central PMCID: PMCPMC4142120. doi:10.1002/hep.27093

Yan, P., Pang, P., Hu, X., Wang, A., Zhang, H., Ma, Y., et al. (2021). Specific MiRNAs in naïve T cells associated with hepatitis C virus-induced hepatocellular carcinoma. *J. Cancer* 12 (1), 1–9. PubMed PMID: 33391397. doi:10.7150/jca.49594

Yang, J. D., and Heimbach, J. K. (2020). New advances in the diagnosis and management of hepatocellular carcinoma. *BMJ* 371, m3544. PubMed PMID: 33106289. doi:10.1136/bmj.m3544

Ye, X., Li, C., Zu, X., Lin, M., Liu, Q., Liu, J., et al. (2019). A large-scale multicenter study validates aldo-keto reductase family 1 member B10 as a prevalent serum marker for detection of hepatocellular carcinoma. *Hepatology* 69 (6), 2489–2501. PubMed PMID: 30672601; PubMed Central PMCID: PMCPMC6593451. doi:10.1002/hep.30519

Ying, H. Y., Gong, C. J., Feng, Y., Jing, D. D., and Lu, L. G. (2017). Serine protease inhibitor Kazal type 1 (SPINK1) downregulates E-cadherin and induces EMT of hepatoma cells to promote hepatocellular carcinoma metastasis via the MEK/ERK signaling pathway. *J. Dig. Dis.* 18 (6), 349–358. PubMed PMID: 28544403. doi:10.1111/1751-2980.12486

Yuan, J., Dong, X., Yap, J., and Hu, J. (2020). The MAPK and AMPK signalings: Interplay and implication in targeted cancer therapy. *J. Hematol. Oncol.* 13 (1), 113. PubMed PMID: 32807225; PubMed Central PMCID: PMCPMC7433213. doi:10.1186/s13045-020-00949-4

Zhang, Q., Rong, Y., Yi, K., Huang, L., Chen, M., and Wang, F. (2020). Circulating tumor cells in hepatocellular carcinoma: Single-cell based analysis, preclinical models, and clinical applications. *Theranostics* 10 (26), 12060–12071. PubMed PMID: 33204329. doi:10.7150/thno.48918

Zhang, S., Huang, Z., Zhou, S., Wang, B., Ding, Y., Chu, J. Z., et al. (2018). The effect and mechanism of metallothionein MT1M on hepatocellular carcinoma cell. *Eur. Rev. Med. Pharmacol. Sci.* 22 (3), 695–701. PubMed PMID: 29461597. doi:10.26355/eurrev_201802_14295

Zhang, T., Guan, G., Zhang, J., Zheng, H., Li, D., Wang, W., et al. (2022). E2F1-mediated AUF1 upregulation promotes HCC development and enhances drug resistance via stabilization of AKR1B10. *Cancer Sci.* 113 (4), 1154–1167. PubMed PMID: 35178834; PubMed Central PMCID: PMCPMC8990806. doi:10.1111/cas.15272

Zhang, X., Ng, H. L. H., Lu, A., Lin, C., Zhou, L., Lin, G., et al. (2016). Drug delivery system targeting advanced hepatocellular carcinoma: Current and future. *Nanomedicine* 12 (4), 853–869. PubMed PMID: 26772424. doi:10.1016/j.nano.2015.12.381

Zhong, B-Y., Ni, C-F., Ji, J-S., Yin, G-W., Chen, L., Zhu, H-D., et al. (2019). Nomogram and artificial neural network for prognostic performance on the albumin-bilirubin grade for hepatocellular carcinoma undergoing transarterial chemoembolization. *J. Vasc. Interv. Radiol.* 30 (3), 330–338. PubMed PMID: 30819473. doi:10.1016/j.jvir.2018.08.026

Zhu, R., Xiao, J., Luo, D., Dong, M., Sun, T., and Jin, J. (2019). Serum AKR1B10 predicts the risk of hepatocellular carcinoma - a retrospective single-center study. *Gastroenterol. Hepatol.* 42 (10), 614–621. PubMed PMID: 31495535. doi:10.1016/j.gastrohep.2019.06.007

frontiers | Frontiers in Genetics

TYPE Original Research
PUBLISHED 07 December 2022
DOI 10.3389/fgene.2022.1004467

Check for updates

OPEN ACCESS

EDITED BY
Hua Tan,
National Human Genome Research Institute (NIH), United States

REVIEWED BY
Avantika Lal,
National Centre for Biological Sciences, India
Zeguo Sun,
Icahn School of Medicine at Mount Sinai, United States

*CORRESPONDENCE
Roujun Peng,
pengrj@sysucc.org.cn
Yujing Zhang,
zhangyj@sysucc.org.cn

†These authors contributed equally to this work and share first authorship

SPECIALTY SECTION
This article was submitted to *Cancer* Genetics and Oncogenomics, a section of the journal Frontiers in Genetics

RECEIVED 27 July 2022
ACCEPTED 24 November 2022
PUBLISHED 07 December 2022

CITATION
Ruan Z, Zhang Y, Quan Q, Jiang J, Wang Q, Zhang Y and Peng R (2022), Pan-cancer analysis identifies DDX56 as a prognostic biomarker associated with immune infiltration and drug sensitivity. *Front. Genet.* 13:1004467. doi: 10.3389/fgene.2022.1004467

COPYRIGHT
© 2022 Ruan, Zhang, Quan, Jiang, Wang, Zhang and Peng. This is an open-access article distributed under the terms of the Creative Commons Attribution License (CC BY). The use, distribution or reproduction in other forums is permitted, provided the original author(s) and the copyright owner(s) are credited and that the original publication in this journal is cited, in accordance with accepted academic practice. No use, distribution or reproduction is permitted which does not comply with these terms.

Pan-cancer analysis identifies DDX56 as a prognostic biomarker associated with immune infiltration and drug sensitivity

Zhaohui Ruan[1†], Yuetong Zhang[2†], Qi Quan[1], Jiaxin Jiang[1], Qianyu Wang[1], Yujing Zhang[2*] and Roujun Peng[1*]

[1]VIP Department, State Key Laboratory of Oncology in South China, Guangdong Key Laboratory of Nasopharyngeal Carcinoma Diagnosis and Therapy, Sun Yat-sen University Cancer Center, Guangzhou, China, [2]Radiation Oncology, State Key Laboratory of Oncology in South China, Guangdong Key Laboratory of Nasopharyngeal Carcinoma Diagnosis and Therapy, Sun Yat-sen University Cancer Center, Guangzhou, China

DDX56, a member of the RNA helicase family, is upregulated in colon adenocarcinoma, lung squamous cell carcinoma, and osteosarcoma. However, the relationships between DDX56 and other tumors are not clear, and the molecular mechanism of its action is not fully understood. Here, we explore the biological functions of DDX56 in 31 solid tumors and clarify that DDX56 can promote oncogenesis and progression in multiple tumor types based on multi-omics data. Bioinformatics analysis revealed that the cancer-promoting effects of DDX56 were achieved by facilitating tumor cell proliferation, inhibiting apoptosis, inducing drug resistance, and influencing immune cell infiltration. Furthermore, we found that copy number alterations and low DNA methylation of *DDX56* were likely to be related to aberrantly high *DDX56* expression. Our results suggest that DDX56 is a potential pan-cancer biomarker that could be used to predict survival and response to therapy, as well as a potential novel therapeutic target. We validated some of our results and illustrated their reliability using CRISPR Screens data. In conclusion, our results clarify the role of DDX56 in the occurrence and development of multiple cancers and provide insight into the molecular mechanisms involved in the process of pathogenesis, indicating a direction for future research on DDX56 in cancers.

KEYWORDS

DDX56, pan-cancer, multi-omics data, bio-marker, survival

Introduction

Cancer poses a great threat to human health and is a leading cause of death, with more than 19.3 million people diagnosed with cancer and more than 10.0 million deaths each year (Sung et al., 2021). The identification of key molecular targets in various cancers has helped to enhance treatment effects and improve the prognosis of cancer patients. For instance, sorafenib, which can inhibit multiple tyrosine kinases including VEGFR1,

VEGFR2, KIT, and PDGFR-α, is widely used in hepatocellular carcinoma (HCC) and renal cell cancer (Bedard et al., 2020). In breast cancer, individual treatment strategies targeting molecular subtypes have dramatically improved survival outcomes in 70–80% of patients (Loibl et al., 2021). These reports show that identification of critical molecules can lead to innovation in cancer therapeutic strategies, with massive application potential. Therefore, the exploration of new key molecules and underlying mechanisms is of great significance.

In addition to molecular targeted therapies, immunotherapy is a prospective treatment for multiple cancer types. The focus of immunotherapy has shifted from the tumor itself to the host's immune system and tumor microenvironment, with the aim of mobilizing immune cells to discern and eventually eliminate cancer cells (Sharma et al., 2017). Immunotherapy based on immune checkpoint inhibitors has dramatically changed management strategies for various advanced cancers, including non-small-cell lung cancer, extensive small-cell lung cancer, HCC, and classical Hodgkin lymphoma) (Lee et al., 2022). Combination therapy with anti-CTLA4 and anti-PD-1 checkpoint inhibition is an effective option for advanced melanoma and unresectable malignant pleural mesothelioma (Baas et al., 2021; Carlino et al., 2021). Treatment targeting LAG3 has also shown good response (Andrews et al., 2017). However, not all patients can benefit from immunotherapy, and there is a lack of effective markers to predict response to immunotherapy. Therefore, it is urgent to screen more therapeutic targets and identify predictive biomarkers of immunotherapy.

DDX56 is a member of the DEAD box RNA helicase family that plays a key part in various RNA-related biological processes (Cordin et al., 2006; Linder and Jankowsky, 2011). Previous studies have shown that DDX56 can promote the occurrence and development of colon cancer, osteosarcoma, glioblastoma, and lung squamous cell carcinoma (Kouyama et al., 2019; Zhu et al., 2020; Pryszlak et al., 2021; Wu et al., 2021). However, the role of DDX56 in other tumors has not been reported. In addition, it has been reported that other members of DEAD box RNA helicase family can induce resistance of tumor cells to chemotherapeutic agents (Park et al., 2018; Mani et al., 2020). Whether DDX56 contributes to tumor progression or could be used as a biomarker remains to be determined. Here, based on bioinformatics analysis of multi-omics data, we illustrate that DDX56 is involved in the occurrence and development of multiple tumors. Further, we conduct co-expression and enrichment analyses of the biological functions of DDX56 in various solid cancers. We also investigate the potential associations between *DDX56* expression and immune infiltration levels and immune-related markers. Finally, we explore the possible mechanisms of high DDX56 expression in tumor tissues. Our results demonstrate the role of DDX56 in oncogenesis in multiple tumors and its potential to serve as a therapeutic target and prognostic indicator.

Materials and methods

Data collection and expression analysis

We compared *DDX56* RNA expression among different tissues using RNA sequencing (RNA-seq) datasets from The Cancer Genome Atlas (TCGA). RNA-seq data (TPM) and related clinical data were downloaded from UCSC Xena (http://xena.ucsc.edu/) (Goldman et al., 2020). The data corresponded to 31 solid tumor types: adrenocortical carcinoma (ACC), bladder urothelial carcinoma (BLCA), breast invasive carcinoma (BRCA), cervical squamous cell carcinoma and endocervical adenocarcinoma (CESC), cholangiocarcinoma (CHOL), colon adenocarcinoma (COAD), esophageal carcinoma (ESCA), glioblastoma multiforme (GBM), head and neck squamous cell carcinoma (HNSC), kidney chromophobe (KICH), kidney renal clear cell carcinoma (KIRC), kidney renal papillary cell carcinoma (KIRP), brain lower grade glioma (LGG), liver hepatocellular carcinoma (LIHC), lung adenocarcinoma (LUAD), lung squamous cell carcinoma (LUSC), mesothelioma (MESO), ovarian serous cystadenocarcinoma (OV), pancreatic adenocarcinoma (PAAD), pheochromocytoma and paraganglioma (PCPG), prostate adenocarcinoma (PRAD), rectum adenocarcinoma (READ), sarcoma (SARC), skin cutaneous melanoma (SKCM), stomach adenocarcinoma (STAD), testicular germ cell tumors (TGCT), thyroid carcinoma (THCA), thymoma (THYM), uterine corpus endometrial carcinoma (UCEC), uterine carcinosarcoma (UCS), uveal melanoma (UVM). Using the "Gene" module of TISCH (http://tisch.comp-genomics.org/search-gene/), we determined the RNA expression of *DDX56* in multiple cell types based on single-cell RNA-seq data (Sun et al., 2021). UALCAN carried out a comparative analysis of protein expression (http://ualcan.path.uab.edu/index.html) (Chandrashekar et al., 2017). Only tumors with matched normal tissue data were used for differential analysis. We defined clinical stages as follows: early stages, TNM stages I/II; advanced stages, TNM stages III/IV.

Survival analysis

Univariate Cox regression was used to assess the prognostic significance of DDX56 across cancer types. Multivariate Cox regression was used to identify independent prognostic factors. The surv_cutpoint function (from R package "survminer", https://github.com/kassambara/survminer) was used to determine the optimal cutoff values of *DDX56* expression level. Only solid tumor data with complete clinical information were included in the survival analysis.

Co-expression and functional enrichment

Genes co-expressed with DDX56 were screened by calculating the Spearman correlation coefficient between DDX56 and all other genes in each cancer. The Benjamini–Hochberg method was used to decrease the false discovery rate (adjusted *p*-value). To gain functional and mechanistic insights regarding DDX56, we performed a pre-ranked gene set enrichment analysis (GSEA) (Subramanian et al., 2005) based on Hallmarker's gene sets, which were downloaded from the MSigDB database (https://www.gsea-msigdb.org/gsea/msigdb/) (Liberzon et al., 2015). The genes with significant correlation coefficients (adjusted $p < 0.05$) were sorted according to Spearman correlation coefficient and then used in GSEA.

Validation of functional enrichment results of DDX56 based on CRISPR screens

The CRISPR pooled libraries consist of thousands of plasmids, each containing multiple gRNAs for each target gene (Shalem et al., 2014). In a CRISPR screening experiment, target cells are treated with the pooled library to create a population of mutant cells that are then screened for a phenotype of interest. Essential genes for specific phenotypic screens can be curated by comparing sgRNA abundance. Therefore, the database includes research information on whether a particular gene is essential for a certain phenotype in a particular tumor cell line (Joung et al., 2017). Compiled CRISPR screen data were obtained from the Biological General Repository for Interaction Datasets (BioGRID) (https://orcs.thebiogrid.org/) (Oughtred et al., 2019). Data from proliferation-based CRISPR screens in solid tumor cancer cell lines were selected. These datasets were used to verify the mitogenic activity of DDX56. Resistance-related CRISPR screening evidence was also retrieved from the BioGRID database. The methods were as previously described except that the studies chosen focused on the "response to chemicals" phenotype.

Drug sensitivity analysis

Half-maximal inhibitory concentration (IC50) data and associated RNA-seq data from multiple cancer cell lines were obtained from the CellMiner database (https://discover.nci.nih.gov/cellminer/) (Reinhold et al., 2012). We conducted Spearman correlation analysis between *DDX56* expression and drug IC50 in order to investigate the relationship between *DDX56* expression and drug sensitivity.

Profiling tumor-infiltrating immune cells (TILs)

Proportions of TILs were estimated using the CIBERSORT function (https://cibersort.stanford.edu/). (Newman et al., 2015; Chen et al., 2018). Based on the Spearman correlation coefficient, we assessed the statistical correlation between *DDX56* expression level and the proportion of TILs.

Prediction analysis for immunotherapy

We evaluated the value of DDX56 in predicting immunotherapy response in an immune checkpoint blockade therapy cohort. The transcriptomic data and relevant clinical data from this cohort were obtained from dbGaP (phs000452) (Liu et al., 2019a). Univariate Cox regression was used to assess the prognostic significance of DDX56.

Gene mutation and methylation analysis of DDX56 and identification of related transcription factors

We conducted gene mutation analysis on cBioportal (https://www.cbioportal.org/) based on TCGA Pan-Cancer Atlas data (Cerami et al., 2012). The correlation of *DDX56* RNA expression level with copy number variation (CNV) was evaluated by MEXPRESS (https://mexpress.be/) (Koch et al., 2019). The correlation between the expression data and the DNA methylation data was estimated by using MEXPRESS (https://mexpress.be/). Oncodb (http://oncodb.org/) was used to compare methylation profiles between tumor tissues and normal tissues (Koch et al., 2019; Tang et al., 2022). We used the Toolkit for CistromeDB (http://dbtoolkit.cistrome.org/) to predict which transcription factors had the greatest potential to enhance expression of DDX56 (Zheng et al., 2019).

Statistical analysis

We compared non-normally distributed continuous variables using Wilcoxon rank-sum test and compared categorical variables using chi-square test between two groups. Kaplan–Meier and log-rank tests were conducted for survival analysis. Unless otherwise stated, all data analysis was performed in R (version 4.1.0). Unless otherwise specified, $p < 0.05$ was considered to indicate statistical significance in all analyses. The tumors involved in each analysis are recorded in Supplementary Table S1.

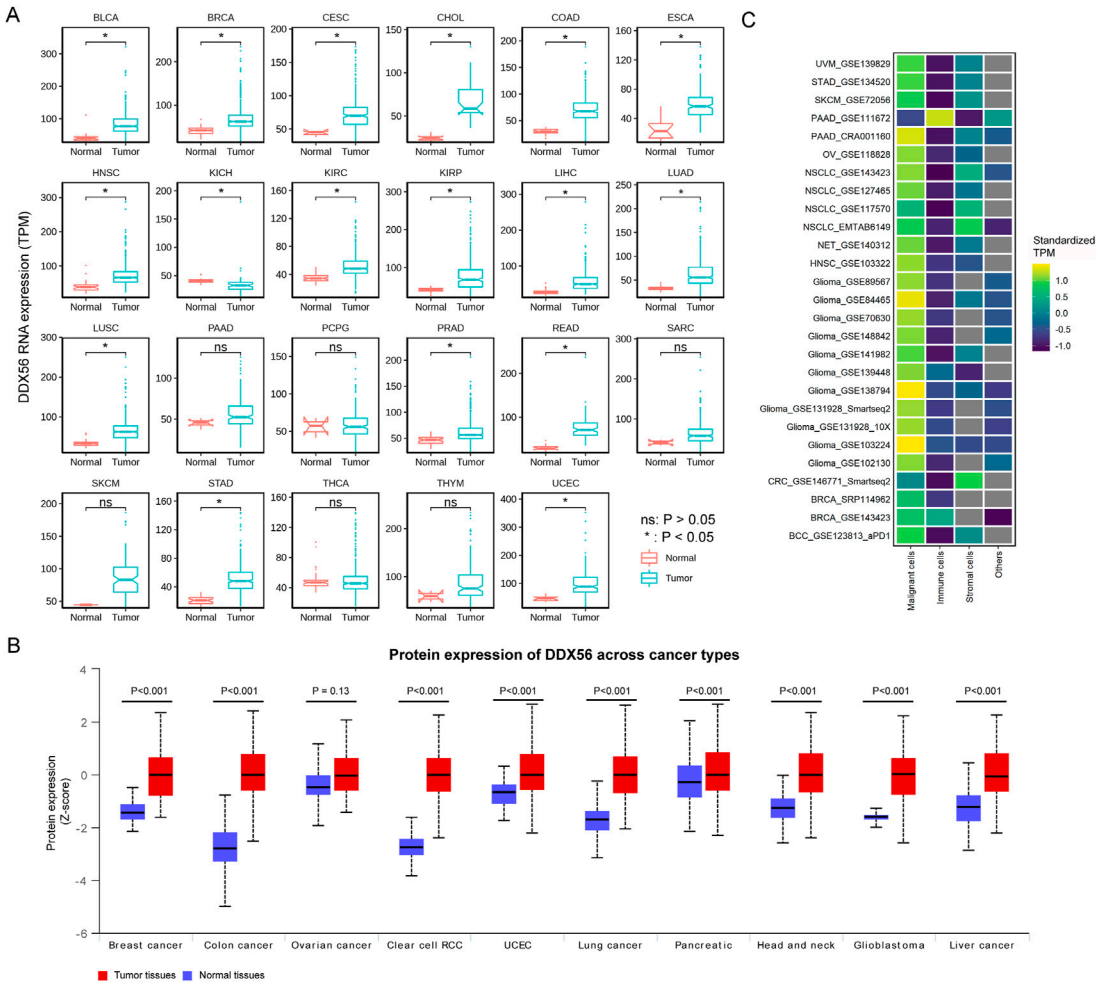

FIGURE 1
RNA and protein expression of DDX56 in various tumors. **(A)** Box plots showing RNA expression of *DDX56* in different tissues (Wilcoxon test). *P*-values are marked. **(B)** Box plots showing protein expression levels of DDX56 in different tissues (T test). *P*-values are marked. **(C)** Heat map showing RNA expression in different cell types of various tumors. TPM values were standardized for each tumor. The colors indicate the TPM value after standardization. The X-axis indicates single-cell RNA-seq datasets. The Y-axis indicates the cell type. Abbreviations: BLCA, bladder urothelial carcinoma; BRCA, breast invasive carcinoma; CESC, cervical squamous cell carcinoma and endocervical adenocarcinoma; CHOL, cholangiocarcinoma; COAD, colon adenocarcinoma; ESCA, esophageal carcinoma; GBM, glioblastoma multiforme; HNSC, head and neck squamous cell carcinoma; KICH, kidney chromophobe; KIRC, kidney renal clear cell carcinoma; KIRP, kidney renal papillary cell carcinoma; LIHC, liver hepatocellular carcinoma; LUAD, lung adenocarcinoma; LUSC, lung squamous cell carcinoma; PAAD, pancreatic adenocarcinoma; PCPG, pheochromocytoma and paraganglioma; PRAD, prostate adenocarcinoma; READ, rectum adenocarcinoma; SARC, sarcoma; SKCM, skin cutaneous melanoma; STAD, stomach adenocarcinoma; THCA, thyroid carcinoma; THYM, thymoma; UCEC, uterine corpus endometrial carcinoma; BCC, basal cell carcinoma; NET, Neuroendocrine tumor; CRC, colorectal cancer; RCC, renal cell carcinoma.

Results

Pan-cancer expression profiles of DDX56

We compared *DDX56* RNA expression between different cancer tissues and matched normal tissues based on TCGA data. The pan-cancer analysis showed that the *DDX56* RNA expression level was higher in 16 solid cancers than in their matched normal tissues (Wilcoxon test, $p < 0.05$) (Figure 1A), consistent with findings in lung squamous cell carcinoma (LUSC), osteosarcoma (OV), and colon cancer (COAD) (Zhu et al., 2020; Pryszlak et al., 2021; Wu et al., 2021). UALCAN was used to determine the protein expression of DDX56 in different types of cancer. According to significant unique analyses (provided by UALCAN, Student's t-test), DDX56 protein was significantly over-expressed in nine tumor types ($p < 0.05$, Figure 1B). An effective tumor biomarker and drug target requires specific and high expression in tumor cells compared with other components of the tumor microenvironment. Therefore, we analyzed pan-cancer single-cell RNA-seq data

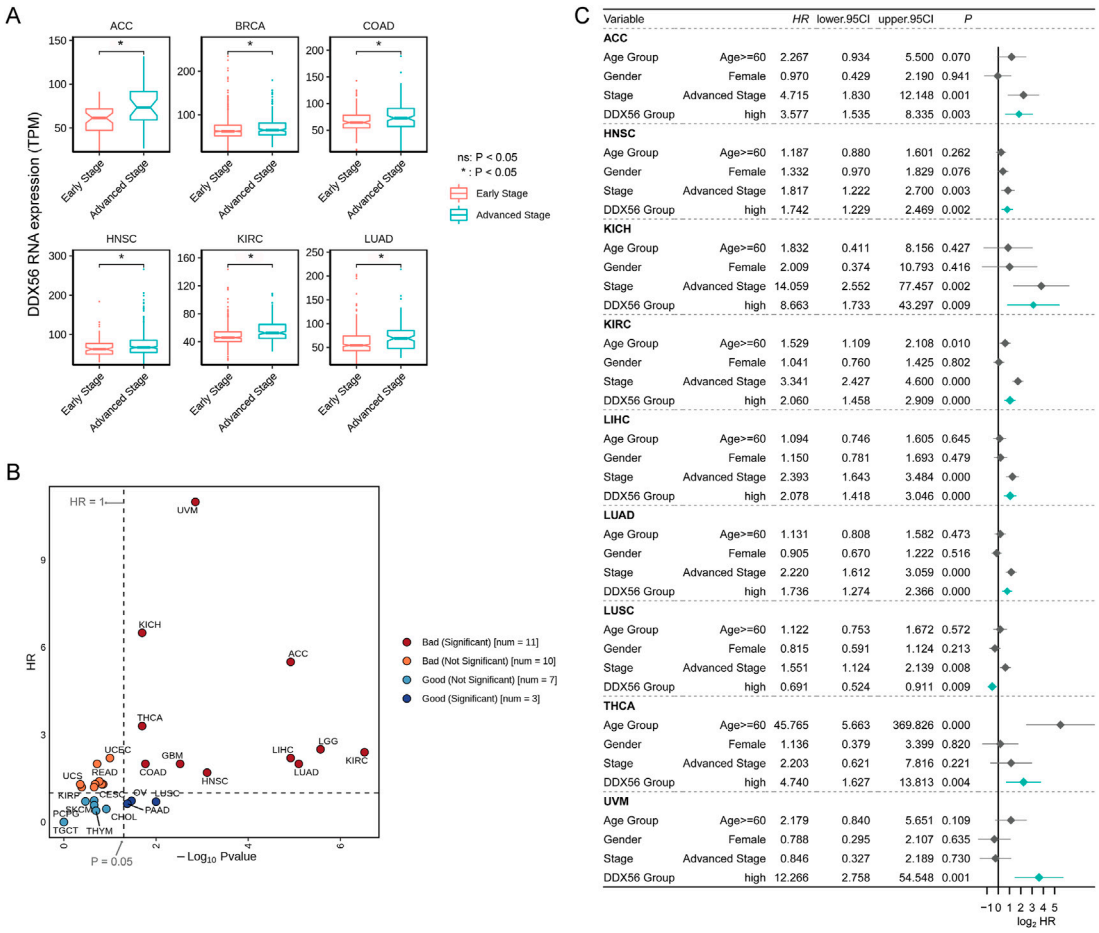

FIGURE 2
Prognostic value of DDX56 in various cancers. **(A)** Box plots showing RNA expression levels of *DDX56* at different clinical stages. For each tumor, stages I and II were classified as early stage; stages III and IV were classified as advanced stage. **(B)** Scatter plot showing outcomes in cancer patients with different *DDX56* expression levels. Statistics were obtained by univariate Cox regression analysis. **(C)** Forest plot showing the results of multivariate Cox regression for multiple tumor types. Abbreviations: ACC, adrenocortical carcinoma; BRCA, breast invasive carcinoma; COAD, colon adenocarcinoma; GBM, glioblastoma multiforme; HNSC, head and neck squamous cell carcinoma; KICH, kidney chromophobe; KIRC, kidney renal clear cell carcinoma; LIHC, liver hepatocellular carcinoma; LUAD lung adenocarcinoma; LUSC, lung squamous cell carcinoma; MESO, mesothelioma; OV, ovarian serous cystadenocarcinoma; PAAD, pancreatic adenocarcinoma; PCPG, pheochromocytoma and paraganglioma; PRAD, prostate adenocarcinoma; READ, rectum adenocarcinoma; SARC, sarcoma; SKCM, skin cutaneous melanoma; STAD, stomach adenocarcinoma; TGCT, testicular germ cell tumors; THCA, thyroid carcinoma; THYM, thymoma; UCEC, uterine corpus endometrial carcinoma; UCS, uterine carcinosarcoma; UVM, uveal melanoma.

using the TISCH database and observed that *DDX56* was mainly expressed in tumor cells rather than immune cells, stromal cells, and others (Figure 1C), indicating the potential of DDX56 as a tumor biomarker and drug target.

Prognostic value of DDX56 in multiple cancers

Next, we assessed the correlation between *DDX56* expression and the clinical features of patients. Although few significant differences were observed between groups in age or gender (Supplementary Figure S1), the expression level of *DDX56* was consistently higher in patients in the advanced stages than those in the early stages of diseases including ACC, BRCA, COAD, HNSC, KIRC, and LUAD (Wilcoxon test, $p < 0.05$, Figure 2A and Supplementary Figure S1). Further, we investigated the prognostic value of DDX56 at a pan-cancer level. The results showed that high *DDX56* expression was correlated with worse outcomes in 11 cancer types (univariate Cox regression, $p < 0.05$, hazard ratio >1) (Figure 2B and Supplementary Figure S2). Then, we implemented multivariate Cox regression analysis based on *DDX56* expression level and other clinical factors and found that DDX56 was an independent predictor for cancer prognosis in

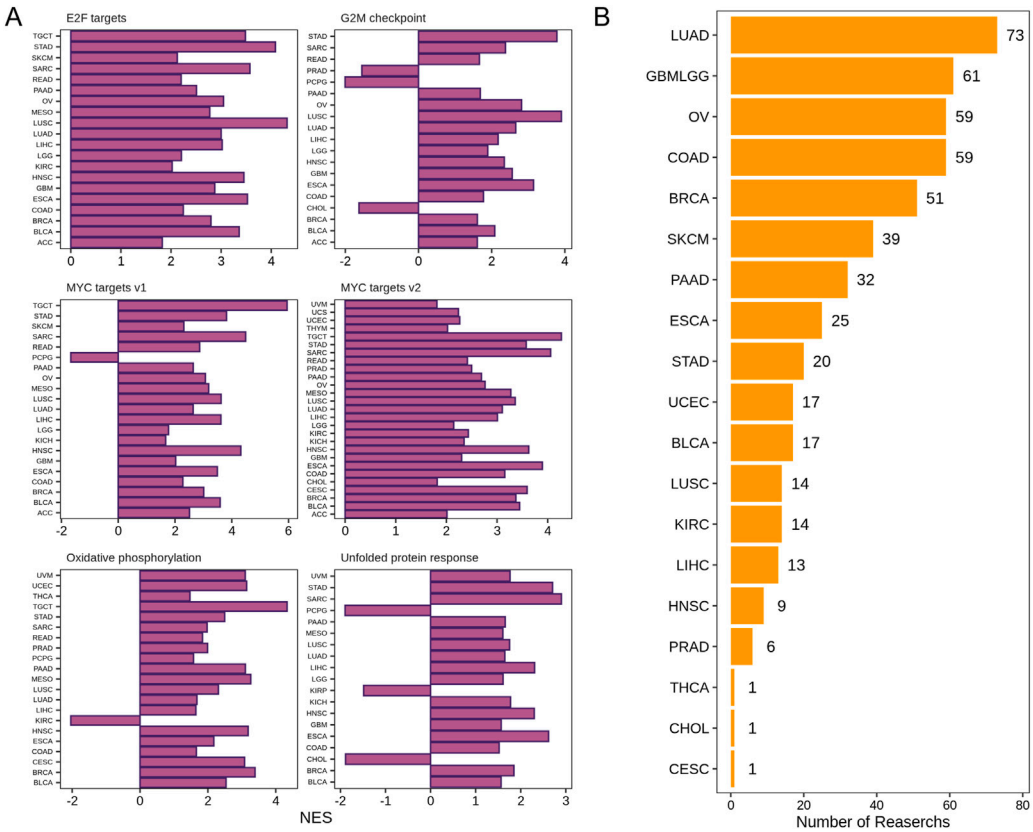

FIGURE 3
DDX56 positively modulates the proliferation of cancer cells. **(A)** GSEA enrichment results for DDX56 in multiple tumor types. Only pathways deemed to be significantly enriched based on GSEA ($p < 0.05$) are illustrated. **(B)** Multiple CRISPR screening studies verifying that DDX56 can positively regulate the proliferation of cancer cells. *X*-axis indicates the number of CRISPR screening studies supporting a pro-proliferative phenotypic role of this gene in tumor cell lines. *Y*-axis indicates the tumor type of the CRISPR screens studies. Abbreviations: ACC: adrenocortical carcinoma; BRCA: breast invasive carcinoma; COAD: colon adenocarcinoma; GBM: glioblastoma multiforme; HNSC: head and neck squamous cell carcinoma; KICH: kidney chromophobe; KIRC: kidney renal clear cell carcinoma; LIHC: liver hepatocellular carcinoma; LUAD: lung adenocarcinoma; LUSC: lung squamous cell carcinoma; MESO: mesothelioma; OV: ovarian serous cystadenocarcinoma; PAAD: pancreatic adenocarcinoma; PCPG: pheochromocytoma and paraganglioma; PRAD: prostate adenocarcinoma; READ: rectum adenocarcinoma; SARC: sarcoma; SKCM: skin cutaneous melanoma; STAD: stomach adenocarcinoma; TGCT: testicular germ cell tumors; THCA: thyroid carcinoma; THYM: thymoma; UCEC: uterine corpus endometrial carcinoma; UCS: uterine carcinosarcoma; UVM: uveal melanoma.

nine tumor types; moreover, worse clinical outcomes in patients with higher expression of *DDX56* were observed in eight tumor types, comprising ACC, HNSC, KICH, KIRC, LIHC, LUAD, THCA, and UVM (Figure 2C). These results suggest that *DDX56* high expression may be a significant predictor of prognosis and function as a promotor in multiple tumor types.

DDX56 has a pro-proliferative property at the pan-cancer level

To explore the molecular mechanism of DDX56 in carcinogenesis, a network of genes co-expressed with DDX56 was first conducted in each tumor dataset, and then pathway enrichment analysis was performed using GSEA. The results revealed that DDX56 mainly participated in cell-proliferation-related signaling pathways, including G2/M checkpoint, MYC targets v1, MYC targets v2, and E2F targets (Figure 3A) (Liberzon et al., 2015). Concomitantly, we observed enrichment of tumor metabolism-related pathways including oxidative phosphorylation and unfolded protein response. In order to validate the possible pro-proliferation function of DDX56, we collected and analyzed CRISPR screens data from the BioGRID Open Respository of CRISPR Screens. CRISPR-based genetic screening is a powerful tool to identify the genes required for specific functions such as cell viability and chemical resistance. We found 512 CRISPR screens studies in 19 tumor types, which confirmed the effects of DDX56 on the proliferation of tumor cells at the pan-cancer level (Figure 3B and Supplementary Table S2).

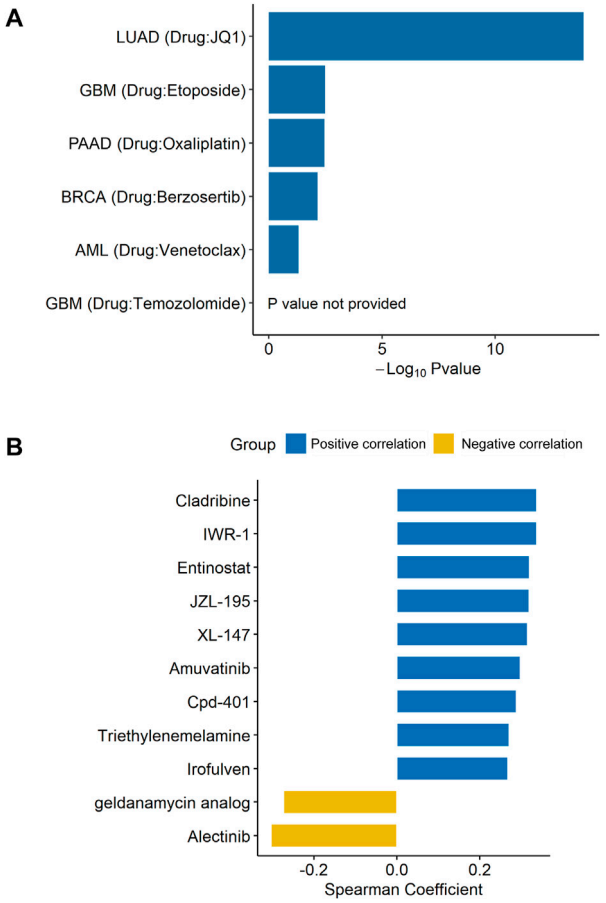

FIGURE 4
DDX56 promotes drug resistance in multiple tumor types. **(A)** Multiple CRISPR screening studies showing that DDX56 is associated with drug resistance. *Y*-axis indicates the tumor type and the associated drug. *X*-axis indicates the logarithm of the negative *p*-value of DDX56 in each CRISPR screening study. **(B)** Bar plot showing the Spearman coefficients for *DDX56* RNA expression and drug IC50. Eleven statistically significant results were obtained from 450 drugs in the screen. Abbreviations: LUAD: lung adenocarcinoma; GBM: glioblastoma multiforme; PAAD: pancreatic adenocarcinoma; BRCA: breast invasive carcinoma; AML: acute myeloid leukemia.

Correlations between DDX56 expression and multiple drug resistance

As the GSEA results had shown enrichment of unfolded protein response (Figure 3A), a chemoresistance-related pathway, (Bahar et al., 2019; Sisinni et al., 2019), we speculated that DDX56 was associated with chemotherapy resistance. To investigate whether DDX56 was relevant to drug resistance, we searched the CRISPR screens evidence in the BioGRID database. We found that DDX56 was an essential gene required for drug resistance in five different tumors (Figure 4A and Supplementary Table S3). Moreover, we obtained IC50 levels of all available drugs for tumor cell lines from the CellMiner database and calculated the Spearman correlation coefficient between the IC50 values and *DDX56* RNA expression in matched tumor cell lines. Our results revealed that high expression of DDX56 was correlated with increased resistance to cladribine, entinostat, amuvatinib, triethylenemelamine, irofulven, IWR-1, JZL-195, XL-147, and Cpd-401 ($p < 0.05$, Figure 4B). On the other hand, high expression of DDX56 could lead to enhanced sensitivity to a geldanamycin analog and alectinib ($p < 0.05$, Figure 4B).

Correlations between DDX56 expression and immune infiltration levels in cancers

The GSEA results suggested that DDX56 may have a critical role in inhibiting cell apoptosis and suppressing antitumor immunity (IL-2 STAT5 signaling, IL-6 JAK STAT3 signaling, and interferon gamma response, Figure 5A) (Liberzon et al., 2015). To further explore the potential relationships between DDX56 and immune cells, we examined the correlations between *DDX56* and several immune cell markers including immune cells (*PTPRC*), T cells (*CD3D*, *CD4*, *CD8A*), B cells (*CD19*), and MHC class II molecules (Supplementary Figure S3). The results suggested that the expression of DDX56 was associated with immune infiltration in the tumor microenvironment. Next, we estimated the proportions of immune cells in each TCGA tumor type by using CIBERSORT. We observed that *DDX56* expression was negatively correlated with immune infiltration levels of plasma cells, resting dendritic cells (DC), and $CD4^+$ memory T cells (Figure 5B). Given that DDX56 participates in the immune infiltration process, it may have crucial biological functions in immunotherapy. Using transcriptome and clinical data from a recently published immunotherapy study (Liu et al., 2019b), we found that anti-PD-1-treated patients with high *DDX56* expression had shorter progression-free survival than those with low *DDX56* expression (Figure 5C).

Pan-cancer analysis of genetic alteration, CNV, and methylation levels of DDX56

The occurrence and development of cancer is related to gene alterations. To determine the genomic characteristics of DDX56 in cancers, comparative analysis of DDX56 was performed using cBioPortal. We observed that the main alterations of *DDX56* were amplifications and mutations in multiple tumors (Figure 6A). The most common mutation type was missense mutation, which could lead to alteration of protein structure and functions (Figure 6B). As CNV can lead to higher gene mRNA levels (Haraksingh and Snyder, 2013), we analyzed the correlation between RNA expression and CNV at the pan-cancer levels. The results showed that the CNV and RNA expression of DDX56 DNA in tumor tissues were significantly associated (Pearson coefficient >0.2,

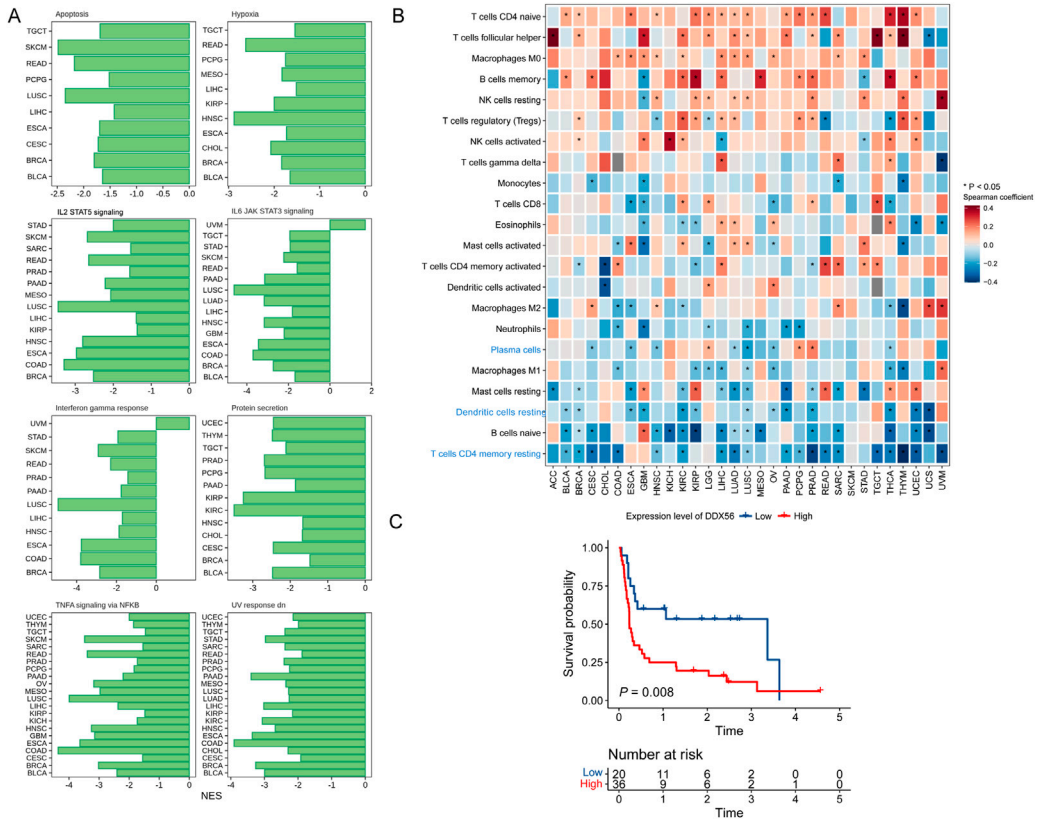

FIGURE 5
Relationships of DDX56 with tumor immune features. **(A)** GSEA enrichment results for DDX56 in multiple tumor types. Only pathways deemed significant enriched based on GSEA ($p < 0.05$) are illustrated. **(B)** Heat map showing Spearman coefficients for *DDX56* RNA expression and proportions of tumor-infiltrating immune cells. **(C)** Kaplan–Meier plots showing worse clinical outcome in immunotherapy cohort patients with higher expression of *DDX56*. Univariate Cox regression was used to assess the statistics.

$p < 0.05$, Figure 6C). In addition, increased RNA transcription may result from low levels of DNA methylation (Bradner et al., 2017). We compared *DDX56* methylation status between various tumors and normal tissues and observed that *DDX56* methylation in five tumor types was lower compared with that in paired normal tissues (Wilcoxon test, $p < 0.05$) (Figure 6D). Furthermore, we estimated the correlation between expression and DNA methylation data using MEXPRESS. We observed that methylation of some CpG dinucleotides and CpG islands, including cg25257687 and cg01998345, was significantly negatively correlated with the RNA expression of *DDX56* (Pearson correlation coefficient <0 and $p < 0.05$, Supplementary Figure S4). Our results suggested that lower methylation levels of *DDX56* DNA may result in high expression levels of *DDX56* RNA in some cancers.

Finally, screening was performed to search candidate transcription factors possibly regulating *DDX56* expression. According to our results, *LYL1*, *MECP2*, *PHF2*, *ETV7*, and *CDK9* were the top five transcription factors with the potential to alter the expression level of DDX56 (Figure 6E). Furthermore, we estimated the co-expression relation of these top five transcription factors and *DDX56* (Spearman correlation, Supplementary Figure S5). We compared the expression levels of the top five transcription factors in tumor tissues and normal tissues (Wilcoxon test, Supplementary Figure S6). For example, we observed that the expression of CDK9 was highly related to the expression of DDX56 in THCA (Spearman correlation coefficient 0.384, $p < 0.05$, Supplementary Figure S5 and Supplementary Table S4). Simultaneously, we observed that the expression levels of CDK9 and DDX56 were both high in THCA tumor tissue (Wilcoxon test, $p < 0.05$, Supplementary Figure S6 and Figure 1A). We thus consider that CDK9 might be responsible for the high expression of DDX56 in THCA.

Discussion

The role of DDX56 in tumorigenesis and development has attracted increasing attention in recent years (Zhu et al., 2020;

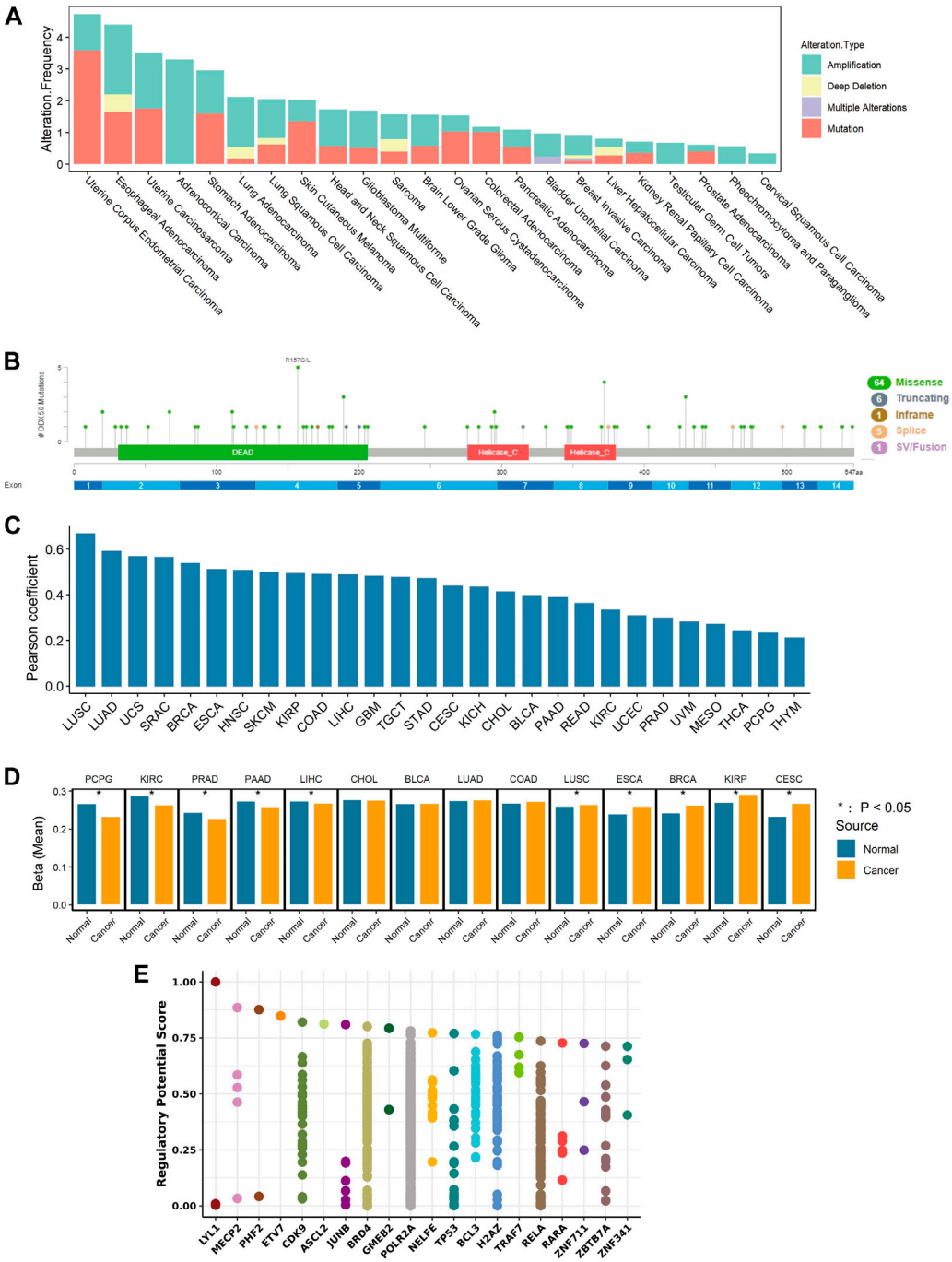

FIGURE 6
Mechanism of regulation of DDX56 expression. **(A)** Analysis of DDX56 alteration frequency in multiple cancer types, colored by mutation type. **(B)** Sites of different mutation types of *DDX56*. **(C)** Bar plot showing the Pearson correlation of CNV and *DDX56* RNA expression in different tumor types. **(D)** Bar plot showing the DNA methylation status of *DDX56* in tumors and normal tissues. *Y*-axis indicates the mean of the beta value. *$p < 0.05$. The statistics are from OncoDB. **(E)** Transcription factors potentially regulating *DDX56* (results obtained from Toolkit). The plot illustrates the top 20 factors. Dots on a single axis line indicate the same factor. Abbreviations: ACC: adrenocortical carcinoma; BRCA: breast invasive carcinoma; COAD: colon adenocarcinoma; GBM: glioblastoma multiforme; HNSC: head and neck squamous cell carcinoma; KICH: kidney chromophobe; KIRC: kidney renal clear cell carcinoma; LIHC: liver hepatocellular carcinoma; LUAD: lung adenocarcinoma; LUSC: lung squamous cell carcinoma; MESO: mesothelioma; OV: ovarian serous cystadenocarcinoma; PAAD: pancreatic adenocarcinoma; PCPG: pheochromocytoma and paraganglioma; PRAD: prostate adenocarcinoma; READ: rectum adenocarcinoma; SARC: sarcoma; SKCM: skin cutaneous melanoma; STAD: stomach adenocarcinoma; TGCT: testicular germ cell tumors; THCA: thyroid carcinoma; THYM: thymoma; UCEC: uterine corpus endometrial carcinoma; UCS: uterine carcinosarcoma; UVM: uveal melanoma.

Pryszlak et al., 2021; Sung et al., 2021; Wu et al., 2021). Although previous studies have reported upregulation of DDX56 in several tumor types, the underlying mechanisms of its pro-oncogenic function remain indistinct. Our results revealed that RNA expression of *DDX56* was indeed higher in 16 tumor types, which was confirmed at the protein level in nine tumor types. On this basis, we found that DDX56 may exert pro-oncogenic effects by enhancing proliferation and restraining apoptosis of tumor cells, affecting the infiltration of immune cells into the tumor microenvironment, and inducing tumor drug resistance. Our results suggest that DDX56 is involved in the occurrence and development of multiple cancers, as well as therapeutic response to chemotherapeutic agents. DDX56 could be an independent predictor of prognosis in a variety of tumor types and may also have value in prediction of immunotherapy efficacy.

Here, we report for the first time that the RNA and protein expression levels of DDX56 are significantly higher in tumor tissues than that in control normal tissues in various tumor types. Based on multi-omics data, we found that the high DDX56 expression in tumor tissues may be due to CNV and aberrant methylation. However, these changes were not present in all patients and may only partially explain the high DDX56 expression. Transcription factors are important components that regulate RNA transcription. We screened the potential transcription factors involved in regulating DDX56 using Toolkit. These transcription factors may be partially responsible for the abnormally high expression of DDX56, but more work needs to be done to reach such a conclusion.

We investigated the molecular mechanisms by which DDX56 promotes tumorigenesis and development through functional enrichment analysis. Our results suggested that DDX56 may promote the proliferation of tumor cells and inhibit tumor apoptosis. Zhu *et al.* showed that the knockdown of *DDX56* could reduce the proliferation and promoted the apoptosis of osteosarcoma cells (Zhu et al., 2020). Kouyama et al. (2019) showed that the overexpression of *DDX56* could enhance the proliferation of colon cancer cells. These results were consistent with our findings. Wu et al. (2021) further revealed that DDX56 could promote the proliferation of tumor cells through the WNT signaling pathway. Our results suggested that there may also be other molecular mechanisms involved, such as “E2F targets” and “MYC targets”, which have not previously been reported in DDX56-related studies. Therefore, we provide additional insights into the signaling pathways by which DDX56 promotes tumor proliferation.

Our functional enrichment results for DDX56 also suggested that DDX56 may be related to the infiltration of immune cells. We found that high *DDX56* expression was closely related to low infiltration levels of DC, plasma cells, and $CD4^+$ T cells. DC are the most powerful antigen-presenting cells and can initiate immune responses (Gardner and Ruffell, 2016; Wculek et al., 2020). As critical mediators in anti-tumor immunity, plasma cells are capable of producing antibodies and $CD4^+$ T cells secrete diverse cytokines that enhance humoral and cellular immunity (Borst et al., 2018; Sharonov et al., 2020). All of them are essential ancillary components in anti-tumor immunity, and their absence is detrimental to the immune reaction to cancer. This may also contribute to the poor prognosis and poor efficacy of immunotherapy in patients with high *DDX56* expression. Here, DDX56 was reported for the first time to be associated with infiltration of several immune cell types in the tumor microenvironment.

Combining all the data, we can conclude that DDX56 has a tumor-promoting function in most solid tumors. However, it may promote tumor progression in different ways in different cancer types. Therefore, we summarized the consistency of those aspects among different cancer types (Supplementary Table S3). For instance, there was no evidence that DDX56 could promote the proliferation of pheochromocytoma and paraganglioma (Figure 3A, $NSE<0$ or insignificant in all proliferation-related pathways). However, we observed that it was related to low level of apoptosis (Figure 5A, Supplementary Table S3) and could affect the infiltration of some immune cell types in pheochromocytoma and paraganglioma (Figure 5B, Supplementary Table S3).

Furthermore, we found that higher expression of DDX56 was associated with worse patient prognosis in multiple tumor types. High DDX56 expression was also found to related to lower efficacy of PD-1 antibody immunotherapy. All these results indicate that DDX56 could be used to predict not only prognosis but also the efficacy of immune checkpoint inhibitors. Our results also indicate that DDX56 may promote multiple anticancer drug resistance in tumor cells, which has not been previously reported.

We acknowledge several limitations of our study. Much more research needs to be done to determine whether DDX56 has the potential to predict prognosis and efficacy of chemotherapy drugs and immunotherapy. Although we has proposed potential pro-tumor molecular mechanisms involving DDX56 based on bioinformatics analysis, we did not perform biological experiments to validate these results. A large amount of CRISPR screens data verified our partial conjecture, giving some credibility to our results (Chow and Chen, 2018). However, the CRISPR screening evidence could not confirm the promoted proliferation ability of DDX56 and further functional experiments are needed to confirm the function of DDX56 and to explore the underlying mechanisms.

Conclusion

In summary, we have clarified the tumor-promoting role of DDX56 based on multi-omics data at a pan-cancer level and elucidated the possible molecular mechanisms involved. These results contribute to our understanding of the biological function of DDX56 in tumors and provide evidence and potential research directions for future studies on DDX56 as an oncogenic driver.

Data availability statement

The datasets presented in this study can be found in online repositories. The names of the repository/repositories and accession number(s) can be found in the article/ Supplementary Material.

Author contributions

ZR, YZ, and RP designed the study. ZR and YZ performed the data analyses. All authors contributed to the conception of the study and drafted the manuscript. All authors contributed significantly to writing the manuscript. ZR and YZ contributed equally to this work and share first authorship.

Funding

The project was supported by the Basic and Applied Basic Research Fund of Guangdong Province (2022A1515012387).

Acknowledgments

We are grateful to all the researchers who provided the data we used.

Conflict of interest

The authors declare that the research was conducted in the absence of any commercial or financial relationships that could be construed as a potential conflict of interest.

Publisher's note

All claims expressed in this article are solely those of the authors and do not necessarily represent those of their affiliated organizations, or those of the publisher, the editors and the reviewers. Any product that may be evaluated in this article, or claim that may be made by its manufacturer, is not guaranteed or endorsed by the publisher.

Supplementary material

The Supplementary Material for this article can be found online at: https://www.frontiersin.org/articles/10.3389/fgene.2022.1004467/full#supplementary-material

SUPPLEMENTARY FIGURE S1
Comparison of DDX56 expression in populations with different clinical characteristics.

SUPPLEMENTARY FIGURE S2
Pan-cancer overall survival analysis of DDX56.

SUPPLEMENTARY FIGURE S3
Pan-cancer correlation analysis of DDX56 RNA expression with several cellular marker genes and MHC class II molecules.

SUPPLEMENTARY FIGURE S4
Correlation analysis of methylation levels of DDX56 DNA and expression levels of DDX56 RNA.

SUPPLEMENTARY FIGURE S5
Pan-cancer correlation analysis of DDX56 RNA expression with top five transcription factors screened by Toolkit (http://dbtoolkit.cistrome.org/).

SUPPLEMENTARY FIGURE S6
Bar plots showing median RNA expression levels of top five DDX56-related transcription factors in different tissues (Wilcoxon test). Significant: P<0.05; Insignificant: P>0.05 or P = 0.05.

SUPPLEMENTARY TABLE S1
Tumors involved in each analysis.

SUPPLEMENTARY TABLE S2
List of CRISPR screening studies showing that DDX56 is associated with the proliferation of cancer cells.

SUPPLEMENTARY TABLE S3
List of CRISPR screening studies showing that DDX56 is associated with drug resistance.

SUPPLEMENTARY TABLE S4
Results of pan-cancer correlation analysis of DDX56 RNA expression with top five transcription factors screened by Toolkit.

SUPPLEMENTARY TABLE S5
Summary of the results.

References

Andrews, L. P., Marciscano, A. E., Drake, C. G., and Vignali, D. A. (2017). LAG3 (CD223) as a cancer immunotherapy target. *Immunol. Rev.* 276, 80–96. doi:10.1111/imr.12519

Baas, P., Scherpereel, A., Nowak, A. K., Fujimoto, N., Peters, S., Tsao, A. S., et al. (2021). First-line nivolumab plus ipilimumab in unresectable malignant pleural mesothelioma (CheckMate 743): A multicentre, randomised, open-label, phase 3 trial. *Lancet* 397, 375–386. doi:10.1016/S0140-6736(20)32714-8

Bahar, E., Kim, J. Y., and Yoon, H. (2019). Chemotherapy resistance explained through endoplasmic reticulum stress-dependent signaling. *Cancers (Basel)* 11 (3), 338. doi:10.3390/cancers11030338

Bedard, P. L., Hyman, D. M., Davids, M. S., and Siu, L. L. (2020). Small molecules, big impact: 20 years of targeted therapy in oncology. *Lancet* 395, 1078–1088.

Borst, J., Ahrends, T., Bąbała, N., Melief, C. J. M., and Kastenmüller, W. (2018). CD4(+) T cell help in cancer immunology and immunotherapy. *Nat. Rev. Immunol.* 18, 635–647. doi:10.1038/s41577-018-0044-0

Bradner, J. E., Hnisz, D., and Young, R. A. (2017). Transcriptional addiction in cancer. *Cell* 168, 629–643. doi:10.1016/j.cell.2016.12.013

Carlino, M. S., Larkin, J., and Long, G. V. (2021). Immune checkpoint inhibitors in melanoma. *Lancet* 398, 1002–1014. doi:10.1016/S0140-6736(21)01206-X

Cerami, E., Gao, J., Dogrusoz, U., Gross, B. E., Sumer, S. O., Aksoy, B. A., et al. (2012). The cBio cancer genomics portal: An open platform for exploring multidimensional cancer genomics data. *Cancer Discov.* 2, 401–404. doi:10.1158/2159-8290.CD-12-0095

Chandrashekar, D. S., Bashel, B., Balasubramanya, S. a. H., Creighton, C. J., Ponce-Rodriguez, I., Chakravarthi, B., et al. (2017). Ualcan: A portal for facilitating tumor subgroup gene expression and survival analyses. *Neoplasia* 19, 649–658. doi:10.1016/j.neo.2017.05.002

Chen, B., Khodadoust, M. S., Liu, C. L., Newman, A. M., and Alizadeh, A. A. (2018). Profiling tumor infiltrating immune cells with CIBERSORT. *Methods Mol. Biol.* 1711, 243–259. doi:10.1007/978-1-4939-7493-1_12

Chow, R. D., and Chen, S. (2018). Cancer CRISPR screens *in vivo*. *Trends Cancer* 4, 349–358. doi:10.1016/j.trecan.2018.03.002

Cordin, O., Banroques, J., Tanner, N. K., and Linder, P. (2006). The DEAD-box protein family of RNA helicases. *Gene* 367, 17–37. doi:10.1016/j.gene.2005.10.019

Gardner, A., and Ruffell, B. (2016). Dendritic cells and cancer immunity. *Trends Immunol.* 37, 855–865. doi:10.1016/j.it.2016.09.006

Goldman, M. J., Craft, B., Hastie, M., Repečka, K., Mcdade, F., Kamath, A., et al. (2020). Visualizing and interpreting cancer genomics data via the Xena platform. *Nat. Biotechnol.* 38, 675–678. doi:10.1038/s41587-020-0546-8

Haraksingh, R. R., and Snyder, M. P. (2013). Impacts of variation in the human genome on gene regulation. *J. Mol. Biol.* 425, 3970–3977. doi:10.1016/j.jmb.2013.07.015

Joung, J., Konermann, S., Gootenberg, J. S., Abudayyeh, O. O., Platt, R. J., Brigham, M. D., et al. (2017). Genome-scale CRISPR-Cas9 knockout and transcriptional activation screening. *Nat. Protoc.* 12, 828–863. doi:10.1038/nprot.2017.016

Koch, A., Jeschke, J., Van criekinge, W., Van engeland, M., and De meyer, T. (2019). MEXPRESS update 2019. *Nucleic Acids Res.* 47, W561–W565. doi:10.1093/nar/gkz445

Kouyama, Y., Masuda, T., Fujii, A., Ogawa, Y., Sato, K., Tobo, T., et al. (2019). Oncogenic splicing abnormalities induced by DEAD-Box Helicase 56 amplification in colorectal cancer. *Cancer Sci.* 110, 3132–3144. doi:10.1111/cas.14163

Lee, J. B., Kim, H. R., and Ha, S. J. (2022). Immune checkpoint inhibitors in 10 Years: Contribution of basic research and clinical application in cancer immunotherapy. *Immune Netw.* 22, e2. doi:10.4110/in.2022.22.e2

Liberzon, A., Birger, C., Thorvaldsdóttir, H., Ghandi, M., Mesirov, J. P., and Tamayo, P. (2015). The Molecular Signatures Database (MSigDB) hallmark gene set collection. *Cell Syst.* 1, 417–425. doi:10.1016/j.cels.2015.12.004

Linder, P., and Jankowsky, E. (2011). From unwinding to clamping - the DEAD box RNA helicase family. *Nat. Rev. Mol. Cell Biol.* 12, 505–516. doi:10.1038/nrm3154

Liu, D., Schilling, B., Liu, D., Sucker, A., Livingstone, E., Jerby-Arnon, L., et al. (2019a). Integrative molecular and clinical modeling of clinical outcomes to PD1 blockade in patients with metastatic melanoma. *Nat. Med.* 25, 1916–1927. doi:10.1038/s41591-019-0654-5

Liu, D., Schilling, B., Liu, D., Sucker, A., Livingstone, E., Jerby-Arnon, L., et al. (2019b). Integrative molecular and clinical modeling of clinical outcomes to PD1 blockade in patients with metastatic melanoma. *Nat. Med.* 25, 1916–1927. doi:10.1038/s41591-019-0654-5

Loibl, S., Poortmans, P., Morrow, M., Denkert, C., and Curigliano, G. (2021). Breast cancer. *Lancet* 397, 1750–1769. doi:10.1016/S0140-6736(20)32381-3

Mani, S. K. K., Yan, B., Cui, Z., Sun, J., Utturkar, S., Foca, A., et al. (2020). Restoration of RNA helicase DDX5 suppresses Hepatitis B virus (HBV) biosynthesis and Wnt signaling in HBV-related hepatocellular carcinoma. *Theranostics* 10, 10957–10972. doi:10.7150/thno.49629

Newman, A. M., Liu, C. L., Green, M. R., Gentles, A. J., Feng, W., Xu, Y., et al. (2015). Robust enumeration of cell subsets from tissue expression profiles. *Nat. Methods* 12, 453–457. doi:10.1038/nmeth.3337

Oughtred, R., Stark, C., Breitkreutz, B. J., Rust, J., Boucher, L., Chang, C., et al. (2019). The BioGRID interaction database: 2019 update. *Nucleic Acids Res.* 47, D529–d541. doi:10.1093/nar/gky1079

Park, S. Y., Kim, W. J., Byun, J. H., Lee, J. J., Jeoung, D., Park, S. T., et al. (2018). Role of DDX53 in taxol-resistance of cervix cancer cells *in vitro*. *Biochem. Biophys. Res. Commun.* 506, 641–647. doi:10.1016/j.bbrc.2018.10.145

Pryszlak, M., Wiggans, M., Chen, X., Jaramillo, J. E., Burns, S. E., Richards, L. M., et al. (2021). The DEAD-box helicase DDX56 is a conserved stemness regulator in normal and cancer stem cells. *Cell Rep.* 34, 108903. doi:10.1016/j.celrep.2021.108903

Reinhold, W. C., Sunshine, M., Liu, H., Varma, S., Kohn, K. W., Morris, J., et al. (2012). CellMiner: A web-based suite of genomic and pharmacologic tools to explore transcript and drug patterns in the NCI-60 cell line set. *Cancer Res.* 72, 3499–3511. doi:10.1158/0008-5472.CAN-12-1370

Shalem, O., Sanjana, N. E., Hartenian, E., Shi, X., Scott, D. A., Mikkelson, T., et al. (2014). Genome-scale CRISPR-Cas9 knockout screening in human cells. *Science* 343, 84–87. doi:10.1126/science.1247005

Sharma, P., Hu-Lieskovan, S., Wargo, J. A., and Ribas, A. (2017). Primary, adaptive, and acquired resistance to cancer immunotherapy. *Cell* 168, 707–723. doi:10.1016/j.cell.2017.01.017

Sharonov, G. V., Serebrovskaya, E. O., Yuzhakova, D. V., Britanova, O. V., and Chudakov, D. M. (2020). B cells, plasma cells and antibody repertoires in the tumour microenvironment. *Nat. Rev. Immunol.* 20, 294–307. doi:10.1038/s41577-019-0257-x

Sisinni, L., Pietrafesa, M., Lepore, S., Maddalena, F., Condelli, V., Esposito, F., et al. (2019). Endoplasmic reticulum stress and unfolded protein response in breast cancer: The balance between apoptosis and autophagy and its role in drug resistance. *Int. J. Mol. Sci.* 20, 857. doi:10.3390/ijms20040857

Subramanian, A., Tamayo, P., Mootha, V. K., Mukherjee, S., Ebert, B. L., Gillette, M. A., et al. (2005). Gene set enrichment analysis: A knowledge-based approach for interpreting genome-wide expression profiles. *Proc. Natl. Acad. Sci. U. S. A.* 102, 15545–15550. doi:10.1073/pnas.0506580102

Sun, D., Wang, J., Han, Y., Dong, X., Ge, J., Zheng, R., et al. (2021). Tisch: A comprehensive web resource enabling interactive single-cell transcriptome visualization of tumor microenvironment. *Nucleic Acids Res.* 49, D1420–d1430. doi:10.1093/nar/gkaa1020

Sung, H., Ferlay, J., Siegel, R. L., Laversanne, M., Soerjomataram, I., Jemal, A., et al. (2021). Global cancer statistics 2020: GLOBOCAN estimates of incidence and mortality worldwide for 36 cancers in 185 countries. *CA Cancer J. Clin.* 71, 209–249.

Tang, G., Cho, M., and Wang, X. (2022). OncoDB: An interactive online database for analysis of gene expression and viral infection in cancer. *Nucleic Acids Res.* 50, D1334–d1339. doi:10.1093/nar/gkab970

Wculek, S. K., Cueto, F. J., Mujal, A. M., Melero, I., Krummel, M. F., and Sancho, D. (2020). Dendritic cells in cancer immunology and immunotherapy. *Nat. Rev. Immunol.* 20, 7–24. doi:10.1038/s41577-019-0210-z

Wu, Q., Luo, X., Terp, M. G., Li, Q., Li, Y., Shen, L., et al. (2021). DDX56 modulates post-transcriptional Wnt signaling through miRNAs and is associated with early recurrence in squamous cell lung carcinoma. *Mol. Cancer* 20, 108. doi:10.1186/s12943-021-01403-w

Zheng, R., Wan, C., Mei, S., Qin, Q., Wu, Q., Sun, H., et al. (2019). Cistrome data browser: Expanded datasets and new tools for gene regulatory analysis. *Nucleic Acids Res.* 47, D729–d735. doi:10.1093/nar/gky1094

Zhu, C., Zhang, X., Kourkoumelis, N., Shen, Y., and Huang, W. (2020). Integrated analysis of DEAD-box helicase 56: A potential oncogene in osteosarcoma. *Front. Bioeng. Biotechnol.* 8, 588. doi:10.3389/fbioe.2020.00588

frontiers | Frontiers in Genetics

TYPE Original Research
PUBLISHED 23 January 2023
DOI 10.3389/fgene.2023.1039813

Check for updates

OPEN ACCESS

EDITED BY
Wei Song,
Wuhan University, China

REVIEWED BY
Liangfang Shen,
Central South University, China
Gehao Liang,
Sun Yat-sen University Cancer Center (SYSUCC), China

*CORRESPONDENCE
Yufu Wang,
estelwyf@163.com
Wenjing Zhang,
wenjingzhang@hrbmu.edu.cn

†These authors have contributed equally to this work and share first authorship

SPECIALTY SECTION
This article was submitted to Cancer Genetics and Oncogenomics, a section of the journal Frontiers in Genetics

RECEIVED 23 September 2022
ACCEPTED 10 January 2023
PUBLISHED 23 January 2023

CITATION
Zhang L, Di L, Liu J, Lei X, Gu M, Zhang W and Wang Y (2023), The LncRNA signature associated with cuproptosis as a novel biomarker of prognosis in immunotherapy and drug screening for clear cell renal cell carcinoma.
Front. Genet. 14:1039813.
doi: 10.3389/fgene.2023.1039813

COPYRIGHT
© 2023 Zhang, Di, Liu, Lei, Gu, Zhang and Wang. This is an open-access article distributed under the terms of the Creative Commons Attribution License (CC BY). The use, distribution or reproduction in other forums is permitted, provided the original author(s) and the copyright owner(s) are credited and that the original publication in this journal is cited, in accordance with accepted academic practice. No use, distribution or reproduction is permitted which does not comply with these terms.

The LncRNA signature associated with cuproptosis as a novel biomarker of prognosis in immunotherapy and drug screening for clear cell renal cell carcinoma

Lishuo Zhang[1†], Longjiang Di[2†], Jinhui Liu[3], Xianli Lei[4], Maoli Gu[1], Wenjing Zhang[3*] and Yufu Wang[3*]

[1]Department of Urology, The First Affiliated Hospital of Harbin Medical University, Harbin, Heilongjiang, China, [2]College of Basic Medicine, Southern Medical University, Guangzhou, Guangdong, China, [3]The Second Affiliated Hospital of Harbin Medical University, Harbin, Heilongjiang, China, [4]Harbin Medical University, Harbin, Heilongjiang, China

Cuproptosis is a new form of cell death, the second form of metal ion-induced cell death defined after ferroptosis. Recently, cuproptosis has been suggested to be associated with tumorigenesis. However, the relationship between cuproptosis and patient prognosis in clear cell renal cell carcinoma (ccRCC) in the context of immunotherapy remains unknown. The aim of this study was to investigate the correlation between cuproptosis-related long non-coding RNA (lncRNA) and ccRCC in terms of immunity as well as prognosis. Clinical information on lncRNAs associated with differences in cuproptosis genes in ccRCC and normal tissues was collected from The Cancer Genome Atlas (TCGA) dataset. Univariate Cox regression was used to screen lncRNAs. A total of 11 lncRNAs closely associated with cuproptosis were further screened and established using the least absolute shrinkage and selection operator (LASSO) algorithm and multivariate Cox regression, and the samples were randomly divided into training and test groups. A risk prognostic model was constructed using the training group, and the model was validated using the test group. We investigated the predictive ability of the prognostic risk model in terms of clinical prognosis, tumor mutation, immune escape, immunotherapy, tumor microenvironment, immune infiltration levels, and tumor drug treatment of ccRCC. Using the median risk score, patients were divided into low and high-risk groups. Kaplan-Meier curves showed that the overall survival (OS) of patients in the high-risk group was significantly worse than low-risk group ($p < 0.001$). Receiver operating characteristic (ROC) curves further validated the reliability of our model. The model consistently and accurately predicted prognosis at 1, 3, and 5 years, with an AUC above 0.7. Tumor cell genes generally precede morphological abnormalities; therefore, the model we constructed can effectively compensate for the traditional method of evaluating the prognosis of patients with renal cancer, and our model was also clinically meaningful in predicting ccRCC staging. In addition, lower model risk scores determined by mutational load indicated a good chance of survival. The high-risk group had greater recruitment of immune cells, while the anti-immune checkpoint immunotherapy was less efficacious overall than that of the low-risk group. Tumor and immune-related pathways were enriched, and anti-tumor agents were selected to improve the survival of ccRCC. This prognostic risk model is based

on the levels of cuproptosis-associated lncRNAs and provides a new perspective in the clinical assessment and precise treatment of ccRCC.

KEYWORDS

clear cell renal cell carcinoma, long non-coding RNA, cuproptosis, prognosis, immunotherapy

1 Introduction

Renal cell carcinoma (RCC) is a relatively rare malignancy of the urinary tract, accounting for approximately 3% of all malignancies. In the urinary system, it is second only to prostate and bladder cancer in terms of incidence (Sung et al., 2021), with a late 5-year survival rate of only 12%. RCC is the deadliest urological cancer (Padala et al., 2020). Based on histological and molecular features, RCC includes a variety of subgroups. Among them, the most notable is renal clear cell carcinoma (ccRCC), which accounts for about 70%–80% of renal cell carcinomas (Srigley et al., 2013). The absence of a specific presentation makes the diagnosis of ccRCC difficult and its treatment ineffective. Even when surgical resection is used for limited-spread ccRCC, recurrence or metastasis occurs in about 30% of patients. Metastatic ccRCC is even more resistant to conventional therapies, resulting in poor patient outcomes (Rabjerg, 2017). The clinical prognosis of ccRCC is generally poor; tumor genetics and immunology need to be explored in order to present possible novel therapies. Avenues with possible therapeutic and prognostic utility include mRNA-lncRNA-miRNA networks, cell death patterns, and other mechanisms.

Copper is a biological element indispensable for the human body. Abnormal copper homeostasis can affect tumor progression through various mechanisms, such as apoptosis, autophagy, reactive oxygen species accumulation, and proteasomes (Ge et al., 2022; Jiang et al., 2022). Recent studies have suggested that copper dominates a specific form of cell death known as cuproptosis, the youngest member of the cell death field, and the second metal ion-induced form of cell death defined after ferroptosis (Kahlson and ScottDixon, 2022). Direct binding of copper to the lipid acylated components of the tricarboxylic acid (TCA) cycle results in lipid acylated protein aggregation and subsequent loss of iron-sulfur cluster proteins, leading to proteotoxic stress and, ultimately, cell death. A recent study screening 489 human cancer cell lines demonstrated that cuproptosis may be associated with tumor growth, multiplication, and invasion; thus, exploring the great potential of cuproptosis as a new avenue for future tumor-targeted therapy is needed (Zheng et al., 2014). However, the impact of cuproptosis on ccRCC prognosis is unclear, and a comprehensive understanding of ccRCC cellular cuproptosis, including the relationship between cuproptosis lncRNA and the tumor immune microenvironment, is still lacking.

Long non-coding RNA (lncRNA) is a heterogeneous set of non-protein-coding transcripts that are greater than 200 nucleotides in length (Kopp and Mendell, 2018; Bridges et al., 2021). During tumor progression, lncRNA can act as an oncogene or as a suppressor, controlling tumor proliferation, differentiation, invasion, and metastasis (Huarte, 2015). Its effects are mainly involved in regulating the transcription and translation of metabolism-related genes, and it even affects post-translational modifications of proteins such as acetylation and ubiquitination (Li et al., 2021). Furthermore, the role of lncRNA interactions with cell death in tumorigenesis, invasion, prognosis, and other aspects has been well-documented. An increasing number of studies have constructed predictive models of ferroptosis-related lncRNAs, which have shown great potential and significance in predicting tumor response and prognosis in various cancers (Xu et al., 2021a; Tang et al., 2022). However, the biological behavior and prognosis of cuproptosis-related lncRNAs in ccRCC has not been explored yet.

In this study, we will explore the relationship ccRCC, cuproptosis, and lncRNA. Firstly, based on the gene expression files of the ccRCC cohort. We studied 11 lncRNA that were associated with cuproptosis and had comparable prognostic significances for ccRCC patients. Using these 11 lncRNAs, we developed a risk prediction model that, upon ROC curve, C-index curve, and survival analysis, as well as other clinical indicators, shows great applicability in patients with ccRCC. Finally, we evaluated the role of these cuproptosis-associated lncRNAs in tumor immune escape and immunotherapy to predict possible target pathways that may hopefully play a role in the development of new treatment drugs and protocols for ccRCC.

2 Materials and methods

2.1 Data acquisition and processing

RNA sequence data and clinical information of renal clear cell carcinoma were obtained using the TCGA database (https://tcga-data.nci.nih.gov/), on 22 May 2022. The TCGA renal clear cell carcinoma cohort included 541 tumor samples and 72 non-tumor samples. Patients with incomplete records of follow-up information were not included in the sample analysis.

2.2 Identification of cuproptosis-associated lncrnas in renal clear cell carcinoma

First, 19 coding genes (mRNAs) associated with cuproptosis were obtained from the previous primary study. The expression levels of 19 cuproptosis-associated genes were obtained from the expression matrix of TCGA using “limma” R software packages. Next, to identify specific lncRNAs associated with cuproptosis, we used correlation tests (cor Filter = 0.1; p-value Filter = 0.05) to screen lncRNAs associated with cuproptosis in ccRCC. Subsequently, we performed correlation tests for the above coding genes and lncRNAs associated with cuproptosis. Sankey diagram and correlation heatmap were drawn with the help of “ggplot2″, “ggalluvial”, “tidyverse”, and “ggExtra” R software packages.

2.3 Model construction of cuproptosis -associated lncRNAs

Following the acquisition of differential cuproptosis-associated lncRNAs, we performed univariate Cox regression, LASSO, and

multivariate Cox regression to assess the corresponding prognostic value. We selected the appropriate lncRNAs using LASSO analysis. Subsequently, we constructed a prognostic model for ccRCC using multivariate Cox regression analysis of these lncRNAs, associated with survival. Patients were divided into high and low-risk groups based on risk scores.

Risk score = $\sum_{i-1}^{n} exp$ *βi. (β denotes coefficient value and exp denotes lncRNA level).

Kaplan-Meier and ROC curves were plotted with the help of the "Survival" and "SurvivalROC" R software packages, while the "scatterplot3d" R package plotted PCA R software packages.

2.4 Construction and verification of nomogram

Using the " survival", "regplot", and "rms" software packages, nomograms were constructed from prognostic features that included clinical characteristics like age, sex, staging, and risk score, allowing the analysis of survival probabilities at 1, 3, and 5 years. The total score ranges from 150 to 400.

2.5 Gene mutation landscape

We obtained data from the TCGA dataset, including RNAseq data, mutated maf data, and clinical information of patients about ccRCC. They were downloaded and visualized using the maftools package.

2.6 Analysis of immune-related function

The ssGSEA analysis was performed first and the scoring was corrected. Heatmap visualization was performed using the "pheatmap" and "reshape2″ packages after difference analysis.

2.7 Immune escape and immunotherapy

Using the tumor immune dysfunction and exclusion (TIDE) algorithm (http://tide.dfci.harvard.edu/), based on TIDE score, the reaction to anti-PD-1 and anti-CTLA4 immunotherapy in the TCGA cohort can be forecast. If TIDE point is > 0, the sample is non-responsive to immune checkpoint inhibitors; if it is < 0, the sample is responding to immune checkpoint inhibitors. Finally, visualization analysis was performed with ggpubr package.

2.8 Screen for potential drugs for disease

According to the Cancer Pharmacosensitivity Genomics (GDSC) (https://www.cancerrxgene.org/), a list of drugs included in, a regression model was constructed using the PRRophetic algorithm. Using the R package "PRRophetic", TCGA-ccRCC gene expression profiles and drugs in high- and low-risk subgroups were utilized to forecast half-maximal inhibitory concentrations (IC50). The smaller the IC50 of a drug, the stronger the drug's efficacy at suppressing cancer cells.

2.9 Gene enrichment

To investigate the basic functions of potential targets, we analyzed the data using functional enrichment. Gene ontology (GO) is a broadly available tool for annotation of gene features, particularly molecular functions, biological pathways and cellular components. The Kyoto Encyclopedia of Genes and Genomes (KEGG) enrichment is a useful access source for investigating the information on genomic functions. To gain a better insight into the oncogenic role of mRNAs, the ClusterProfiler package was used to analyze GO functions and KEGG pathways. The bubble map was plotted using the ggplot2 package of R software; the heatmap map was plotted using the "pheatmap" package of R software.

2.10 RT-PCR

Total RNA extraction was performed as follows: RNA extraction was performed using the Trizol kit. Reverse transcription synthesis of cDNA was performed using RevertAid First Strand cDNA Synthesis Kitt (Thermo Fisher, United States). SYBR Premix Ex Taq (Takara, Japan) instrument was used for relative quantification of data. Relative expression was calculated using the $2^{-\Delta\Delta}$ method (GAPDH was used as an internal reference). primer sequences for SGMS1-AS1. Forward (5′-GGATGGCGATGGTCAGGAAA-3′), reverse (5′-TTGGAGAGA GAGTTGCTTGGTG-3′); primer sequence for GNG12-AS1. Forward (5′-ACCTGCGGATACAGGACT-3′), reverse (5′-CCAGAAGCT GATGGCCGTAT-3′); primer sequence for SMARCA5-AS1. forward (5′-CASGATGTTCCGTCTGCGTC-3′), reverse (5′-GAT TCCCGCCGTGAGGTAAG-3′).

3 Results

3.1 Identification of cuproptosis-related lncRNAs

As shown in the flowchart in Figure 1A, we obtained 16,877 lcnRNAs from the ccRCC cohort using the TCGA database. 19 additional cuproptosis-associated genes were collected from available research. The relationship between ccRCC-associated lcnRNAs and cuproptosis-associated genes was visualized by the Sankey diagram and Pearson correlation analysis (Figure 1B).

3.2 Construction of risk score models

Univariate regression analysis revealed that 30 of the 55 cuproptosis-associated lcnRNAs screened from the ccRCC cohort, such as RAP2C-AS1, SUCLG2-AS1, PAXIP1-AS2, and LlNC01534, were strongly associated with the prognosis of ccRCC (Figure 2A). We then performed LASSO Cox regression to highlight the prognosis of the 11 lncRNAs associated with cuproptosis based on the lowest AIC (Figures 2B, C). Here, we interpreted the expression levels of each lncRNA to calculate the risk score = CDK6-AS1 × (0.0550731091024949)+EIF3J-DT × (−0.0994364819118698); SMARCA5-AS1 × (−0.0398456854170419) + LINC01711 × (0.026179353625897) + APCDD1L-DT × (0.128634099684908) + AP001372.2 × (−0.0654088007155913) + GNG12-AS1 ×

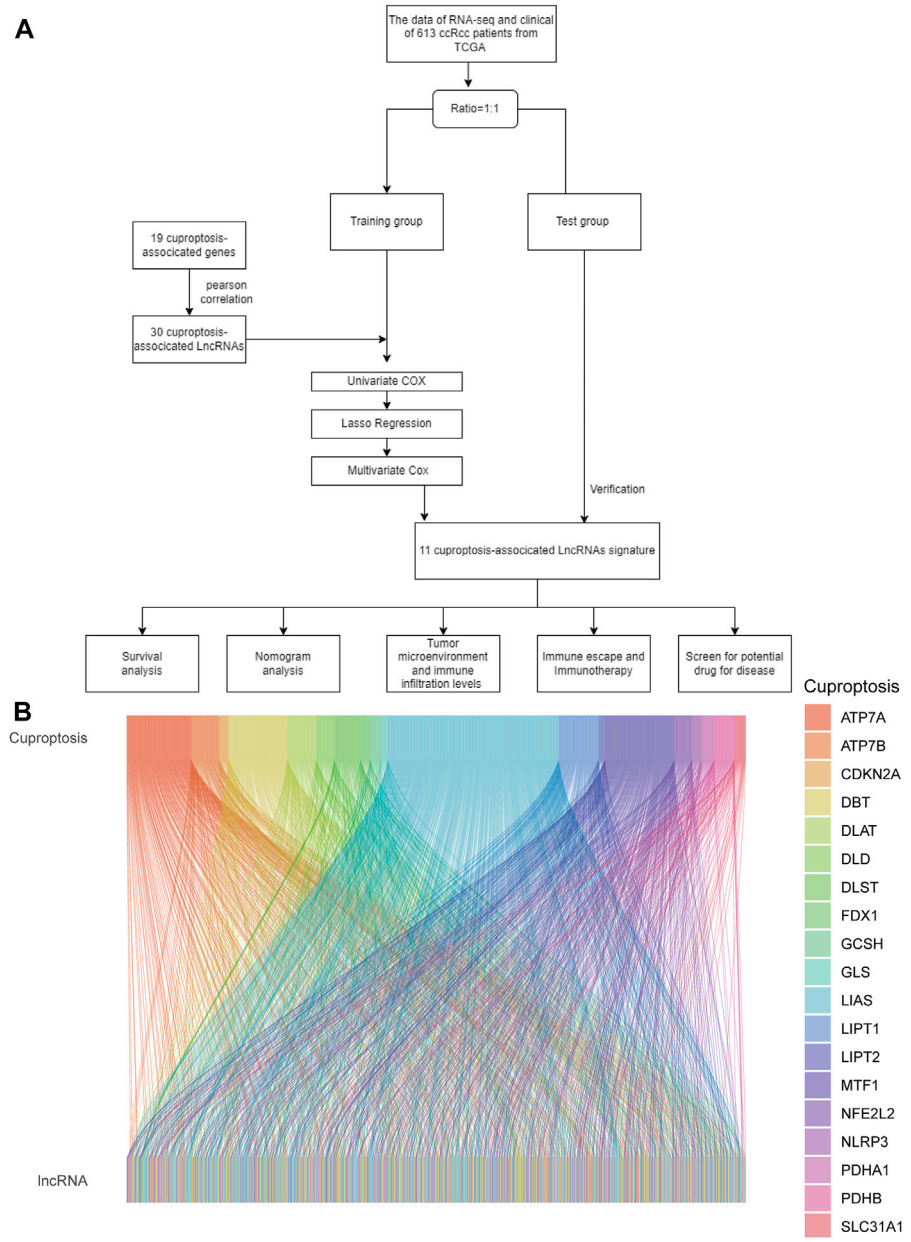

FIGURE 1
(A) Flowchart of the study. **(B)** Sankey diagram shows the association of lncRNAs associated with cuproptosis.

(−0.080630180236459) + SGMS1-AS1 × (−0.159906874521064) + LINC02446 × (0.0682696388752037); SNHG3 × (0.178418983910243) + NNT-AS1 × (−0.142242723024275). Cuproptosis-associated genes and these 11 cuproptosis-associated lncRNAs are closely related. For example, AP001372.2 was positively associated with LIAS, LIPT1, LIPT2 *etc.* APCDD1L-DT was positively correlated with PDHA1, PDHB *etc.* and negatively correlated with LIPT2. (Figure 2D). With the 11 cuproptosis gene-associated lncRNAs, we constructed a prognostic risk model to classify patients with ccRCC into high- and low-risk groups using the median risk score and validated the model with a test group. Risk curves show the correlation between the risk scores and risk levels. Patients were ordered based on the risk points of cuproptosis-associated lncRNAs. The risk was higher with higher scores (Figure 2E is the training; Figure 2F is the test). Scatter plots showed a strong correlation between survival duration and risk scores in ccRCC according to the cuproptosis-associated lncRNA model (Figure 2G is the training; Figure 2H is the test). Our results suggest that the risk score can more accurately predict and reflect the prognosis of ccRCC patients. The heat map then shows the relationship between the levels of cuproptosis-related lncRNAs in the model and the risk score (Figure 2I is the training; Figure 2J is the test).

3.3 Evaluation of the prognostic risk score model

PCA analysis showed that the lncRNAs involved in the construct model were able to most accurately distinguish between high- and low-risk groups compared to other indicators, such as various

10.3389/fgene.2023.1039813

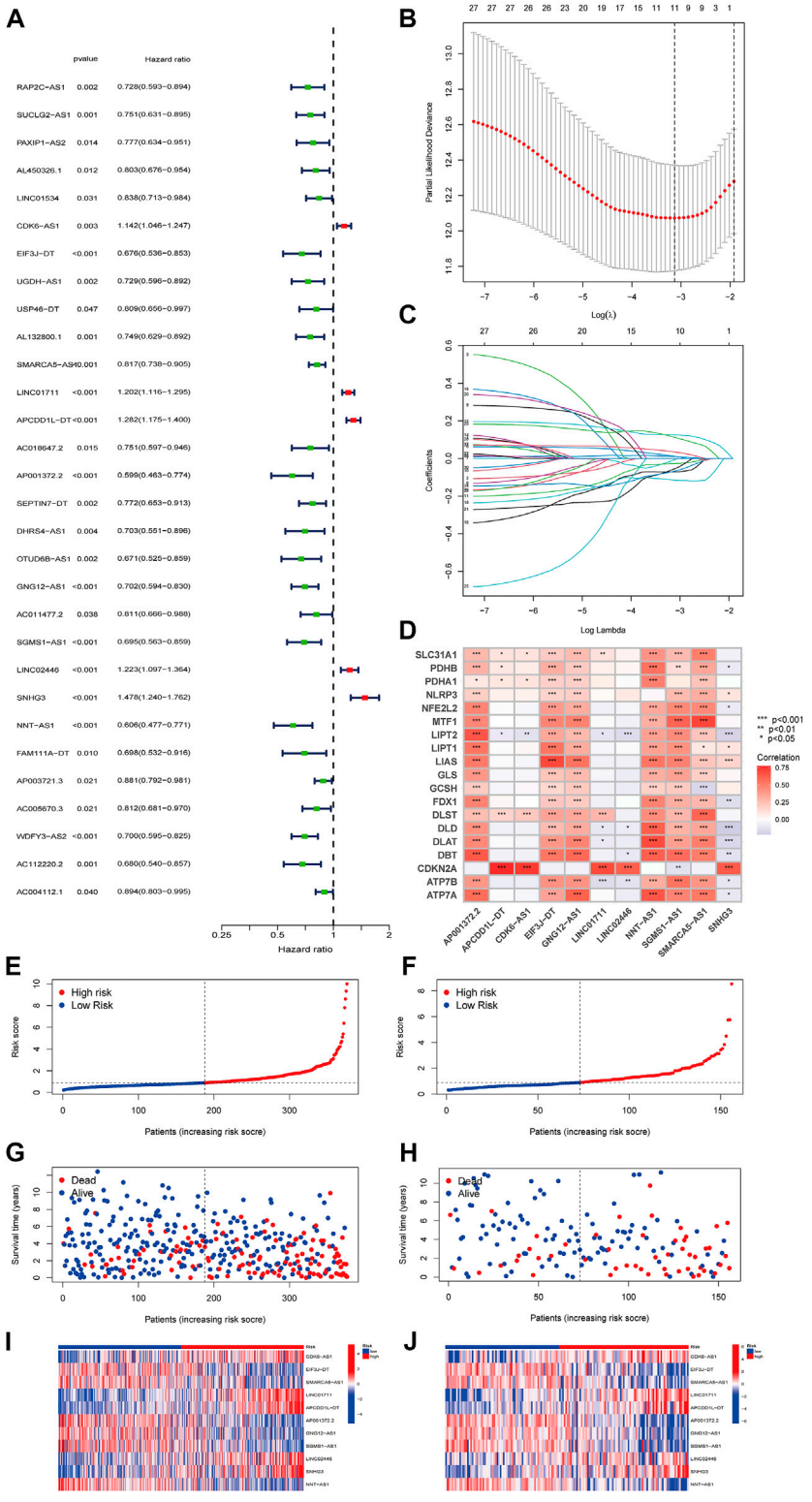

FIGURE 2
(A) Risk Forest Plot (red means high-risk lncRNA; green means low-risk lncRNA). **(B)** LASSO analysis of cuproptosis-related lncRNAs. **(C)** Cross-validation for tuning parameter selection in LASSO regression. **(D)** the correlation between cuproptosis genes and the 11 prognostic cuproptosis-associated lncRNAs in the proposed signature. The abscissa in the figure is lncRNA, ordinate is cuproptosis gene. **(E,F)** Distribution of risk score status in patients with train ccRCC and test ccRCC. **(G,H)** Scatterplot of survival status of patients with train ccRCC and test ccRCC. **(I,J)** Heat map of cuproptosis-related lncRNA expression profiles in train ccRCC and test ccRCC.

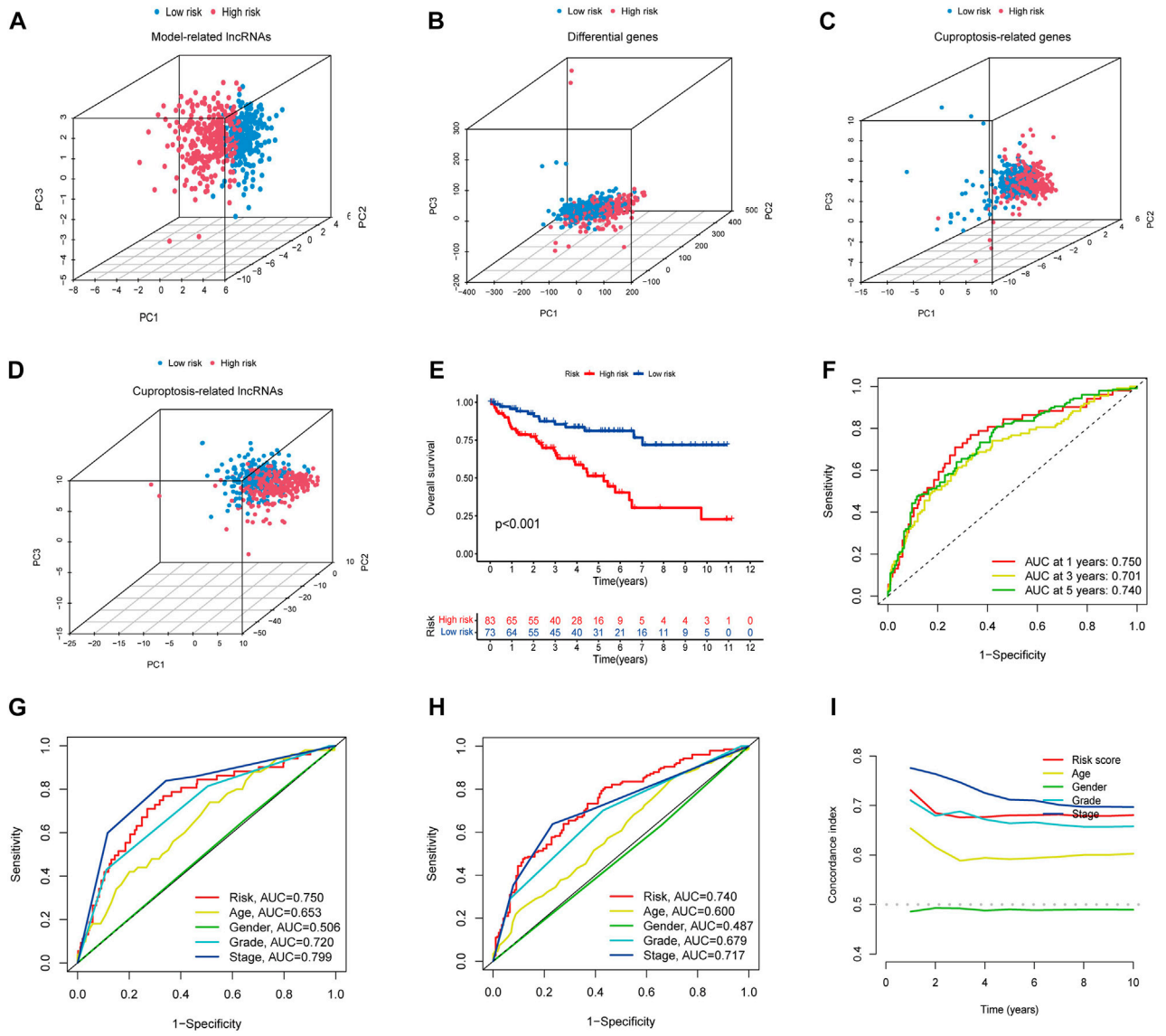

FIGURE 3
(A–D) PCA analysis of model lncRNAs, PCA analysis of cuproptosis-related lncRNAs, PCA analysis of cuproptosis-related genes, and PCA analysis of all genes, respectively. **(E)** Kaplan-Meier curves of high and low-risk group in TCGA. **(F)** ROC curves for 1, 3, and 5-year prognostic characteristics using CGGA risk score. **(G,H)** The ROC curves in TCGA data set. The larger the area under the curve, the greater the accuracy of predicting the survival time of patients through the model. **(I)** The C-index curve of risk score was used to assess the model. The ordinate is that the C-index score is the better the predictability.

differentially expressed ccRCC genes, cuproptosis-related genes, and all cuproptosis-related lncRNAs (Figures 3A–D). Using Kaplan-Meier curves, we found that the survival rate of the high-risk group was significantly lower than that of the low-risk group (Figure 3E). The ROC curves showed that the constructed model had AUC values of 0.750, 0.701, and 0.740 at 1, 2, and 3 years, which indicated the remarkable predictive ability of the model (Figure 3F). The AUC value of the model was second only to tumor stage (AUC = 0.799) upon combined ROC was used to predict 1-year overall survival (OS) curve analysis and predict 5-year overall survival (OS) curve analysis, including age, sex, stage, grade, and risk score (Figures 3G, H). In addition, we further validated the constructed prognostic model by C-index curves and found the results to be as expected (Figure 3I). The results indicated that our model could evaluate the prognosis of patients with ccRCC.

3.4 Correlation of cuproptosis-related lncRNA models with clinical features

Univariate and multivariate Cox regression analysis clinical characteristics including age, sex, staging, and risk score showed that this model, constructed using 11 cuproptosis-associated lcnRNAs, was an independent factor for ccRCC clinical outcomes ($p < 0.001$) (Figures 4A, B). We designed a nomogram, including sex, age, staging, and risk score to predict 1, 3, and 5-year survival of patients with ccRCC. The calibration plots showed that this risk score performed well, that there was a good match between predicted and actual survival, and that the prediction model had a high predictive value (Figures 4C, D). Subsequently, we performed a stratified survival analysis to test the actual application of our prognostic risk model; the results showed that patients with stage

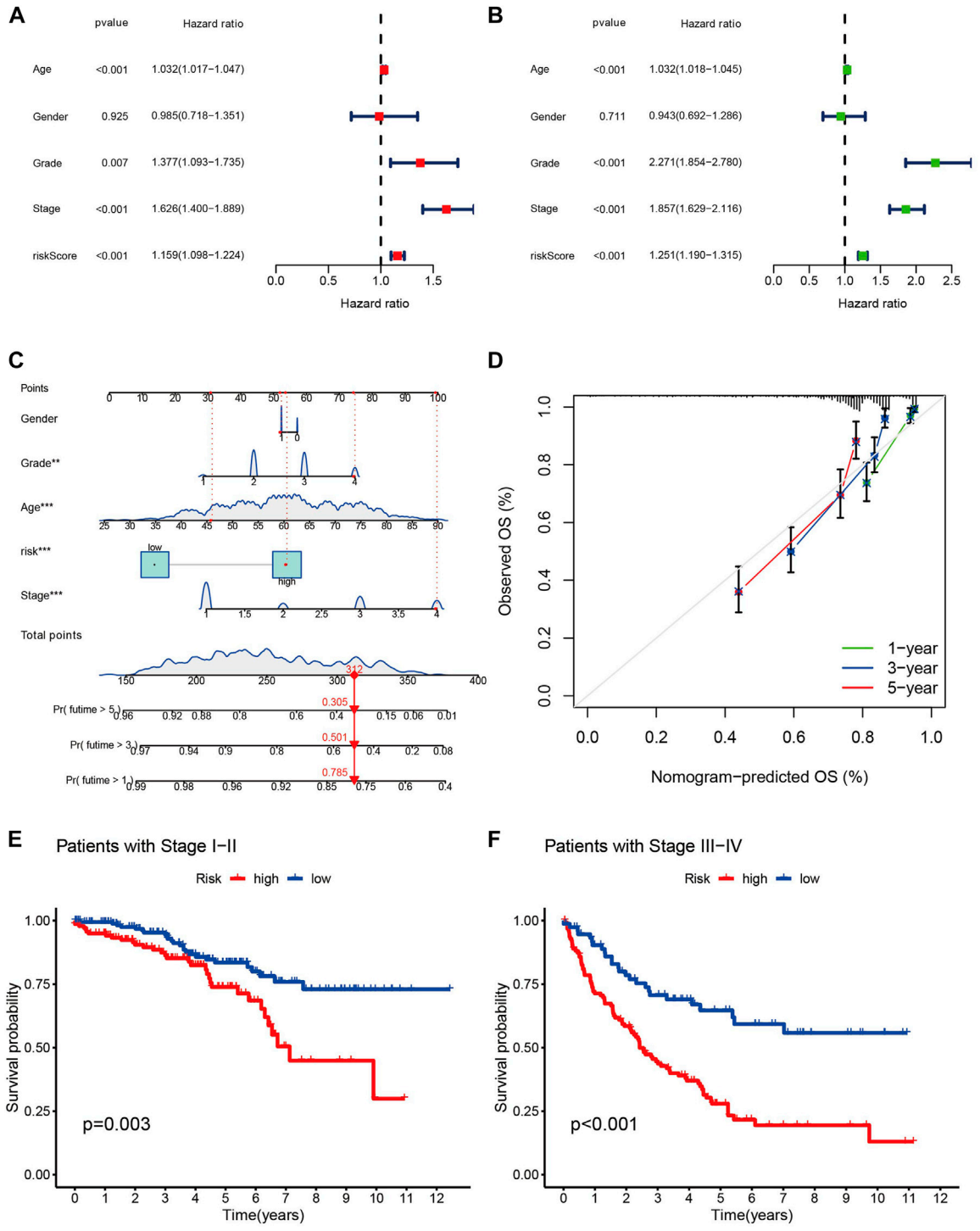

FIGURE 4
(A,B) The forest plots of *p*-value of univariate and multivariate Cox analysis of gene expression and clinical characteristics in TCGA, respectively. **(C)** Nomogram for combining clinicopathological factors and cuproptosis-associated lncRNAs for prediction. **(D)** Nomogram calibration curves. **(E,F)** the clinical survival of patients in the high- and low-risk groups of stage I-II and stage III-IV of ccRCC.

I and II tumors with higher risk scores had a worse prognosis ($p < 0.05$). The same results were found in patients with stage III and IV tumors ($p < 0.001$) (Figures 4E, F). This suggests that the model is not only applicable to predict clinical outcomes in patients with early-stage, but also late-stage tumors.

3.5 Status and impact of tumor mutations in different risk groups

Given the fact that the genetic mutations are an essential cause of oncogenesis, we investigated the distribution of somatic mutations.

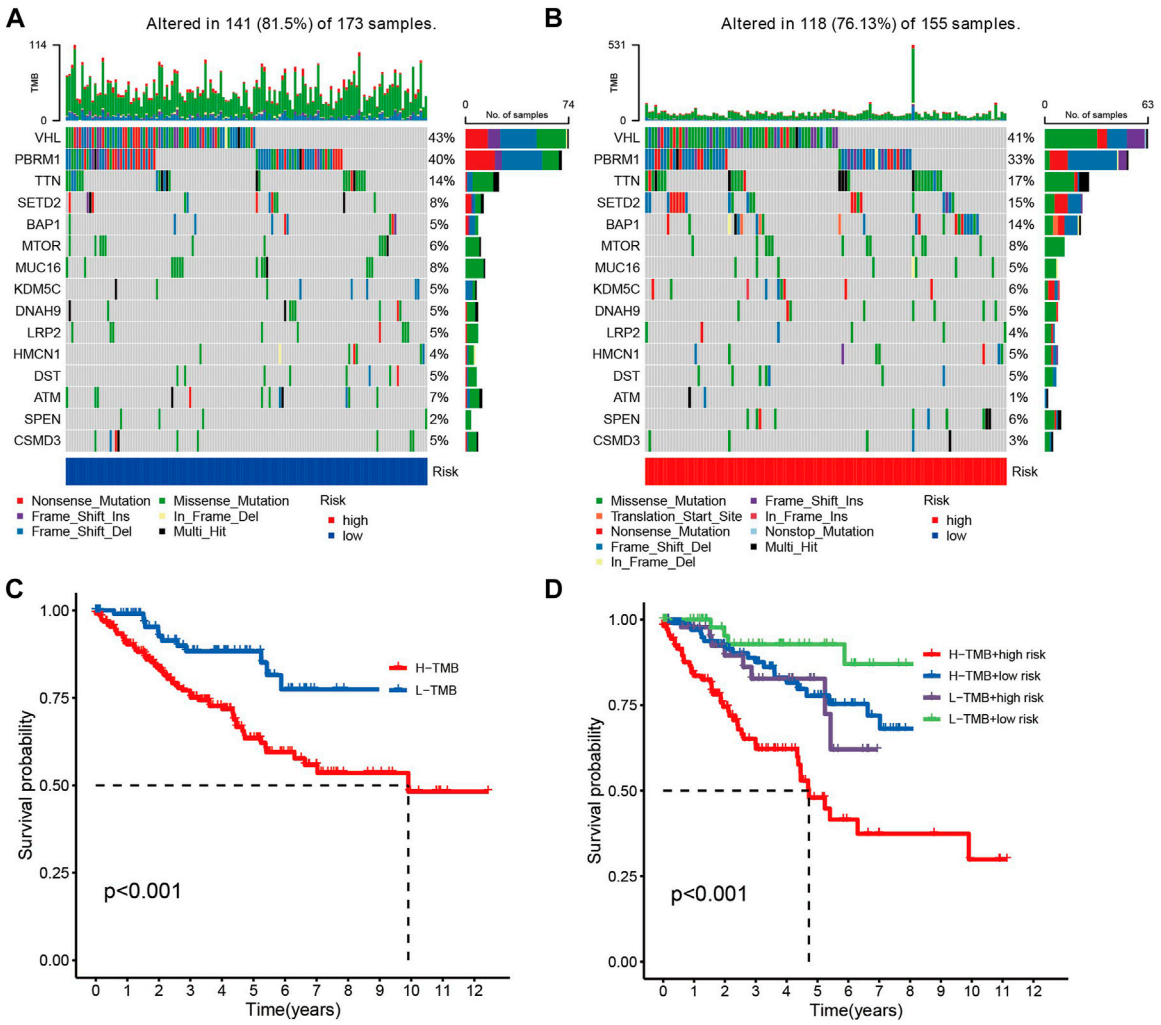

FIGURE 5
(A,B) Comparison chart of gene mutation frequencies. **(C)** Relationship between tumor mutation load and survival (red means high mutation rate, blue represents low mutation rate). **(D)** Relationship between TMB and risk score and prognosis.

The 15 most common mutated genes in both groups are shown on the heat map. The overall mutation rate was similar in both high- and low-risk patients, but in the low-risk group, genes like VHL, PBRM1, and MUC16 showed a higher mutation rate in the low-risk group (Figures 5A, B). Kaplan-Meier curves for overall survival showed that patients in the high tumor mutation load (TMB) group had significantly lower OS than those in the low TMB group (Figure 5C). Combining tumor mutation load and risk score allowed us to classify patients into four groups. The combined survival analysis showed that the high tumor mutation load and high-risk groups had the worst prognoses, and, conversely, the low tumor mutation load and low-risk groups had the best prognoses ($p < 0.001$) (Figure 5D).

3.6 Immune escape immunotherapy tumor microenvironment and immune infiltration levelsBetween the two groups

As immune checkpoint suppression therapy has become a focus of cancer treatment, we explored the role of risk models based on cuproptosis-associated lcnRNAs in predicting tumor-associated immunity As shown in Figure 6. Analysis of 13 immune-associated pathways showed that type I and II IFN response, HLA, checkpoint, co-stimulation, cytolytic activity, pro-inflammation, APC, CCR, and paraneoplastic inflammation were significantly different between high and low-risk groups (Figure 6A). Increased tumor immune dysfunction and rejection (TIDE) scores were detected more frequently in the high-risk group than in the low-risk group (Figure 6B); The results predicted by different software can visually show that immune cells such as B-cell naive and T-cell CD8 + are positively correlated with risk scores. Neutrophils are predominantly negatively correlated with risk score (Figure 6C). Immune checkpoint related genes analysis such as CD40 LGALS9 HAVCR2 TNFRSF18 CD70 were statistically significant in high- and low-risk groups (Figure 6D). Difference analysis of ssGSEA between immune cells and immune-related functions in high- and low-risk groups was mainly in CD8 + T-cell, T helper cells and other immune-related cells, Cytolytic HLA activity, and other immune functions (Figures 6E, F), and immune infiltration of the tumor microenvironment has

10.3389/fgene.2023.1039813

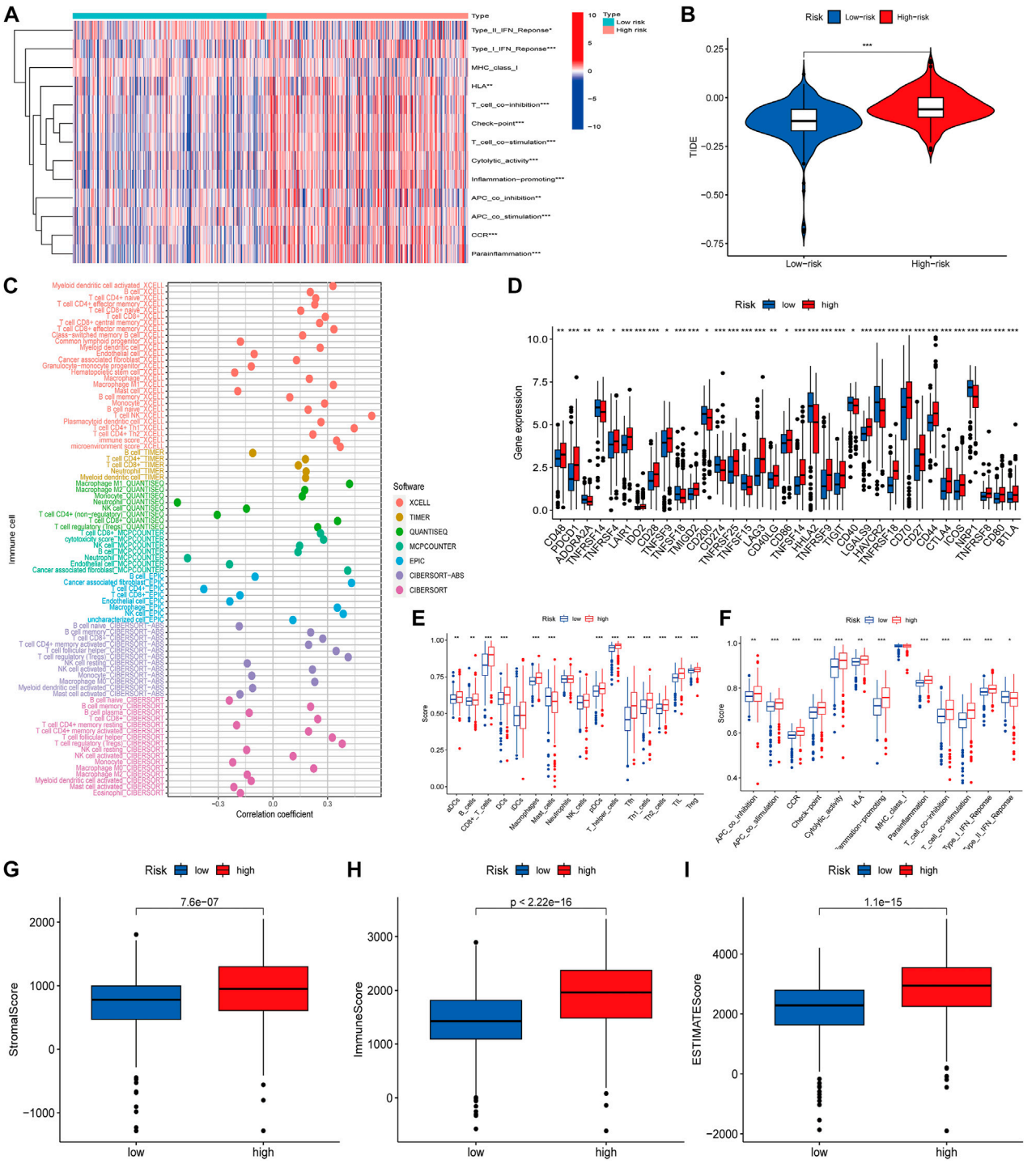

FIGURE 6
(A) Heat map of immune function differences. **(B)** Scoring of immune escape and immunotherapy in high- and low-risk groups. **(C)** Correlation coefficients between immune cells and risk scores, different colors representing different software predictions **(D)** Differential analysis of immune checkpoint related genes between high- and low-risk groups **(E,F)** Difference analysis of ssGSEA between immune cells and immune-related functions in high and low risk groups **(G–I)** The number of stromal cells, immune cell content, and comprehensive scoring of tumor microenvironment were different in the high- and low-risk groups (*$p < 0.05$; **$p < 0.01$; ***$p < 0.001$).

been associated with improved survival for some patients with solid tumors. The number of stromal cells, immune cell contents, and the comprehensive scoring of the tumor microenvironment were significantly different between the high- and low-risk groups. These data support existing studies suggesting that in ccRCC tissue types, heterogeneous immune infiltrates are present, and low-risk groups show an improved prognosis ($p < 0.001$) (Figures 6G–I).

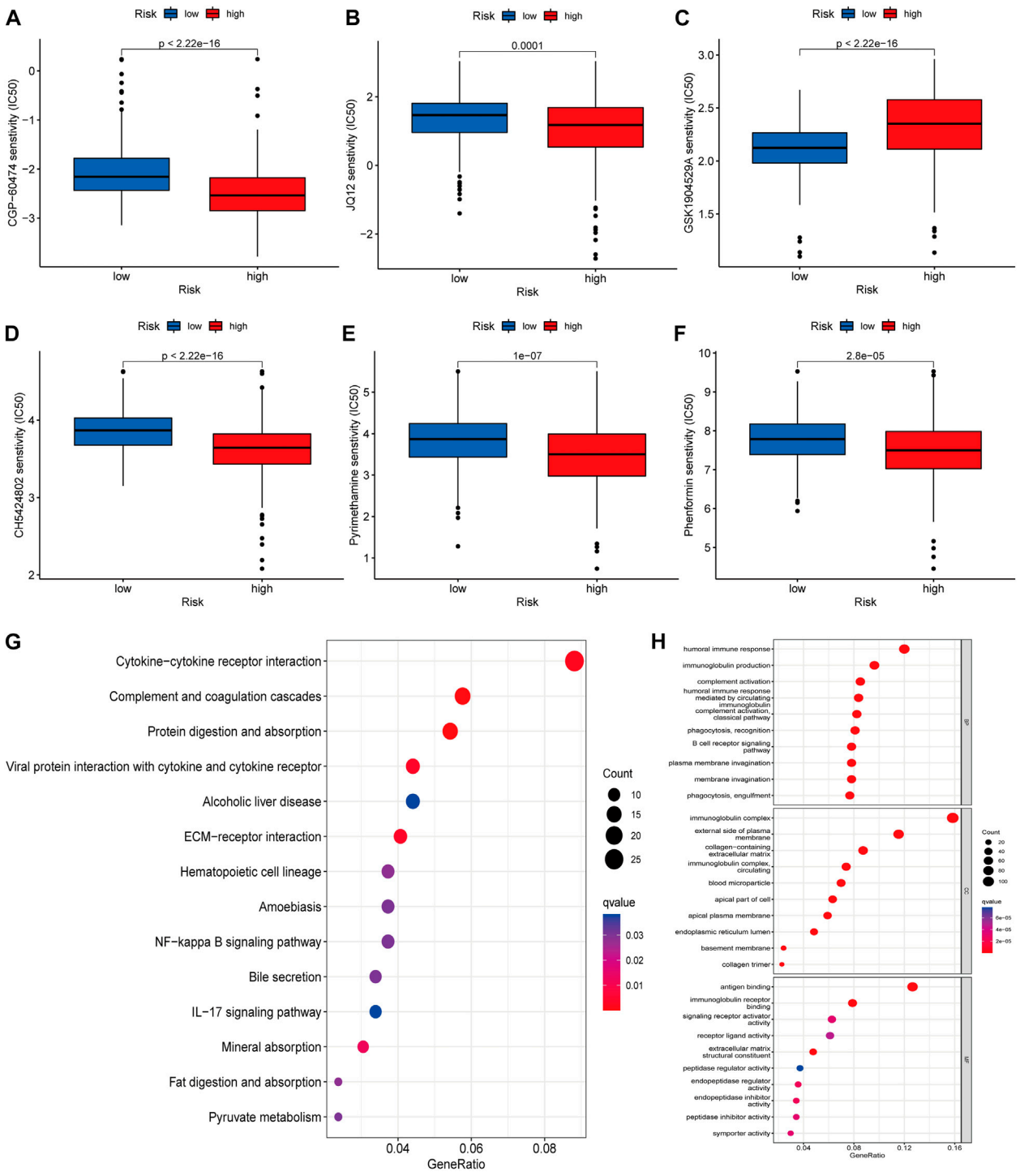

FIGURE 7
(A–F) The IC50 score in high- and low-risk drugs. Asterisks (*) stand for significance levels (*$p < 0.05$, **$p < 0.01$, ***$p < 0.001$) **(G,H)** KEGG and GO of differential genes in high- and low-risk groups, respectively Enrichment analysis, in which different colors represent the significance of differential enrichment results; the smaller the value of fdr, the more the number of circles. Circle size represents the number of enriched genes.

3.7 Screening for disease potential drugs and functional analysis

We using further drug sensitivity studies, we found that patients in the low-risk group were more sensitive to most immunosuppressive agents, such as CGP-6047A, JQ12, CH5424802, pyrimethamine, and phenformin, while the high-risk group only showed better sensitivity to GSK1904529A (Figures 7A–F). This means that patients from the lower risk group have a better chance of responding well to these chemotherapy drugs, and, subsequently have more treatment options. To further explore the mechanism of the role of cuproptosis-associated lcnRNAs in ccRCC, We performed GO and KEGG of

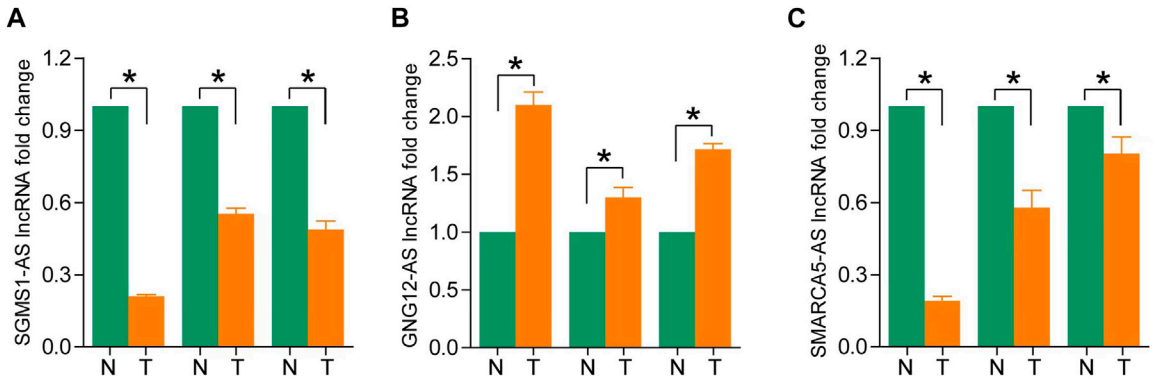

FIGURE 8
(A–C) Expression levels of SGMS1-AS1, GNG12-AS1, and SMARCA5-AS1 in ccRCC paraneoplastic tissues and ccRCC samples by RT-PCR (*$p < 0.05$, **$p < 0.01$, ***$p < 0.001$).

differential genes in high- and low-risk groups. According to KEGG analysis, these RNAs were mainly involved in cytokine-cytokine receptor interactions, complement and coagulation cascades, protein digestion and absorption, alcoholic liver disease, EMC-receptor interactions, among others (Figure 7G). GO analysis was mainly involved in humoral immune responses, immunoglobulin production, immunoglobulin complexes, plasma membrane extrinsic, antigen binding, and immunoglobulin receptor binding (Figure 7H). These functions are vital to tumor the progression and immunotherapy response.

3.8 Validation of lncRNAs expression in ccRCC tissues

To assess differences in the expression of three landmark lncRNAs that constitute prognostic models in ccRCC and normal tissue, we used the unpaired Student's *t*-test to examine expression levels of the three lncRNAs quantified by qRT-PCR. The qRT-PCR data of the three patients showed that lncRNAs SGMS1-AS1 and SMARCA5-AS1 were lower, and lncRNA GNG12-AS1 was higher in cancer tissues than in adjacent normal tissues. This further validated the accuracy of our previous bioinformatics analysis (Figures 8A–C).

4 Discussion

Renal cancer (RCC) is one of the most common tumors of the urinary system, and ccRCC is the most common (75%–80%) and best-studied subtype of RCC. Its treatment and management have always been challenging. Traditional radiotherapy and chemotherapy are essentially ineffective for RCC, and about 30% of RCC patients have metastatic disease at the initial visit, or relapse after complete resection of the primary tumor. Drug resistance of tumor cells in patients with relapse is the key to gauging the prognosis and determining future clinical action (Makhov et al., 2018). Although studies have shown that molecular targeting of vascular endothelial growth factor, platelet-derived growth factor, and inhibitor (PD1-PD-L1/CTLA4) to inhibit immune checkpoints can improve prognosis to a certain extent, tumor cells may grow immune to the new anti-tumor drugs. For example, the drug resistance of sunitinib and erlotinib is gradually increasing, and the overall survival rate of patients is still not optimistic (Barata and Rini, 2017). Therefore, the search for new immune checkpoints and targeted molecules is of great significance and requires urgency for the prognosis of ccRCC patients.

Cuproptosis is a recently defined unique mode of cell death. The mechanism of its occurrence mainly involves the homeostasis of copper ions (intake and output), mitochondrial respiration, energy metabolism—such as the TCA cycle, reduction of Fe-S cluster protein levels, the increase of HSP70 and other protein levels—as well as the triggering of protein toxicity. The researchers also identified key genes, such as FDX1, LIPT1, LIAS, DLD, NLRP3, GLS, among other key genes, associated with cuproptosis through genome-wide CRISPR-Cas9 loss-of-function methods. and ATP7B (Zheng et al., 2014; Tsvetkov et al., 2022). Although the impact of cuproptosis on tumorigenesis, development, prognosis, *etc.* remains to be further explored, the metabolic reprogramming involved in its genesis is based on its defining context in tumor cells and its changes in metabolic pathways of tumor energetics and biosynthesis (Xia et al., 2021). We can foresee that cuproptosis has a great predictive potential in the field of oncology. Related studies have demonstrated that ccRCC is also often accompanied by reprogramming of glucose and fatty acid metabolism, as well as TCA cycle dysfunction (Schaeffeler et al., 2019). Exploring the mechanisms associated with these metabolic pathways and exploiting the close link between cuproptosis and energy metabolism may contribute to the treatment of ccRCC.

The regulatory effects of lncRNAs on tumorigenesis, metastasis, and infiltration have gradually been comprehensively studied. The related mechanisms mainly include mediating post-translational modifications, regulating immune responses, promoting immune escape, and participating in metabolic reprogramming (Zhang et al., 2020; Li et al., 2021; Tan et al., 2021). Some studies have shown that lncRNAs regulate some elements of copper ion homeostasis and cuproptosis, such as SLC31A1 (CTR1), ATP7B, and GLS, and exert their influence on tumors. The lncRNA NEAT1 reduces the expression of CTR1 to regulate the function of cancer stem cells (Jiang et al., 2018). The lncRNA GLS-AS participates in the nutritional stress of pancreatic cancer by inhibiting GLS-mediated metabolism and controls tumor progression (Deng et al., 2019). In addition, lncRNAs themselves—or their encoded peptides—are also involved in the regulation of the carboxylic acid cycle of tumor cells (Stein et al., 2018; Sang et al., 2021). In summary, in tumor cells, lncRNAs regulate the expression of

cuproptosis-related genes and the related mechanisms affect the occurrence and development of tumors. However, the role of cuproptosis-related lncRNAs on the treatment and prognosis of ccRCC tumors still needs further research.

In our study, we screened 55 lncRNAs associated with cuproptosis in ccRCC and constructed a model with the final selected 11 lncRNAs. These 11 lncRNAs have good discriminatory ability for high- and low-risk groups. There was a significant difference in OS between the high and low-risk groups. The 1, 3, and 5-year survival rates for this model corresponded to areas under the ROC curve that were all greater than 0.70. The results mentioned prior reflect the strength of the model in predicting the prognosis of ccRCC. The reliability of the model was further validated by the results of methods such as C-index, risk curve, calibration curve, and validation of clinical characteristics. Based on the above series of analysis, we found that most lncRNAs were protective in ccRCC patients, while only CDK6-AS1, LINC01711, APCDD1L-DT, LINC02446, and SNHG3 were independent risk factors for ccRCC. Studies have shown that LINC01711 is an independent prognostic factor for esophageal squamous cell carcinoma (ESCC) and, combined with other autophagy-related lncRNAs, can help forecast the prognosis and treatment of ESCC (Shi et al., 2021). The experiments carried out by the Mei-Ling Xu team proved that LINC01711 promotes the proliferation, migration, and invasion of ESCC (Xu et al., 2021b). The predictive effect of LINC02446 combined with other lncRNAs on tumor overall survival has been studied in bladder cancer and melanoma (Zhang et al., 2021a; Tong et al., 2021). The molecular mechanisms involved in bladder cancer mainly involve EIF3G-related translational activation as well as mTOR signaling pathway activation (Zhang et al., 2021b). SNHG3 plays a more prominent role in tumors, involving endogenous competing miRNAs, encoding peptides, *etc.* As an independent predictor of ccRCC, research relating to SNHG3 has recently improved (Yang et al., 2020). Topoisomerase II Alpha (TOP2A) is an enzyme that controls and changes the topological state of DNA, and can exert anti-tumor effects (Buzun et al., 2020). SNHG3 promotes ccRCC cell proliferation through a TOP2A-dependent pathway (Zhang et al., 2019). Baculoviral inhibitor of apoptosis repeat-containing 5 (BIRC5) is another regulatory target of lncRNA SNHG3 in ccRCC (Xu et al., 2021c). Cuproptosis-related lncRNAs can participate in the regulation of tumorigenesis and progression by binding to DNA, miRNA, and proteins, thereby affecting tumor progression, patient prognosis, and treatment outcomes. There is no study that examines the mechanisms of lncRNA and cuproptosis interactions in tumors. We established a cuproptosis-related lncRNA-based risk model to predict ccRCC and assist its early diagnosis and treatment.

The immune escape of tumor cells is a vital factor in tumor progression. Many studies have shown that lncRNAs can regulate tumor immune responses and promote tumor immune escape. Hepatocyte-derived exosomal lncRNA TUC339 is involved in cytokines, chemokines, Toll-like receptors and other related signaling molecules (Li et al., 2018). LncRNA MIAT is positively correlated with immune checkpoint molecules, such as PD-1 and CTLA4, in liver cancer cells (Peng et al., 2020). Therefore, we further carried out the immune-related analysis of 11 cuproptosis-related lncRNAs. We found significant differences in 13 immune-related pathways, TIDE scores, tumor microenvironment, and immune infiltration levels between high- and low-risk groups. These results suggest that lncRNAs associated with cuproptosis play a key role in regulating the associated immunity and patient prognoses in ccRCC cases. We analyzed the clinical sensitivity of immunotherapy drugs and found that the drug sensitivity of the high-risk group was significantly lower than that of the low-risk group, and that there were very few effective for the high-risk group; the low-risk group is more likely to have an effective immunotherapy course. In addition, in order to explore further functions of cuproptosis-related lncRNAs in ccRCC in the future, we performed GO and KEGG functional analysis, and found that most of these functions are related to tumor development and tumor immunotherapy. Finally, we detected lncRNAs in normal tissue and ccRCC tissue prognostic model using qRT-PCR method. These results confirmed the conclusions obtained earlier and made the study more accurate and complete.

There are several limitations in this study. First, we analyzed the prognostic role of cellular cuproptosis-related lncRNAs in ccRCC, but the interactions with target genes, signaling pathways, as well as themselves, needs further elucidation. In addition, our study verified the different expression levels of 3 representative lncRNAs associated with risk models quantified by RT-PCR. However, due to the difficulty of specimen collection, we did not measure the levels of all 11 cuproptosis-related lncRNAs.

In conclusion, our study marks the first analysis of cuproptosis-related lncRNA in ccRCC. We have exhaustively verified the predictive ability and reliability of the associated risk assessment model.

Data availability statement

Publicly available datasets were analyzed in this study. This data can be found here: TCGA.

Author contributions

LZ and LD conceived and designed the study, reviewed the paper, and provided comments. LZ, JL, WZ, and YW performed data mining and analysis. LD, MG, WZ, and YW wrote the manuscript. All authors contributed to the article and approved the submitted version.

Funding

This work was supported by Financial asistance under Heilongjiang Postdoctoral Fund (Grant No. LBH-Z18121), National Natural Science Foundation of China (Grant No. 82001715), Health and Family Planning Commission of Heilongjiang Provincial (Grant No. 2018286), The Fundamental Research Funds for the Provincial Universities (Grant No. 2017LCZX67).

Acknowledgments

We would like to thank Editage (www.editage.cn) for English language editing.

Conflict of interest

The authors declare that the research was conducted in the absence of any commercial or financial relationships that could be construed as a potential conflict of interest.

Publisher's note

All claims expressed in this article are solely those of the authors and do not necessarily represent those of their affiliated organizations, or those of the publisher, the editors and the reviewers. Any product that may be evaluated in this article, or claim that may be made by its manufacturer, is not guaranteed or endorsed by the publisher.

Supplementary material

The Supplementary Material for this article can be found online at: https://www.frontiersin.org/articles/10.3389/fgene.2023.1039813/full#supplementary-material

References

Barata, P. C., and Rini, B. I. (2017). Treatment of renal cell carcinoma: Current status and future directions. *CA a cancer J. Clin.* 67 (6), 507–524. doi:10.3322/caac.21411

Bridges, M. C., Daulagala, A. C., and Kourtidis, A. (2021). LNCcation: lncRNA localization and function. *J. Cell Biol.* 220 (2), e202009045. doi:10.1083/jcb.202009045

Buzun, K., Bielawska, A., Bielawski, K., and Gornowicz, A. (2020). DNA topoisomerases as molecular targets for anticancer drugs. *J. enzyme inhibition Med. Chem.* 35 (1), 1781–1799. doi:10.1080/14756366.2020.1821676

Deng, S-J., Chen, H. Y., Zeng, Z., Deng, S., Zhu, S., Ye, Z., et al. (2019). Nutrient stress-dysregulated antisense lncRNA GLS-AS impairs GLS-mediated metabolism and represses pancreatic cancer progression. *Cancer Res.* 79 (7), 1398–1412. doi:10.1158/0008-5472.CAN-18-0419

Ge, E. J., Bush, A. I., Casini, A., Cobine, P. A., Cross, J. R., DeNicola, G. M., et al. (2022). Connecting copper and cancer: From transition metal signalling to metalloplasia. *Nat. Rev. Cancer* 22 (2), 102–113. doi:10.1038/s41568-021-00417-2

Huarte, M. (2015). The emerging role of lncRNAs in cancer. *Nat. Med.* 21 (11), 1253–1261. doi:10.1038/nm.3981

Jiang, P., Chen, A., Wu, X., Zhou, M., Ul Haq, I., Mariyam, Z., et al. (2018). NEAT1 acts as an inducer of cancer stem cell-like phenotypes in NSCLC by inhibiting EGCG-upregulated CTR1. *J. Cell. physiology* 233 (6), 4852–4863. doi:10.1002/jcp.26288

Jiang, Y., Huo, Z., Qi, X., Zuo, T., and Wu, Z. (2022). Copper-induced tumor cell death mechanisms and antitumor theragnostic applications of copper complexes. *Nanomedicine Lond. Engl.* 17 (5), 303–324. doi:10.2217/nnm-2021-0374

Kahlson, M. A., and ScottDixon, J. (2022). Copper-induced cell death. *Sci. (New York, N.Y.)* 375 (6586), 1231–1232. doi:10.1126/science.abo3959

Kopp, F., and Mendell, J. T. (2018). Functional classification and experimental dissection of long noncoding RNAs. *Cell* 172 (3), 393–407. doi:10.1016/j.cell.2018.01.011

Li, G., Kryczek, I., Nam, J., Li, X., Li, S., Li, J., et al. (2021). LIMIT is an immunogenic lncRNA in cancer immunity and immunotherapy. *Nat. Cell Biol.* 23 (5), 526–537. doi:10.1038/s41556-021-00672-3

Li, X., Lei, Y., Wu, M., and Li, N. (2018). Regulation of macrophage activation and polarization by HCC-derived exosomal lncRNA TUC339. *Int. J. Mol. Sci.* 19, 2958. doi:10.3390/ijms19102958

Makhov, P., Joshi, S., Ghatalia, P., Kutikov, A., Uzzo, R. G., and Kolenko, V. M. (2018). Resistance to systemic therapies in clear cell renal cell carcinoma: Mechanisms and management strategies. *Mol. cancer Ther.* 17 (7), 1355–1364. doi:10.1158/1535-7163.MCT-17-1299

Padala, S. A., Barsouk, A., Thandra, K. C., Saginala, K., Mohammed, A., Vakiti, A., et al. (2020). Epidemiology of renal cell carcinoma. *World J. Oncol.* 11 (3), 79–87. doi:10.14740/wjon1279

Peng, L., Chen, Y., Ou, Q., Wang, X., and Tang, N. (2020). LncRNA MIAT correlates with immune infiltrates and drug reactions in hepatocellular carcinoma. *Int. Immunopharmacol.* 89, 107071. doi:10.1016/j.intimp.2020.107071

Rabjerg, M. (2017). Identification and validation of novel prognostic markers in Renal Cell Carcinoma. *Dan. Med. J.* 64, 10B5339.

Sang, L., Ju, H. Q., Yang, Z., Ge, Q., Zhang, Z., Liu, F., et al. (2021). Mitochondrial long non-coding RNA GAS5 tunes TCA metabolism in response to nutrient stress. *Nat. Metab.* 3 (1), 90–106. doi:10.1038/s42255-020-00325-z

Schaeffeler, E., Buttner, F., Reustle, A., Klumpp, V., Winter, S., Rausch, S., et al. (2019). Metabolic and lipidomic reprogramming in renal cell carcinoma subtypes reflects regions of tumor origin. *Eur. Urol. focus* 5 (4), 608–618. doi:10.1016/j.euf.2018.01.016

Shi, X., Liu, X., Pan, S., Ke, Y., Li, Y., Guo, W., et al. (2021). A novel autophagy-related long non-coding RNA signature to predict prognosis and therapeutic response in esophageal squamous cell carcinoma. *Int. J. general Med.* 14, 8325–8339. doi:10.2147/IJGM.S333697

Srigley, J. R., Delahunt, B., Eble, J. N., Egevad, L., Epstein, J. I., Grignon, D., et al. (2013). The international society of urological pathology (ISUP) vancouver classification of renal neoplasia. *Am. J. Surg. pathology* 37, 101469–101489. doi:10.1097/PAS.0b013e318299f2d1

Stein, C. S., Jadiya, P., Zhang, X., McLendon, J. M., Abouassaly, G. M., Witmer, N. H., et al. (2018). Mitoregulin: A lncRNA-encoded microprotein that supports mitochondrial supercomplexes and respiratory efficiency. *Cell Rep.* 23 (13), 3710–3720. e8. doi:10.1016/j.celrep.2018.06.002

Sung, H., Ferlay, J., Siegel, R. L., Laversanne, M., Soerjomataram, I., Jemal, A., et al. (2021). Global cancer statistics 2020: GLOBOCAN estimates of incidence and mortality worldwide for 36 cancers in 185 countries. *CA a cancer J. Clin.* 71 (3), 209–249. doi:10.3322/caac.21660

Tan, Y-T., Lin, J. F., Li, T., Li, J. J., Xu, R. H., and Ju, H. Q. (2021). LncRNA-mediated posttranslational modifications and reprogramming of energy metabolism in cancer. *Cancer Commun. Lond. Engl.* 41 (2), 109–120. doi:10.1002/cac2.12108

Tang, R., Wu, Z., Rong, Z., Xu, J., Wang, W., Zhang, B., et al. (2022). Ferroptosis-related lncRNA pairs to predict the clinical outcome and molecular characteristics of pancreatic ductal adenocarcinoma. *Briefings Bioinforma.* 23 (1), bbab388. doi:10.1093/bib/bbab388

Tong, H., Gao, S., Yin, H., Cao, H., and He, W. (2021). An epithelial-mesenchymal transition-related long noncoding RNA signature correlates with the prognosis and progression in patients with bladder cancer. *Biosci. Rep.* 41 (1), BSR20203944. doi:10.1042/BSR20203944

Tsvetkov, P., Coy, S., Petrova, B., Dreishpoon, M., Verma, A., Abdusamad, M., et al. (2022). Copper induces cell death by targeting lipoylated TCA cycle proteins. *Sci. (New York, N.Y.)* 375 (6586), 1254–1261. doi:10.1126/science.abf0529

Xia, L., Oyang, L., Lin, J., Tan, S., Han, Y., Wu, N., et al.(2021). The cancer metabolic reprogramming and immune response. *Mol. cancer* 20 (1), 28. doi:10.1186/s12943-021-01316-8

Xu, M-L., Liu, T. C., Dong, F. X., Meng, L. X., Ling, A. X., and Liu, S. (2021). Exosomal lncRNA LINC01711 facilitates metastasis of esophageal squamous cell carcinoma via the miR-326/FSCN1 axis. *Aging* 13 (15), 19776–19788. doi:10.18632/aging.203389

Xu, Z., Peng, B., Liang, Q., Chen, X., Cai, Y., Zeng, S., et al.(2021). Construction of a ferroptosis-related nine-lncRNA signature for predicting prognosis and immune response in hepatocellular carcinoma. *Front. Immunol.* 12, 719175. doi:10.3389/fimmu.2021.719175

Xu, Z., Ye, J., Bao, P., Wu, Q., Xie, F., and Li, P. (2021). Long non-coding RNA SNHG3 promotes the progression of clear cell renal cell carcinoma via regulating BIRC5 expression. *Transl. cancer Res.* 10 (10), 4502–4513. doi:10.21037/tcr-21-1802

Yang, W., Zhang, K., Li, L., Ma, K., Hong, B., Gong, Y., et al.(2020). Discovery and validation of the prognostic value of the lncRNAs encoding snoRNAs in patients with clear cell renal cell carcinoma. *Aging* 12 (5), 4424–4444. doi:10.18632/aging.102894

Zhang, C., Dang, D., Cong, L., Sun, H., and Cong, X. (2021). Pivotal factors associated with the immunosuppressive tumor microenvironment and melanoma metastasis. *Cancer Med.* 10 (14), 4710–4720. doi:10.1002/cam4.3963

Zhang, C., Qu, Y., Xiao, H., Xiao, W., Liu, J., Gao, Y., et al.(2019). LncRNA SNHG3 promotes clear cell renal cell carcinoma proliferation and migration by upregulating TOP2A. *Exp. Cell Res.* 384 (1), 111595. doi:10.1016/j.yexcr.2019.111595

Zhang, M., Wang, N., Song, P., Fu, Y., Ren, Y., and Li, Z.(2020). LncRNA GATA3-AS1 facilitates tumour progression and immune escape in triple-negative breast cancer through destabilization of GATA3 but stabilization of PD-L1. *Cell Prolif.* 53 (9), e12855. doi:10.1111/cpr.12855

Zhang, X., Zhang, J., Zhao, W., Dong, X., Xin, P., Liu, X., et al.(2021). Long non-coding RNA LINC02446 suppresses the proliferation and metastasis of bladder cancer cells by binding with EIF3G and regulating the mTOR signalling pathway. *Cancer gene Ther.* 28 (12), 1376–1389. doi:10.1038/s41417-020-00285-2

Zheng, G., Zhang, J., Xu, Y., Shen, X., Song, H., Jing, J., et al.(2014). Involvement of CTR1 and ATP7A in lead (Pb)-induced copper (Cu) accumulation in choroidal epithelial cells. *Toxicol. Lett.* 225 (1), 110–118. doi:10.1016/j.toxlet.2013.11.034

Frontiers in Genetics

Highlights genetic and genomic inquiry relating to all domains of life

The most cited genetics and heredity journal, which advances our understanding of genes from humans to plants and other model organisms. It highlights developments in the function and variability of the genome, and the use of genomic tools.

Discover the latest Research Topics

See more →

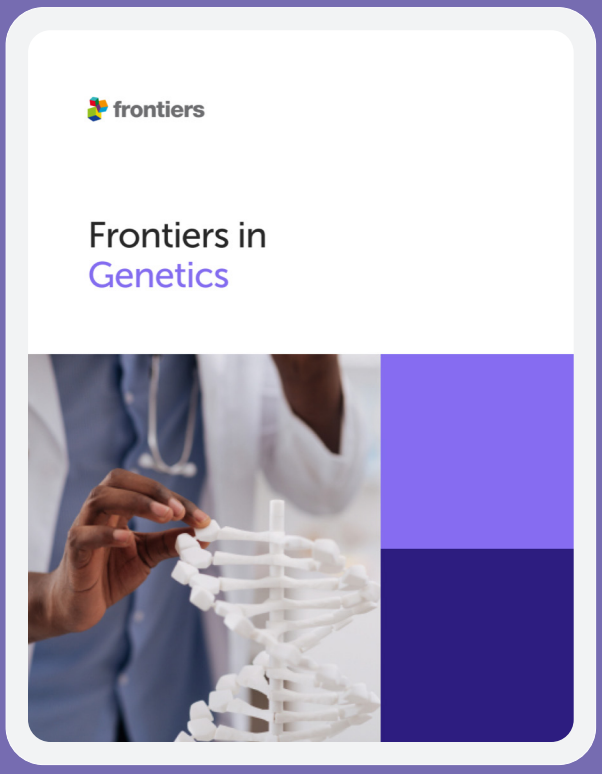

Frontiers

Avenue du Tribunal-Fédéral 34
1005 Lausanne, Switzerland
frontiersin.org

Contact us

+41 (0)21 510 17 00
frontiersin.org/about/contact